RADIATION-INDUCED AND OXIDATIVE DNA DAMAGES

EDITED BY: Antonio Monari, Elise Dumont and Chryssostomos Chatgilialoglu
PUBLISHED IN: Frontiers in Chemistry

frontiers Research Topics

frontiers

Frontiers Copyright Statement

© Copyright 2007-2015 Frontiers Media SA. All rights reserved.

All content included on this site, such as text, graphics, logos, button icons, images, video/audio clips, downloads, data compilations and software, is the property of or is licensed to Frontiers Media SA ("Frontiers") or its licensees and/or subcontractors. The copyright in the text of individual articles is the property of their respective authors, subject to a license granted to Frontiers.

The compilation of articles constituting this e-book, wherever published, as well as the compilation of all other content on this site, is the exclusive property of Frontiers. For the conditions for downloading and copying of e-books from Frontiers' website, please see the Terms for Website Use. If purchasing Frontiers e-books from other websites or sources, the conditions of the website concerned apply.

Images and graphics not forming part of user-contributed materials may not be downloaded or copied without permission.

Individual articles may be downloaded and reproduced in accordance with the principles of the CC-BY licence subject to any copyright or other notices. They may not be re-sold as an e-book.

As author or other contributor you grant a CC-BY licence to others to reproduce your articles, including any graphics and third-party materials supplied by you, in accordance with the Conditions for Website Use and subject to any copyright notices which you include in connection with your articles and materials.

All copyright, and all rights therein, are protected by national and international copyright laws.

The above represents a summary only. For the full conditions see the Conditions for Authors and the Conditions for Website Use.

ISSN 1664-8714
ISBN 978-2-88919-660-9
DOI 10.3389/978-2-88919-660-9

About Frontiers

Frontiers is more than just an open-access publisher of scholarly articles: it is a pioneering approach to the world of academia, radically improving the way scholarly research is managed. The grand vision of Frontiers is a world where all people have an equal opportunity to seek, share and generate knowledge. Frontiers provides immediate and permanent online open access to all its publications, but this alone is not enough to realize our grand goals.

Frontiers Journal Series

The Frontiers Journal Series is a multi-tier and interdisciplinary set of open-access, online journals, promising a paradigm shift from the current review, selection and dissemination processes in academic publishing. All Frontiers journals are driven by researchers for researchers; therefore, they constitute a service to the scholarly community. At the same time, the Frontiers Journal Series operates on a revolutionary invention, the tiered publishing system, initially addressing specific communities of scholars, and gradually climbing up to broader public understanding, thus serving the interests of the lay society, too.

Dedication to Quality

Each Frontiers article is a landmark of the highest quality, thanks to genuinely collaborative interactions between authors and review editors, who include some of the world's best academicians. Research must be certified by peers before entering a stream of knowledge that may eventually reach the public - and shape society; therefore, Frontiers only applies the most rigorous and unbiased reviews.
Frontiers revolutionizes research publishing by freely delivering the most outstanding research, evaluated with no bias from both the academic and social point of view.
By applying the most advanced information technologies, Frontiers is catapulting scholarly publishing into a new generation.

What are Frontiers Research Topics?

Frontiers Research Topics are very popular trademarks of the Frontiers Journals Series: they are collections of at least ten articles, all centered on a particular subject. With their unique mix of varied contributions from Original Research to Review Articles, Frontiers Research Topics unify the most influential researchers, the latest key findings and historical advances in a hot research area! Find out more on how to host your own Frontiers Research Topic or contribute to one as an author by contacting the Frontiers Editorial Office: **researchtopics@frontiersin.org**

RADIATION-INDUCED AND OXIDATIVE DNA DAMAGES

Topic Editors:
Antonio Monari, Université de Lorraine, Theory-Simulatio-Modeling Group, France
Elise Dumont, Ecole Normale Supérieure de Lyon, France
Chryssostomos Chatgilialoglu, Institute of Nanoscience and Nanotechnology (INN), NCSR Demokritos, Athens

Interaction of a sensitizer (palmatine) with a B-DNA double strand.
Image by Antonio Monari

DNA stores and passes the genetic information of almost all living organisms. Its molecular structure and their intramolecular interactions are particularly suitable to maximize stability against oxidative stress and UV-light absorption. Yet the protection and repair strategies are still error-prone: DNA lesions are produced, including the most complex and highly mutagenic ones. An important threat to DNA stability comes from photosensitization, i.e. from the dramatic multiplication of radiation-induced defects mediated by the presence of organic or organometallic dyes compared to the direct exposure to UVA radiation. Moreover, the photo-induced production of singlet oxygen generates an extremely high oxidative stress on DNA that, in vivo, normally results in extended cellular apoptosis.

Elucidating the processes leading to DNA damages, from the production of a simple radical entity to deleterious lesions, as well as the opportunities of repair by devoted enzymes, is a cornerstone towards the development of more efficient protection strategies.

Sensitization and selective production of DNA lesions can also be exploited to induce the selective apoptosis of cancer cells upon exposition to radiation or to oxidative stress, for instance in the field of photodynamic therapy.

The importance and relevance of the field is witnessed by the impressive amount of high-level papers dealing with this complex subject, and notably tackling the structural elucidation of DNA and DNA-drug adducts, the mechanisms of formation of DNA lesions (including the precise detection of the final lesion products), as well as the influence of the lesions on the DNA

stability and dynamics and the consequences on the ease of repair. Due to the complexity of the field lying at the frontiers between chemistry, physics and biology, multidisciplinary strategies allying modeling and experience are needed.

This topic aims at giving an extended overview of the current research in the domain, with fundamental contribution from the leading groups in the field of DNA reactivity, structural characterization, photo-chemistry and photo-physics, as well as repair mechanism. It will therefore be a fundamental guide for scientists wanting to address the field of DNA lesion and repair, but also more generally for researchers working in rational drug design or in the development of biomarkers and medical imaging techniques.

Citation: Monari, A., Dumont, E., Chatgilialoglu, C., eds. (2015). Radiation-Induced and Oxidative DNA Damages. Lausanne: Frontiers Media. doi: 10.3389/978-2-88919-660-9

Table of Contents

05 ***Editorial: Radiation-induced and oxidative DNA damages***
Antonio Monari, Elise Dumont and Chryssostomos Chatgilialoglu

07 ***Stress-induced DNA damage biomarkers: applications and limitations***
Zacharenia Nikitaki, Christine E. Hellweg, Alexandros G. Georgakilas and Jean-Luc Ravanat

22 ***Understanding DNA under oxidative stress and sensitization: the role of molecular modeling***
Elise Dumont and Antonio Monari

37 ***An ameliorative protocol for the quantification of purine 5',8-cyclo-2'-deoxynucleosides in oxidized DNA***
Michael A. Terzidis and Chryssostomos Chatgilialoglu

46 ***Radiation-induced formation of purine lesions in single and double stranded DNA: revised quantification***
Michael A. Terzidis, Carla Ferreri and Chryssostomos Chatgilialoglu

53 ***The association constant of 5',8-cyclo-2'-deoxyguanosine with cytidine***
Amedeo Capobianco, Tonino Caruso, Sandra Fusco, Michael A. Terzidis, Annalisa Masi, Chryssostomos Chatgilialoglu and Andrea Peluso

59 ***Mutagenic effects induced by the attack of NO_2 radical to the guanine-cytosine base pair***
José P. Cerón-Carrasco, Alberto Requena, José Zúñiga and Denis Jacquemin

66 ***DNA oxidation profiles of copper phenanthrene chemical nucleases***
Zara Molphy, Creina Slator, Chryssostomos Chatgilialoglu and Andrew Kellett

75 ***Flexibility of short ds-DNA intercalated by a dipyridophenazine ligand***
Fuchao Jia, Stéphane Despax, Jean-Pierre Münch and Pascal Hébraud

82 ***Deciphering the photochemical mechanisms describing the UV-induced processes occurring in solvated guanine monophosphate***
Salvatore F. Altavilla, Javier Segarra-Martí, Artur Nenov, Irene Conti, Ivan Rivalta and Marco Garavelli

frontiers in Chemistry

EDITORIAL
published: 25 August 2015
doi: 10.3389/fchem.2015.00054

Editorial: Radiation-induced and oxidative DNA damages

Antonio Monari[1]*, *Elise Dumont*[2]* and *Chryssostomos Chatgilialoglu*[3]*

[1] Theory-Simulatio-Modeling Group, Centre National de la Recherche Scientifique, Université de Lorraine, Nancy, France, [2] École normale supérieure de Lyon and Centre National de la Recherche Scientifique, Lyon, France, [3] National Center for Scientific Research Demokritos, Athens, Greece

Keywords: DNA lesions, radiation and UV induced, simulation and modeling, spectroscopies, analytical chemistry

The study of DNA lesions and changes, produced by interaction with UV or ionizing radiation and by the effects of oxidative stress, is a multidisciplinary research field in life sciences that has yelded exciting discoveries in the last few decades. The importance of this study is clearly enhanced by its strong societal impact, because of the connections of DNA lesions with carcinogenetic processes, which lead to the disruption or mismatching of the genetic information. As well, the controlled and selective production of lesions is a promising tool for the development of novel antitumoral strategies and drugs. The multidisciplinary character requires a combined effort from simulation and modeling studies, together with high-level experimental and analytical chemistry, spectroscopy, up to biochemical or cellular biology tools. In this Research Topic, we present a collection of articles focusing on DNA bases photoinduced and radiation damages, on the DNA interactions, on potential drug development and on the effect of radicals on DNA constituents.

The fundamental reactions of DNA constituents are taken into account for instance by the investigation of the potential mutagenic effects of NO_2 radical to guanine and cytosine base pairs (Cerón-Carrasco et al., 2015) by high level simulation protocols. An ameliorated protocol has also been developed and validated to achieve a better accuracy in the determination of radiation-induced lesions in purine moieties (Terzidis et al., 2015) embedded in double- and single-strand DNA. The improved quantification of purine 5′,8-cyclonucleosides resulting from the cyclization of C5′ radical on DNA has also been tackled (Terzidis and Chatgilialoglu, 2015). The association constant of lipophilic derivatives of the 5′,8-cyclo-2′-deoxyguanosine with 2′-deoxycytidine has been studied by voltammetry NMR techniques (Capobianco et al., 2015).

DNA sensitization by endogenous molecules has also been covered. The oxidative profile of copper phenanthrene chemical nucleases interacting with DNA has been presented (Molphy et al., 2015) together with a variety of biophysical data. Furthermore, Förster Resonant-Energy-Transfer has been used to prove the flexibility and dynamical behavior of short double-strand DNA sequences intercalated by organometallic compounds (Jia et al., 2015). Connected to spectroscopy a very detailed analysis of the excited state potential energy landscape of solvated guanine monophosphate has been reported with high level *ab initio* techniques, together with an analysis of principal photochemical pathways (Altavilla et al., 2015).

Furthermore, two reviews, one on simulation and modeling of DNA lesions (Dumont and Monari, 2015) and the other on stress-induced DNA biomarkers (Nikitaki et al., 2015), help to clearly define the state of the art of this very active scientific field.

This scientific topic is also closely related to the COST in Chemistry Action CM1201 "Biomimetic Radical Chemistry" and in particular to its Working Group 2 devoted to "Models of DNA Damages and Consequences." The COST Action members have actively participated with most of the contributions derived from the scientific collaborations ongoing in its framework. As such the Research Topic also represents a very nice overview of the effectiveness and added value brought about by the creation of a large multinational

OPEN ACCESS

Edited and reviewed by:
John D. Wade, Florey Institute of Neuroscience and Mental Health, Australia

***Correspondence:**
Antonio Monari, antonio.monari@cbt.uhp-nancy.fr; Elise Dumont, elise.dumont@ens-lyon.fr; Chryssostomos Chatgilialoglu, c.chatgilialoglu@inn.demokritos.gr

Specialty section:
This article was submitted to Chemical Biology, a section of the journal Frontiers in Chemistry

Received: *29 July 2015*
Accepted: *10 August 2015*
Published: *25 August 2015*

Citation:
Monari A, Dumont E and Chatgilialoglu C (2015) Editorial: Radiation-induced and oxidative DNA damages. Front. Chem. 3:54. doi: 10.3389/fchem.2015.00054

scientific network. Furthermore, the financial support of the COST Action CM1201 has allowed the open source publication of exciting scientific contributions from its members.

We believe that the "Radiation Induced and Oxidative DNA Damage" Research Topic nicely illustrates most of the complex and fascinating challenges that scientists working on DNA damages should tackle. At the same time, it highlights the scientific maturity of this field, foreseeing even more exciting perspectives that will undoubtedly blossom in the forthcoming years.

Acknowledgments

Support from COST in Chemistry CM1201 Biomimetic Radical Chemistry is gratefully acknowledged.

References

Altavilla, S. F., Segarra-Martí, J., Nenov, A., Conti, I., Rivalta, I., and Garavelli, M. (2015). Deciphering the photochemical mechanisms describing the UV-induced processes occurring in solvated guanine monophosphate. *Front. Chem.* 3:29. doi: 10.3389/fchem.2015.00029

Capobianco, A., Caruso, T., Fusco, S., Terzidis, M. A., Masi, A., Chatgilialoglu, C., et al. (2015). The association constant of 5′,8-cyclo-2′-deoxyguanosine with cytidine. *Front. Chem.* 3:22. doi: 10.3389/fchem.2015.00022

Cerón-Carrasco, J. P., Requena, A., Zúñiga, J., and Jacquemin, D. (2015). Mutagenic effects induced by the attack of NO_2 radical to the guanine-cytosine base pair. *Front. Chem.* 3:13. doi: 10.3389/fchem.2015.00013

Dumont, E., and Monari, A. (2015). Understanding DNA under oxidative stress and sensitization: the role of molecular modeling. *Front. Chem.* 3:43. doi: 10.3389/fchem.2015.00043

Jia, F., Despax, S., Münch, J.-P., and Hébraud, P. (2015). Flexibility of short ds-DNA intercalated by a dipyridophenazine ligand. *Front. Chem.* 3:25. doi: 10.3389/fchem.2015.00025

Molphy, Z., Slator, C., Chatgilialoglu, C., and Kellett, A. (2015). DNA oxidation profiles of copper phenanthrene chemical nucleases. *Front. Chem.* 3:28. doi: 10.3389/fchem.2015.00028

Nikitaki, Z., Hellweg, C. E., Georkakilas, A. G., and Ravanat, J.-L. (2015). Stress-induced DNA damage biomarkers: applications and limitations. *Front. Chem.* 3:35. doi: 10.3389/fchem.2015.00035

Terzidis, M. A., Chatgilialoglu, C. (2015). An ameliorative protocol for the quantification of purine 5′,8-cyclo-2′-deoxynucleosides in oxidized DNA. *Front. Chem.* 3:47. doi: 10.3389/fchem.2015.00047

Terzidis, M. A., Ferreri, C., and Chatgilialoglu, C. (2015). Radiation-induced formation of purine lesions in single and double stranded DNA: revised quantification. *Front. Chem.* 3:18. doi: 10.3389/fchem.2015.00018

Conflict of Interest Statement: The authors declare that the research was conducted in the absence of any commercial or financial relationships that could be construed as a potential conflict of interest.

Copyright © 2015 Monari, Dumont and Chatgilialoglu. This is an open-access article distributed under the terms of the Creative Commons Attribution License (CC BY). The use, distribution or reproduction in other forums is permitted, provided the original author(s) or licensor are credited and that the original publication in this journal is cited, in accordance with accepted academic practice. No use, distribution or reproduction is permitted which does not comply with these terms.

frontiers in Chemistry

REVIEW
published: 02 June 2015
doi: 10.3389/fchem.2015.00035

Stress-induced DNA damage biomarkers: applications and limitations

Zacharenia Nikitaki[1], *Christine E. Hellweg*[2], *Alexandros G. Georgakilas*[1] and *Jean-Luc Ravanat*[3,4]*

[1] DNA Damage and Repair Laboratory, Physics Department, School of Applied Mathematical and Physical Sciences, National Technical University of Athens, Athens, Greece, [2] Radiation Biology Department, German Aerospace Center (DLR), Institute of Aerospace Medicine, Köln, Germany, [3] Laboratoire des Lésions des Acides Nucléiques, Institut des Nanosciences et Cryogénie, Service de Chimie Inorganique et Biologique, Université Grenoble Alpes, Grenoble, France, [4] CEA, Institut des Nanosciences et Cryogénie, Service de Chimie Inorganique et Biologique, Grenoble, France

A variety of environmental stresses like chemicals, UV and ionizing radiation and organism's endogenous processes such as replication stress and metabolism can lead to the generation of reactive oxygen and nitrogen species (ROS/RNS) that can attack cellular vital components like DNA, proteins and lipid membranes. Among them, much attention has been focused on DNA since DNA damage plays a role in several biological disorders and aging processes. Thus, DNA damage can be used as a biomarker in a reliable and accurate way to quantify for example radiation exposure and can indicate its possible long term effects and cancer risk. Based on the type of DNA lesions detected one can hypothesize on the most probable mechanisms involved in the formation of these lesions for example in the case of UV and ionizing radiation (e.g., X- or α-, γ-rays, energetic ions, neutrons). In this review we describe the most accepted chemical pathways for DNA damage induction and the different types of DNA lesions, i.e., single, complex DNA lesions etc. that can be used as DNA damage biomarkers. We critically compare DNA damage detection methods and their limitations. In addition, we suggest the use of DNA repair gene products as biomarkes for identification of different types of stresses i.e., radiation, oxidative, or replication stress, based on bioinformatic approaches and meta-analysis of literature data.

Keywords: DNA damage, oxidative stress, biomarkers, ionizing radiation, UV radiation, clustered DNA lesions

OPEN ACCESS

Edited by:
Antonio Monari,
Université de Lorraine, France

Reviewed by:
Richard Wagner,
Université de Sherbrooke, Canada
Peter O'Neill,
University of Oxford, UK

***Correspondence:**
Jean-Luc Ravanat,
Laboratory "Lésions des Acides Nucléiques," Institut des Nanosciences et Cryogénie, Service de Chimie Inorganique et Biologique, CEA-Grenoble, 17 rue des Martyrs, 38054 Grenoble, France
jravanat@cea.fr

Specialty section:
This article was submitted to Chemical Biology, a section of the journal Frontiers in Chemistry

Received: *23 January 2015*
Accepted: *07 May 2015*
Published: *02 June 2015*

Citation:
Nikitaki Z, Hellweg CE, Georgakilas AG and Ravanat J-L (2015) Stress-induced DNA damage biomarkers: applications and limitations. Front. Chem. 3:35. doi: 10.3389/fchem.2015.00035

Introduction

DNA Damage Formation and Consequences also Including DNA Repair

In all cells and tissues a significant level of DNA damage is formed on a daily basis from exposure to various intracellular and extracellular agents. Endogenous sources of damage targeting nuclear and mitochondrial DNA are but not limited to replication stress and oxidative stress i.e., free radicals resulting from metabolism as by-products and at the level of the organism from various mechanisms like inflammatory responses such as reactive oxygen species (ROS) released from macrophages (Kryston et al., 2011). In addition, the so-called oncogene-induced ROS can fuel high proliferation, replication stress and DNA damage response (DDR) activation (Ogrunc et al., 2014). Replication stress manifested as stalled replication forks and possible collapse results in

DNA double strand breaks (DSBs) which must be repaired immediately usually by the homologous recombination (HR) pathway (Halazonetis et al., 2008). This continuous challenging process may lead to genomic instability and cancer, especially if it is combined with exposure for example to natural radiation and low doses of ionizing radiation from medical exams (X-rays). This "naturally" occurring combination of DNA damage (DSBs and oxidized bases) may be considered as the most common form of complex DNA damage, triggering different repair mechanisms in the cell, such as DSB repair (HR and non-homologous end joining-NHEJ), base excision repair (BER), mismatch repair (MMR), and possibly nucleotide excision repair (NER) especially for UV-induced DNA lesions (Aziz et al., 2012). In order to complete the picture one should add the fact that specific regions of the human genome are prone to breaks i.e., the fragile sites are highly preferable targets for DNA breakage due to replication or oxidative stress (Tsantoulis et al., 2008; Georgakilas et al., 2014). These problematic regions of possible DNA breaks do not relate necessarily with the genome sites where radiation interacts creating may be an accumulative phenomenon of genome "damage burden." Last but not least, at the organism level, these phenomena maybe augmented by the initiation of systemic effects inducing DNA damage in distant sites of the human body as a result of innate or adaptive immune response (Sprung et al., 2015).

In this review we summarize the current knowledge of DNA damage induction mechanisms and the primary methodology utilized for detection and quantification of DNA lesions generated by a variety of stresses expected to induce the majority of DNA lesions in the cell. Although these classifications are introduced for the first time in this work in general there are considered as "classical" examples of DNA damage sources (Aziz et al., 2012). Since we consider the critical use of DNA damage-based biomarkers not only for biological dosimetry of radiation exposure but also for prediction of radiation effects and prognosis of cancer radiotherapy, we performed a meta-analysis of literature available data, to identify putative DDR genes implicated in the cellular reaction to three primary types of DNA damage inducing stresses: ionizing radiation, oxidative, and replication stress. Our results suggest some genes which are possibly "unique" for each type of stress and may be candidates for DNA damage biomarkers i.e., markers indicating that DNA damage has occurred and most possibly DDR initiation. The critical parameter here is that these markers are assigned in each case to three different types of "stress": (1) ionizing radiation, (2) oxidative stress, and (3) replication stress.

Formation of DNA Damages: Mechanistic Aspects

Non-Ionizing Radiation: UV Induced DNA Damage

We initiate our discussion on possible stress DNA damage markers with UV radiation since some of the lesions (as discussed below) induced by this type of radiation are highly specific and characteristic for UV radiation. DNA absorbs UV light mostly in the UVC and UVB ranges and only a little in the UVA wavelengths. However, the UVC light is filtered by the ozone layer of the Earth's atmosphere and does not reach the surface of the Earth. Thus, UVB and UVA represent a major risk factor for the development of skin cancers. Following photon absorption, DNA bases are excited and two major classes of damages can be produced at bi-pyrimidine sequences. Cyclobutane bi-pyrimidine dimers (CPD) are generated through a cycloaddition of the two C5–C6 double bounds of two adjacent pyrimidine bases located on the same strand (**Figure 1**). The four possible dimeric products, i.e., TT, TC, CT, and CC are produced in cells and skin exposed to UV light (Mouret et al., 2006). The second class of dimeric lesions, identified as a pyrimidine (6-4) pyrimidone photoproducts (6-4PP), are produced by a $[2+2]$ cycloaddition between the C5–C6 double bond of the 5′-end base and the C4 carbonyl group of a 3′-end pyrimidine. These above mentioned lesions are specifically produced by UV light and thus could serve as a signature for UV exposure. It has been also shown that UVA can induce the formation of pyrimidine dimers most probably through the excitation of an endogenous photosensitizer that could transfer its energy to DNA bases, generating exclusively CPDs (Mouret et al., 2006). In addition, photoactivated endogenous sensitizers may also induce oxidation of DNA, either directly through a one electron oxidation reaction (Type I) or through the transient formation of singlet oxygen (Type II) (Cadet et al., 2015). These two latter mechanisms are able to produce oxidized DNA bases and mostly 8-oxo-7,8-dihydro-2′-deoxyguanosine (8-oxodGuo) (*vide infra*). This lesion has been extensively used as a biomarker of DNA oxidation, but since it can be produced by several mechanisms, it cannot be indicative of a specific stress. In contrast, pyrimidine dimers (CPD and 6-4PP) are only produced by UV light (Cadet et al., 2000).

Ionizing Radiation and Oxidative Stress

In cells, following exposure to ionizing radiation, DNA lesions can be produced directly or indirectly. The direct effect induces a one-electron oxidation of DNA, the indirect effect generates ROS through water radiolysis that can subsequently damage DNA. The relative contribution of both effects is still a matter of debates and will be discussed below.

One electron induced DNA oxidation (direct effect) is known to produce mostly guanine damages since this base has the lowest

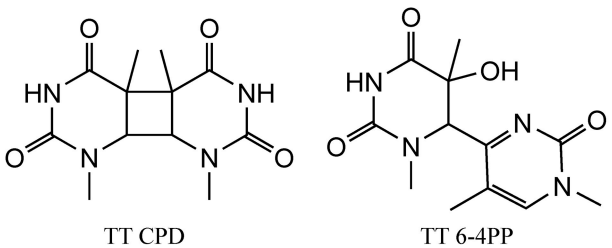

FIGURE 1 | Structure of the main UV induced pyrimidine dimers, including CPD (left) and 6-4PP (right) dimer generated at TT sequences.

ionization potential among the DNA constituents. Thus, even if oxidation occurs on another DNA base, a fast electron transfer takes place from guanine to the initially produced radical cation that is thus "chemically" repaired (Cadet et al., 2004). Such transfer reaction can take place *in vitro* over large ranges of DNA bases (Hall et al., 1996). The generated guanine radical cation can then decompose through deprotonation or hydration, the second reaction being at the origin of the formation of the well-known 8-oxodGuo.

The indirect effect produces ROS through water radiolysis, among them the hydroxyl radical $HO^{\bullet}$ is the most reactive one, it reacts at a diffusion controlled rate with any biomolecule, including DNA. Reaction of $HO^{\bullet}$ with DNA involves either addition onto aromatic moieties of DNA bases, or through hydrogen abstraction. It has been estimated that about 70% reacts with DNA bases, and 30% with deoxyribose moieties, the latter reaction is giving rise mostly to single strand breaks (SSB). Reaction of $HO^{\bullet}$ with DNA bases involves mostly addition onto aromatic rings giving rise to about 70 different decomposition products. Information on the identified products can be obtained from recent review articles on that topic (Cadet et al., 2012a; Ravanat et al., 2012). It should be highlighted that most of the radiation-induced DNA lesions have been initially characterized using isolated nucleosides or sometimes short oligonucleotides. Thereafter efforts have been made to develop analytical methods (*vide infra*) to search for the formation of these identified modifications first in irradiated DNA following DNA hydrolysis, and when detection sensitivity was high enough, directly in cells exposed to radiation, subsequently to DNA extraction.

More recent efforts have been made to study the decomposition reaction of initially produced radicals, directly in dsDNA. A general observation that could be made from the recent data is that initially produced radicals could efficiently react with surrounding DNA constituents to produce complex lesions, including so-called tandem damage involving two adjacent DNA modifications. Two examples of this kind of reaction will be described below in detail; additional information can be obtained from recent review articles (Cadet et al., 2012b; Ravanat et al., 2014). The first one concerns the formation of tandem lesions containing 8-oxodGuo and also 2′-deoxy-7,8-dihydro-2′-deoxyadenosine (8-oxodAdo). These two lesions have been detected in cells exposed to ionizing radiation and one striking observation was that the yield of 8-oxodGuo formation was found to be about one order of magnitude higher than that of 8-oxodAdo (Cadet et al., 2004). It was initially proposed that these two modifications were produced by addition of $HO^{\bullet}$ (indirect effect) onto the C8 atom of guanine and adenine. However, since $HO^{\bullet}$ is very reactive and reacts with a similar efficacy with the two purine bases, such a mechanism, that was supposed to be the predominant one, could not explain the difference in the yield of formation of the two modified purine lesions. More recently, it has been shown *in vitro* that other reactions can generate 8-oxodGuo and 8-oxodAdo. In fact, it has been demonstrated (Bergeron et al., 2010) that the addition of the $HO^{\bullet}$ radical at C8 of guanine and adenine is a minor process (only 5%). Moreover, 50% of the produced 8-oxodGuo has been attributed to the addition of a pyrimidine peroxyl radical onto C8 of an adjacent guanine base, preferably when the purine is located at the 5′ position of the pyrimidine peroxyl radical. Such addition produces an endoperoxide that, following decomposition, gives rise to 8-oxodGuo (or 8-oxodAdo) and an adjacent pyrimidine modification, including formylamine (Bourdat et al., 2000). A third mechanism, that involves an electron transfer reaction, probably from guanine to the initially produced peroxyl radical, explains why formation of 8-oxodGuo is relatively higher than that of 8-oxodAdo. Indeed, as explained previously, such an electron transfer produces mostly guanine damages. Interestingly, in the absence of oxygen, a direct reaction of the pyrimidine radical with a purine base could also occur to generate intra-strand crosslinks (Bellon et al., 2002). These reactions detailed in **Figure 2**, have been observed *in vitro* using dsDNA, and up to now there is no experimental evidence that implication of the hydroperoxyl radicals is involved in the formation of tandem lesions in cells. However, the fact that at the cellular level the yield of 8-oxodAdo formation is one order of magnitude lower to that of 8-oxodGuo strongly suggests that formation of tandem lesions in cellular DNA following initial formation of a single oxidation event is highly probable. Additional evidence comes from the fact that an unexpected high frequency of spontaneous proximal multiple mutations has been reported in cell and animal models (Hill et al., 2004). Formation of intra-strand crosslinks (produced in the absence of oxygen) has been observed in cells (Hong et al., 2007). It should be also highlighted that the mechanisms of formation of such tandem lesions have been confirmed by theoretical studies (Labet et al., 2008; Dupont et al., 2013).

The second example of complex DNA lesions produced by a single oxidation event concerns the formation of damages arising from initial 2-deoxyribose oxidation. Such reactions were initially supposed to give rise to SSB when hydrogen abstraction occur on C5′, C4′, or C3′ of 2-deoxyribose. Hydrogen abstraction occurring at C1′ generates an abasic site. These two types of lesions are known to be very rapidly and efficiently repaired in cells. However, it was also reported that reactive aldehydes could be produced following 2-deoxyribose oxidation (Pogozelski and Tullius, 1998). Interestingly, DNA bases are known to react very efficiently with conjugated aldehydes. Using an innovative approach to search for new radiation-induced DNA lesions directly in dsDNA exposed to ionizing radiation (Regulus et al., 2004), a cytosine adduct has been identified and its formation was explained by the initial formation of a reactive aldehyde, as schematized in **Figure 3**. The first single oxidation event involves hydrogen atom abstraction which occurs at the C4′ position (Regulus et al., 2007). Reaction with oxygen produces a conjugated aldehyde that is then able to react with a surrounding cytosine base mostly located onto the complementary strand (Sczepanski et al., 2008). Thus, the produced lesion implies a strand break and an inter-strand crosslink. This lesion has been also measured in cells, and its yield of formation following exposure to ionizing radiation is within the same range than the formation of DSB. In addition, kinetics of repair of such damage was found to be significantly lower (half-life about 10 h) compared to single lesions that could be totally repaired within a few hours. Other examples of complex DNA lesions produced

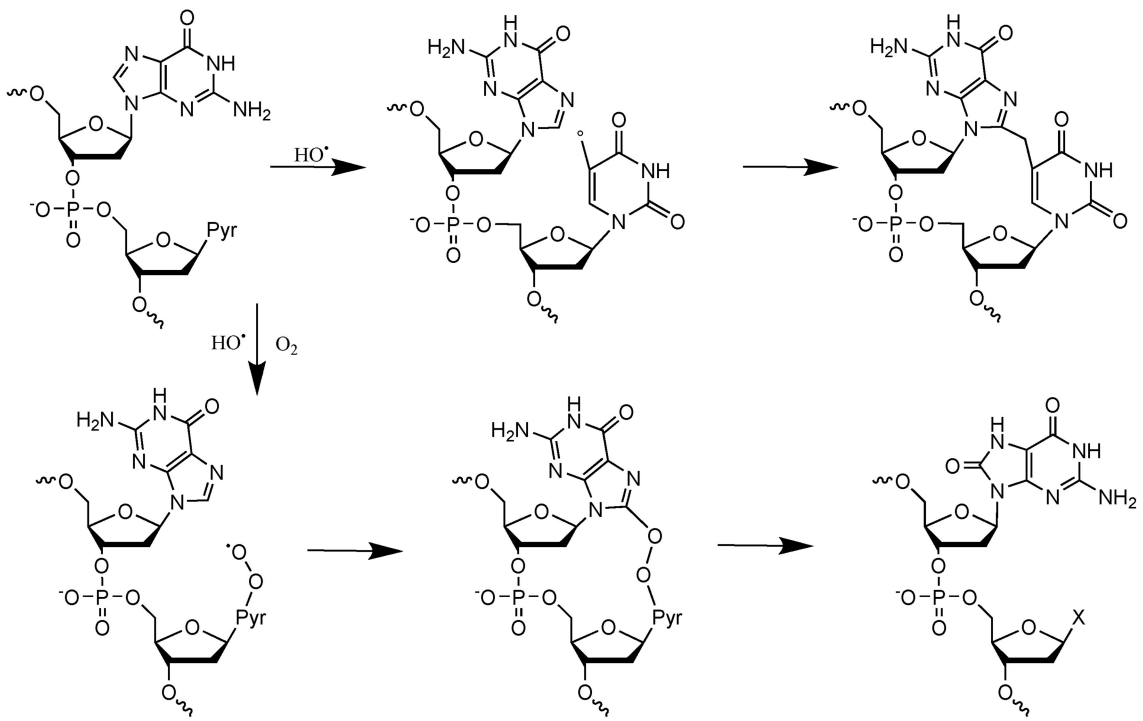

FIGURE 2 | Mechanisms of formation of tandem DNA lesions induced by HO•. In the absence of oxygen intra-strand crosslinks are produced, whereas in the presence of oxygen tandem lesions containing 8-oxodGuo adjacent to a pyrimidine modification (indicated by an X) are generated.

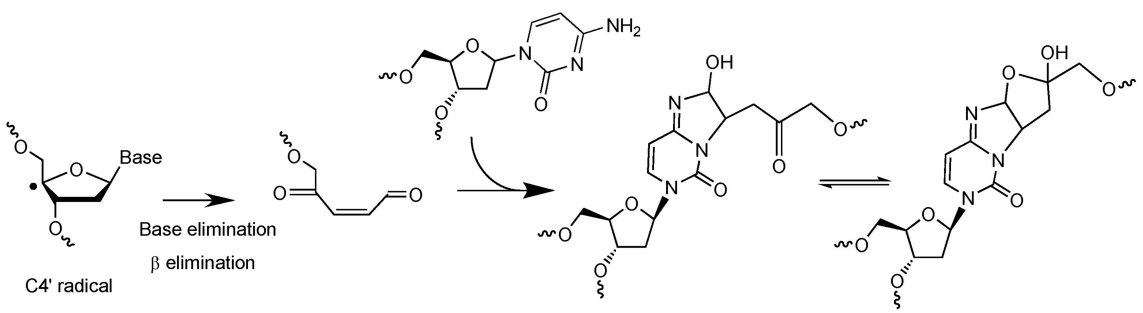

FIGURE 3 | Mechanism of formation of a complex lesion induced by C4′ hydrogen abstraction. Following formation of the C4′ radical the produced aldehyde is able to react with a cytosine base located onto the complementary strand to generate an inter-strand crosslink.

by initial 2-deoxyribose oxidation have been reported (Dedon, 2008).

These two above detailed examples of chemical reactions illustrate the complexity of the undergoing reactions taking place when radicals are produced in dsDNA. Since the initial event is the formation of a single radical, these lesions could be produced both by ionizing radiation and also by endogenous oxidative stress. It is important to distinguish these modifications arising from the initial formation of a single oxidation event that we call "tandem lesions" to clustered lesions or so-called multiply damaged sites (MDS) that arose from multiple ionization processes due to the spatial distribution of energy depositions events following exposure to ionizing radiation. However, it is interesting to notice that at the molecular level, up to now, no known specific radiation-induced lesions have been identified, and all identified lesions produced by ionizing radiation could also be produced by endogenous oxidative stress. The main difference is the higher complexity of DNA damage in the case of ionizing radiation as supported by experimental (as reviewed in Hada and Georgakilas, 2008; Georgakilas et al., 2013) and theoretical studies (Nikjoo et al., 2001). This also explains why it is a challenging task to measure radiation-induced DNA lesions, since these lesions are already present in absence of radiation, and their yield of formation per unit dose ∼1 lesion per 10 million normal bases and per Gy is relatively low. Thus, the harmful effects of ionizing radiation could not be attributed primarily

to the produced single lesions. In fact, more than the chemical nature of the modification, the localization of their formation in clusters could explain the genotoxicity of ionizing radiation (**Figure 4**). Interestingly, it has been shown that increasing the linear energy transfer (LET) of the particle (Prise et al., 1994) increases the lethality of the irradiated cells due to the high repair resistance of clustered DNA damages (Eccles et al., 2011). Paradoxically, it has been determined that the absolute number of modifications produced per unit dose (Gy), is lower in cells exposed to higher LET particles (such as heavy ions) compared to cells irradiated with gamma or X rays (Pouget et al., 2002). From these observations it could be concluded that the toxicity of ionizing radiation compared to endogenous oxidative stress, is due to the presence of so-called clustered DNA lesions, or MDS (Kryston et al., 2011). In other words, in cells endogenous oxidative stress produces randomly distributed oxidative lesions that could be repaired efficiently by the cell machinery. However, following exposure to radiation, formation of the lesions is localized around the particle track.

When the LET of the particle increases, clusters contain an increasing number of modifications (Tsao et al., 2007; Pachnerova Brabcova et al., 2014). We exemplify this phenomenon in **Figure 4**. These clustered lesions are difficult to be repair and thus more harmful for the cell. DSB are one of the best examples of these clustered lesions. Their formation through endogenous oxidative stress is very rare since this requires simultaneous oxidation occurring onto the two complementary strands in close vicinity (less than one or two helix turn). With ionizing radiation, the probability of two events taking place locally on the two strands, increases when LET increases. At the chemical level, a damage induced by high LET radiation, will resemble at a mixture of the above 70 different identified DNA lesions plus a SSB (Stewart et al., 2011; Georgakilas et al., 2013). This illustrates the complexity at the molecular level of the lesions that could be produced in the DNA of cells exposed to ionizing radiation. Only little information is available regarding the formation of radiation-induced DNA-protein crosslinks. At the molecular level, only a few examples of reactions involving amino acids and DNA bases have been reported. Formation of guanine-lysine adducts generated through a one-electron oxidation reaction following nucleophilic addition of ε-amino group of lysine onto C8 of guanine is one of the possible mechanisms (Perrier et al., 2006). Further work has to be done to better estimate the importance of such damages in cells (Jaruga and Dizdaroglu, 2008).

Methods for Measuring DNA Lesions

Measuring DNA damage in cells is a challenging analytical problem since the level of damages to be measured is relatively

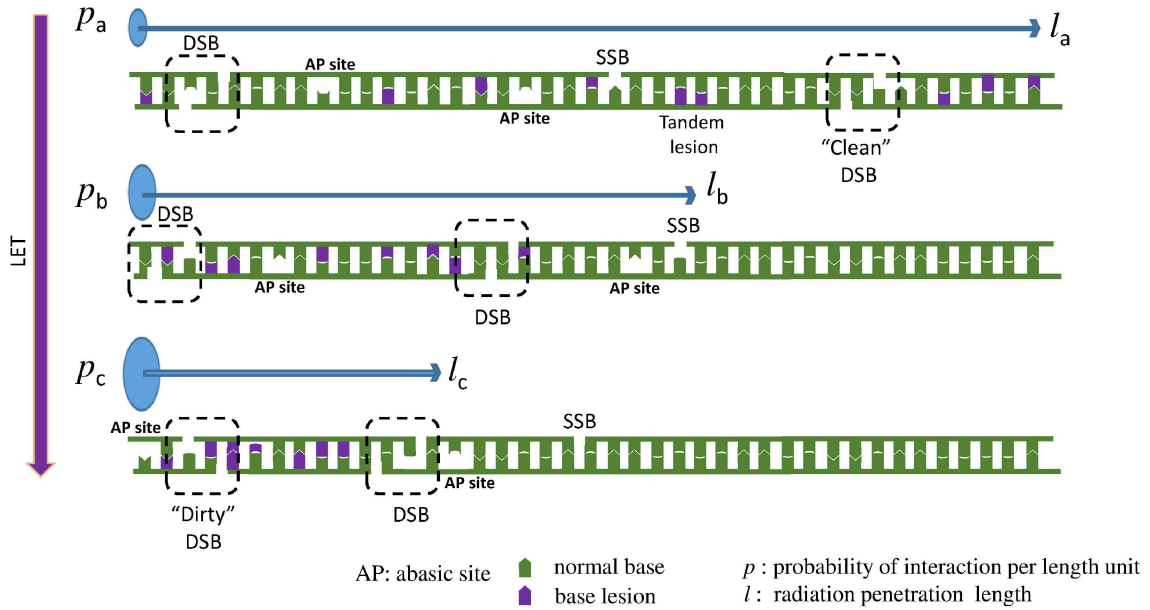

FIGURE 4 | When LET increases the DNA lesions are denser (clustered). Here we present a one dimensional example: Three different particles with the same energy, but with different LET interact with a DNA molecule. Assuming that $LET_a < LET_b < LET_c$, then $p_a < p_b < p_c$, where $p = P/l$ is the interaction probability per length unit. Thereafter $l_a > l_b > l_c$, where l is the radiation penetration length, the distance that the particle travels until it loses all of its energy inducing different types of DNA lesions, like double strand break (DSB), single strand break (SSB), abasic sites (AP) and oxidized bases. Since all the three particles (low to high LET) carry the same energy and they are able to cause about the same number of lesions and they travel for different distances then the particle with the higher LET will cause more dense lesions, because the same number of lesions (here 2 DSBs, 1 SSB, 8 base lesions, and 2 AP sites) will occur in a smaller distance. This increased complexity is considered a major challenge for the cellular DNA repair systems. To illustrate that increase in complexity, an example of a "clean" DSB containing only two SSB is illustrated for low LET radiation, compared to a "dirty" DSB produced by high LET radiation involving two SSB and base damages. In addition, an example of tandem lesion produced by a single oxidation event is illustrated.

low and represents generally less than one modification per million normal bases. In addition, such a measurement has to be performed with a limited amount of biological material. Two different strategies have been used for this purpose.

Direct methods are based on analytical chemistry, requiring first extraction and then digestion of DNA, followed by the measurement of specific DNA lesions (at the nucleotide, nucleoside or base level) using a more or less specific detector coupled to a chromatographic separation.

Indirect biochemical methods have been also developed. These assays measure generally strand breaks. By coupling to DNA repair enzymes that convert lesions into strand breaks, or by using specific antibodies raised against DNA lesions, several modifications can be quantified. More recently, antibodies were raised against protein or protein modifications belonging to the DDR mechanisms allowing detection of "repair" foci of active repair that could be directly correlated to DNA damages. Finally, biological consequences of the generated lesions, such as micronuclei or chomosomal aberrations could be also used to monitor damages to DNA.

Direct Methods

The principle of the direct measurement of DNA lesions involves first extraction of genomic DNA from the cells, followed by the complete hydrolysis to monomeric units, being either nucleotides, nucleosides or bases (Ravanat, 2012). Then analytical methods are used to separate the hydrolyzed products and a specific detection method is used to detect and quantify the lesions.

High performance liquid chromatography coupled to electrochemical detection (HPLC-ECD) was one of the first methods developed in the early eighties for the detection of 8-oxodGuo (Floyd et al., 1984). As this lesion has an ionization potential lower than that of normal bases, it can be detected selectively and quantitatively. This approach has been also extended to a few other DNA modifications including 5-hydroxy-2′-deoxycytidine (5-HO-dCyd) and 8-oxodAdo. The system is also usually equipped with a less sensitive UV detector that monitors normal bases, and thus results could directly be expressed as the number of modification per million normal nucleosides, in enzymatically hydrolyzed DNA samples.

During the same period of time, a method based on gas chromatography coupled to mass spectrometry (GC-MS) has been also developed (Dizdaroglu, 1984). Such a method has been applied to acid hydrolyzed DNA samples that release free bases. This method requires also an additional derivatization step since DNA bases are not volatile enough to be separated by GC. The derivatized products could then be detected by mass spectrometry in the so-called selected ion monitoring (SIM) mode. This approach is thus more versatile than the HPLC-ECD method that is limited to the detection of only a few DNA lesions. However, it has been rapidly highlighted that the two methods reported significant different background levels of lesions measured in eukaryotic cells in the absence of any stress (Halliwell and Dizdaroglu, 1992). At the end of the last century, it was clearly established that the difference was attributed to the derivatization step of the GC-MS assay that, by oxidizing DNA bases (Ravanat et al., 1995), artefactually creates DNA lesions and thus provides overestimated levels of damages (Cadet et al., 1997).

Nowadays, HPLC coupled to tandem mass spectrometry (through electrospray ionization, HPLC-MS/MS) is the method of choice for measuring low levels of DNA damages (Ravanat, 2012). This method, due to a soft ionization technique, is very sensitive, at least in the so-called multiple reaction monitoring (MRM) mode that requires tandem mass spectrometry. Isotopically labeled internal standards could be used to increase the accuracy of the quantitation. If an analytical tool is currently available, it should be kept in mind that artefactual formation of DNA lesions during the work-up, including DNA extraction, is always possible. Thus, through a European collaborative project named "European Standard Committee on Oxidative DNA Damage" (ESCODD) (ESCODD, 2002, 2003) efforts have been made to minimize spurious oxidation that could occur during the work-up. Optimized protocols are now available (Ravanat et al., 2002).

Using HPLC-ECD and HPLC-MS/MS (and appropriated protocols for DNA extraction and hydrolysis) the amount of a several DNA lesions has been measured in cells exposed to increasing doses of gamma irradiation (Pouget et al., 1999, 2002). Thymidine glycols were found to be the major lesions and their yield of formation, around 0.1 modification per 10^6 bases and per Gy, was found to be 4 times higher than that of 8-oxodGuo, whereas a recent work reported similar levels for the two lesions (Madugundu et al., 2014). Interestingly, the yield of formation of the formamido-pyrimidine derivative of guanine was higher (about 2 times) to that of 8-oxodGuo suggesting that the DNA is in a reducing cellular environment since both lesions arose from the same intermediate and formation of 8-oxodGuo requires oxidizing conditions. It should be noticed that the complex lesion involving formation of cytosine adducts was also detected in cells by HPLC-MS/MS and its level of formation is about two orders of magnitude lower than that of 8-oxodGuo (Regulus et al., 2007), and thus almost similar to that of DSB estimated to be about 40 DSB per cell and per Gy. More recently 2′,3′-dideoxyribonucleosides were also measured in cells exposed to ionizing radiation (Madugundu et al., 2012). Their yield of formation is relatively low, similar to that of DSB, but they are supposed to be specifically generated by secondary electrons with an average kinetic energy of 10 eV and they can react with DNA components by a mechanism involving dissociative electron attachment (Sanche, 2009; Park et al., 2013; Kouass Sahbani et al., 2014). Further work has to be done to clearly establish the role of these low energy electrons to induce strand breaks and base damage at the cellular level.

Indirect Methods

Indirect or biochemical approaches have been also used to detect DNA lesions in cells. First attempts have been made to use antibodies raised against DNA lesions. Thus, specific antibodies raised against pyrimidine dimers were developed and were found to be specific enough to detect formation of these UV-induced lesions (Perdiz et al., 2000). For oxidative DNA lesions, and mostly 8-oxodGuo, the developed antibodies were found to be

not specific enough and thus cross-reaction with guanine base was found to give overestimated results (Breton et al., 2003).

Other indirect methods are based on the detection of DNA strand breaks. Among them, the alkaline elution (AE) or the more recently developed comet assay are well suited. These methods enable the measurement of strand breaks (mostly single strand breaks: SSB) based on the fact that an alkaline elution of DNA through a filter is faster if it contains breaks (AE) (Pflaum and Epe, 2000), or that electrophoresis of DNA embedded in an agarose gel is increased in the presence of a SSB (single cell gel electrophoresis—SCGE or "Comet" assay) (Boysen et al., 2010). To increase the versatility of the assay, the approach could be combined with DNA repair enzymes like human (OGG1, NTH1) or bacterial glycosylases (Fpg, EndoIII) that excise oxidative DNA lesions and thus induce additional breaks. Thus, prior to electrophoresis (or elution), DNA can be treated by these glycosylases and thus the additional strand breaks are interpreted as the base modifications that have been recognized by the DNA repair enzymes. By running the electrophoresis under alkaline (denaturing) conditions, total lesions are measured, while under neutral (non-denaturing) conditions, bistranded DNA lesions, i.e., two lesions located on opposing strands, are quantified. An adaptation of this approach for the detection of bistranded clustered DNA lesions is presented in the next section (Georgakilas et al., 2010; Georgakilas, 2011). Coming back to the idea of using DNA repair enzymes as damage probes, for example, it is accepted that Fpg-sensitive sites are mostly due to the presence of oxidized purine bases, including mostly 8-oxodGuo. Using such an approach the relative proportion of direct strand breaks (including also alkali-labile sites), oxidized purine and pyrimidine bases has been determined in cells exposed to ionizing radiation (Cadet et al., 1999). Formation of these lesions was found to increase linearly with the radiation dose (0–20 Gy). The amount of Fpg-sensitive sites was found to be similar to that of EndoIII sensitive sites, suggesting that an almost similar amount of oxidized pyrimidine and purine bases is produced. In addition, the number of direct strand breaks (including also alkali-labile sites) was found to be similar to the number of modified bases. As already mentioned, increasing the LET of the particle was found to lower the yield of formation of the individual lesions (Pouget et al., 2002). For comparison it has been demonstrated that singlet oxygen only produced 8-oxodGuo in cellular DNA (Ravanat et al., 2000), in the absence of significant formation of strand breaks (Ravanat et al., 2004).

Using the specific measurement of several DNA lesions, attempts have been made to determine the relative importance of the direct vs. indirect effect (Douki et al., 2006). This remains to determine the relative proportion of lesions produced by a one-electron oxidation mechanism, compared to lesions produced by $HO^{\bullet}$. As mentioned above, one-electron oxidation of DNA produces mostly 8-oxodGuo, and this has been demonstrated experimentally using a two photons ionization system (high intensity 266 nm laser pulses) (Douki et al., 2004). $HO^{\bullet}$ produces several lesions, including also 8-oxodGuo. Thus, one would expect that increasing the LET of the radiation, that is supposed to increase the proportion of the direct effect, would also increase the relative formation of 8-oxodGuo. However, this was not observed experimentally, strongly suggesting that the direct effect plays a minor role in the formation of the radiation-induced DNA lesions. Additional experiments are required, using lesions specifically produced by an one electron oxidation reaction (that is not the case for 8-oxodGuo that could be also produced by hydroxyl radicals) to confirm such results. Recently, identified polyamine-guanine adducts (Silerme et al., 2014) could potentially be used for such a purpose.

Others Methods to Measure DNA Damages through their Consequences

Another possible approach to measure cell damage is flow cytometry. Since flow cytometry gives information of cell size and fluorescence intensity, the most explored application in the frame of DNA damage is the detection of aneuploidy or polyploidy. More precisely, speaking for oxidatively-induced DNA damage, the application of flow cytometry is to explore the relative levels of fluorescence between treated and untreated cells, stained with antibodies binding to oxidative stress related proteins. This is a rather old but relatively rapid and reliable technique, while it is quite indirect, since it measures changes in light scattering and fluorescence of nucleoids after cellular irradiation (Milner et al., 1987). Newer approaches target simultaneously DDR proteins (by use of specific antibodies) as a marker of DNA damage like DNA repair proteins γ-H2AX and BER enzymes. For example Ong et al. report the first estimation of OGG1 levels by flow cytometry (Peng et al., 2003). The most explored DDR proteins using flow cytometry are TP53 (Sarasqueta et al., 2013), γ-H2AX (Li et al., 2013), CHEK1, ATR, ATM, TP53BP1, CASP3, and PRKDC.

In addition, an alternative way to measure DNA lesions is to measure the consequences of the produced damages. This concerns for example the measurement of the mutations induced by the damages or chromosomal abnormalities, using for example the micronuclei test or determining chromosomal aberrations. These methods will not be described in the present article.

Measuring Clustered DNA Lesions (DSBs and Non-DSB Lesions)

There is a quite limited number of methodologies for detecting and measuring clustered DNA lesions and especially non-DSB lesions. An alternative approach to measure DNA lesions is to measure the activation of the DDR system that is triggered following formation of lesions. This approach has been extensively used to assess in cells the formation and repair of DSB. Indeed, following formation of a DSB, the ATM protein is able to phosphorylate a histone variant H2AX located nearby the DSB, the purpose of such phosphorylation is to signal to the DNA repair machinery the presence of a damage. Antibodies raised against the phosphorylated form of H2AX, named γ-H2AX, allow to detect foci of the phosphorylated protein that could then been attributed to the presence of a DSB (Rothkamm and Horn, 2009). These foci could be directly observed using a fluorescent microscope and counted to determine the number of DSBs. Measurement at different time points after irradiation allows determination of the repair kinetics of radiation-induced

DSBs. Other proteins (like MRE11, 53BP1 etc.) involved in DNA repair could be used in a similar way to localize and follow over time the presence and processing of radiation-induced DNA lesions. The sensitivity of γ-H2AX immunofluorescence is high, with one focus corresponding to one DSB, and ca. 20–30 foci induced per Gy and per cell. Therefore, all these methodologies can be applied to relative low doses of a few mGy up to 2–3 Gy where usually saturation is reached.

Electrophoretic Approaches

The most reliable quantitative approaches to measure DSB are considered to be the electrophoretic ones like Pulse Field Gel Electrophoresis (PFGE) and its various adaptations using DNA repair enzymes as described above. First experimental evidence for the existence of clustered DNA damage following exposure to low- or high-LET radiation was provided in the 90's as described in these reviews (Hada and Georgakilas, 2008; Georgakilas et al., 2013). One major breakthrough though has been done by Sutherland et al. measuring very accurately different types of clustered DNA lesions using a sensitive adaptation of non-denaturing electrophoresis (Sutherland et al., 2000). Focusing on the bistranded DNA lesions i.e., DSBs and non-DSB oxidative clustered DNA lesions (OCDLs) (Georgakilas, 2011), we rely on the fact that repair enzymes participating in BER like DNA glycosylases and AP endonucleases will function also *in vitro*, i.e., on isolated DNA carrying different patterns of non-DSB lesions. Once they detect the lesion in each strand and in each cluster, they will excise it and cleave the DNA strand 3′-prime to the DNA lesion by their intrinsic lyase activity (DNA glycosylases: human OGG1 or NTH1) or cleave directly 5′-prime to the abasic (AP) site in the case of an AP endonuclease, like human APE1 and create a SSB in each strand, i.e., a DSB in the case of a cluster. These additional indirect DSBs which are formed *in vitro* by the assay are different from the ones induced directly by the irradiation. Therefore, in the same gel both DSBs and OCDLs can be measured using any electrophoresis combined with number average length analysis (NALA) (Sutherland et al., 2003). The sensitivity of the assay is quite satisfactory and while for DSBs there is a limiting dose of 3–5 Gy where one can measure reliably these lesions, for OCDLs the dose can be even below 1 Gy with the use of DNA repair enzymes and appropriate electrophoretic protocols (Sutherland et al., 2002). By the use of the above approaches one can measure a few DSBs and OCDLs per Gy per cell and the suggesting ratio is 1 DSB: 3-5 OCDLs for a wide range of doses (Hada and Georgakilas, 2008; Georgakilas et al., 2013). A significant methodological improvement for measuring DSBs and OCDLs in individual cells has been done by different groups using different adaptations of the Comet assay (Blaisdell and Wallace, 2001; Georgakilas et al., 2010). The adaptations of the Comet assay under alkaline (denaturing) conditions offer a high sensitivity and detection of DNA damage even in the dose range of a few mGy up to 1–2 Gy. The drawback in this case is the fact that this assay is not as quantitative as the PFGE, and thus does not allow quantifying the number of lesions per cell per Gy. Another possible disadvantage of all electrophoretic approaches is that the running conditions and the so-called "electrophoretic regime" have to be carefully chosen, so the small DNA fragments not to be "lost" during the electrophoresis and therefore DSBs and OCDLs to be underestimated (Hada and Georgakilas, 2008). The importance of small DNA fragments usually less than 10 kbp becomes very important in the case of high-LET radiation where the complexity of DNA damage and therefore the proximity of DNA lesions are expected to be high and in general much higher than that of low-LET radiations.

Immunostaining

For the detection of DSBs and OCDLs using other more modern methods, "DNA staining" methods were adapted lately, such as immunohistochemistry (IHC), immunocytochemistry (ICC), immunofluorescence (IF), flow cytometry, ELISA and Western Blotting. These techniques utilize properly developed antibodies in order to detect the presence of a specific protein. A general description of an antibody could be like a Y-shaped protein, that its upper region, the edges of the branches, is devoted to the recognition (recognition area) of the so-called antigen, while the trunk of the Y is the functional region. Immunofluorescence is the branch of immunostaining that uses fluorescence dyes for the visualization of the target molecules in the fluorescence microscope.

Among DNA lesions, the most hazardous is accepted to be the DSB, since this lesion may lead to changes of DNA sequence and thereby into mutations if repaired by the error-prone NHEJ and not through HR pathway. As discussed above, a very informative DSB repair protein is the H2AX, which under a DSB turns into its phosphorylated form (γ-H2AX). γ-H2AX forms foci that can be microscopically observed as fluorescent spots after immunofluorescence staining. The γ-H2AX assay is considered as the gold standard of DSB detection, since a linear dependence of foci number on radiation dose has been verified and there is a "1:1" correlation between foci number and DSBs. Since the importance of γ-H2AX is given, it is a worthwhile task to look for sites of colocalization of γ-H2AX foci with potent foci of other DDR proteins. Both epifluorescence and confocal microscopy can be utilized. Although confocal is by definition more informative, epi-fluorescence could be approved as more time-effective. γ-H2AX foci detection can be carried out through epifluorescence using a high throughput image analysis software, making foci imaging and scoring almost fully automated (like the Metasystems Metafer 4 system).

A recent publication by Asaithamby et al. (2011) utilized the idea of detecting clustered DNA lesions in human cells using the foci colocalization approach for low and high-LET ions. Generally speaking, colocalization is referred to the detection of two different color foci (each one corresponding to a different DDR protein) that coexist in the same cell area. For calculating the level of co-localization, highly specific software like the Imaris (Bitplane) can be used. Usually the criterion for foci colocalization is the coverage of a minimum percentage (e.g., 70%) of focus A area by the focus of protein B and vice versa. This is useful for estimation of co-occurrence between foci of similar size. As an example and using a freely available software (JCount), colocalization of APE1 and γ-H2AX foci in HepG2 cells irradiated with argon ions (Ar-36,

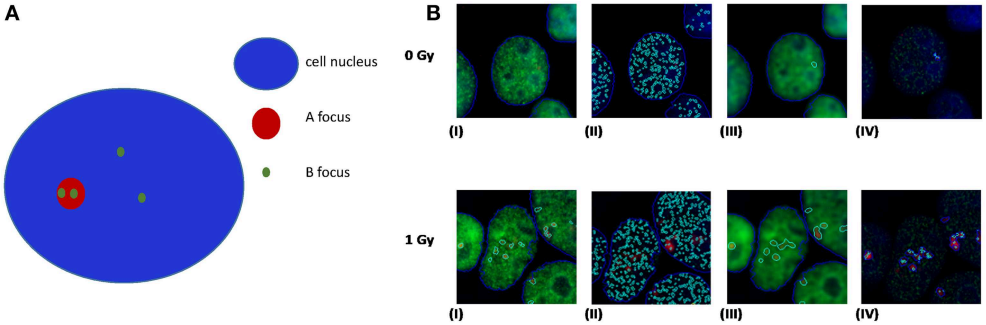

FIGURE 5 | (A) Principles of colocalization between foci of dissimilar size. Colocalization exists if the ratio of B foci number per A nucleus area is greater than the ratio of B foci number per cell nucleus area. **(B)** Realistic example of colocalization between APE1 and γ-H2AX foci in human HepG2 cells irradiated with high-LET Ar heavy ions (Ar-36, LET 269.4 keV/μm). In our case γ-H2AX forms large and bright red foci with clear boundaries, while APE1 gives a punctuated and diffused staining, forming numerous small "foci," even in case of non-irradiated cells. In an attempt of using a freely available software, we have performed the analysis using the Jcount software (courtesy of Dr. Pavel Lobachevsky group, Peter McCallum Institute, Australia). As expected a significant increase in the colocalization of APE1 foci with the DSB focus is observed for all irradiated samples compared to non-irradiated (0 Gy). (I)–(IV): 0 Gy 1 h and 1 Gy 1 h. (I) γ-H2AX foci (per cell); (II) APE1 foci (per cell); (III) complex γ-H2AX foci that would serve as the area for estimation APE1 foci per complex γ-H2AX focus in (IV).

LET 269.4keV/μm) is presented (**Figure 5**). In this case one can see that γ-H2AX forms large and bright foci with clear boundaries, while APE1 gives a punctuate and diffused staining, forming numerous small "foci," even in case of non-irradiated cells.

The origin of this difference is that γ-H2AX appears only after induction of a DSB, while APE1 protein pre-exists in cells, and under a DSB, it is just localized at the site of damage. Moreover, one γ-H2AX focus may extend through 2×10^6 bp, consisting of about 2000 molecules of phosphorylated histone H2AX (Rogakou et al., 1998), while in case of APE1 the task is to identify the migration of some tens of molecules at the site of DSB. There are however some limitations in this approach. It cannot be easily claimed that one is able to detect the fluorescence of individual molecules and thus to count the number of APE1 or other repair protein molecules (corresponding to abasic sites or oxidized bases using for example OGG1), thereby specifying precisely the number of non-DSB lesions that accompany a DSB. Taking into account these limitations, it is a logical consequence that the resulting non-DSB foci number is highly dependent on software specified parameters. In addition and toward the optimization of this methodology, the use of high-LET particles might be helpful since the colocalization can be tested on the particle track and not anywhere in the cell like in the case of X- or γ-rays. Last but not least and according to our experience, the first step for unbiased foci analysis is to capture comparable images. For that the microscope imaging software can be set to integrate for different but specified intervals for each fluorochrome. The proper integration time, i.e., the period of time that the CCD camera collects the emitted fluorescent light, can be defined as the maximum that for the highest signal to observe no color oversaturation. By this way, a reliable evaluation of colocalization between two proteins can be performed like for example APE1 and γ-H2AX.

Future Developments

Utilizing Meta-Analysis Tools in Order to Reveal Potent and Existent DNA Damage Biomarkers

Toward the necessity of developing reliable markers for different types of stresses inducing DNA damage and under consideration of the overlap between the different DDR pathways including DNA repair, we use meta-analysis tools, wishing to suggest possible biomarkers for future applications.

Based exclusively in previously published data, we present in this section suggestions for potent DNA damage biomarkers. Our results are presented in two tables. Considering that the three more hazardous types of DNA damage are due to: (a) exposure to ionizing radiation, (b) occurrence of oxidative stress, and (c) replication stress, in **Table 1**, we suggest that the products of those DDR and repair genes could serve potentially for "exclusive" identification of each stress type. Thus, the usage of the DDR genes of **Table 1** targets the detection of the type of the stress occurring in the cell through the type of DDR response initiated. In **Table 2**, we quote the most common genes that have been correlated in literature with the above mentioned three situations. We must mention that the genes in **Table 2** can participate in more than one DDR pathways or types of responses in contrast to **Table 1**, that each gene can be assigned with a relative safety to a specific type of stress-induced DNA damage, for example radiation-induced DDR. Thus, the usage of **Table 2** is to suggest in general genes for the confirmation and quantitative assessment of existent DNA damage not knowing necessarily the type of agent or situation which induced it. In order to mine the genes for these two tables, two independent sequences of searching were performed.

Firstly, we run multiple times the *GLAD4U* (Jourquin et al., 2012), testing different query terms. In order to define the most suitable genes for oxidative stress we unified the results of the query terms: "oxidative stress and DNA repair," "oxidative

TABLE 1 | DNA repair genes that could serve for better identification of exposure to ionizing radiation, occurrence of oxidative stress or identification of DNA replication processes.

Response to ionizing radiation	Response to oxidative stress	DNA replication
FAM175A	*PSEN1*	*POLE3*
BRE		*RECQL5*
BABAM1		*IGHMBP2*
UIMC1		*POLG2*
NABP2		*RFC2_HUMAN*
NABP1		*RFC4_HUMAN*
EYA3		*RFC3_HUMAN*
EYA1		*RFC5_HUMAN*
BRCC3		*RFA1_HUMAN*
INIP		*RFA3_HUMAN*
INTS3		*RFA2_HUMAN*
RNF8		*INO80E*
RNF168		*RNASEH2A*
C10orf90		*ATR_HUMAN*
RFWD3		*RBM14*
AEN		*CDK2_HUMAN*
USP28		
BRSK1		
PAXIP1		

The analysis was based only in literature available data running multiple times the GLAD4U, testing specific query terms as described in the text. For the evaluation of the results, some genes and terms were further sampled in other search engines like Quertle.

stress and DNA Repair," "DNA repair and oxidative stress." We kept only those with score greater than 10, as it arises in *GLAD4U*. Score is a measure of relevance between the genes and the query terms, it serves for the prioritization of the results. It is defined as the negative logarithm of the hypergeometric *p*-value. Respectively, the same was done for the other two entries. "Ionizing radiation and DNA repair," "DNA repair and ionizing radiation," and "ionizing radiation and DDR" were unified in order to produce the gene list for "Ionizing Radiation." Accordingly, for "Replication Stress" the results of the queries "DNA repair and replication stress," "replication stress and DNA repair" and "replication stress and DDR" were taken into account. Especially for replication stress PANTHER library was also utilized. For the evaluation of the results, some genes and terms were sampled in other search engines (like Quertle, LLC, 2014). Thus, **Table 2** was created. We have to emphasize here, that genes of **Table 2**, in contrast with **Table 1**, are not suitable for "exclusive" identification of the nature of the DNA stress, although some of them seem to appear only in one category. This happened because we kept only those genes with score greater than 10.

For **Table 1** in addition to the previous analysis, a second one was performed. We searched with *AmiGO2*, a tool of the *Gene Ontology Consortium* search engine (The Gene Ontology, 2015), using the proper of the available filters. The resulting genes were tested with *BioVenn* (Hulsen et al., 2008) in all combinations with the other two categories, and also with the categories that resulted with *GLAD4U*. We kept only the unique genes of each category. To enhance the significance of our results, we run extra tests using other search engines (see below). Our results indicate a variety of gene products that maybe possibly used as "signatures" for each type of stress and be further tested experimentally. We cannot exclude the existence of other possible genes that equally or better characterize for example exclusively radiation response and not replication nor oxidative stress. Our findings were based on published data and the specific search engine tools (see supporting information).

Evaluation of Meta-Analysis Results by Manual Searching in Quertle and other Bibliographic Data Bases

In order to more efficiently scrutinize our results we performed for all of the above found genes (**Table 1**) a manual search in Quertle (LLC, 2014) and also using databases GeneCards (Safran et al., 2010), Uniprot (Apweiler et al., 2004), Entrez Gene (Maglott et al., 2005) and PANTHER (Moussavi Nik et al., 2012). No Quertle search result overlap was found for any of these genes between each of them and the other two categories (columns). For example, ionizing radiation genes (column 1) with the terms "oxidative or replication" stress suggesting a possible "uniqueness" for each of these markers. As a result, these genes or their encoded proteins are potential biomarkers, but they need to be validated in further studies. Some examples are listed below:

Ionizing Radiation

- ***FAM175A, BRE, BRCC3, BABAM1, and UIMIC1***: They are all located in different chromosomes and their protein products belong to the BRCA1-A complex that is involved in DDR and DSB repair. The BRCA1-A complex specifically recognizes "Lys-63"-linked ubiquitinated histones H2A and H2AX at DNA lesion sites, leading to target the BRCA1-BARD1 heterodimer to sites of DNA damage at DSBs. This complex also possesses deubiquitinase activity that specifically removes "Lys-63"-linked ubiquitin on histones H2A and H2AX+ (Apweiler et al., 2004). This complex takes part in G2 DNA damage check point and particularly participates in X-ray induced DDR.
- ***NABP1 and NABP2***: They are components of the SOSS complex, a multiprotein complex that functions downstream of the MRN complex to promote DNA repair and G2/M checkpoint. In the SOSS complex, NABP1 and NABP2 act as a sensor of single-stranded DNA that binds to single-stranded DNA, in particular to polypyrimidines. The SOSS complex associates with DNA lesions and influences diverse endpoints in the cellular DDR including cell-cycle checkpoint activation, recombinational repair and maintenance of genomic stability. Required for efficient HR-dependent repair of DSBs and ATM-dependent signaling pathways (Safran et al., 2010).

Oxidative Stress

- ***PSEN1***: It was rather surprising for us that only one gene "survived" our screening as described above. The close bonds between oxidative stress and ionizing radiation when it comes

TABLE 2 | Genes most commonly used in bibliography in order to identify exposure to ionizing radiation, occurrence of oxidative stress and DNA replication process.

Ionizing radiation						Oxidative stress		Replication stress	
Score	**gene**	**score**	**gene**	**score**	**gene**	**Score**	**gene**	**Score**	**gene**
194.8	*ATM*	31.8	*ERCC5*	15.5	*RAD9A*	127.8	*OGG1*	113.6	*ATR*
87.5	*DDB2*	29.9	*XRCC6*	14.5	*FANCD2*	43.7	*APEX1*	48.3	*CHEK1*
79.3	*TP53*	29.9	*TP53BP1*	14.4	*RNF8*	29.2	*SOD2*	42.5	*ATM*
73.5	*H2AFX*	29.4	*ERCC2*	14.2	*RAD51B*	28.1	*PARP1*	32.4	*CLSPN*
71.7	*NBN*	29.0	*XRCC3*	14.2	*CDKN1A*	27.3	*ATM*	29.0	*ATRIP*
71.2	*PRKDC*	29.0	*XRCC5*	13.8	*BARD1*	23.7	*GSTM1*	23.8	*RPA1*
56.5	*ATR*	27.3	*XRCC4*	13.6	*NTHL1*	23.3	*XRCC1*	20.8	*RPA2*
55.2	*CHEK2*	23.5	*APEX1*	13.6	*CDC25C*	18.7	*CAT*	17.0	*H2AFX*
54.6	*MRE11A*	22.8	*DCLRE1C*	13.4	*XRCC2*	18.5	*GSTT1*	15.6	*SMARCAL1*
53.8	*BRCA1*	22.1	*RAD18*	13.3	*NHEJ1*	17.9	*GPX1*	14.3	*BLM*
52.8	*XRCC1*	21.1	*OGG1*	13.3	*BRCA2*	17.0	*ERCC6*	14.0	*RAD17*
52.7	*CHEK1*	19.5	*CDC25A*	13.0	*ATRIP*	16.8	*NFE2L2*	13.7	*WRN*
52.3	*RAD51*	19.5	*RAD52*	12.8	*ERCC1*	15.7	*ERCC2*	11.4	*CDC25A*
51.1	*XPA*	19.1	*ERCC8*	12.5	*LIG4*	13.9	*NUDT1*	10.5	*RAD9A*
50.3	*DDB1*	18.4	*ERCC4*	12.0	*POLD1*	12.5	*NEIL1*	10.3	*FANCM*
47.1	*PCNA*	18.2	*CUL4A*	11.8	*PNKP*	11.4	*WRN*	10.3	*NBN*
44.9	*XPC*	17.9	*ERCC3*	11.5	*KAT5*	11.0	*MUTYH*		
39.8	*ERCC6*	16.7	*UIMC1*	11.4	*MDM2*	10.8	*TP53*		
39.6	*RAD50*	16.5	*RPA1*	10.4	*PPM1D*				
37.6	*MDC1*	16.4	*PARP1*	10.2	*ABL1*				
32.2	*POLH*	16.0	*RPA2*						

*In this table and in contrast with **Table 1**, these proteins are not suitable for exclusive identification, but there are the most informative, although some of proteins seem to appear only in one category. That is because in **Table 2** only the proteins with the higher score are displayed. In each case, the term "score" as it arises in GLAD4U. "Score" is a measure of relevance between the query terms, it serves for the prioritization of the results. It is defined as the negative logarithm of the hypergeometric p-value.*

to induction of DNA damage can probably explain this result i.e., very difficult to identify oxidative-stress unique genes. According to Gene Ontology, PSEN1 is a gene belonging in the DDR family of genes and especially damage resulting from oxidative stress inducers like hypoxia (Moussavi Nik et al., 2012). The encoded protein belongs to gamma secretase complex, which is a cellular component. Gamma-secretase cleaves several transmembrane proteins including the cell surface receptor Notch and the beta-amyloid precursor protein. Presenilin is a protein which forms a complex with Aph1, Nicastrin and others to cause intramembranous proteolysis of Notch subsequent to its extracellular cleavage by TACE after ligand binding. Presenilin is the actual peptidase in the complex. Its name derives from the fact that it is separately also the peptidase involved in cleavage of the β-amyloid precursor protein or β-APP, and in this role, mutations in Presenilin1 and Presenilin 2 in humans have been linked to familial early onset Alzheimer's disease as researched in PANTHER database database (Mi et al., 2005). It also participates in metabolic processes, through oxidoreductase activity. PSEN1 interacts selectively and non-covalently with oxygen. Searching in Quertle that provides correlated results, gave no direct results when we combined this gene with ionizing radiation or replication stress. Collectively, PSEN1 has been correlated with signal transduction in response to DNA damage, and activation of MAPKK activity.

DNA Replication

- ***POLE3***: is a histone-fold protein that interacts with other histone-fold proteins to bind DNA in a sequence-independent manner. These histone-fold protein dimers combine within larger enzymatic complexes for DNA transcription, replication, and packaging (Maglott et al., 2005).
- ***RECQL5***: is a DNA repair gene, the encoded proteins of which contribute to DNA replication being responsible for DNA duplex unwinding. It is required for mitotic chromosome separation after cross-over events and cell cycle progress. It is required for efficient DNA repair, including repair of inter-strand cross-links. Stimulates DNA decatenation mediated by TOP2A. It prevents sister chromatid exchange and HR (Apweiler et al., 2004).
- ***IGHMBP2***: This gene encodes a helicase superfamily member that binds a specific DNA sequence from the immunoglobulin μ chain switch region (Maglott et al., 2005). The encoded protein is a 5′–3′ helicase that unwinds RNA and DNA duplexes in an ATP-dependent reaction. It acts as a transcription regulator and is required for the transcriptional activation of the flounder liver-type antifreeze protein gene (Apweiler et al., 2004).
- ***POLG2:*** This gene encodes a DNA repair and also DNA replication protein (Apweiler et al., 2004). This protein enhances DNA binding and promotes processive DNA synthesis (Maglott et al., 2005).

- ***RFC2_HUMAN, RFC3_HUMAN, RFC4_HUMAN and RFC5_HUMAN***: These genes encode a member of the activator 1 small subunits family. The elongation of primed DNA templates by DNA polymerase δ and ϵ requires the action of the accessory proteins, proliferating cell nuclear antigen (PCNA) and replication factor C (RFC). Replication factor C, also called activator 1, is a protein complex consisting of five distinct subunits. The core complex possesses DNA-dependent ATPase activity, which was found to be stimulated by PCNA in an *in vitro* system (Maglott et al., 2005).
- ***RFA1_HUMAN, RFA2_HUMAN and RFA3_HUMAN***: They play an essential role in several cellular processes in DNA metabolism including replication, recombination and DNA repair. They bind and subsequently stabilize single-stranded DNA intermediate and thus prevent complementary DNA from reannealing. They function as components of the alternative replication protein A complex (aRPA). aRPA binds single-stranded DNA and probably plays a role in DNA repair; it does not support chromosomal DNA replication and cell cycle progression through S-phase. *In vitro*, aRPA cannot promote efficient priming by DNA polymerase alpha but supports DNA polymerase delta synthesis in the presence of PCNA and replication factor C (RFC), the dual incision/excision reaction of NER and RAD51-dependent strand exchange (Apweiler et al., 2004).

Conclusions

Measuring oxidative DNA lesions at the cellular level is a challenging task since the chosen methodology should be sensitive enough to measure using a few μg of DNA less than one modification per million DNA bases. In addition, the possibility to artefactually produce such lesions during for example DNA isolation increases the difficulty to obtain reliable results. Thus, effort should be made to compare different and independent experimental approaches in order to better assess the formation and biological consequences of DNA lesions. In the field of ionizing radiation, it is not only the chemical nature of the lesions that is important, but it is their localization in a cluster of damage i.e., MDS. This dense distribution of lesions increases their biological importance since the DNA repair systems are often challenged while processing of these clusters. In the future, effort should be also made to search for specific radiation-induced lesions. Since, following irradiation, several radicals could be produced in a close vicinity, one could imagine that such specific lesions could be generated by the recombination of two initially produced radicals. Such damage would have a very low probability to be generated by endogenous oxidative stress. Recently, it has been shown that such a lesion can be generated by the recombination of two initially produced radicals (Uvaydov et al., 2014).

Based on the current experimental tools one can envision that in the future the radiation-induced clustered DNA lesions will be more efficiently and more accurately detected at the level of human cells or tissues and will constitute the signature of this type of radiation, as it is the case for pyrimidine dimers with UV irradiation. In addition, by using various gene product markers one can hypothesize the development of biomarker libraries suggesting response to the specific type of stresses i.e., ionizing radiation, oxidative or replication stress.

Acknowledgments

This work was supported by an EU Marie Curie Reintegration Grant MC-CIG-303514, Greek National funds through the Operational Program 'Educational and Lifelong Learning of the National Strategic Reference Framework (NSRF)-Research Funding Program: THALES (Grant number MIS 379346), Labex PRIMES (ANR-11-LABX-0063). The sponsorship of the COST Action CM1201 "Biomimetic Radical Chemistry" is gratefully acknowledged. The argon ion beamtime at GANIL was supported by the European Community through the European Nuclear Science and Applications Research (ENSAR) contract in the framework of FP7 Integrated Infrastructure Initiative (Grant Agreement n° 262010).

Supplementary Material

The Supplementary Material for this article can be found online at: http://journal.frontiersin.org/article/10.3389/fchem.2015.00035/abstract

References

Apweiler, R., Bairoch, A., Wu, C. H., Barker, W. C., Boeckmann, B., Ferro, S., et al. (2004). UniProt: the Universal Protein knowledgebase. *Nucleic Acids Res.* 32, D115–D119. doi: 10.1093/nar/gkh131

Asaithamby, A., Hu, B., and Chen, D. J. (2011). Unrepaired clustered DNA lesions induce chromosome breakage in human cells. *Proc. Natl. Acad. Sci. U.S.A.* 108, 8293–8298. doi: 10.1073/pnas.1016045108

Aziz, K., Nowsheen, S., Pantelias, G., Iliakis, G., Gorgoulis, V. G., and Georgakilas, A. G. (2012). Targeting DNA damage and repair: embracing the pharmacological era for successful cancer therapy. *Pharmacol. Ther.* 133, 334–350. doi: 10.1016/j.pharmthera.2011.11.010

Bellon, S., Ravanat, J.-L., Gasparutto, D., and Cadet, J. (2002). Cross-linked thymine-purine base tandem lesions: synthesis, characterization, and measurement in gamma-Irradiated isolated DNA. *Chem. Res. Toxicol.* 15, 598–606. doi: 10.1021/tx015594d

Bergeron, F., Auvré, F., Radicella, J. P., and Ravanat, J.-L. (2010). HO° radicals induce an unexpected high proportion of tandem base lesions refractory to repair by DNA glycosylases. *Proc. Natl. Acad. Sci. U.S.A.* 107, 5528–5533. doi: 10.1073/pnas.1000193107

Blaisdell, J. O., and Wallace, S. S. (2001). Abortive base-excision repair of radiation-induced clustered DNA lesions in *Escherichia coli*. *Proc. Natl. Acad. Sci. U.S.A.* 98, 7426–7430. doi: 10.1073/pnas.131077798

Bourdat, A.-G., Douki, T., Frelon, S., Gasparutto, D., and Cadet, J. (2000). Tandem base lesions are generated by hydroxyl radical within isolated DNA in aerated aqueous solution. *J. Am. Chem. Soc.* 122, 4549–4556. doi: 10.1021/ja994282i

Boysen, G., Collins, L. B., Liao, S., Luke, A. M., Pachkowski, B. F., Watters, J. L., et al. (2010). Analysis of 8-oxo-7,8-dihydro-2'-deoxyguanosine by ultra high pressure liquid chromatography-heat assisted electrospray ionization-tandem mass spectrometry. *J. Chromatogr. B* 878, 375–380. doi: 10.1016/j.jchromb.2009.12.004

Breton, J., Sichel, F., Bianchini, F., and Prevost, V. (2003). Measurement of 8-hydroxy-2′-deoxyguanosine by a commercial available ELISA test: comparison with HPLC/Electrochemical detection in calf thymus DNA and determination in human serum. *Anal. Lett.* 36, 123–134. doi: 10.1081/AL-120017267

Cadet, J., Bardet, M., Delatour, T., Douki, T., Gasparutto, D., Molko, D., et al. (1999). "Radiation chemistry of DNA: damage induced by ionizing and UV radiations," in *Fundamentals for the Assessment of Risks from Environmental Radiation,* al., C.B.-K.e. (ed.)., (Dordrecht: Kluwer Academic Publishers), 91–102. doi: 10.1007/978-94-011-4585-5_13

Cadet, J., Bellon, S., Douki, T., Frelon, S., Gasparutto, D., Muller, E., et al. (2004). Radiation-Induced DNA damage: formation, measurement, and biochemical features. *J. Env. Path. Toxico. Oncol.* 23, 33–43. doi: 10.1615/JEnvPathToxOncol.v23.i1.30

Cadet, J., Bourdat, A. G., D'Ham, C., Duarte, V., Gasparutto, D., Romieu, A., et al. (2000). Oxidative base damage to DNA: specificity of base excision repair enzymes. *Mutat. Res.* 462, 121–128. doi: 10.1016/S1383-5742(00)00022-3

Cadet, J., Douki, T., and Ravanat, J. L. (2015). Oxidatively generated damage to cellular DNA by UVB and UVA radiation. *Photochem. Photobiol.* 91, 140–155. doi: 10.1111/php.12368

Cadet, J., Douki, T., and Ravanat, J.-L. (1997). Artifacts associated with the measurement of oxidized DNA bases. *Environ. Health Perspect.* 105, 1033–1039. doi: 10.2307/3433836

Cadet, J., Douki, T., Gasparutto, D., Ravanat, J.-L., and Wagner, R. (2012a). "Oxidatively generated nucleobase modifications in isolated and cellular DNA," in *Encyclopedia of Radicals in Chemistry, Biology and Materials*, eds. C. Chatgilialoglu and A. Studer (Chichester: John Wiley & Sons Ltd), 1319–1344. doi: 10.1002/9781119953678.rad038

Cadet, J., Ravanat, J.-L., Taverna-Porro, M., Menoni, H., and Angelov, D. (2012b). Oxidatively generated complex DNA damage: tandem and clustered lesions. *Cancer Lett.* 327, 5–15. doi: 10.1016/j.canlet.2012.04.005

Dedon, P. C. (2008). The chemical toxicology of 2-deoxyribose oxidation in DNA. *Chem. Res. Toxicol.* 21, 206–219. doi: 10.1021/tx700283c

Dizdaroglu, M. (1984). The use of capillary gas chromatography-mass spectrometry for identification of radiation induced DNA bases damage and DNA base-amino acid cross-links. *J. Chromatogr.* 295, 103–121. doi: 10.1016/S0021-9673(01)87602-0

Douki, T., Ravanat, J.-L., Angelov, D., Wagner, R. J., and Cadet, J. (2004). Effects of duplex stability on charge-transfer efficiency within DNA. *Top. Current. Chem.* 236, 1–25. doi: 10.1007/b94409

Douki, T., Ravanat, J.-L., Pouget, J.-P., Testard, I., and Cadet, J. (2006). Minor contribution of direct ionization to DNA base damage induced by heavy ions. *Int. J. Radiat. Biol.* 82, 119–127. doi: 10.1080/09553000600573788

Dupont, C., Patel, C., Ravanat, J. L., and Dumont, E. (2013). Addressing the competitive formation of tandem DNA lesions by a nucleobase peroxyl radical: a DFT-D screening. *Org. Biomol. Chem.* 14, 3038–3045. doi: 10.1039/c3ob40280k

Eccles, L. J., O'Neill, P., and Lomax, M. E. (2011). Delayed repair of radiation induced clustered DNA damage: friend or foe? *Mutat. Res.* 711, 134–141. doi: 10.1016/j.mrfmmm.2010.11.003

ESCODD, A. (2002). Inter-laboratory validation of procedures for measuring 8-oxo-7,8-dihydroguanine/8-oxo-7,8-dihydrodeoxyguanosine in DNA. *Free Radic. Res.* 36, 239–245. doi: 10.1080/10715760290019246

ESCODD, A. (2003). Measurement of DNA oxidation in human cells by chromatographic and enzymic methods. *Free Radic. Biol. Med.* 34, 1089–1099. doi: 10.1016/S0891-5849(03)00041-8

Floyd, R. A., Watson, J. J., and Wong, P. K. (1984). Sensitive assay of hydroxyl free radical formation utilizing high pressure liquid chromatography with electrochemical detection of phenol and salicylate hydroxylation products. *J. Biochem. Biophys. Methods* 10, 221–235. doi: 10.1016/0165-022X(84)90042-3

Georgakilas, A. (2011). Detection of clustered DNA lesions: biological and clinical applications. *World J. Biol. Chem.* 2, 173–176. doi: 10.4331/wjbc.v2.i7.173

Georgakilas, A. G., Holt, S. M., Hair, J. M., and Loftin, C. W. (2010). Measurement of oxidatively-induced clustered DNA lesions using a novel adaptation of single cell gel electrophoresis (comet assay). *Curr. Protoc. Cell Biol.* Chapter 6:Unit 6.11. doi: 10.1002/0471143030.cb0611s49

Georgakilas, A. G., O'Neill, P., and Stewart, R. D. (2013). Induction and repair of clustered DNA lesions: what do we know so far? *Radiat. Res.* 180, 100–109. doi: 10.1667/RR3041.1

Georgakilas, A. G., Tsantoulis, P., Kotsinas, A., Michalopoulos, I., Townsend, P., and Gorgoulis, V. G. (2014). Are common fragile sites merely structural domains or highly organized "functional" units susceptible to oncogenic stress? *Cell. Mol. Life Sci.* 71, 4519–4544. doi: 10.1007/s00018-014-1717-x

Hada, M., and Georgakilas, A. G. (2008). Formation of clustered DNA damage after high-LET irradiation: a review. *J. Radiat. Res.* 49, 203–210. doi: 10.1269/jrr.07123

Halazonetis, T. D., Gorgoulis, V. G., and Bartek, J. (2008). An oncogene-induced DNA damage model for cancer development. *Science* 319, 1352–1355. doi: 10.1126/science.1140735

Hall, D. B., Holmlin, R. E., and Barton, J. K. (1996). Oxidative DNA damage through long-range electron transfer. *Nature* 382, 731–735. doi: 10.1038/382731a0

Halliwell, B., and Dizdaroglu, M. (1992). Commentary. The measurement of oxidative damage to DNA by HPLC and GC/MS techniques. *Free Radic. Res. Commun.* 16, 75–87. doi: 10.3109/10715769209049161

Hill, K. A., Wang, J., Farwell, K. D., Scaringe, W. A., and Sommer, S. S. (2004). Spontaneous multiple mutations show both proximal spacing consistent with chronocoordinate events and alterations with p53-deficiency. *Mutat. Res.* 554, 223–240. doi: 10.1016/j.mrfmmm.2004.05.005

Hong, H., Cao, H., and Wang, Y. (2007). Formation and genotoxicity of a guanine-cytosine intrastrand cross-link lesion *in vivo*. *Nucleic Acids Res.* 35, 7118–7127. doi: 10.1093/nar/gkm851

Hulsen, T., de Vlieg, J., and Alkema, W. (2008). BioVenn - a web application for the comparison and visualization of biological lists using area-proportional Venn diagrams. *BMC Genomics* 9:488. doi: 10.1186/1471-2164-9-488

Jaruga, P., and Dizdaroglu, M. (2008). 8,5′-Cyclopurine-2′-deoxynucleosides in DNA: mechanisms of formation, measurement, repair and biological effects. *DNA Repair (Amst.)* 7, 1413–1425. doi: 10.1016/j.dnarep.2008.06.005

Jourquin, J., Duncan, D., Shi, Z., and Zhang, B. (2012). GLAD4U: deriving and prioritizing gene lists from PubMed literature. *BMC Genomics* 13(Suppl, 8):S.20. doi: 10.1186/1471-2164-13-S8-S20

Kouass Sahbani, S., Rezaee, M., Cloutier, P., Sanche, L., and Hunting, D. J. (2014). Non-DSB clustered DNA lesions induced by ionizing radiation are largely responsible for the loss of plasmid DNA functionality in the presence of cisplatin. *Chem. Biol. Interact.* 217, 9–18. doi: 10.1016/j.cbi.2014.04.004

Kryston, T. B., Georgiev, A. B., Pissis, P., and Georgakilas, A. G. (2011). Role of oxidative stress and DNA damage in human carcinogenesis. *Mutat. Res.* 711, 193–201. doi: 10.1016/j.mrfmmm.2010.12.016

Labet, V., Morell, C., Grand, A., Cadet, J., Cimino, P., and Barone, V. (2008). Formation of cross-linked adducts between guanine and thymine mediated by hydroxyl radical and one-electron oxidation: a theoretical study. *Org. Biomol. Chem.* 6, 3300–3305. doi: 10.1039/b805589k

Li, P., Du, C. R., Xu, W. C., Shi, Z. L., Zhang, Q., Li, Z. B., et al. (2013). Correlation of dynamic changes in gamma-H2AX expression in peripheral blood lymphocytes from head and neck cancer patients with radiation-induced oral mucositis. *Radiat. Oncol.* 8:155. doi: 10.1186/1748-717X-8-155

LLC, Q. (2014). *Quertle Relationship-driven Biomedical Search, v4.1.1. Quertle LLC.* Available online at: http://www.quertle.info/ (Accessed December 22, 2014).

Madugundu, G. S., Cadet, J., and Wagner, J. R. (2014). Hydroxyl-radical-induced oxidation of 5-methylcytosine in isolated and cellular DNA. *Nucleic Acids Res.* 42, 7450–7460. doi: 10.1093/nar/gku334

Madugundu, G. S., Park, Y., Sanche, L., and Wagner, J. R. (2012). Radiation-induced formation of 2′,3′-dideoxyribonucleosides in DNA: a potential signature of low-energy electrons. *J. Am. Chem. Soc.* 134, 17366–17368. doi: 10.1021/ja306810w

Maglott, D., Ostell, J., Pruitt, K. D., and Tatusova, T. (2005). Entrez gene: gene-centered information at NCBI. *Nucleic Acids Res.* 33, D54–D58. doi: 10.1093/nar/gki031

Mi, H., Lazareva-Ulitsky, B., Loo, R., Kejariwal, A., Vandergriff, J., Rabkin, S., et al. (2005). The PANTHER database of protein families, subfamilies, functions and pathways. *Nucleic Acids Res.* 33, D284–D288. doi: 10.1093/nar/gki078

Milner, A. E., Vaughan, A. T. M., and Clark, I. P. (1987). Measurement of DNA damage in mammalian cells using flow cytometry. *Radiat. Res.* 110, 108–117. doi: 10.2307/3576888

Mouret, S., Baudouin, C., Charveron, M., Favier, A., Cadet, J., and Douki, T. (2006). Cyclobutane pyrimidine dimers are predominant DNA lesions in whole human skin exposed to UVA radiation. *Proc. Natl. Acad. Sci. U.S.A.* 103, 13765–13770. doi: 10.1073/pnas.0604213103

Moussavi Nik, S. H., Wilson, L., Newman, M., Croft, K., Mori, T. A., Musgrave, I., et al. (2012). The BACE1-PSEN-AbetaPP regulatory axis has an ancient role in response to low oxygen/oxidative stress. *J. Alzheimers Dis.* 28, 515–530. doi: 10.3233/JAD-2011-110533

Nikjoo, H., O'Neill, P., Wilson, W. E., and Goodhead, D. T. (2001). Computational approach for determining the spectrum of DNA damage induced by ionizing radiation. *Radiat. Res.* 156, 577–583. doi: 10.1667/0033-7587(2001)156[0577:CAFDTS]2.0.CO;2

Ogrunc, M., Di Micco, R., Liontos, M., Bombardelli, L., Mione, M., Fumagalli, M., et al. (2014). Oncogene-induced reactive oxygen species fuel hyperproliferation and DNA damage response activation. *Cell Death Differ.* 21, 998–1012. doi: 10.1038/cdd.2014.16

Pachnerova Brabcova, K., Sihver, L., Yasuda, N., Matuo, Y., Stepan, V., and Davidkova, M. (2014). Clustered DNA damage on subcellular level: effect of scavengers. *Radiat. Environ. Biophys.* 53, 705–712. doi: 10.1007/s00411-014-0557-2

Park, Y., Peoples, A. R., Madugundu, G. S., Sanche, L., and Wagner, J. R. (2013). Side-by-side comparison of DNA damage induced by low-energy electrons and high-energy photons with solid TpTpT trinucleotide. *J. Phys. Chem. B* 117, 10122–10131. doi: 10.1021/jp405397m

Peng, T., Shen, H. M., Liu, Z. M., Yan, L. N., Peng, M. H., Li, L. Q., et al. (2003). Oxidative DNA damage in peripheral leukocytes and its association with expression and polymorphisms of hOGG1: a study of adolescents in a high risk region for hepatocellular carcinoma in China. *World J. Gastroenterol.* 9, 2186–2193.

Perdiz, D., Grof, P., Mezzina, M., Nikaido, O., Moustacchi, E., and Sage, E. (2000). Distribution and repair of bipyrimidine photoproducts in solar UV-irradiated mammalian cells. Possible role of Dewar photoproducts in solar mutagenesis. *J. Biol. Chem.* 275, 26732–26742. doi: 10.1074/jbc.m001450200

Perrier, S., Hau, J., Gasparutto, D., Cadet, J., Favier, A., and Ravanat, J.-L. (2006). Characterization of lysine-guanine cross-links upon one-electron oxidation of a guanine-containing oligonucleotide in the presence of a trilysine peptide. *J. Am. Chem. Soc.* 128, 5703–5710. doi: 10.1021/ja057656i

Pflaum, M., and Epe, B. (2000). "Measuring oxidative DNA damage by alkaline elution," in *Measuring in vivo Oxidative Damage: A Practical Course*, eds. J. Lunec and H. R. Griffiths (Chischester: John Wiley & Sons, LTD), 95–104.

Pogozelski, W. K., and Tullius, T. D. (1998). Oxidative strand scission of nucleic acids: routes initiated by hydrogen abstraction from the sugar moiety. *Chem. Rev.* 98, 1089–1108. doi: 10.1021/cr960437i

Pouget, J.-P., Frelon, S., Ravanat, J.-L., Testard, I., Odin, F., and Cadet, J. (2002). Formation of modified DNA bases in cells exposed either to gamma radiation or to high-LET particles. *Radiat. Res.* 157, 589–595. doi: 10.1667/0033-7587(2002)157[0589:FOMDBI]2.0.CO;2

Pouget, J.-P., Ravanat, J.-L., Douki, T., Richard, M.-J., and Cadet, J. (1999). Measurement of DNA base damage in cells exposed to low doses of gamma radiation: comparison between the HPLC-EC and the comet assays. *Int. J. Radiat. Biol.* 75, 51–58. doi: 10.1080/095530099140807

Prise, K. M., Folkard, M., Newman, H. C., and Michael, B. D. (1994). Effect of radiation quality on lesion complexity in cellular DNA. *Int. J. Radiat. Biol.* 66, 537–542. doi: 10.1080/09553009414551581

Ravanat, J. L., Breton, J., Douki, T., Gasparutto, D., Grand, A., Rachidi, W., et al. (2014). Radiation-mediated formation of complex damage to DNA: a chemical aspect overview. *Br. J. Radiol.* 87:20130715. doi: 10.1259/bjr.20130715

Ravanat, J.-L. (2012). Chromatographic methods for the analysis of oxidatively damaged DNA. *Free Radic. Res.* 46, 479–491. doi: 10.3109/10715762.2011.623161

Ravanat, J.-L., Cadet, J., and Douki, T. (2012). Oxidatively generated DNA lesions as potential biomarkers of *in vivo* oxidative stress. *Curr. Mol. Med.* 12, 655–674. doi: 10.2174/156652412800792651

Ravanat, J.-L., Di Mascio, P., Martinez, G. R., Medeiros, M. H., and Cadet, J. (2000). Singlet oxygen induces oxidation of cellular DNA. *J. Biol. Chem.* 275, 40601–40604. doi: 10.1074/jbc.M006681200

Ravanat, J.-L., Douki, T., Duez, P., Gremaud, E., Herbert, K., Hofer, T., et al. (2002). Cellular background level of 8-oxo-7,8-dihydro-2′-deoxyguanosine: an isotope based method to evaluate artefactual oxidation of DNA during its extraction and subsequent work-up. *Carcinogenesis* 23, 1911–1918. doi: 10.1093/carcin/23.11.1911

Ravanat, J.-L., Sauvaigo, S., Caillat, S., Martinez, G. R., Medeiros, M. H. G., Di Mascio, P., et al. (2004). Singlet oxygen-mediated damage to cellular DNA as determined by the comet assay associated with DNA repair enzymes. *Biol. Chem.* 385, 17–20. doi: 10.1515/BC.2004.003

Ravanat, J.-L., Turesky, R. J., Gremaud, E., Trudel, L. J., and Stadler, R. H. (1995). Determination of 8-oxoguanine in DNA by gas chromatography-mass spectrometry and HPLC-electrochemical detection. Overestimation of the background level of the oxidized base by the gas chromatography-mass spectrometry assay. *Chem. Res. Toxicol.* 8, 1039–1045. doi: 10.1021/tx00050a007

Regulus, P., Duroux, B., Bayle, P. A., Favier, A., Cadet, J., and Ravanat, J. L. (2007). Oxidation of the sugar moiety of DNA by ionizing radiation or bleomycin could induce the formation of a cluster DNA lesion. *Proc. Natl. Acad. Sci. U.S.A.* 104, 14032–14037. doi: 10.1073/pnas.0706044104

Regulus, P., Spessotto, S., Gateau, M., Cadet, J., Favier, A., and Ravanat, J.-L. (2004). Detection of new radiation-induced DNA lesions by liquid chromatography coupled to tandem mass spectrometry. *Rapid. Commun. Mass Spectrom.* 18, 2223–2228. doi: 10.1002/rcm.1612

Rogakou, E. P., Pilch, D. R., Orr, A. H., Ivanova, V. S., and Bonner, W. M. (1998). DNA double-stranded breaks induce histone H2AX phosphorylation on serine 139. *J. Biol. Chem.* 273, 5858–5868. doi: 10.1074/jbc.273.10.5858

Rothkamm, K., and Horn, S. (2009). gamma-H2AX as protein biomarker for radiation exposure. *Ann. Ist. Super. Sanita* 45, 265–271.

Safran, M., Dalah, I., Alexander, J., Rosen, N., Iny Stein, T., Shmoish, M., et al. (2010). GeneCards version 3: the human gene integrator. *Database (Oxford)* 2010:baq020. doi: 10.1093/database/baq020

Sanche, L. (2009). Biological chemistry: beyond radical thinking. *Nature* 461, 358–359. doi: 10.1038/461358a

Sarasqueta, A. F., Forte, G., Corver, W. E., de Miranda, N. F., Ruano, D., van Eijk, R., et al. (2013). Integral analysis of p53 and its value as prognostic factor in sporadic colon cancer. *BMC Cancer* 13:277. doi: 10.1186/1471-2407-13-277

Sczepanski, J. T., Jacobs, A. C., and Greenberg, M. M. (2008). Self-promoted DNA interstrand cross-link formation by an abasic site. *J. Am. Chem. Soc.* 130, 9646–9647. doi: 10.1021/ja8030642

Silerme, S., Bobyk, L., Taverna-Porro, M., Cuier, C., Saint-Pierre, C., and Ravanat, J. L. (2014). DNA-polyamine crosslinks generated upon one electron oxidation of DNA. *Chem. Res. Toxicol.* 27, 1011–1018. doi: 10.1021/tx500063d

Sprung, C. N., Ivashkevich, A., Forrester, H. B., Redon, C. E., Georgakilas, A., and Martin, O. A. (2015). Oxidative DNA damage caused by inflammation may link to stress-induced non-targeted effects. *Cancer Lett.* 356, 72–81. doi: 10.1016/j.canlet.2013.09.008

Stewart, R. D., Yu, V. K., Georgakilas, A. G., Koumenis, C., Park, J. H., and Carlson, D. J. (2011). Effects of radiation quality and oxygen on clustered DNA lesions and cell death. *Radiat. Res.* 176, 587–602. doi: 10.1667/RR2663.1

Sutherland, B. M., Bennett, P. V., Sidorkina, O., and Laval, J. (2000). Clustered DNA damages induced in isolated DNA and in human cells by low doses of ionizing radiation. *Proc. Natl. Acad. Sci. U.S.A.* 97, 103–108. doi: 10.1073/pnas.97.1.103

Sutherland, B. M., Bennett, P. V., Sutherland, J. C., and Laval, J. (2002). Clustered DNA damages induced by x rays in human cells. *Radiat. Res.* 157, 611–616. doi: 10.1667/0033-7587(2002)157[0611:CDDIBX]2.0.CO;2

Sutherland, B. M., Georgakilas, A. G., Bennett, P. V., Laval, J., and Sutherland, J. C. (2003). Quantifying clustered DNA damage induction and repair by gel electrophoresis, electronic imaging and number average length analysis. *Mutat. Res.* 531, 93–107. doi: 10.1016/j.mrfmmm.2003.08.005

The Gene Ontology, C. (2015). Gene ontology consortium: going forward. *Nucleic Acids Res.* 43, D1049–D1056. doi: 10.1093/nar/gku1179

Tsantoulis, P. K., Kotsinas, A., Sfikakis, P. P., Evangelou, K., Sideridou, M., Levy, B., et al. (2008). Oncogene-induced replication stress preferentially targets common fragile sites in preneoplastic lesions. A genome-wide study. *Oncogene* 27, 3256–3264. doi: 10.1038/sj.onc.1210989

Tsao, D., Kalogerinis, P., Tabrizi, I., Dingfelder, M., Stewart, R. D., and Georgakilas, A. G. (2007). Induction and processing of oxidative clustered DNA lesions in 56Fe-ion-irradiated human monocytes. *Radiat. Res.* 168, 87–97. doi: 10.1667/RR0865.1

Uvaydov, Y., Geacintov, N. E., and Shafirovich, V. (2014). Generation of guanine-amino acid cross-links by a free radical combination mechanism. *Phys. Chem. Chem. Phys.* 16, 11729–11736. doi: 10.1039/c4cp00675e

Conflict of Interest Statement: The authors declare that the research was conducted in the absence of any commercial or financial relationships that could be construed as a potential conflict of interest.

Copyright © 2015 Nikitaki, Hellweg, Georgakilas and Ravanat. This is an open-access article distributed under the terms of the Creative Commons Attribution License (CC BY). The use, distribution or reproduction in other forums is permitted, provided the original author(s) or licensor are credited and that the original publication in this journal is cited, in accordance with accepted academic practice. No use, distribution or reproduction is permitted which does not comply with these terms.

frontiers in Chemistry

REVIEW
published: 14 July 2015
doi: 10.3389/fchem.2015.00043

Understanding DNA under oxidative stress and sensitization: the role of molecular modeling

Elise Dumont[1]* *and Antonio Monari*[2,3]*

[1] Laboratoire de Chimie, UMR 5182 Centre National de la Recherche Scientifique, École Normale Supérieure de Lyon, Lyon, France, [2] Université de Lorraine - Nancy, Theory-Modeling-Simulation, Structure et Réactivité des Systèmes Moléculaires Complexes (SRSMC), Vandoeuvre-les-Nancy, France, [3] Centre National de la Recherche Scientifique, Theory-Modeling-Simulation, Structure et Réactivité des Systèmes Moléculaires Complexes (SRSMC), Vandoeuvre-les-Nancy, France

OPEN ACCESS

Edited by:
John D. Wade,
Florey Institute of Neuroscience and Mental Health, Australia

Reviewed by:
Robert Vianello,
Rudjer Boskovic Institute, Croatia
Giampaolo Barone,
University of Palermo, Italy

***Correspondence:**
Elise Dumont,
Laboratoire de Chimie, UMR 5182 Centre National de la Recherche Scientifique, École Normale Supérieure de Lyon, 46, Allée d'Italie, 69364 Lyon 07, France
elise.dumont@ens-lyon.fr;
Antonio Monari,
Faculté de Sciences et Techniques, Boulevard des Aiguillettes, Vandoeuvre-les-Nancy, 54506 Nancy, France
antonio.monari@univ-lorraine.fr

Specialty section:
This article was submitted to Chemical Biology, a section of the journal Frontiers in Chemistry

Received: 27 March 2015
Accepted: 29 June 2015
Published: 14 July 2015

Citation:
Dumont E and Monari A (2015) Understanding DNA under oxidative stress and sensitization: the role of molecular modeling. Front. Chem. 3:43. doi: 10.3389/fchem.2015.00043

DNA is constantly exposed to damaging threats coming from oxidative stress, i.e., from the presence of free radicals and reactive oxygen species. Sensitization from exogenous and endogenous compounds that strongly enhance the frequency of light-induced lesions also plays an important role. The experimental determination of DNA lesions, though a difficult subject, is somehow well established and allows to elucidate even extremely rare DNA lesions. In parallel, molecular modeling has become fundamental to clearly understand the fine mechanisms related to DNA defects induction. Indeed, it offers an unprecedented possibility to get access to an atomistic or even electronic resolution. Ab initio molecular dynamics may also describe the time-evolution of the molecular system and its reactivity. Yet the modeling of DNA (photo-)reactions does necessitate elaborate multi-scale methodologies to tackle a damage induction reactivity that takes place in a complex environment. The double-stranded DNA environment is first characterized by a very high flexibility, but also a strongly inhomogeneous electrostatic embedding. Additionally, one aims at capturing more subtle effects, such as the sequence selectivity which is of critical important for DNA damage. The structure and dynamics of the DNA/sensitizers complexes, as well as the photo-induced electron- and energy-transfer phenomena taking place upon sensitization, should be carefully modeled. Finally the factors inducing different repair ratios for different lesions should also be rationalized. In this review we will critically analyze the different computational strategies used to model DNA lesions. A clear picture of the complex interplay between reactivity and structural factors will be sketched. The use of proper multi-scale modeling leads to the in-depth comprehension of DNA lesions mechanisms and also to the rational design of new chemo-therapeutic agents.

Keywords: DNA, photosensitization, photodynamic therapy, photochemistry, molecular modeling, energy/electron transfer

1. Introduction

DNA stability is essential to maintain cellular integrity of living organisms and avoid genetic mutations. Threats to DNA stability can be triggered by oxidative stress induced by the presence of metabolic reactive radical and oxygen species (ROS) or by photoreactivity. Oxidative and light-induced stress can have a very strong influence on the biological processes governed by DNA, as

well as in the indirect activation or transduction of signal cascades, that may result in different malignant outcomes for the life of the involved cells (Salmon et al., 2004; Kujoth et al., 2005; Klaunig et al., 2010). Although, in the following we will focus more on $OH^{\bullet}$ induced pathways, it is worth mentioning that superoxide radical (0_2^-) is also connected to the induction of DNA lesions (Fridovich, 1995; Cadenas and Davies, 2000; Valko et al., 2007), as well as reactive nitrogen species (RNS) that are known for their potential carcinogenic activity (Pryor and Squadrito, 1995; Pacher et al., 2007; Sainz et al., 2012).

In contrast to photochemical degradation mechanisms, oxidative stress sources can also derive from endogenous processes and mechanism. Inflammatory conditions are a known source of ROS (Kamp et al., 2011), such as $OH^{\bullet}$, and remarkably ROS and free radicals are also exploited by the cells for signal transduction (Hamanaka and Chandel, 2010; Finkel, 2011), and hence are a key factor of cell metabolism. Moreover, ROS ultimately attacking DNA, may also derive as byproducts of the degradation of oxidized lipids or proteins, via the endocytosis process (Lim et al., 2004; Miyamoto and Di Mascio, 2014). In addition an other important source of endogenous ROS production, also related to neurodegenerative diseases, is due to the metabolism of dietary and biogenic amines (Chaiyen et al., 2012; Ramsay, 2012; Vianello et al., 2012; Repic et al., 2014). Indeed, this metabolic pathway performed by monoamide oxidase enzymes leads to the production of H_2O_2 and subsequently of $OH^{\bullet}$.

DNA is also constantly exposed to light, and hence efficient dissipative channels exist to hamper potentially dangerous photochemical pathways. Nevertheless, inherently stable DNA photoproducts have been reported and their photochemistry has been deeply analyzed (Sinha and Hader, 2002; Brash, 2015). Indeed, the correlation between DNA photo-lesions and the emergence of threatening mutations is now well accepted, and in particular the correlation between some types of skin cancers and uncontrolled sun exposure (Sage et al., 2005). Furthermore, the absorption range of native DNA can be significantly extended from the UVB region (where the constitutive nucleobases individually absorb) to the less energetic UVA because of the excitonic coupling within the macromolecular DNA structure, or thanks to the interaction with endogenous or exogenous chromophores, i.e., the photosensitization (Epe, 2012).

The cells response to the oxidative and photochemical stress normally results in an acceleration of protective mechanisms aimed to expel the stress enhancing factors. In the case of DNA lesions the activation of "repair" proteins, that may vary greatly in terms of specificity and efficiency, is invoked. The latter enzymes usually excise the damaged DNA area (Sancar and Sancar, 1988; Radzimanowski et al., 2013), therefore hampering any mismatch in the replication process. However some situations exist where the repair mechanisms fail to efficiently eradicate the lesions. In this case two scenarios are possible. On the one hand mismatches can occur during transcription, ultimately leading to mutations and eventually to carcinogenesis. On the other hand if the stress is too strong or the replication is impossible, for instance because it is blocked by interstrand cross-links, cells may induce their programmed death (apoptosis).

Apoptosis induction favored by the controlled production of DNA lesions has a very important therapeutic significance. Indeed, the formation of irreversible DNA lesions, and the interference with the replication process, has been and is currently exploited in the development of chemotherapeutic agents. For instance, we may cite the renown case of the cisplatin (Florea and Büsselberg, 2011), whose therapeutic effects are known since the 60's. More recently the cytotoxic action of other organometallic compounds, in particular Ruthenium complexes (Rademaker-Lakhai et al., 2004; Yan et al., 2005; Antonarakis and Emadi, 2010; Suss-Fink, 2010), has gained great attention in the development of novel chemotherapeutic drugs that are presently in clinical trial phase. Furthermore, since DNA lesions can be induced not only by ground state chemistry, but may also results from photochemical or photophysical activated energy- or electron-transfer processes the use of light-triggered therapeutic strategies and drugs appears promising in enhancing specificity of action and hence reduce unwanted side-effects. A particular attention should be paid to the light-induced activation of singlet oxygen that is promoted by opportune sensitizers such as porphyrins and lies at the heart of photodynamic therapy strategies (Dougherty et al., 1998; Pandey, 2000; Agostinis et al., 2011; Ethirajan et al., 2011).

From an experimental point of view, one relies on the use of techniques able to identify and possibly quantify the different lesions formed in DNA. Combination of mass-spectrometry with gas-phase chromatography is usually used to provide such informations both for isolated and cellular DNA (Frelon et al., 2000). Indeed, the difficulty in studying the reactions taking place in the complex macromolecular environment usually pushes toward the use of simple models, such as (artificial) mono- or dinucleotide. Even if such simplified techniques allow to infer and extrapolate valuable information on the nucleobase reactivity, still it is important to recall that the role of the DNA environment is almost totally neglected, while it may have huge chemical consequences. On the other hand NMR and X-ray spectrometry may provide extremely useful structures of lesioned DNA double-strand (Gold et al., 2014; Jain et al., 2014; Zalesak et al., 2014; Mutter et al., 2015). Even if in this case most often DNA inherent flexibility and complex dynamic are not properly taken into account, and hence the structural evolution and the role played by different lesions in driving such reorganization may be totally neglected. Obviously, to assess the response of DNA to UV/vis radiation the use of spectroscopic techniques is crucial. This can go from the standard and bench-scale use of optical techniques such as absorption, luminescence and electronic dichroism (Vorlickova and Palecek, 1974; Brabec et al., 1992; Ding et al., 2009) to more sophisticated time-resolved technique (Gustavsson et al., 2010, 2013; Vaya et al., 2012), allowing to follow the time-evolution of the different excited states. Furthermore, dichroism and spectroscopic titration are commonly used to infer the different and possibly competitive interaction modes between DNA and sensitizers (Carvlin et al., 1982; Wang et al., 2012; Lauria et al., 2014).

As this brief survey evidences, the induction of DNA lesions triggered by different sources of stress involves a very complex

interplay between different phenomena taking place at molecular level, and having more general and systemic consequences. On the other hand, it is precisely that complexity that strongly suggests a multidisciplinary approach to tackle this non trivial problem, in particular combining adequate spectroscopic techniques with state-of-the-art molecular multiscale modeling. Molecular modeling is invaluable in providing atomistic or even electronic scale description of the involved phenomena. For instance, molecular dynamics techniques allow to assess for the structural deformation of lesioned DNA and its time evolution, as well as to infer the existence of different stable interaction modes with smaller sensitizers. The ground- and excited- state behavior and the reactivity, for instance in terms of free energy profiles along reaction coordinates, are described by using hybrid quantum mechanics/ molecular mechanics (QM/MM) methods allowing to take into account the role of the environment (Senn and Thiel, 2007, 2009; Meier et al., 2013; Monari et al., 2013). QM/MM also allows to validate the experimental use of simpler and more homogeneous model systems (Ding et al., 2009). The growing computational power experienced in the latter years, as well as the presence of more and more efficient algorithms and codes allows to tackle more and more complex problems and environments, providing an unprecedented comprehension of biologically relevant mechanisms.

In the present review we will present some examples of the molecular modeling of DNA under external stress, both concerning ground-state and photochemical pathways, underlying the fundamental questions that may be answered by a proper simulation and modeling.

2. Modeling of DNA Oxidative Stress

DNA oxidative stress is dominated by a combinatorial radical chemistry, in biological media hydroxyl ($HO^{\bullet}$) and peroxyl ($HOO^{\bullet}$) radical being by far the principal players. However, other non-radical reactive chemical moieties can play a role and have a strong biological influence: $^1O_2$, H_2O_2, alkylating agents, low-energy electrons, and each of them has been tackled by simulation means.

2.1. An Ubiquitous First Step: Hydrogen Abstraction

We will hereby focus on radical induced ground-state reactivity, and mostly on the hydroxyl radical $HO^{\bullet}$, as its study exemplifies the methods employed in DNA damage molecular modeling. The hydroxyl radical is prone to abstract an hydrogen, with subsequent production of one water molecule and an highly reactive radical specie embedded in the biological macromolecule (see **Figure 1**); hence, this first step may also constitute the initiation step in radical chain reactions.

It has been shown that for a given double-strand DNA fragment (ds-DNA), an hydrogen uptake can occur at many positions, on the nucleobase (Cadet et al., 1999) but also on the sugar moiety (Pogozelski and Tullius, 1998), with a ratio of 9:1. Another reactive pathway activated by the hydroxyl radical is the direct addition of $HO^{\bullet}$ onto the an ethylenic position of a given nucleobase B, thus forming *in situ* a radical entity $[B–OH]^{\bullet}$. Once

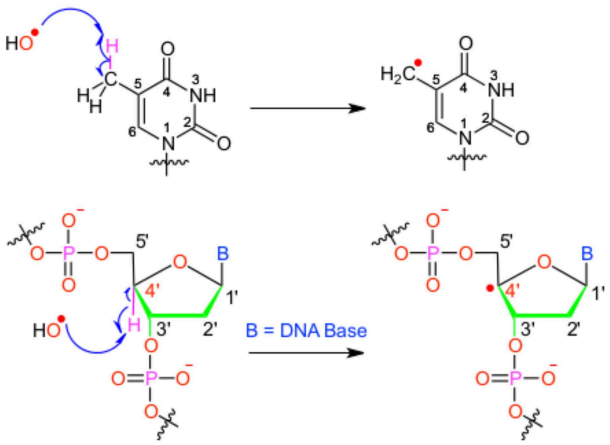

FIGURE 1 | Scheme of the different possible oxidative attacks by OH• on DNA nucleobase or backbone sugar moiety.

again $[B–OH]^{\bullet}$ may undergo further fragmentation or evolve toward the formation of a peroxyl nucleobase. Thus $HO^{\bullet}$ has a deleterious and versatile, chemical outcome with many possible subsequent fragmentation patterns. For instance, as schematized in **Figure 2**, a possible evolution may lead to the generation of abasic sites, or to the oxidative strand scission of nucleic acids (Cooke et al., 2003). Abasic lesions are characterized by oxidative pathways that lead to the disruption of the base pyrimidine or purine kernel, leaving only the sugar as part of the strand. On the other hand strand scission, mostly affect the sugar and the backbone (**Figure 2**) and ultimately results in a breaking of the strand continuity. If the previous lesions may easily be recognized and repaired by specific enzymes, also more dangerous lesions, particularly refractory to the repair may be produced (Bergeron et al., 2010). The former are produced by the attack of an oxidized nucleobase onto a vicinal one (either situated on the same strand or on the opposite strand), this gives rise to intra- or interstrand cross-links respectively. This particularly complex and significant case will be dealt to in Section 2.3.

Modeling has been early invoked to provide a rationale, and ultimately predict, the preferential hydrogen abstraction sites: indeed, because of its general high reactivity, the hydroxyl radical selectivity is governed by the accessibility to the solvent. The latter is an information reliably estimated by bioinformatics approaches such as the computation of Solvent Accessible Surface Area (SASA). Tullius et al. have exploited this approach to rationalize the $HO^{\bullet}$-induced DNA strand breaking (Balasubramanian et al., 1998), hence providing a clear-cut structural basis to rationalize the abstraction site preference. Indeed the authors have clearly shown the existence of a very good correlation between the reactivity of the different sites and their solvent. The C5 carbon atom was indeed found to contribute to the total cleavage by 57%, the C4 position accounting for the 22% and the C3 for the 17%. The most reactive C5 position on the other hand shows a solvent accessible area of 46%, while the C4 and C3 are characterized by 28 and 14% accesible surface, respectively. Furthermore, this rather simple

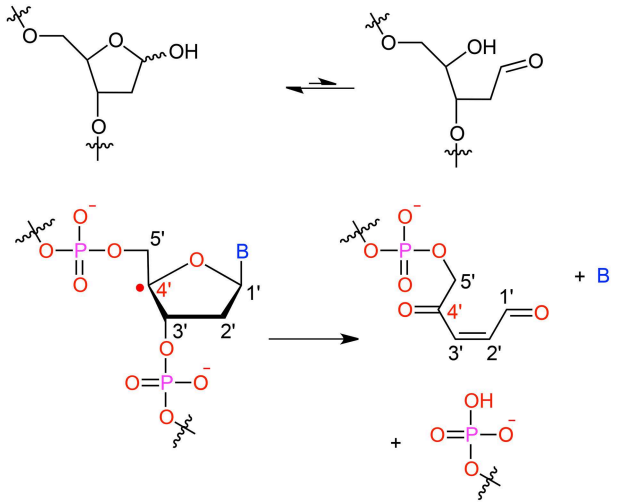

FIGURE 2 | Evolution to abasic site and DNA strand scission following oxidative attack on the DNA sugar moiety.

approach may easily be generalized to preview the reactivity in presence of diffusion controlled reactants and may be extended to the investigations of RNA reactivity and repair processes. Monte-Carlo simulations of site-specific radical attack to DNA bases have also proved their usefulness (Nijkoo et al., 1999; Bulent et al., 2008), with the advantage to go beyond the single-structure and static description. On the other hand, the almost immediate estimate of SASA paves the way toward massive parallel-sequencing-based hydroxyl radical probing of RNA accessibility (Kielpinski and Vinther, 2014).

The hydrogen abstraction is the key limiting step of the whole damage process (Regulus et al., 2007; Nikitaki et al., 2015), and its in-depth understanding can take full profit from quantum mechanics calculations: the latter are most often rooted in density functional theory (DFT), which allows to discriminate the most stable radical centers. Most particularly, DFT can easily be used to calculate the carbon–hydrogen bond dissociation energy (BDE) on different nucleobase and sugar potential reactive sites. This description allows to go beyond the simple solvent accessibility, indeed a lower BDE will be recognized as a crucial factor favoring the reactivity of the specific site.

For instance, DFT confirms that hydrogen abstraction for pyrimidine nucleobases, i.e., cytosine and thymine, occurs preferentially on C5 positions and on the corresponding methyl group (C5 m), not only because of solvent accessibility but also due to electronic favors (Ji et al., 2005; Frances-Monneris et al., 2013; Yadav and Mishra, 2013). Interestingly enough, while most natural occuring nucleobases lead to the formation of π-radicals upon H abstraction, the substitution of the carbonyl oxygen with sulfur induces the formation of the quite rare σ-radicals (Besic et al., 2001; Vianello and Maksic, 2003; Gomzi, 2011).

It is remarkable that a sound agreement can be achieved between experiment and theory even when calculations on model, isolated moieties are performed (Bera and Schaefer, 2005). More recently, Papiez et al. have employed Car-Parrinello molecular dynamics (CPMD) to describe the hydrogen abstraction on a solvated guanine (Wu et al., 2004; Abolfath et al., 2012). This work nicely underlines the contrast between the static approaches where temperature effects and hence thermal fluctuations are neglected and the dynamic picture. Indeed while in vacuum the hydrogen abstraction occurs at around $t = 0.07$ *ps*, water solution slows down the reaction rate roughly by a factor of two ($t = 0.12$ *ps*). The hampering effect of the water environment is due to thermal fluctuation of the solvent molecules, that are also highly organized because of hydrogen-bond networks, ultimately resulting in a strong disturbance of the OH· motion. The extension of this protocol to a ds-DNA model would constitute an interesting perspective. However reaching such a goal will require describing most of the system at the molecular mechanics (MM) level, while the reactive center (i.e., the nucleobase) should be described quantum mechanically (QM). Furthermore, water molecules close to the nucleobase should be included in the QM partition, but due to water high mobility one has to take into account the fact that some solvent molecules may move out from the significant QM partition while others may enter. Such schemes, known as adaptative QM/MM, have been pushed forward over the last years (Nielsen et al., 2010) but are for now applied only to model reactions. An interesting alternative for large scale molecular modeling could rely on the use of *reactive* MD, which has been realized relying on the ReaxFF force field (Abolfath et al., 2011).

However, QM/MM-MD simulatons, e.g., in a Car-Parrinello framework, have nowadays been successfully performed both for reactivity in DNA double strands and in solvated nucleoside (Abolfath et al., 2012; Garrec et al., 2012). Compared with reactive MD force-fields and previous calculations, these studies have the advantage to exploit a less-parameterized density functional. Furthermore, they also provide a more direct comparison of free-energy profiles between an isolated system and a DNA fragment. Indeed, it is worth emphasizing that DFT has been employed in a near-exclusive way not only for ground-state reactivity, but also for calculating eletronical vertical excitation (Durbeej and Eriksson, 2003). More recently, several works have also described *photo-induced* hydrogen abstraction (Szabla et al., 2015), resorting to a multi-reference description of the electronic density through complete active space self-consistent (CASSCF) or second order perturbation theory (CASPT2) approaches. Remarkably, in the previous contribution the authors identified a reactive conical intersection joining the S_0/S_1 of β-2′-deoxycytidine. Although, from the S_1 minimum the system should overcome a rather large barrier of 0.59 eV to reach the conical intersection, the excess vibrational energy at Franck-Condon geometry safely allows for its crossing and hence justify the active photochemistry. Even if multi-configurational methods can in principle be used within a QM/MM-MD framework, they are mostly restricted to the treatment of excited states due to their efficiency in the description of non-adiabatic potential energy points (conical intersection) and to the computational bottleneck that limits the time-scale of the MD trajectory to hundreds of fs (Szabla et al., 2015). However, unlike for other systems or reactions, the exchange-correlation density

functional dependence is less prononouced for the study of DNA and nucleobase hydrogen abstraction reactivity, and different functional classes usually provide the same insights. In contrast, the inclusion of a dispersion is particularly important as it was evidenced for instance by the Bickelhaupt's group (Poater et al., 2011).

2.2. Probing the Role of the Environment for Single-nucleobase Reactions

When coming to DNA reactivity and damage generations, experiments are performed on isolated nucleobases, small DNA fragments (trinucleotides), longer oligonucleotides or even larger ds-DNA structures. It is now well recognized that reactivity in model systems can largely differ due to the geometrical constraint imposed within a ds-DNA and the strongly heterogenous environment. Providing a most direct comparison between reaction profiles for isolated moieties vs. nucleobases embedded in a complex macromolecular environment allows to pinpoint the structural and electrostatic factors that can dramatically tune or reserve the intrinsic reactivity of nucleobases. Many elementary lesions in DNA subunits have been first targeted based on QM studies on isolated fragments (Duncan Lyngdoh and Schaefer, 2009).

Predictions of the reactivity order between different nucleobases can indeed be assessed on model π-stacked systems (thymine propensity to form lower triplet states or dimerize (Durbeej and Eriksson, 2003), lower ionization potential of guanine, ...). Both DFT and (multireference) post Hartree-Fock approaches can be employed, (e.g., on the guanine radical cation Hutter and Clark, 1996; Sponer et al., 2001; Jurecka et al., 2006). DNA reactivity has been a field of investigation for conceptual DFT, with derivation of DFT-based descriptors to rationalize intrinsic trends in DNA reactivity (Labet et al., 2014). Yet, this supposes that reactivity is governed only by electronic factors, neglecting the influence of the strongly heterogeneous environment, and the fact that the flexibility of short oligonucleotides can induce noticeable deviations from the canonical B-DNA parameters.

Cluster models where a reaction profile is obtained employing hybrid QM/MM (Barnett et al., 2006) or QM/QM$'$ approaches (Cauët et al., 2013; Ceron-Carrasco and Jacquemin, 2013; Jacquemin et al., 2014) provide a first step toward more realistic systems. However in these models dynamics is neglected and implicitly such schemes assume that reactivity occurs with no distortion of the B-helix (extremal nucleobases are kept frozen). Furthermore, even larger deviation of the ideal B-DNA structure can be induced by the lesions themselves, with consequences that can be crucial for further reactivity or for the repair ratio.

Structural and dynamic changes of an oxidized abasic site in ds-DNA have been studied by molecular dynamics to unravel representative conformation(s) of the double-helix and infer the role played by structural modifications on the DNA chemical reactivity (Chen et al., 2008; Patel et al., 2013). Indeed it has been shown that abasic sites shows a great conformational flexibility (Patel et al., 2013), and most notably MD has unambiguously shown that abasic site is much better stabilized in the B-DNA double strand when coupled with a cytosine. Indeed in this case the lesion is accomodated in the duplex and stabilized by a pair of hydrogen bonds, in contrast purines nucleobases may at most form one hydrogen bonds and as a consequences the lesions constantly flip in and out of the duplex. The blocking of the abasic site inside the B-DNA by cytosine has a strong consequence on reactivity since it can favor reactive conformations leading to interstrand cross-links.

Indeed, MD simulations provide a starting point for tackling the reactivity, within the framework of hybrid QM/MM-MD simulations. A decade ago Parrinello and coworkers rationalized the role of the B-DNA (Gervasio et al., 2004) on the reactivity of the guanine radical cation. This pioneer work constitutes a first probe of a reversal for the stability of the GC^+:C vs. G(−H)C :C(H)+ couple in B-DNA, which is due to the electrostatic interaction with the negatively charged backbone as well as to the different geometrical structures adopted by the pair.

QM/MM-MD simulations of DNA reactivity are becoming more and more popular, with several choices concerning the biais techniques (metadynamics Gervasio et al., 2004, umbrella sampling, thermodynamic integration Garrec et al., 2012) to sample the free energy reaction profile along one or several reaction coordinate(s).

The next subsection is devoted to theoretical studies focusing on reactions implying two nucleobases, where the distortion of the DNA structure is even larger and hence a proper dynamic description of the reaction becomes crucial.

2.3. Bridging Two Nucleobases: Structure and Reactivity

After the initial radical hit, modified nucleobases (X), such as oxidized AP, see **Figure 2**, can be formed which are prone to form covalent intra- or interstrand cross-links (ICL) with vicinal nucleobases. One often lacks the knowledge of a proper experimental structure of the damage to ascertain the conformation of the reactant, or to probe the final structure of the product (Patel et al., 2013).

Formation of ICLs obeys a multistep pathway that can be studied based on model systems (Labet et al., 2008; Sviatenko et al., 2012). But the study of ICLs also differs from single-nucleobase lesions since the B-DNA structure is much strongly impacted by the formation of this kind of defect, which could be in line with the fact they are refractory to repair.

The formation of ICLs can be formally written as X → B, where X denotes the modified (oxidized) nucleobase and B one of the four canonical nucleobases (**Figure 2**). Their modeling covers two central aspects:

1. The reactivity to situate the barrier to covalently bind two nucleobases together. This can rely on DFT calculations performed on dinucleoside monophosphate, in gas-phase or with implicit solvation. Alternatively the reactivity can be treated within a B-DNA fragment, to account notably for the helical embedding. The barrier to overcome to bridge up two nucleobases together is strongly dependent on DNA conformation and on the nucleobases themselves. However

this dependence is non trivial, and attacks corresponding to strand offset have also been reported.
2. The structural consequences of the formation of such bonds, and in particular the free-energy necessary to induce the helical deformation. In this case molecular modeling can palliate the lack of experimental structures. In particular modeling provides starting conformations of the reactant, but perhaps more importantly, provides a computationally efficient way to build up in silico the structures of a given modified oligonucleotide.

The latter point is fundamental in the absence of NMR or X-ray structure even for the most commonly formed intra- and inter-strand oxidatively-generated lesions. Also, from a modeling perspective, the typical timescale for the reorganization of a 12 base-pair oligonucleotide bearing a central defect, poses a central challenge since it spans tens of nanoseconds, to be compared to the current limitations of 10–100 ps for QM/MM-MD schemes. The identification of suitable reaction coordinates and collective variables describing the process will allow the use of rare-event accelerating methods such as meta-dynamics, however the problem is still far from being trivial. Their inherent complexity also explains why the modeling of this class of lesions is much less developed, despite their strong biological significance.

One important breakthrough in the study of intrastrand-cross links has been recently performed using Car-Parrinello QM/MM molecular dynamics (Garrec et al., 2012). In this paper the authors have performed thermodynamic integration to unravel the free-energy profile of the reaction between cytosine and a nearby C5m-thymine radical leading to the so called G[8,5-Me]T lesion. The geometrical constrains imposed by the B-DNA environment helps in keeping the reactant in an optimal π-stacked conformations, and as a results the process is characterized by a relatively low activation energy (about 10.0 Kcal/mol) on the other hand isolated nucleotides shows a rather larger deviation from the ideal conformations and as a result the activation free energy goes up to about 70.0 Kcal/mol. Furthermore, the relatively small disruption of the ideal B-helix structure induced by G[8,5-Me]T could also explain the observed low reparation rate.

All in all it clearly appears that the modeling of ground-state DNA reactivity is an extremely complicated problem requiring the correct equilibrium between a proper description of the electronic factors and a suitable sampling of the conformational space of a very flexible macromolecule. To tackle the latter problems some techniques developed in particular in the field of the enzymatic catalysis (Garcia-Mesenguer et al., 2013; Zinovjev et al., 2013; Zinovjev and Tunon, 2014) should be considered both to define proper reaction pathways and to perform a good sampling compatible with the reaction time-scale. On the other hand the problem of an accurate sampling of the conformational space or of the definition of suitable collective variables is less dramatic when dealing with excited-state phenomena, i.e., photochemistry and photophysics, even if still the coupling of electronic factors with vibrational and dynamical ones cannot be underestimated. These aspects will be the focus of the next section.

3. Interaction between DNA and UV Radiation

DNA is constituted by π-stacked nucleobases that can be regarded as chromophores and whose absorbance is mostly confined in the UVB regions of the spectrum. The absorption region capable of producing DNA lesions can be enlarged for instance by photosensitization, i.e., by the interaction with endogenous or exogenous compounds (Epe, 2012; Cadet and Wagner, 2013).

3.1. Direct UV Absorption and Decay

Even if UVB wavelengths are normally filtered by the ozone layer, and efficient deactivation pathways of the nucleobases excited states exist, DNA lesions resulting from direct photoactivation are usually reported and are considered as extremely dangerous for their potential carcinogenicity.

The photochemical pathways leading to the formation of the cyclobutane thymine dimer ($T <> T$) and of the 6-4 photoadducts [(64)-PP] in the case of stacked nucleobases has been the subject of interesting combined theoretical and spectroscopic study (Banyasz et al., 2012). After a thoughtful validation of TDDFT techniques by comparison with high-level CASPT2 techniques the authors efficiently analyze the differences between the paths leading to the two main photoproducts [$T <> T$ or (64)-PP]. In particular in the case of $T <> T$ dimerization, after absorption at 5.36 eV, an efficient and barrierless path in the first $\pi\pi^\star$ excited state leads to a short lived minimum at 4.45 eV connected to the conical intersection (CI) region. Furthermore, the CI is characterized by a very short inter-monomer distance, most notably the C5-C5′ and the C6-C6′ distances have been found to be of 2.5 and 2.06 Å, respectively, hence the topology of the CI clearly favors dimerization. Notably, no sterical hindrance or electrostatic effect due to the backbone are observed. On the contrary the formation of the (64)-PP adducts, and in particular of the key oxetane intermediate, involves the population of a charge transfer (CT) state. The CT state involves both thymines and is found at 5.50 eV. From Franck-Condon region the excited states may relax toward a very short living minimum that efficiently evolves toward the oxetane conical intersection region. Once again, the geometrical features of this conical intersection favor dimerization, in particular very short intermonomer distances are found (C6-C4′ 2.46 Åand C5-O8′ 1.65 Å). Note that environment effects are crucial since the backbone charges efficiently stabilize the charge-separated state compared to the gas-phase situation, and hence strongly favor its population. Furthermore, a barrier in the CT state potential energy surface, and probably due to dynamical solvent effects, needs to be overcome. This fact supports the evidence that although the CT state is reachable upon UVA irradiation, shorter wavelengths excitation are needed to allow the system the excess kinetic energy.

Recently, more complex photochemical mechanisms have been taken into account (Esposito et al., 2014). Once again combining spectroscopy and modeling, the study of a trinucleotide of sequence TCG allowed to gain insight into the competition between the formation of cyclobutane pyrimidine

dimer (CPD) and (64)-PP adducts. Interestingly the role of the methylation of the 5′ position of guanine has been shown to be far from innocent in dictating the relative ratio between the CPD and (64)-PP. Indeed, the authors found that upon methylation the ratio between the quantum efficiency for the CPD production versus the (6-4)PP one ($\varphi_{CPD}/\varphi_{(6-4)PP}$) goes from 1.52 to 3.68. The important increase of the selectivity toward CPD has been rationalized by combining QM and MD calculations and ascribed to the sugar puckering which modulates the stacking arrangement of the reactants. Indeed, methylation strengthens interaction with flanking T and globally stabilizes conformers that are more reactive toward CPD formation. Since C5 position metyhylation of guanine is known to play important role in epigenetic gene regulations and is found as hot-spot in skin cancer the biological relevance of these findings are evident. The influence of the double helical pairing has also been taken into account, globally confirming the previous results.

The same group (Vayá et al., 2012) has also revealed the role of the DNA structural organization in dictating its spectroscopic and photochemical properties. Indeed the exciton coupling of the nucleobases is reflected in an energy- and charge-transfer along the double helix that is reflected in the fact that DNA lesions hot-spot depend on the nearby base sequence and are not randomly distributed. From a photophysical point of view an interplay between charge and energy transfer is observed. Still it will be important to determine the sequence effects favoring charge-separation and charge-recombination.

Barbatti and Lischka have reported a systematic study of the deactivation pathways for the four DNA nucleobases (adenine, thymine, guanine and cytosine) as well as for uracil (Barbatti et al., 2010). The use of non-adiabatic state-hopping molecular dynamics (Barbatti, 2011) has allowed the authors to give clear insights on the deactivation pathways and to reveal two distinct behaviors between purines and pyrimidines. Indeed, adenine and guanine have a relatively simple photodynamic, characterized by a rapid evolution from the $\pi\pi^\star$ up to the conical intersection, where they are funneled back to the S_0 ground state. This simple mechanism is also reflected in the extremely fast deactivation with an estimated excited state life time of 0.28 and 0.77 ps for guanine and adenine, respectively. In contrast, for pyrimidines a much more complicated situation is found with the competition of two channels: one evolving to the $\pi\pi^\star$ conical intersection and the other one toward the $n\pi^\star$ crossing seam. The ratio between the two channels depending on the bases, for instance in cytosine the direct $\pi\pi^\star$ path is not activated at all. The more complex photochemistry of pyrimidine bases, also due to the presence of low lying $\pi\pi^\star$ states with flatter potential energy surfaces, is reflected in the longer life-time of excited states spanning values from 0.53 to several ps.

Robb group (Groenhof et al., 2007) also reported a computational study of the deactivation pathways of a cytosine-guanine base-pair both in gas phase and embedded in a DNA environment. Their QM and QM/MM multiconfigurational calculations revealed that the deactivation pathway starts with a proton transfer, that is followed by a radiationless decay leading to an extended conical intersection seams. Indeed, the particular topology of the conical intersection systems may lead to a number of crossings between the first excited and the ground state, that may ultimately lead to a diabatic blockage. After the crossing to the ground state the proton is transferred back and in a majority of situation the initial conformation is restored. Interestingly, comparing QM and QM/MM calculations, the authors conclude that the Watson-Crick pairing keeping the base pair closer together enhanced photostability minimizing the fraction of trajectory ending up in a different tautomeric state compared to the initial configuration.

Novel strategies to prove the photostability of DNA nucleobases start emerging, notably very recently Garavelli's group reported the modeling of near UV 2D-electronic spectroscopy as a tool to characterize the double excited, multi excimer and charge-transfer states that may be responsible of the ultrafast deactivation dynamics. These advancements could pave the way toward a better interplay between theory and modeling to give an atomistic level description of the different dynamic phenomena (Nenov et al., 2015).

Although, extremely efficient DNA relaxation pathways may lead to a drawback evidenced by the works of Gonzalez's group that have underlined a femtosecond intersystem crossing taking place in the case of cytosine (Richter et al., 2012). The explicit inclusion of spin-orbit coupling in the calculation of the hopping probability has evidenced a non-negligible population of the triplet state manifold, indeed after 140 fs the $T1$ state has an important population of 10%. This striking result, even if it neglects the environment, is extremely important from a photophysical point of view, since it illustrates a situation in which the quasi-degeneracy between triplets and singlets compensates the moderate, but non-negligible, value for the spin-orbit coupling. Moreover, from a more biological point of view, if confirmed in the DNA embedding it may open the way to the population of triplet states, that could be responsible of indirect production of DNA lesions.

3.2. DNA Photosensitization

In DNA photosensitization the absorption of light and the subsequent photochemical pathways are mediated by an interacting chromophore. By definition in the case of sensitization the chromophore needs to be recovered inaltered at the end of the process, acting in an almost catalytical way. This excludes covalent interactions with DNA that characterize the action of important antitumoral drugs such as the cisplatin.

The study of DNA photosensitization is complicated by the fact that one should be able to achieve a good knoweldge of different phenomena. First of all, a clear picture of the structure of the DNA/sensitizers aggregate is compulsory. Usually three main modes of interaction have been characterized for canonical B-DNA (Zeglis et al., 2007), see **Figure 3**:

- **Groove Binding**. In which the sensitizer lies close to the DNA grooves, and stabilization is mostly driven by electrostatic interactions with the negatively charged backbone. Note that usually a rather important selectivity is evidenced between the minor or major groove, and that the double-helical structure is only scarcely distorted.

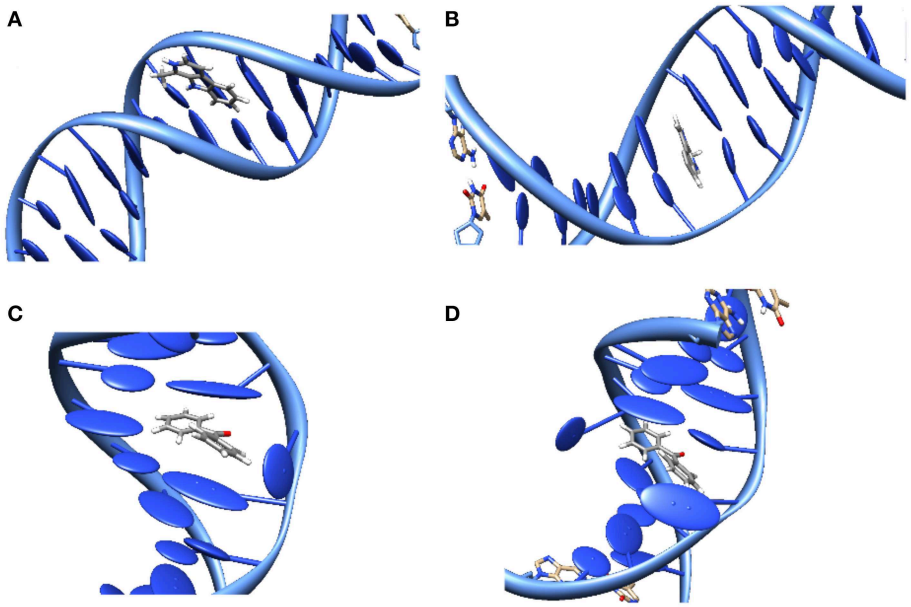

FIGURE 3 | Representation of the main interaction modes between DNA and sensitizers. (A) Groove-Binding; **(B)** Intercalation; **(C)** Insertion; **(D)** Double Insertion.

- **Intercalation**. In which the sensitizer slips between two base pairs. The stabilizing interactions are mostly due to dispersion and π-stacking with the DNA nucleobases, and hence this mode is predominant for rather large, planar, conjugated structures. The DNA helix is slightly more perturbed since an intercalation pocket needs to be created.
- **Insertion**. In which the sensitizer ejects one of the bases from its Watson-Crick pairing, taking its place in the helix. Conjugated systems with non-collinear fused rings, i.e., mimicking the pyrimidine geometries, are the most likely to prefer insertion over intercalation.

Moreover the three interaction modes can most often coexist, with a population ratio strongly dependent on the environmental factors such as the DNA sequence or the salt concentration. As a consequence, X-Ray resolved structures are quite rare, and structural determination becomes crucial, requiring a proper modeling that may confirm more indirect experimental observation such as the ones based on circular dichroism.

On that context we should cite the extensive molecular simulations performed by the Lavery group using molecular dynamics and different sampling techniques such as metadynamics and umbrella sampling (Wilhelm et al., 2012). The authors were able to unambigously determine two stable states for the binding of Daunomycin drug to DNA: minor groove binding and intercalation. Furthermore, they were able to recover the free energy profile along the pathway connecting the two modes. A thermally accessible low barrier of about 6.5 kcal/mol was indeed found to separate the two stable modes, with intercalation being about 2.0 kcal/mol more stable. Interestingly, also an intermediate state was found with the drug only partially intercalated while DNA is strongly bended away from the drug. This intermediate state, sometimes called semi-intercalation, is also found in a number of other drugs or even in the case of minor-groove binding protein. In the case of daunomycin, however, the particularity lies in the fact that it is only connected to a very shallow minimum in the free energy profile, and hence does not constitute a kinetic blockage for the full intercalation.

Also the interaction between simple organic molecules and DNA should be described most carefully, which necessitates the resort to molecular dynamic simulations to sample the relevant possible conformations. A particularly striking case is the one of benzophenone, a paradigmatic sensitizers (Cuquerella et al., 2012), for which no experimental structure has ever been reported for the interaction with DNA. Indeed, by analyzing the molecular dynamics trajectory only 2 stable interaction modes were evidenced (Dumont and Monari, 2013), one of them was the usual minor-groove binding, but the second one was a novel mode called "double insertion" (**Figure 3**). In this mode the sensitizer, benzophenone, ejects both the bases constituting the Watson-Crick pair and take the place of both in the stacked structure. The use of the so-called non covalent interactions (NCI) technique to visualize non-covalent interaction (Johnson et al., 2010) allowed to pinpoint the emergence of a very strong hydrogen-bond between the ejected base and the phosphate of the backbone as one of the factors explaining the stabilization of the double-insertion mode, even in presence of a strong helical deformation. Furthermore, the calculation of induced circular dichroism, using QM/MM methods coupled to the MD simulation, evidenced a clear spectroscopic signature for the double-insertion in the UVA region that could allow for an easy experimental confirmation (Dumont and Monari, 2013). Indeed, while the minor groove-bound benzophenone does not show any

induced circular dichroism spectra, the double-inserted mode presents a well resolved negative band at 350 nm, corresponding to the $n\pi^\star$ excitation. Since this band belongs to the UVA and is far from the native DNA absorbing region it is supposed that it could allow for a quite straightforward discrimination of the interaction modes. Recently and independently the double-inserted mode has been also evidenced in the case of copper complexes interacting with DNA (Galindo-Murillo et al., 2015) using very long scale molecular dynamics up to the μs scale.

Photosensitization involving the excitation of the chromophore, and the subsequent excited-state interactions with the nearby nucleobases, the influence of the environment on excited state properties is crucial and should be thoughtfully taken into account. Indeed the optical properties of many chromophores can be modulated by the environment, one of the most well known cases being the light-switch effects (Friedman et al., 1990), i.e., the activation of luminescence induced by DNA for the Ruthenium complex $[Ru(dppz)(bipy)_2]^{2+}$ (bpy = 2,2′-bipyridine; dppz = dipyridophenazine). Indeed the latter complex happens to be dark in water, weakly luminescent in non protic solvent like acetonitrile and strongly luminescent in water. One of the first rationalization of this phenomenon was proposed by Batista, using TDDFT calculations coupled with a continuum description of the environment and a micro-hydration scheme (Batista and Martin, 2005). Batista suggested the presence of two quasi-degenererate triplet states: one metal to ligand charge-transfer (MLCT) centered on the dppz ($^3MLCT_{dppz}$) and one intraligand (IL) $\pi\pi\star$ triplet still centered on the dppz ($^3IL_{dppz}$). The authors attribute the quenching of luminescence by water to the stabilization of the dark $^3MLCT_{dppz}$ that becomes the lowest triplet state and hence easily populated. The stabilization would be mostly due to hydrogen bonds between solvent molecules and the nitrogen dppz atoms.

More recently a refined explanation for the light-switch effect was offered coupling a multiscale modeling to describe the interactions with the surroundings together with TDDFT and high level ab-initio calculations. Firstly the intercalation interaction mode and the main features of the absorption spectrum of $[Ru(dppz)(bipy)_2]^{2+}$ interacting with DNA were modeled, also taking into account polarizable embedding and validating the computational protocol (Very et al., 2012). To this end the presence of the charge-transfer band due to the Ruthenium complex was evidenced at around 450 nm. The band was assigned to a complex manifold of different metal-to-ligand (MLCT) transitions. Subsequently (Very et al., 2014), the triplet excited state manifold of $[Ru(dppz)(bipy)_2]^{+2}$ in different environments, namely water, acetophenone and DNA was computed, and the distribution of electronic density analyzed. The authors concluded that in water the dark $^3MLCT_{dppz}$ state was populated being the lowest one upon geometry relaxation, in acetonitrile on the other hand the lowest triplet excited state was still of MLCT character but was centered both on the dppz and bipy ligands ($^3MLCT_{dppz/bipy}$) since in contrast to the dppz centered one the $^3MLCT_{bipy}$ are brights the mixed $^3MLCT_{dppz/bipy}$ can be considered as weakly emissive, coherently with the experiment. Finally in the case of intercalation in DNA the triplet state becomes now entirely centered on the bipy ancillary ligand ($^3MLCT_{bipy}$) giving rise to a bright state and hence to the triggering of luminescence. Therefore, the light-switch effect does not happen because of a competition between MLCT and IL triplet states but instead by a change in the electronic density reorganization of the MLCT states operated by the environment.

Usually photosensitization can be classified considering the physical phenomenon producing the lesion with DNA. Type I photosensitization is due to a charge transfer usually toward guanine, type II sensitization on the other hand is based on an energy-transfer between the sensitizer (triplet) excited state and molecular oxygen giving raise to $^1O_2$ and the subsequent oxidative events. Finally, one should also take into account triplet photosensitization characterized by an energy-transfer between the photosensitizers and DNA bases, usually thymine; thymine dimers are the most common final products of triplet sensitization. Since the physical processes underlining these photosensitization pathways are different, modeling strategies should be tailored to provide a satisfactory description.

Concerning type I photosensitization some evidences of important electron transfer between nearby guanine and different ruthenium complexes have been reported already at Franck-Condon level using QM/MM performed with an extended QM partition and TDDFT calculations (Chantzis et al., 2013). Indeed, in this contribution the authors have calculated the absorption spectrum of ruthenium complexes intercalated in DNA extending the QM partition to accommodate the nearby guanine and adenine base. By analyzing the electron density reorganization, it has been shown that some vertical transitions exist around 300 nm characterized by a very strong charge-transfer, the calculation of natural population analysis (NPA) charges have allowed to estimate such charge-transfer to be close to 0.7 electron.

Also in the case of type II sensitization the role of the environment may be far from innocent. For instance in the case of a DNA interacting drug known as palmatine the production of $^1O_2$ as well as fluorescence is triggered only by interaction with DNA (Hirakawa et al., 2012). Once again only QM/MM methods coupled with MD allows for a rationalization of the photochemical pathways (Dumont and Monari, 2015). Indeed, it was shown that in water solution upon excitation to a valence $\pi\pi\star$ (3.0 eV), state palmatine relaxation crosses a CT state that happens to be, at his relaxed geometry, lower in energy than the valence state (3.8 against 4.0 eV, respectively). This fact opens the way to efficient non-radiative pathways and hence induces quenching of luminescence and the inhibition of singlet oxygen production. In the case of the interactions with DNA (happening through minor-groove or insertion) already at Franck-Condon geometry the CT state is strongly destabilized by more than 1 eV comparing to the water-solution case. As a consequence the crossing with the $\pi\pi\star$ state is impossible even after geometry relaxation. Therefore, when interacting with DNA, palmatine evolves toward the S_1 ($\pi\pi\star$) state that can subsequently either relax radiatively (fluorescence) or give intersystem crossing to populate the triplet state and produce $^1O_2$. Intersystem crossing is also supported by the high spin-orbit

coupling calculated to be of the order of 40 cm^{-1}. We note that in this contribution (Dumont and Monari, 2015), it was evidenced that in the case of planar conjugated systems, the calculation of the absorption spectrum necessitates to take into account the effect of the low-frequency vibration modes, for instance through the coupling with MD. Indeed the calculation of absorption spectrum with static procedures gives totally unreliable results. Indeed, static absorption spectrum has a shift of about 100 nm compared to experimental results, while the inclusion of dynamic effects allows to perfectly match the observed absorption maximum (420 nm) providing one uses a long-range corrected functional. This situation was also observed for other DNA interacting systems such as the β-carboline harmane both for absorption and fluorescence spectra (Etienne et al., 2013, 2014).

The role of the environment in tuning type II photosensitization, and in particularly in driving the population of the triplet manifold was recently pointed out by Nogueira et al. in the case of the interaction between DNA and phenothiazinium dyes (Nogueira et al., 2015). The author evidenced that while in water solution intersystem-crossing is only driven by relatively inefficient vibronic spin-orbit coupling, the interaction with DNA modifies the energy order of the excited states and hence opens the way to a second symmetry allowed crossing. Indeed, in water solution the dye has to overcome significant barriers both from Franck-Condon region and S_1 minimum (0.77 and 0.51 eV, respectively) to reach the symmetry allowed intersystem crossing between S_1 and T_3. On the other hand in DNA, mostly because of the hydrogen-bonding networks, the modified potential energy landscape for singlet and triplet results in a significant lowering of the barriers that assume values of 0.15 and 0.30 eV, for Franck-Condon or S_1 minimum, respectively hence the intersystem crossing region can now be safely reached thanks to thermal energy and $^1O_2$ ne produced. The observed production of singlet oxygen in water is ascribed to the coupling between electronic and vibrational movements, i.e., to the so called vibronic spin-orbit coupling, happening between S_1 and T_2 state, however this channel being less effective that the fully allowed electronic spin-orbit coupling with T_3 the enhancement in the production of $^1O_2$ by the DNA environment is confirmed.

Triplet photosensitization is also an experimentally-known component of DNA damage that can be timely tackled by modeling. Since it involves the preliminary population of the photosensitizer triplet state manifold, one may ask if the macromolecular environment keeps the road to photosensitization open, or if it hinders its development. Acetophenone is a known triplet photosensitizer (Epe, 2012) and its efficiency is due to a very efficient population of the triplet state in gas phase (Huix-Rotllant et al., 2013). Molecular dynamics simulations have allowed to identify acetophenone stable interaction mode with DNA, namely intercalation (Huix-Rotllant et al., 2015). Furthermore, QM/MM calculations, performed both at CAS-PT2 and TDDFT level of theory, have shown that the gas-phase quasi-degeneracy of the first singlet excited state S_1 with the two $\pi\pi\star$ and $n\pi\star$ triplet state is not significantly altered by the environment (Huix-Rotllant et al., 2015). The authors have also evidenced that all along the MD trajectory the spin-orbit coupling between the S_1 and at least one of the triplet is always quite high (about 20 cm^{-1}), i.e., a value that allows efficient intersystem crossing if the energy difference between the states is small (Richter et al., 2012). One of the most striking features of gas phase acetophenone photohysics, explaining the high-efficiency of the intersystem crossing is indeed the presence of a three-point crossing between the singlet and the two triplets. In presence of DNA although the perfect crossing is lifted the two intersections still happens in a very close-by region of the configuration space (Huix-Rotllant et al., 2015). All these results point toward the fact that the DNA environment does not alter the efficient photophysical pathways leading to acetophenone triplet population during the very first vibrational motions. This in turn points toward the rationalization of the efficient DNA photosensitization experienced by acetophenone.

But in order to be efficient in terms of triplet-photosensitization, the population of the triplet manifold should be rapidly followed by energy transfer to the nearby thymine. This aspect has been recently deeply analyzed for the case of benzophenone (Dumont et al., 2015). The energy profile for the benzophenone-DNA triplet transfer has been obtained following an approximate reaction coordinate both for a double-inserted and a minor-groove bound benzophenone. Calculations have been performed by QM/MM to take into account the environment effects, while triplet energy has been obtained both at CASPT2 and TD-DFT level. In particular it has been evidenced that for double-insertion two very efficient and barrierless sensitization channels exist one proceeding from the T_1 state ($n\pi\star$) and the other from the T_2 ($\pi\pi\star$) triplet. On the contrary in the case of minor-groove binding the T_1 sensitization channel is hampered by a significant barrier (0.30 eV), while the T_2 channel is still active and virtually barrierless. Furthermore, it has been evidenced that due to the close-by distance of the interacting chromophores the transfer will proceed through the Dexter mechanism mainly driven by the electronic densities overlap. Estimation of the overlap has shown a slightly pronounced kinetic preference for the double-insertion mode, but still shows that the transfer from minor-groove is possible and efficient although with a 100 times lower efficiency compared to the double-inserted situation.

Obviously a deeper characterization of energy- and electron-transfer processes will necessitate to take into account non-adiabatic and state-hopping dynamics. Furthermore, since the triplet manifolds are involved in most of the cases the spin-orbit coupling should not be neglected. This aspect coupled with the necessity to take into account the environment and many interacting chromophores and the relative long time scale of the full sensitization process will necessitate a considerable computational effort that can be achieved only through a proper methodological development. Still significant progresses have been made allowing to get a clearer vision of a fundamental and rather complicated process whose biological relevance cannot be underestimated.

4. Sensitizing Non-canonical DNA Structures

Even if the canonical B-DNA form is by far the most common one, particular DNA sequences may adopt the so-called non-canonical conformations. The biological relevance of such structures is now clearly evidenced. On that context particular significance has to be attributed to the guanine-quadruplex (G4), that are present in guanine-rich sequences such as the telomeres (Neidle and Parkinson, 2003). Telomeres protecting activity is a key factor to regulate cellular apoptosis, indeed the activation of telomerase, which is overexpressed in a vast majority of tumor cell lines, is strongly related to cancer cells uncontrolled replication (Neidle and Parkinson, 2002). The stabilization of G4 structures by DNA sensitization may result in an inhibition of the telomerase (Neidle, 2010), hence opening the way to novel anticancer therapies. In particular the selectivity of the sensitizer toward G4, instead of canonical DNA structure, will be a key factor governing the overall selectivity of the drug toward cancer cells.

The relative peculiar structure of G4 has necessitated an important computational effort to rationalize their structure and their stability (Ilchenko and Dubey, 2014), as well as the the sequence effects governing their formation. Furthermore, since G4 are stabilized by interactions with cations to compensate the negative charges the pH and salt concentrations are key factors determining their appearance. In a vast majority of studies (Ilchenko and Dubey, 2014) QM methods were used to analyze the stabilizing factors of G4. Systematic DFT studies were performed (Jissy et al., 2011), in addition the role of different cations stabilizing the central channel was investigated in particularly connected to the emergence of polarizability anisotropy that may induce birifrangence potentially exploitable in biomolecular imaging.

A rather serious complication in the study of G4 is connected to the polymorphism observed for such structures (Ilchenko and Dubey, 2014). This experimentally observed evidence, has also been rationalized by other DFT calculations (Fonseca Guerra et al., 2010), in particular the role of the hydrogen-bond networks has been evidenced. Some of the same authors have also proposed new possible monomers leading to the formation of quadruplexes structure such as substituted xanthines (Szolomajer et al., 2011).

In parallel, the necessity to correctly represent the polymorphism of the G4 non-canonical structures has pushed toward the validation of force-fields, which are usually parameterized to reproduce the behavior of canonical B-DNA (Grunenberg et al., 2014). The comparison of force field descriptions with DFT calculations shows that extreme care should be taken to model the competitive rotamers. In particular while the OPLS and the MMFF force fields correctly reproduce experimental and DFT results, the DNA-popular Amber force field gives the opposite energy-order.

However, the combination of well parameterized force fields and of QM and QM/MM techniques allows to correctly reproduce the interaction of sensitizers with G4. The most common G4 sensitizers are rather extended and planar π-conjugated cations (Ilchenko and Dubey, 2014). Recently, Barone group (Terenzi et al., 2014) has used molecular modeling to predict the relative stability of G4 vs. B-DNA aggregates with square-planar organometallic Schiff-base complexes containing copper and zinc. MD simulations have shown that the Schiff-base strongly interact with G4 both via electrostatic interactions and through efficient π-stacking. The estimation of the G4/sensitizer free energy of formation gives values ranging from -34.6 to -14.4 kcal/mol therefore speaking in favor of a stable complex. It is noteworthy that these results have also been supported by biological tests confirming a potential anti-cancer activity.

It is evident that despite some difficulty the sensitization of non-canonical DNA structure, both at the ground and for the excited-state, is no more considered as an exotic novelty. On the contrary it is displaying all its potentiality in the rational design of novel therapeutic strategies. Molecular modeling is playing an active role on the field and will certainly drive not only the comprehension of the mechanisms leading to a selective sensitization, but also the prediction of entirely novel sensitizers.

5. Conclusions

The impressive progresses of modeling and simulation techniques have now made possible tackling problems as complex as the generation of oxidatively-induced DNA lesions and the interaction of DNA with potential drugs. However, this domain should still be considered very challenging also from a computational chemistry point of view. Indeed, many different factors should be taken into account and treated on the same footing to have a proper, and biologically relevant, description of the various phenomena comming into play.

Particular attention should be taken for instance to model the conformational degrees of freedom of the very flexible DNA macromolecule, this of course calls for adequate and long-scale molecular dynamics trajectory. Techniques allowing a good estimate of the free-energy, especially but not exclusively, in the case of sensitization binding energies are also of paramount importance. This aspect will of course require the development of efficient force fields as well as of proper sampling techniques.

The study of the electron density reorganization taking place on the ground- or on the excited states is also fundamental to go beyond the simple structural description and propose hints on the reactivity or the photochemistry of DNA alone or in presence of sensitizers. The envisaged QM or QM/MM techniques should conjugate the precision of the description with the efficiency necessary to make possible the sampling of important region of the configuration space, and hence having access to good statistical properties. This is especially true since in many case energy- or electron-transfer phenomena have to be taken into due accounts, i.e., one has to deal with some of the most challenging situations for QM methods.

We believe that from a methodological point of view the development of novel multiscale techniques in particular for what concerns excited state non-adiabatic dynamics as well as ab-initio QM/MM dynamics will allow the treatment of more and more complex scenarios, coupling a good accuracy with good statistics. On that context the development of proper sampling techniques allowing the definition of good and physical relevant

reaction coordinates taking into account all the relevant collective variables will certainly be one of the most important challenges of the next years.

Nowadays, the atomistic scale description of DNA related phenomena offered by multiscale modeling allows to rationalize and properly describe phenomena as diverse as the behavior of DNA under oxidative stress or the environment controlled behavior of phototherapy drugs. The selectivity of potential drug candidates toward different DNA configurations as well as the differential dynamical behavior of different DNA sequences are now accessible at least at a semi-quantitative level.

Modern day molecular modeling is therefore able to provide a molecular and electronic description of the factor governing DNA chemistry under external perturbation, therefore molecular modeling can nowadays be considered as a fundamental tool to provide unprecedented insights in chemical biology. Conversely, the knowledge of the mechanism of DNA lesions induction are also paving the way to the rational design of novel therapeutic agents. Therefore we may safely say that the communication between the *in silico* world of molecular modeling and the *in vitro* world of biological chemistry and cellular biology is now a sounding and promising reality.

Author Contributions

Both authors contributed equally to the present review.

Acknowledgments

This work has been performed in the framework of the COST Action "Biomimetic Radical Chemistry" whose support is gratefully acknowledged. AM thanks CNRS for the funding of the "chaire d'excellence" program. The authors thanks Dr. Raymond Grüber for useful discussion and for providing some of the figures.

References

Abolfath, R. M., Biswas, P. K., Rajnarayanam, R., Brabec, T., Kodym, R., and Papiez, L. (2012). Multiscale QM/MM molecular dynamics study on the first steps of guanine damage by free hydroxyl radicals in solution. *J. Phys. Chem. A* 116, 3940–3945. doi: 10.1021/jp300258n

Abolfath, R. M., van Duin, A. C. T., and Brabec, T. (2011). Reactive molecular dynamics study on the first steps of DNA damage by free hydroxyl radicals. *J. Phys. Chem. A* 115, 11045–11049. doi: 10.1021/jp204894m

Agostinis, P., Berg, K., Cengel, K. A., Foster, T. H., Girotti, A. W., Gollnick, S. O., et al. (2011). Photodynamic therapy of cancer: an update. *Cancer J. Clin.* 61, 250–281. doi: 10.3322/caac.20114

Antonarakis, E. S., and Emadi, A. (2010). Ruthenium-based chemotherapeutics: are they ready for prime time? *Cancer Chemother. Pharmacol.* 66, 1–9. doi: 10.1007/s00280-010-1293-1

Balasubramanian, B., Pogozelski, W. K., and Tullius, T. D. (1998). DNA strand breaking by the hydroxyl radical is governed by the accessible surface areas of the hydrogen atoms of the DNA backbone. *Proc. Natl. Acad. Sci. U.S.A.* 95, 9738–9743. doi: 10.1073/pnas.95.17.9738

Banyasz, A., Douki, T., Improta, R., Gustavsson, T., Onidas, D., Vayá, I., et al. (2012). Electronic excited states responsible for dimer formation upon UV absorption directly by thymine strands: joint experimental and theoretical study. *J. Am. Chem. Soc.* 134, 14834–14845. doi: 10.1021/ja304069f

Barbatti, M. (2011). Nonadiabatic dynamics with trajectory surface hopping method. *Wiley Interdiscipl. Rev. Comput. Mol. Sci.* 1, 620–633. doi: 10.1002/wcms.64

Barbatti, M., Aquino, A. J. A., Szymczak, J. J., Nachtigallová, D., Hobza, P., and Lischka, H. (2010). Relaxation mechanisms of UV-photoexcited DNA and RNA nucleobases. *Proc. Natl. Acad. Sci. U.S.A.* 107, 21453–21458. doi: 10.1073/pnas.1014982107

Barnett, R. N., Bongiorno, A., Cleveland, C. L., Joy, A., Landman, U., and Schuster, G. B. (2006). Oxidative damage to DNA: counterion-assisted addition of water to ionized dna. *J. Am. Chem. Soc.* 128, 10795–10800. doi: 10.1021/ja061795y

Batista, E. R., and Martin, R. L. (2005). On the excited states involved in the luminescent probe [Ru(bpy)2dppz]2+. *J. Phys. Chem. A* 109, 3128–3133. doi: 10.1021/jp050673+

Bera, P. P., and Schaefer, H. F. (2005). (GH)$^{\bullet}$C and G(CH)$^{\bullet}$ radicals derived from the guanine–cytosine base pair cause dna subunit lesions. *Proc. Natl. Acad. Sci. U.S.A.* 102, 6698–6703. doi: 10.1073/pnas.0408644102

Bergeron, F., Auvre, F., Radicella, J. P., and Ravanat, J.-L. (2010). HO· radicals induce an unexpected high proportion of tandem base lesions refractory to repair by DNA glycosylases. *Proc. Natl. Acad. Sci. U.S.A.* 107, 5528–5533. doi: 10.1073/pnas.1000193107

Besic, E., Sankovic, K., Gomzi, V., and Herak, J. N. (2001). Sigma radicals in gamma-irradiated single crystals of 2-thiothymine. *Phys. Chem. Chem. Phys.* 3, 2723–2725. doi: 10.1039/b103210k

Brabec, V., Reedijk, J., and Leng, M. (1992). Sequence-dependent distortions induced in dna by monofunctional platinum(II) binding. *Biochemistry* 31, 12397–12402. doi: 10.1021/bi00164a014

Brash, D. E. (2015). UV signature mutations. *Photochem. Photobiol.* 91, 15–26. doi: 10.1111/php.12377

Bulent, A., Wesley, E. B., Steven, G. S., James, E. T., and David, T. M. (2008). (monte carlo) simulations of site-specific radical attack to DNA bases. *Radiat. Res.* 169, 223–231. doi: 10.1667/RR0293.1

Cadenas, E., and Davies, K. J. (2000). Mitochondrial free radical generation, oxidative stress, and aging1. *Free Rad. Biol. Med.* 29, 222–230. doi: 10.1016/S0891-5849(00)00317-8

Cadet, J., Delatour, T., Douki, T., Gasparutto, D., Pouget, J.-P., Ravanat, J.-L., et al. (1999). Hydroxyl radicals and DNA base damage. *Mutat. Res. Fundament. Mol. Mech. Mutagenes.* 424, 9–21. doi: 10.1016/S0027-5107(99)00004-4

Cadet, J., and Wagner, J. R. (2013). DNA base damage by reactive oxygen species, oxidizing agents, and UV radiation. *Cold Spring Harb. Perspect. Biol.* 5:a012559. doi: 10.1101/cshperspect.a012559

Carvlin, M. J., Datta-Gupta, N., and Fiel, R. J. (1982). Circular dichroism spectroscopy of a cationic porphyrin bound to DNA. *Biochem. Biophys. Res. Commun.* 108, 66–73. doi: 10.1016/0006-291X(82)91832-0

Cauët, E., Bogatko, S., Lievin, J., De Proft, F., and Geerlings, P. (2013). Electron-attachment-induced DNA damage: instantaneous strand breaks. *J. Phys. Chem. B* 117, 9669–9676. doi: 10.1021/jp406320g

Ceron-Carrasco, J. P., and Jacquemin, D. (2013). Electric field induced DNA damage: an open door for selective mutations. *Chem. Commun.* 49, 7578–7580. doi: 10.1039/c3cc42593b

Chaiyen, P., Fraaije, M. W., and Mattevi, A. (2012). The enigmatic reaction of flavins with oxygen. *Trends Biochem. Sci.* 37, 373–380. doi: 10.1016/j.tibs.2012.06.005

Chantzis, A., Very, T., Daniel, C., Monari, A., and Assfeld, X. (2013). Theoretical evidence of photo-induced charge transfer from DNA to intercalated ruthenium (II) organometallic complexes. *Chem. Phys. Lett.* 578, 133–137. doi: 10.1016/j.cplett.2013.05.068

Chen, J., Dupradeau, F.-Y., Case, D. A., Turner, C. J., and Stubbe, J. (2008). DNA oligonucleotides with A, T, G or C opposite an abasic site: structure and dynamics. *Nucleic Acids Res.* 36, 253–262. doi: 10.1093/nar/gkm622

Cooke, M. S., Evans, M. D., Dizdaroglu, M., and Lunec, J. (2003). Oxidative DNA damage: mechanisms, mutation, and disease. *FASEB J.* 17, 1195–1214. doi: 10.1096/fj.02-0752rev

Cuquerella, M. C., Lhiaubet-Vallet, V., Cadet, J., and Miranda, M. A. (2012). Benzophenone photosensitized dna damage. *Accoun. Chem. Res.* 45, 1558–1570. doi: 10.1021/ar300054e

Ding, S., Kolbanovskiy, A., Durandin, A., Crean, C., Shafirovich, V., Broyde, S., et al. (2009). Absolute configurations of DNA lesions determined by comparisons of experimental ECD and ORD spectra with DFT calculations. *Chirality* 21, E231–E241. doi: 10.1002/chir.20804

Dougherty, T. J., Gomer, C. J., Henderson, B. W., Jori, G., Kessel, D., Korbelik, M., et al. (1998). Photodynamic therapy. *J. Natl. Cancer Inst.* 90, 889–905. doi: 10.1093/jnci/90.12.889

Dumont, E., and Monari, A. (2013). Benzophenone and DNA: evidence for a double insertion mode and its spectral signature. *J. Phys. Chem. Lett.* 4, 4119–4124. doi: 10.1021/jz4021475

Dumont, E., and Monari, A. (2015). Interaction of palmatine with DNA: an environmentally controlled phototherapy drug. *J. Phys. Chem. B* 119, 410–419. doi: 10.1021/jp5088515

Dumont, E., Wibowo, M., Roca-Sanjuan, D., Garavelli, M., Assfeld, X., and Monari, A. (2015). Resolving the benzophenone DNA-photosensitization mechanism at QM/MM level. *J. Phys. Chem. Lett.* 6, 576–580. doi: 10.1021/jz502562d

Duncan Lyngdoh, R. H., and Schaefer, H. F. (2009). Elementary lesions in DNA subunits: electron, hydrogen atom, proton, and hydride transfers. *Acc. Chem. Res.* 42, 563–572. doi: 10.1021/ar800077q

Durbeej, B., and Eriksson, L. A. (2003). On the formation of cyclobutane pyrimidine dimers in UV-irradiated DNA: why are thymines more reactive? *Photochem. Photobiol.* 78, 159–167. doi: 10.1562/0031-8655(2003)078<0159:OTFOCP>2.0.CO;2

Epe, B. (2012). DNA damage spectra induced by photosensitization. *Photochem. Photobiol. Sci.* 11, 98–106. doi: 10.1039/C1PP05190C

Esposito, L., Banyasz, A., Douki, T., Perron, M., Markovitsi, D., and Improta, R. (2014). Effect of c5-methylation of cytosine on the photoreactivity of DNA: a joint experimental and computational study of TCG trinucleotides. *J. Am. Chem. Soc.* 136, 10838–10841. doi: 10.1021/ja5040478

Ethirajan, M., Chen, Y., Joshi, P., and Pandey, R. K. (2011). The role of porphyrin chemistry in tumor imaging and photodynamic therapy. *Chem. Soc. Rev.* 40, 340–362. doi: 10.1039/B915149B

Etienne, T., Gattuso, H., Monari, A., and Assfeld, X. (2014). QM/MM modeling of Harmane cation fluorescence spectrum in water solution and interacting with DNA. *Comput. Theor. Chem.* 1040–1041, 367–372. doi: 10.1016/j.comptc.2014.03.026

Etienne, T., Very, T., Perpète, E. A., Monari, A., and Assfeld, X. (2013). A QM/MM study of the absorption spectrum of harmane in water solution and interacting with DNA: the crucial role of dynamic effects. *J. Phys. Chem. B* 117, 4973–4980. doi: 10.1021/jp4017882

Finkel, T. (2011). Signal transduction by reactive oxygen species. *J. Cell Biol.* 194, 7–15. doi: 10.1083/jcb.201102095

Florea, A.-M., and Büsselberg, D. (2011). Cisplatin as an anti-tumor drug: cellular mechanisms of activity, drug resistance and induced side effects. *Cancers* 3, 1351–1371. doi: 10.3390/cancers3011351

Fonseca Guerra, C., van der Wijst, T., Poater, J., Swart, M., and Bickelhaupt, F. (2010). Adenine versus guanine quartets in aqueous solution: dispersion-corrected DFT study on the differences in π-stacking and hydrogen-bonding behavior. *Theor. Chem. Acc.* 125, 245–252. doi: 10.1007/s00214-009-0634-9

Frances-Monneris, A., Merchan, M., and Roca-Sanjuan, D. (2013). Electronic UV-Vis transient spectra of the oh reaction products of uracil, thymine, cytosine, and 5,6-dihydrouracil by using the complete active space self-consistent field second-order perturbation (CASPT2//CASSCF) theory. *J. Chem. Phys.* 139:071101. doi: 10.1063/1.4818727

Frelon, S., Douki, T., Ravanat, J.-L., Pouget, J.-P., Tornabene, C., and Cadet, J. (2000). High-performance liquid chromatographytandem mass spectrometry measurement of radiation-induced base damage to isolated and cellular DNA. *Chem. Res. Toxicol.* 13, 1002–1010. doi: 10.1021/tx000085h

Fridovich, I. (1995). Superoxide radical and superoxide dismutases. *Annu. Rev. Biochem.* 64, 97–112. doi: 10.1146/annurev.bi.64.070195.000525

Friedman, A. E., Chambron, J. C., Sauvage, J. P., Turro, N. J., and Barton, J. K. (1990). A molecular light switch for DNA: Ru(bpy)2(dppz)2+. *J. Am. Chem. Soc.* 112, 4960–4962. doi: 10.1021/ja00168a052

Galindo-Murillo, R., Garcia-Ramos, J. C., Ruiz-Azuara, L., Cheatham, T. E., and Cortes-Guzman, F. (2015). Intercalation processes of copper complexes in DNA. *Nucleic Acids Res.* doi: 10.1093/nar/gkv467

Garcia-Mesenguer, R., Marti, S., Ruiz-Pernia, J. J., Moliner, V., and Tunon, I. (2013). Studying the role of protein dynamics in an SN2 enzyme reaction using free-energy surfaces and solvent coordinates. *Nat. Chem.* 5, 566–571. doi: 10.1038/nchem.1660

Garrec, J., Patel, C., Rothlisberger, U., and Dumont, E. (2012). Insights into intrastrand cross-link lesions of DNA from QM/MM molecular dynamics simulations. *J. Am. Chem. Soc.* 134, 2111–2119. doi: 10.1021/ja2084042

Gervasio, F. L., Laio, A., Iannuzzi, M., and Parrinello, M. (2004). Influence of DNA structure on the reactivity of the guanine radical cation. *Chem. Eur. J.* 10, 4846–4852. doi: 10.1002/chem.200400171

Gold, B., Stone, M. P., and Marky, L. A. (2014). Looking for Waldo: a potential thermodynamic signature to DNA damage. *Acc. Chem. Res.* 47, 1446–1454. doi: 10.1021/ar500061p

Gomzi, V. (2011). {DFT} study of radicals formed in 2-thiothymine single crystals at 77k: 1- and 2-molecule models revised. *Comput. Theor. Chem.* 963, 497–502. doi: 10.1016/j.comptc.2010.11.019

Groenhof, G., Schäfer, L. V., Boggio-Pasqua, M., Goette, M., Grubmüller, H., and Robb, M. A. (2007). Ultrafast deactivation of an excited cytosineguanine base pair in DNA. *J. Am. Chem. Soc.* 129, 6812–6819. doi: 10.1021/ja069176c

Grunenberg, J., Barone, G., and Spinello, A. (2014). The right answer for the right electrostatics: force field methods are able to describe relative energies of DNA guanine quadruplexes. *J. Chem. Theory Comput.* 10, 2901–2905. doi: 10.1021/ct500329f

Gustavsson, T., Improta, R., and Markovitsi, D. (2010). DNA/RNA: building blocks of life under UV irradiation. *J. Phys. Chem. Lett.* 1, 2025–2030. doi: 10.1021/jz1004973

Gustavsson, T., Sarkar, N., Vaya, I., Jimenez, M. C., Markovitsi, D., and Improta, R. (2013). A joint experimental/theoretical study of the ultrafast excited state deactivation of deoxyadenosine and 9-methyladenine in water and acetonitrile. *Photochem. Photobiol. Sci.* 12, 1375–1386. doi: 10.1039/c3pp50060h

Hamanaka, R. B., and Chandel, N. S. (2010). Mitochondrial reactive oxygen species regulate cellular signaling and dictate biological outcomes. *Trends Biochem. Sci.* 35, 505–513. doi: 10.1016/j.tibs.2010.04.002

Hirakawa, K., Hirano, T., Nishimura, Y., Arai, T., and Nosaka, Y. (2012). Dynamics of singlet oxygen generation by DNA-binding photosensitizers. *J. Phys. Chem. B* 116, 3037–3044. doi: 10.1021/jp300142e

Huix-Rotllant, M., Dumont, E., Ferré, N., and Monari, A. (2015). Photophysics of acetophenone interacting with DNA: why the road to photosensitization is open. *Photochem. Photobiol.* 91, 323–330. doi: 10.1111/php.12395

Huix-Rotllant, M., Siri, D., and Ferré, N. (2013). Theoretical study of the photochemical generation of triplet acetophenone. *Phys. Chem. Chem. Phys.* 15, 19293–19300. doi: 10.1039/c3cp52703d

Hutter, M., and Clark, T. (1996). On the enhanced stability of the guaninecytosine base-pair radical cation. *J. Am. Chem. Soc.* 118, 7574–7577. doi: 10.1021/ja953370+

Ilchenko, M., and Dubey, I. (2014). "Quantum chemical approaches in modeling the structure of DNA quadruplexes and their interaction with metal ions and small molecules," in *Application of Computational Techniques in Pharmacy and Medicine*, Volume 17 of *Challenges and Advances in Computational Chemistry and Physics*, eds L. Gorb, V. Kuz'min, and E. Muratov (Berlin: Springer), 181–206.

Jacquemin, D., Zuniga, J., Requena, A., and Ceron-Carrasco, J. P. (2014). Assessing the importance of proton transfer reactions in DNA. *Acc. Chem. Res.* 47, 2467–2474. doi: 10.1021/ar500148c

Jain, V., Vaidyanathan, V. G., Patnaik, S., Gopal, S., and Cho, B. P. (2014). Conformational insights into the lesion and sequence effects for arylamine-induced translesion DNA synthesis: 19F NMR, surface plasmon resonance, and primer kinetic studies. *Biochemistry* 53, 4059–4071. doi: 10.1021/bi5003212

Ji, Y., Xia, Y., Zhao, M., Li, F., and Huang, B. (2005). Reactions of ·OH with thymine studied using density functional theory. *Int. J. Quant. Chem.* 101, 211–218. doi: 10.1002/qua.20293

Jissy, A., Ashik, U., and Datta, A. (2011). Nucleic acid G-quartets: insights into diverse patterns and optical properties. *J. Phys. Chem. C* 115, 12530–12546. doi: 10.1021/jp202401b

Johnson, E. R., Keinan, S., Mori-Sánchez, P., Contreras-García, J., Cohen, A. J., and Yang, W. (2010). Revealing noncovalent interactions. *J. Am. Chem. Soc.* 132, 6498–6506. doi: 10.1021/ja100936w

Jurecka, P., Sponer, J., Cerny, J., and Hobza, P. (2006). Benchmark database of accurate (MP2 and CCSD(T) complete basis set limit) interaction energies of small model complexes, DNA base pairs, and amino acid pairs. *Phys. Chem. Chem. Phys.* 8, 1985–1993. doi: 10.1039/b600027d

Kamp, D. W., Shacter, E., and Weitzman, S. A. (2011). Chronic inflammation and cancer: the role of the mitochondria. *Oncology* 25, 400–410, 413.

Kielpinski, L. J., and Vinther, J. (2014). Massive parallel-sequencing-based hydroxyl radical probing of RNA accessibility. *Nucleic Acids Res.* 42:e70. doi: 10.1093/nar/gku167

Klaunig, J. E., Kamendulis, L. M., and Hocevar, B. A. (2010). Oxidative stress and oxidative damage in carcinogenesis. *Toxicol. Pathol.* 38, 96–109. doi: 10.1177/0192623309356453

Kujoth, G. C., Hiona, A., Pugh, T. D., Someya, S., Panzer, K., Wohlgemuth, S. E., et al. (2005). Mitochondrial DNA mutations, oxidative stress, and apoptosis in mammalian aging. *Science* 309, 481–484. doi: 10.1126/science.1112125

Labet, V., Morell, C., Grand, A., Cadet, J., Cimino, P., and Barone, V. (2008). Formation of cross-linked adducts between guanine and thymine mediated by hydroxyl radical and one-electron oxidation: a theoretical study. *Organ. Biomol. Chem.* 6, 3300–3305. doi: 10.1039/b805589k

Labet, V., Morell, C., Tognetti, V., Syzgantseva, O. A., Joubert, L., Jorge, N., et al. (2014). "Characterization of the chemical reactivity and selectivity of DNA bases through the use of DFT-based descriptors," in *Structure, Bonding and Reactivity of Heterocyclic Compounds*, Volume 38 of *Topics in Heterocyclic Chemistry*, eds F. De Proft and P. Geerlings (Berlin; Heidelberg: Springer), 35–70.

Lauria, A., Bonsignore, R., Terenzi, A., Spinello, A., Giannici, F., Longo, A., et al. (2014). Nickel(ii), copper(ii) and zinc(ii) metallo-intercalators: structural details of the DNA-binding by a combined experimental and computational investigation. *Dalton Trans.* 43, 6108–6119. doi: 10.1039/c3dt53066c

Lim, P., Wuenschell, G. E., Holland, V., Lee, D.-H., Pfeifer, G. P., Rodriguez, H., et al. (2004). Peroxyl radical mediated oxidative DNA base damage: implications for lipid peroxidation induced mutagenesis. *Biochemistry* 43, 15339–15348. doi: 10.1021/bi048276x

Meier, K., Choutko, A., Dolenc, J., Eichenberger, A. P., Riniker, S., and van Gunsteren, W. F. (2013). Multi-resolution simulation of biomolecular systems: a review of methodological issues. *Angewandte Chemie Int. Edn.* 52, 2820–2834. doi: 10.1002/anie.201205408

Miyamoto, S., and Di Mascio, P. (2014). "Lipid hydroperoxides as a source of singlet molecular oxygen," in *Lipid Hydroperoxide-Derived Modification of Biomolecules*, Volume 77 of *Subcellular Biochemistry*, ed Y. Kato (Berlin: Springer), 3–20.

Monari, A., Rivail, J.-L., and Assfeld, X. (2013). Theoretical modeling of large molecular systems. advances in the local self consistent field method for mixed quantum mechanics/molecular mechanics calculations. *Acc. Chem. Res.* 46, 596–603. doi: 10.1021/ar300278j

Mutter, S. T., Margiotta, N., Papadia, P., and Platts, J. A. (2015). Computational evidence for structural consequences of kiteplatin damage on DNA. *JBIC J. Biol. Inorgan. Chem.* 20, 35–48. doi: 10.1007/s00775-014-1207-5

Neidle, S. (2010). Human telomeric G-quadruplex: the current status of telomeric G-quadruplexes as therapeutic targets in human cancer. *FEBS J.* 277, 1118–1125. doi: 10.1111/j.1742-4658.2009.07463.x

Neidle, S., and Parkinson, G. (2002). Telomere maintenance as a target for anticancer drug discovery. *Nat. Rev. Drug Dis.* 1, 383–393. doi: 10.1038/nrd793

Neidle, S., and Parkinson, G. N. (2003). The structure of telomeric DNA. *Curr. Opin. Struct. Biol.* 13, 275–283. doi: 10.1016/S0959-440X(03)00072-1

Nenov, A., Segarra-Marti, J., Giussani, A., Conti, I., Rivalta, I., Dumont, E., et al. (2015). Probing deactivation pathways of DNA nucleobases by two-dimensional electronic spectroscopy: first principles simulations. *Faraday Discuss.* 177, 345–362. doi: 10.1039/C4FD00175C

Nielsen, S. O., Bulo, R. E., Moore, P. B., and Ensing, B. (2010). Recent progress in adaptive multiscale molecular dynamics simulations of soft matter. *Phys. Chem. Chem. Phys.* 12, 12401–12414. doi: 10.1039/c004111d

Nijkoo, H., O'Neill, P. M. T., and Goodhead, D. T. (1999). Quantitative modelling of DNA damage using Monte Carlo track structure method. *Radiat. Environ. Biophys.* 38, 31–38.

Nikitaki, Z., Hellweg, C. E., Georgakilas, A. G., and Ravanat, J.-L. (2015). Stress-induced DNA damage biomarkers: applications and limitations. *Front. Chem.* 3:35. doi: 10.3389/fchem.2015.00035

Nogueira, J. J., Oppel, M., and Gonzlez, L. (2015). Enhancing intersystem crossing in phenotiazinium dyes by intercalation into DNA. *Angewandte Chemie Int. Edn.* 54, 4375–4378. doi: 10.1002/anie.201411456

Pacher, P., Beckman, J. S., and Liaudet, L. (2007). Nitric oxide and peroxynitrite in health and disease. *Physiol. Rev.* 87, 315–424. doi: 10.1152/physrev.00029.2006

Pandey, R. K. (2000). Recent advances in photodynamic therapy. *J. Porphyr. Phthalocyan.* 4, 368–373. doi: 10.1002/(SICI)1099-1409(200006/07)4:4<368::AID-JPP244>3.0.CO;2-6

Patel, C., Drsata, T., Lankas, F., and Dumont, E. (2013). Structure, dynamics, and interactions of a C4'-oxidized abasic site in DNA: a concomitant strand scission reverses affinities. *Biochemistry* 52, 8115–8125. doi: 10.1021/bi401268q

Poater, J., Swart, M., Guerra, C. F., and Bickelhaupt, F. M. (2011). Selectivity in DNA replication. interplay of steric shape, hydrogen bonds, π-stacking and solvent effects. *Chem. Commun.* 47, 7326–7328. doi: 10.1039/c0cc04707d

Pogozelski, W. K., and Tullius, T. D. (1998). Oxidative strand scission of nucleic acids: routes initiated by hydrogen abstraction from the sugar moiety. *Chem. Rev.* 98, 1089–1108. doi: 10.1021/cr960437i

Pryor, W. A., and Squadrito, G. L. (1995). The chemistry of peroxynitrite: a product from the reaction of nitric oxide with superoxide. *Am. J. Physiol. Lung Cell. Mol. Physiol.* 268, L699–L722.

Rademaker-Lakhai, J. M., van den Bongard, D., Pluim, D., Beijnen, J. H., and Schellens, J. H. M. (2004). A phase I and pharmacological study with imidazolium-trans-DMSO-imidazole-tetrachlororuthenate, a novel ruthenium anticancer agent. *Clin. Cancer Res.* 10, 3717–3727. doi: 10.1158/1078-0432.CCR-03-0746

Radzimanowski, J., Dehez, F., Round, A., Bidon-Chanal, A., McSweeney, S., and Timmins, J. (2013). An 'open' structure of the RecOR complex supports ssDNA binding within the core of the complex. *Nucleic Acids Res.* 7972–7986. doi: 10.1093/nar/gkt572

Ramsay, R. R. (2012). Monoamine oxidases: the biochemistry of the proteins as targets in medicinal chemistry and drug discovery. *Curr. Topics Med. Chem.* 12, 2189–2209. doi: 10.2174/156802612805219978

Regulus, P., Duroux, B., Bayle, P.-A., Favier, A., Cadet, J., and Ravanat, J.-L. (2007). Oxidation of the sugar moiety of DNA by ionizing radiation or bleomycin could induce the formation of a cluster DNA lesion. *Proc. Natl. Acad. Sci. U.S.A.* 104, 14032–14037. doi: 10.1073/pnas.0706044104

Repic, M., Vianello, R., Purg, M., Duarte, F., Bauer, P., Kamerlin, S. C. L., et al. (2014). Empirical valence bond simulations of the hydride transfer step in the monoamine oxidase B catalyzed metabolism of dopamine. *Proteins Struct. Funct. Bioinform.* 82, 3347–3355. doi: 10.1002/prot.24690

Richter, M., Marquetand, P., Gonzlez-Vázquez, J., Sola, I., and González, L. (2012). Femtosecond intersystem crossing in the DNA nucleobase cytosine. *J. Phys. Chem. Lett.* 3, 3090–3095. doi: 10.1021/jz301312h

Sage, E., Drouin, R., and Rouabhia, M. (eds.). (2005). "Chemical sequencing profiles of photosensitized DNA damage," in *From DNA Photolesions to Mutations, Skin Cancer and Cell Death* (Cambridge, UK: The Royal Society of Chemistry), 15–31.

Sainz, R. M., Lombo, F., and Mayo, J. C. (2012). Radical decisions in cancer: redox control of cell growth and death. *Cancers* 4, 442–474. doi: 10.3390/cancers4020442

Salmon, T. B., Evert, B. A., Song, B., and Doetsch, P. W. (2004). Biological consequences of oxidative stress-induced DNA damage in saccharomyces cerevisiae. *Nucleic Acids Res.* 32, 3712–3723. doi: 10.1093/nar/gkh696

Sancar, A., and Sancar, G. B. (1988). DNA repair enzymes. *Annu. Rev. Biochem.* 57, 29–67. doi: 10.1146/annurev.bi.57.070188.000333

Senn, H., and Thiel, W. (2007). "QM/MM methods for biological systems," in *Atomistic Approaches in Modern Biology*, Volume 268 of *Topics in Current Chemistry*, ed M. Reiher (Berlin; Heidelberg: Springer), 173–290.

Senn, H. M., and Thiel, W. (2009). QM/MM methods for biomolecular systems. *Angewandte Chemie Int. Edn.* 48, 1198–1229. doi: 10.1002/anie.200802019

Sinha, R. P., and Hader, D.-P. (2002). UV-induced DNA damage and repair: a review. *Photochemist. Photobiol. Sci.* 1, 225–236. doi: 10.1039/b201230h

Sponer, J., Leszczynski, J., and Hobza, P. (2001). Electronic properties, hydrogen bonding, stacking, and cation binding of DNA and RNA bases. *Biopolymers* 61, 3–31.

Suss-Fink, G. (2010). Arene ruthenium complexes as anticancer agents. *Dalton Trans.* 39, 1673–1688. doi: 10.1039/B916860P

Sviatenko, L., Gorb, L., Hovorun, D., and Leszczynski, J. (2012). Interaction of 2-deoxyadenosine with cis-2-butene-1,4-dial: Computational approach to analysis of multistep chemical reactions. *J. Phys. Chem. A* 116, 2333–2342. doi: 10.1021/jp211911u

Szabla, R., Campos, J., Sponer, J. E., Sponer, J., Gora, R. W., and Sutherland, J. D. (2015). Excited-state hydrogen atom abstraction initiates the photochemistry of β-2′–deoxycytidine. *Chem. Sci.* 6, 2035–2043. doi: 10.1039/C4SC03761H

Szolomajer, J., Paragi, G., Batta, G., Guerra, C. F., Bickelhaupt, F. M., Kele, Z., et al. (2011). 3-substituted xanthines as promising candidates for quadruplex formation: computational, synthetic and analytical studies. *New J. Chem.* 35, 476–482. doi: 10.1039/c0nj00612b

Terenzi, A., Bonsignore, R., Spinello, A., Gentile, C., Martorana, A., Ducani, C., et al. (2014). Selective g-quadruplex stabilizers: schiff-base metal complexes with anticancer activity. *RSC Adv.* 4, 33245–33256. doi: 10.1039/C4RA05355A

Valko, M., Leibfritz, D., Moncol, J., Cronin, M. T., Mazur, M., and Telser, J. (2007). Free radicals and antioxidants in normal physiological functions and human disease. *Int. J. Biochem. Cell Biol.* 39, 44–84. doi: 10.1016/j.biocel.2006.07.001

Vaya, I., Brazard, J., Gustavsson, T., and Markovitsi, D. (2012). Electronically excited states of DNA oligonucleotides with disordered base sequences studied by fluorescence spectroscopy. *Photochem. Photobiol. Sci.* 11, 1767–1773. doi: 10.1039/c2pp25180a

Vayá, I., Gustavsson, T., Douki, T., Berlin, Y., and Markovitsi, D. (2012). Electronic excitation energy transfer between nucleobases of natural DNA. *J. Am. Chem. Soc.* 134, 11366–11368. doi: 10.1021/ja304328g

Very, T., Ambrosek, D., Otsuka, M., Gourlaouen, C., Assfeld, X., Monari, A., et al. (2014). Photophysical properties of ruthenium(II) polypyridyl DNA intercalators: effects of the molecular surroundings investigated by theory. *Chem. Euro. J.* 20, 12901–12909. doi: 10.1002/chem.201402963

Very, T., Despax, S., Hebraud, P., Monari, A., and Assfeld, X. (2012). Spectral properties of polypyridyl ruthenium complexes intercalated in DNA: theoretical insights into the surrounding effects of $[Ru(dppz)(bpy)_2]^{2+}$. *Phys. Chem. Chem. Phys.* 14, 12496–12504. doi: 10.1039/c2cp40935f

Vianello, R., and Maksic, Z. B. (2003). A combined ab initio and density functional study of the electronic structure of thymine and 2-thiothymine radicals. *Collect. Czechoslovak Chem. Commun.* 68, 2322–2334. doi: 10.1135/cccc 20032322

Vianello, R., Repic, M., and Mavri, J. (2012). How are biogenic amines metabolized by monoamine oxidases? *Eur. J. Organ. Chem.* 2012, 7057–7065. doi: 10.1002/ejoc.201201122

Vorlickova, M., and Palecek, E. (1974). A study of changes in DNA conformation caused by ionizing and ultra-violet radiation by means of pulse polarography and circular dichroism. *Int. J. Radiat. Biol.* 26, 363–372. doi: 10.1080/09553007414551341

Wang, K., Poon, C. T., Choi, C. Y., Wong, W.-K., Kwong, D. W., Yu, F. Q., et al. (2012). Synthesis, circular dichroism, DNA cleavage and singlet oxygen photogeneration of 4-amidinophenyl porphyrins. *J. Porphyr. Phthalocyan.* 16, 85–92. doi: 10.1142/S108842461100435X

Wilhelm, M., Mukherjee, A., Bouvier, B., Zakrzewska, K., Hynes, J. T., and Lavery, R. (2012). Multistep drug intercalation: molecular dynamics and free energy studies of the binding of daunomycin to DNA. *J. Am. Chem. Soc.* 134, 8588–8596. doi: 10.1021/ja301649k

Wu, Y., Mundy, C. J., Colvin, M. E., and Car, R. (2004). On the mechanisms of OH radical induced DNA-base damage: a comparative quantum chemical and CarParrinello molecular dynamics study. *J. Phys. Chem. A* 108, 2922–2929. doi: 10.1021/jp0363592

Yadav, A., and Mishra, P. C. (2013). Reactivities of hydroxyl and perhydroxyl radicals toward cytosine and thymine: a comparative study. *Int. J. Quant. Chem.* 113, 56–62. doi: 10.1002/qua.24050

Yan, Y. K., Melchart, M., Habtemariam, A., and Sadler, P. J. (2005). Organometallic chemistry, biology and medicine: ruthenium arene anticancer complexes. *Chem. Commun.* 4764–4776. doi: 10.1039/b508531b

Zalesak, J., Lourdin, M., Krejci, L., Constant, J.-F., and Jourdan, M. (2014). Structure and dynamics of DNA duplexes containing a cluster of mutagenic 8-oxoguanine and abasic site lesions. *J. Mol. Biol.* 426, 1524–1538. doi: 10.1016/j.jmb.2013.12.022

Zeglis, B. M., Pierre, V. C., and Barton, J. K. (2007). Metallo-intercalators and metallo-insertors. *Chem. Commun.* 4565–4579. doi: 10.1039/b710949k

Zinovjev, K., Ruiz-Pernia, J. J., and Tunon, I. (2013). Toward an automatic determination of enzymatic reaction mechanisms and their activation free energies. *J. Chem. Theory Comput.* 9, 3740–3749. doi: 10.1021/ct 400153r

Zinovjev, K., and Tunon, I. (2014). Exploring chemical reactivity of complex systems with path-based coordinates: role of the distance metric. *J. Comput. Chem.* 35, 1672–1681. doi: 10.1002/jcc.23673

Conflict of Interest Statement: The authors declare that the research was conducted in the absence of any commercial or financial relationships that could be construed as a potential conflict of interest.

Copyright © 2015 Dumont and Monari. This is an open-access article distributed under the terms of the Creative Commons Attribution License (CC BY). The use, distribution or reproduction in other forums is permitted, provided the original author(s) or licensor are credited and that the original publication in this journal is cited, in accordance with accepted academic practice. No use, distribution or reproduction is permitted which does not comply with these terms.

frontiers in Chemistry

ORIGINAL RESEARCH
published: 28 July 2015
doi: 10.3389/fchem.2015.00047

An ameliorative protocol for the quantification of purine 5′,8-cyclo-2′-deoxynucleosides in oxidized DNA

Michael A. Terzidis[1] *and Chryssostomos Chatgilialoglu*[1,2]*

[1] *Istituto per la Sintesi Organica e la Fotoreattività, Consiglio Nazionale delle Ricerche, Bologna, Italy,* [2] *Institute of Nanoscience and Nanotechnology, National Centre of Scientific Research "Demokritos", Athens, Greece*

OPEN ACCESS

Edited by:
Huib Ovaa, Netherlands Cancer Institute, Netherlands

Reviewed by:
Mark Helm, Johannes Gutenberg-Universität Mainz, Germany
Rui Zhao, Institute of Chemistry, Chinese Academy of Sciences, China

***Correspondence:**
Chryssostomos Chatgilialoglu, Institute of Nanoscience and Nanotechnology, National Centre of Scientific Research "Demokritos", Patriarchou Grigoriou & Neapoleos Str., 15310 Agia Paraskevi, Athens, Greece
c.chatgilialoglu@inn.demokritos.gr; chrys@isof.cnr.it

Specialty section:
This article was submitted to Chemical Biology, a section of the journal Frontiers in Chemistry

Received: *08 March 2015*
Accepted: *13 July 2015*
Published: *28 July 2015*

Citation:
Terzidis MA and Chatgilialoglu C (2015) An ameliorative protocol for the quantification of purine 5′,8-cyclo-2′-deoxynucleosides in oxidized DNA. Front. Chem. 3:47. doi: 10.3389/fchem.2015.00047

5′,8-Cyclo-2′-deoxyadenosine (cdA) and 5′,8-cyclo-2′-deoxyguanosine (cdG) are lesions resulting from hydroxyl radical ($HO^{\cdot}$) attack on the 5′H of the nucleoside sugar moiety and exist in both 5′*R* and 5′*S* diastereomeric forms. Increased levels of cdA and cdG are linked to Nucleotide Excision Repair (NER) mechanism deficiency and mutagenesis. Discrepancies in the damage measurements reported over recent years indicated the weakness of the actual protocols, in particular for ensuring the quantitative release of these lesions from the DNA sample and the appropriate method for their analysis. Herein we report the detailed revision leading to a cost-effective and efficient protocol for the DNA damage measurement, consisting of the nuclease benzonase and nuclease P1 enzymatic combination for DNA digestion followed by liquid chromatography isotope dilution tandem mass spectrometry analysis.

Keywords: DNA damage, cyclonucleosides, enzymatic digestion protocols, isotope dilution analysis, liquid chromatography-tandem mass spectrometry

Introduction

Hydroxyl radicals ($HO^{\cdot}$) are known for their reactivity toward DNA leading to nucleobase modifications and strand breaks. In particular, the attack at H5′ of DNA by $HO^{\cdot}$ is estimated to occur with a 55% probability over all possible sugar positions, and produces the C5′ radical (Aydogan et al., 2002). The chemistry of C5′ radical is very peculiar with respect to the other positions of 2-deoxyribose in the sense that it does not generate an abasic site, but unique cyclic base-sugar adducts are formed denominated cyclopurine lesions (**Figure 1**). Therefore, apart from the usual glycosidic bond, another covalent bond between the C5′ sugar and the C8 purine carbon atoms is present (Chatgilialoglu et al., 2011). 5′,8-Cyclo-2′-deoxyadenosine (cdA) and 5′,8-cyclo-2′-deoxyguanosine (cdG) in their 5′*R* and 5′*S* diastereomeric forms are tandem-type lesions observed among the DNA modifications and identified in mammalian cellular DNA *in vivo* (Chatgilialoglu et al., 2011). Nowadays these lesions are considered as robust biomarkers for oxidative stress and might be resistant to repair machinery in cells. Indeed, it has been recently found that these tandem lesions accumulate with aging in a tissue-specific manner (liver > kidney > brain), providing evidence that DNA repair mechanisms are inadequate to preserve the integrity of genetic material from these lesions (Wang et al., 2011, 2012). Results from competitive transcription and adduct bypass assay revealed that 5′*S*-cdG strongly inhibits transcription *in vitro* and in mammalian cells, and induces transcriptional mutagenesis both *in vitro* and *in vivo* (You et al., 2012). Recent

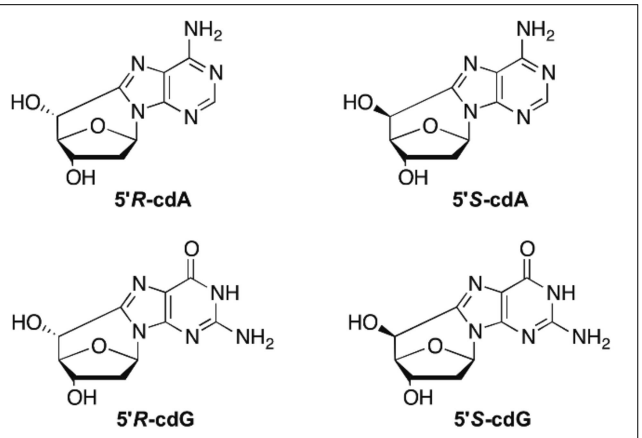

FIGURE 1 | 5′,8-Cyclo-2′-deoxyadenosine (cdA) and 5′,8-cyclo-2′-deoxyguanosine (cdG) lesions.

studies reported cyclopurine lesions as reliable oxidative stress biomarkers in animal models for examination of liver injury pathophysiology in Wilson's disease and pigmentation (Wang et al., 2011; Mitra et al., 2012). A direct comparison of relative Nucleotide Excision Repair (NER) efficiencies of the four cyclopurines has been determined in the identical sequence contexts and in the same HeLa cell extract preparations (Kropachev et al., 2014). The cdA and cdG lesions were excised with similar efficiencies, but the efficiencies for both 5′*R* cyclopurines were greater by a factor of ∼2 than for the 5′*S* lesions. Based on molecular modeling and molecular dynamics simulations, the structural and energetic origins of this difference in NER efficiencies have been suggested. Indeed, the greater stacking impairment in the 5′*R* stereoisomer correlates well with its greater relative NER excision efficiency.

Modified oligonucleotides and dimers containing the cyclopurines were synthesized and used by different research groups for the development of enzymatic protocols aiming at the quantitative liberation of the lesions as nucleoside units, prior to quantification (Romieu et al., 1998, 1999; Jaruga et al., 2004). The cocktails used in the latter studies contain the nuclease enzyme P1, which is dependent on both zinc and water co-factors and is known to recognize and hydrolyze single-stranded DNA and RNA to the level of 5′-mononucleotides by concerted endo- and exonucleolytic action (Fujimoto et al., 1975; Volbeda et al., 1991; Romier et al., 1998). The mechanism behind the action of the snake venom phosphodiesterase (3′-exo) and phosphodiesterase II (5′-exo), also used in digestion mixtures, has been identified to proceed through the formation of a nucleotidyl-enzyme intermediate by an active-site threonine insult, on which a double-displacement takes place (Culp et al., 1985; Cummins and Potter, 1987). Results reported for irradiated samples of calf thymus DNA have been critically reviewed, highlighting that the available protocols are not the best performing test available, and revision is needed in order to get precise damage values and foster the potential involvement of these lesions in human health (Chatgilialoglu et al., 2011). The objectives of this work were to (i) develop and validate a sensitive analytical method based on the stable isotope-dilution tandem mass spectrometry technique using triple quadrupole mass spectrometry, and (ii) to elucidate the hydrolytic action of several enzymes for the satisfactory DNA digestion and quantitative release of single nucleoside cyclopurines. We anticipate that our revised protocol, consisting of the nuclease benzonase and nuclease P1 enzymatic combination for DNA digestion followed by liquid chromatography isotope dilution tandem mass spectrometry analysis, provides benefits for costs and efficiency related to DNA damage measurement including cyclopurine lesions.

Materials and Methods

Chemicals

8-Bromo-2′-deoxyadenosine, 2′-deoxyadenosine monohydrated, 7,8-dihydro-8-oxo-2′-deoxyadenosine (8-oxo-dA), 2′-deoxyguanosine monohydrated, 7,8-dihydro-8-oxo-2′-deoxyguanosine 8-oxo-dG), and 8-bromo-2′-deoxyguanosine were purchased from Berry & Associates Inc. (Dexter, USA). [$^{15}N_5$]-2′-deoxyadenosine monohydrated and [$^{15}N_5$]-2′-deoxyguanosine monohydrated (all >98% isotopic purity) were purchased from Cambridge Isotope Laboratories (Andover, USA). All the salts and solvents, thymidine, 2′-deoxycytidine, activated calf thymus DNA, nuclease P1 from *Penicillium citrinum*, phosphodiesterase II, phosphodiesterase I from *Crotalus Adamanteus venom*, DNAse I, DNAse II, alkaline phosphatase from bovine intestinal mucosa, erythro-9-(2-hydroxy-3-nonyl)adenine hydrochoride (EHNA), benzonase 99%, deferoxamine mesylate salt, BHT and pentostatin, were obtained from Sigma (Taufkirchen, Germany and Milan, Italy) while the 3 kDa filters were purchased from Millipore (Bedford, USA). Distilled and deionized water (ddH2O) was purified by a Milli-Q system (Millipore, Bedford, USA).

Synthesis of Reference Compounds and Internal Standards

The four diastereoisomers 5′*R*-cdA, 5′*S*-cdA, 5′*R*-, and 5′*S*-cdG were synthesized according to published synthetic protocol (Jimenez et al., 2004; Terzidis and Chatgilialoglu, 2013) (e.g., see Figure S1 for cdA). Synthesis of ^{15}N labeled of adenine derivatives was performed as previously reported for the unlabeled compounds (Boussicault et al., 2008). In particular, 1 mL of aqueous solution containing 1.5 mM of [$^{15}N_5$]-dA was prepared, flushed with N_2O for 15 min and γ-irradiated with a total dose of 2 kGy at a dose rate of 4.5 Gy min^{-1}. After the reaction crude mixture was submitted to HPLC purification and the peaks corresponding to [$^{15}N_5$]-5′*R*-cdA, [$^{15}N_5$]-5′*S*-cdA, and [$^{15}N_5$]-8-oxo-dA were collected (Figures S2, S3). The two diastereoisomers in ESI MS/MS analysis gave m/z 255 for the $[M+H]^+$ and the two diagnostic fragment ions at m/z 169 and at m/z 141, whereas [$^{15}N_5$]-8-oxo-dA gave m/z 273 for the $[M + H]^+$ and two fragment ions at m/z 157 and m/z 130, which correspond to the protonated 2-deoxyribose and [$^{15}N_5$]-8-oxo-adenine, respectively. The synthesis of [$^{15}N_5$]-8-bromo-2′-deoxyguanosine has been achieved starting from [$^{15}N_5$]-dG and following a known procedure for the unlabeled compound

(Münzel et al., 2011). In particular, 1 mg (3.5 μmol) of [$^{15}N_5$]-dG was suspended to 500 μL of acetonitrile/water mixture 4:1 in a microcentrifuge tube of 1.5 mL volume. Then 1.3 mg *N*-bromosuccinimide (7.3 μmol) was added to the suspension in three portions and the mixture stirred at room temperature for 2 h. After the solvent was removed under a stream of argon, acetone (100 μL) was added. The mixture was stirred at room temperature for 4 h and then stored at −20°C overnight. Next, the mixture was centrifuged at 1000 g for 1 min and the supernatant was removed with a pipette. The precipitate was washed with cold acetone (60 μL), centrifuged again and the liquid removed with a pipette. The bromo derivative was irradiated as previously reported for the unlabeled compounds (Chatgilialoglu et al., 2007): 1 mM solution in ddH_2O was transferred into the UV irradiation apparatus, flushed with argon for 15 min, and irradiated for 30 min with a UV light (5 W low pressure Hg lamp). The reaction mixture was quenched with a 5% $NaHCO_3$ solution (final pH 7) and submitted to HPLC for purification (Figure S4) affording the two diastereomers [$^{15}N_5$]-5′*R*-cdG and [$^{15}N_5$]-5′*S*-cdG (Figures S4, S5). [$^{15}N_5$]-8-oxo-dG was prepared following a literature protocol (Taghizadeh et al., 2008). In particular, [$^{15}N_5$]-dG (0.24 mg, 0.82 μmol) was dissolved in 164 μL of water in an ultrasound bath. After, 5.45 μL of 0.5 M freshly prepared ascorbic acid (2.7 μmol) were added followed by 3.3 μL of 0.1 M $CuSO_4$ (3.3 μmol) and 9.4 μL of 30% hydrogen peroxide. The reaction mixture was stirred at room temperature and quenched after 2 h with a 5% Na_2SO_3 solution. The crude was purified by HPLC (Figures S6, S7). The two diastereoisomers in ESI MS/MS analysis gave m/z 271 for the $[M + H]^+$ and the two diagnostic fragment ions at m/z 185 and at m/z 206, whereas [$^{15}N_5$]-8-oxo-dG gave m/z 289 for the $[M + H]^+$ and two fragment ions at m/z 173 and m/z 145, which correspond to the protonated 2-deoxyribose and [$^{15}N_5$]-8-oxo-guanine respectively. The isotopic purities of the ^{15}N labeled compounds were found to be >99.9% by tandem mass spectrometry analysis using an ion-trap Bruker Daltonics MS^n system. The calculations were based on the ratio between the signals of the fragment ions corresponding to the labeled and the natural compounds. Their UV spectra were identical to those of the unlabeled compounds.

Determination of Purine 5′,8-Cyclo-2′-Deoxynucleosides Extinction Coefficients

The purity of the natural standard references of purine 5′,8-cyclo-2′-deoxynucleosides was determined after the synthesis according to published procedures (Jimenez et al., 2004; Terzidis and Chatgilialoglu, 2013). They were all controlled by HPLC-UV and LC-MS^2 (Agilent-Bruker Daltonics ion trap) for purity. The purine 5′,8-cyclo-2′-deoxynucleosides obtained by the previous procedure were desalinated using solid phase extraction cartridges (Waters Sep-Pak® C18-E, 120 Å, 360 mg) by following the manufacturer's instruction. For the determination of the extinction coefficients (ε) at the λ_{max} of each nucleoside and, in order to reduce pipetting errors, aqueous solutions of each were prepared involving a five digital balance. The UV spectra were recorded by a UV spectrophotometer.

Isotope Dilution Tandem Mass Spectrometry Quantification

The quantification of the lesions was carried out by liquid chromatography isotope dilution tandem mass spectrometry technique. The calibration of the spectrometer with the natural lesions was based on the parameters reported previously (Belmadoui et al., 2010). The analytes were resolved on a 2 mm × 150 mm Luna C18 (2) 100 Å column (3 μ min particle size, Phenomenex) loaded with a pre-column C18 (2) cartridge using an LC system (Perkin Elmer Inc., USA) coupled with an AB Sciex 4000 triple quadrupole mass spectrometer (AB Sciex Inc., USA) working on multiple reaction monitoring mode. The chromatographic method used for the separation of the analytes started with 99% of 2 mM ammonium formate (solvent A) and 1% acetonitrile (solvent B). A gradient program using 2 mM ammonium formate (A) and acetonitrile (B) was involved, 0 → 20 min solvent B 1 → 9.8%. The system was washed for extra 5 min with isocratic solution B 15% and additional 10 min were given for re-equilibration after each analysis. The flow rate remained constant at 0.2 mL/min, the column was thermostated at 30°C and the injection volume was 15 μL. Linear responses were found for injection volumes up to 30 μL and upon dilution (see Figures S8, S10, respectively, in Supplementary Material).

Preparation of the Calibration Curves

The construction of the calibration curves of the isotopic $^{15}N_5$ labeled and unlabeled lesions of the four purine 5′,8-cyclo-2′-deoxynucleosides and the two 8-oxo-7,8-dihydro-2′-deoxynucleosides were prepared by plotting the MRM signal area ratios of the lesions and their isotopic equivalents against their corresponding concentration of the lesions. The concentration of the labeled lesions were chosen carefully be close to the concentration of the analytes in the samples (nM) and kept constant both for the construction of the curves and the quantification of the lesions in the samples. The latter was based on the comparison of the MRM signal areas between the lesions and their internal standards, and their respective response curves (see Table S2 in Supplementary Material). For this reason the horizontal axis values in the curves are given as analyte concentration (Figure S9). The concentrations of the lesions used for building up the calibration curves are reported in Table S3. For the preparation of the different solutions a five-digital balance was used in order to avoid pipetting errors. The determination of concentrations of the internal standard solutions containing the purine [$^{15}N_5$]-5′,8-cyclo-2′-deoxynucleosides and [$^{15}N_5$]-7,8-dihydro-8-oxo-2′-deoxyadenosine was based on their traces after HPLC-UV analyses (at 260 nm) and the corresponding response curves of the unlabeled equivalent compounds. The quantification of the [$^{15}N_5$]-7,8-dihydro-8-oxo-2′-deoxyguanosine solution was performed by UV spectroscopy.

HPLC-UV Analysis, Off-line Sample Cleanup and Enrichment

HPLC-UV analysis, cleanup and enrichment of the samples were performed on a 4.6 mm × 150 mm Luna C18 (2) 100 Å column (5 μ min particle size, Phenomenex) loaded with a pre-column

C18 (2) cartridge, on an Agilent 1100 HPLC-UV system (Agilent, USA). The gradient program used an eluent composed by 2 mM ammonium formate (solvent A), acetonitrile (solvent B), and methanol (solvent C) (Table S5). The time windows used for the collection of fractions containing the lesions are reported in Table S6 (Figure S11). The collected fractions were freeze-dried, pooled, freeze-dried again, and redissolved in 50 μL ddH_2O before LC-MS/MS analysis. The quantification of the dA, dG, dC, and Thy was based on their absorbance at 260 nm (Cui et al., 2013). The same analytical protocol was used also for the quantification of the normal 2′-deoxyribonucleosides in the enzymatic digestion studies.

Lesion Stability under Acidic Conditions

The stability of the lesions against the acidic hydrolysis was also investigated. Six aqueous mixtures of 10 μL containing a mixture of 19 pmol 8-oxo-dG, 6 pmol 5′*R*-cdG, 1 pmol 5′*S*-cdG, 5 pmol 8-oxo-dA, 5 pmol 5′*R*-cdA and 3 pmol 5′*S*-cdA were prepared and 10 μL of formic acid solutions with different concentrations were added in order to reach 0, 0.1, 0.5, 1, 5, and 10% final formic acid concentrations. The solutions were incubated at 37°C for 4 h and then quenched with cold NH_4OH solution (Das et al., 2012). The mixture of internal standard references (labeled) was added. The samples were freeze-dried, reconstituted in 50 μL of ddH_2O and analyzed by LC-MS/MS. The experiments were repeated three times.

Enzymatic Digestion Protocols

Protocol A (Wang et al., 2011): 40 μg DNA were dissolved in 10 μL of Ar flushed buffer containing 0.3 M AcONa pH 5.6, 10 mM $ZnCl_2$, 3 mM deferoxamine mesylate, and 1 mM EHNA. Next, 4 U of Nuclease P1 (in 30 mM AcONa pH 5.3, 5 mM $ZnCl_2$ and 50 mM NaCl) and 5 mU phosphodiesterase II were added and the mixture was incubated in 37°C. After 48 h, 20 μL of 0.5 M Tris-HCl buffer pH 8.9 flushed with Ar were added along with 4 U of alkaline phosphatase and 5 mU of phosphodiesterase I. The mixture was incubated for extra 2 h. After quenching with 10% formic acid, the mixture was transferred in a microspin filter (3 kDa) and centrifuged at ∼14,000 *g* for 20 min (4°C). The filtrate was submitted to lyophilization (n.b., the original protocol does not use deferoxamine, degased solutions and argon atmosphere, but we found necessary to be added according to the recoveries studies we performed).

Protocol B (Jaruga et al., 2004): 50 μg DNA were dissolved in 50 μL of 10 mM Tris-HCl buffer pH 7.5 containing 2.5 μL of 1 M AcONa and 45 mM $ZnCl_2$ (final pH 6.0). Next, 5 U of Nuclease P1 (in 30 mM AcONa pH 5.3, 5 mM $ZnCl_2$ and 50 mM NaCl), 4 mU phosphodiesterase I and 32 U of alkaline phosphatase were added and the mixture was incubated at 37°C. After 24 h, the mixture was transferred in a microspin filter (3 kDa) and centrifuged at ∼14,000 *g* for 20 min (4°C). The filtrate was lyophilized overnight.

Protocol C (Belmadoui et al., 2010): 50 μg DNA were dissolved in 100 μL of buffer containing succinic acid 20 mM pH 6, 10 mM $CaCl_2$, 3 mM deferoxamine mesylate, and 1 mM EHNA. Next, 5 U of Nuclease P1 (in 30 mM AcONa pH 5.3, 5 mM $ZnCl_2$ and 50 mM NaCl), 4 mU phosphodiesterase II and 0.25 U DNAse II were added and the mixture was incubated at 37°C. After 2 h, 10 μL of Tris-HCl buffer 0.5 M pH 8 were added along with 5 U of alkaline phosphatase and 3 mU of phosphodiesterase I. The mixture was incubated for extra 2 h at 37°C. Finally, 10 μL of buffer containing 0.2 M succinic acid pH 6, 0.1 M $CaCl_2$ together with 5 U of nuclease P1, 4 mU phosphodiesterase II and 0.25 U DNAse II were added and the mixture was incubated at 37°C for 2 h before being transferred in a microspin filter (3 kDa) and centrifuged ∼14,000 *g* for 20 min (4°C). The filtrate was submitted to lyophilization.

Protocol D: 50 μg DNA were dissolved in 100 μL of Ar flushed 10 mM Tris-HCl buffer pH 7.9 containing 10 mM $MgCl_2$, 50 mM NaCl, 0.2 mM pentostatin, 5 μM BHT, and 3 mM deferoxamine. Next, 3 U of benzonase (in 20 mM Tris HCl pH 8.0, 2 mM $MgCl_2$, and 20 mM NaCl), 4 mU phosphodiesterase I, 3 U DNAse I, 2 mU of PDE II and 2 U of alkaline phosphatase were added and the mixture was incubated at 37°C. Finally the mixture was quenched with 1% formic acid, transferred in a microspin filter (3 kDa) and centrifuged at ∼14,000 *g* for 20 min (4°C). The filtrate was submitted to lyophilization.

Protocol E: The same procedure as described in protocol D was followed but after the first incubation, 35 μL of Ar flushed buffer containing 0.3 M AcONa pH 5.6 and 10 mM $ZnCl_2$ along with 0.5 U of Nuclease P1 (in 30 mM AcONa pH 5.3, 5 mM $ZnCl_2$, and 50 mM NaCl), 4 mU phosphodiesterase II and 125 mU of DNAse II were added. The mixture was incubated at 37°C for extra 21 h, then 20 μL of 0.5 M Tris HCl pH 8.9 were added and the incubation continued for other 2 h, before quenching and removal of the enzymes as described in the previous protocols.

In the cases, when the samples were used for the LC-MS/MS analysis, internal standards of all analytes were added prior to enzymatic digestion.

Results and Discussion

Quantification of Lesions by Isotope Dilution LC-MS/MS

Initially we have developed an HPLC-UV analytical protocol for the satisfactory separation of the four natural 2′-deoxyribonucleosides, the four diastereoisomers of the purine 5′,8-cyclo-2′-deoxynucleosides and the two 8-oxo- products of dG and dA (see Figure S11 in Supplementary Material). The quantification of the lesions was based on the liquid chromatography isotope dilution tandem mass spectroscopy technique. The LOD (s/n = 3) and LOQ (s/n = 10) for the 5′*R*-cdG, 5′*S*-cdG, 5′*R*-cdA, 5′*S*-cdA, 8-oxo-dG and 8-oxo-dA were found 0.9, 0.6, 0.6, 0.2, 1.2, 0.2 fmol and 3.1, 2.2, 2.0, 0.8, 4.1 and 0.8 fmol respectively. Noteworthy, the LOD and LOQ values found here are lower than those reported in the literature (Wang et al., 2011, 2012) for the quantification of the lesions in cellular DNA. A typical LC-MS/MS trace (TIC) of the six lesions is depicted in **Figure 2A** together with the analytical traces of the 5′*R*-cdG and isotopic labeled 5′*R*-cdG (**Figure 2B**) and the fragmentation profiles of 5′*R*-cdA and 5′*R*-cdG (**Figures 2C,D**).

Regarding the stability of the lesions under acidic conditions, it is known that the 5′*S*-diastereoisomers of the cdA and cdG

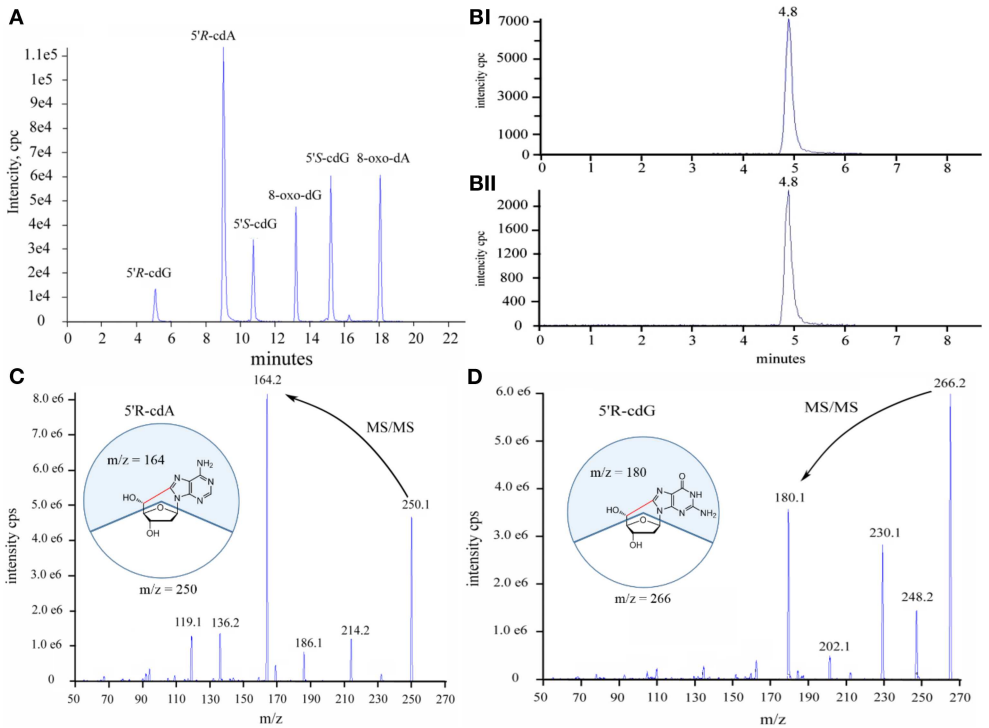

FIGURE 2 | (A) Total ion current traces of the six lesions, **(B)** Selective ion current traces of (i) the unlabeled and (ii) isotopic labeled 5′*R*-cdG, **(C)** Diagnostic MS/MS fragmentation profiles of the 5′*R*-cdA, **(D)** Diagnostic MS/MS fragmentation profiles of the 5′*R*-cdG.

are more resistant to acidic hydrolysis than the normal purine 2′-deoxyribonucleosides (dA, dG), the most resistant one being 8-oxo-dG. To our knowledge there is no information regarding the stability of the 5′*R*-diastereomers under acidic hydrolysis conditions (Das et al., 2012). In order to investigate the relative stability of the lesions and the recovery yields under acidic conditions, solutions containing the six lesions were added with different percentages of formic acid and incubated at 37°C for 4 h. The LC-MS/MS analyses showed that all the lesions are highly resistant to acidic hydrolysis and the order of resistance increase following the pattern: 5′*S*-cdG < 5′*R*-cdG < 5′*S*-cdA < 5′*R*-cdA ≈ 8-oxo-dG ≈ 8-oxo-dA. The recoveries of the lesions after 4 h incubation with formic acid are shown in **Figure 3**.

The investigation of the lesion stability in the enzymatic digestion buffers (pH = 5.6 and pH = 9) and the conditions followed until the LC-MS/MS analysis, autosampler storage, etc., showed that 8-oxo-dG is the only nucleoside resulting in low recoveries when protection from oxidation (use of metal chelators, argon, and antioxidants) is not taken into account. The lesions stock solutions were prepared by taking in to account their extinction coefficients, and particularly for 5′*R*- or 5′*S*-cdG found λ_{max} = 258 nm, ε = 13850 M^{-1} cm^{-1} and for 5′*R*- or 5′*S*-cdA found λ_{max} = 266 nm, ε = 14900 M^{-1} cm^{-1}. Regarding the [$^{15}N_5$]-7,8-dihydro-8-oxo-2′-deoxynucleosides were used the values reported in the literature (Taghizadeh et al., 2008).

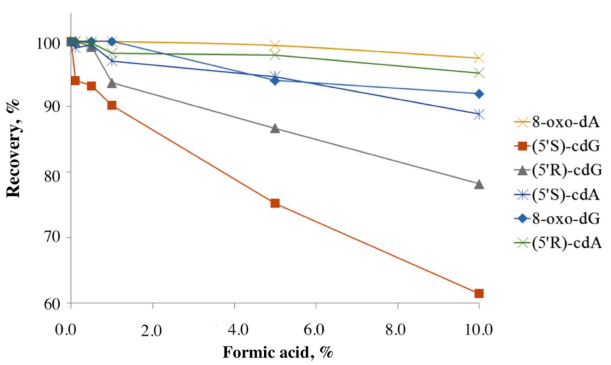

FIGURE 3 | Recovery of the lesions treated with different percentages of formic acid after incubation at 37°C for 4 h. The experiments were conducted in triplicates and errors are within the size of the symbols.

Enzymatic Digestibility Studies

One of the most important steps for the accurate quantification of the purine 5′,8-cyclonucleosides is the enzymatic digestion for the liberation of the lesions and the natural nucleotides to single molecules. To our knowledge in the literature three relatively recent enzymatic digestion protocols exist (protocols A, B, and C), that are used to release the purine 5′,8-cyclonucleosides from DNA. The amount of the purine 5′,8-cyclonucleosides per million of normal nucleosides (Lesions/10^6 Nu) produced

after gamma irradiation of calf thymus DNA, and the ratio of the 5′*R*/5′*S* diastereoisomers display very different values among the research groups working in this field (Chatgilialoglu et al., 2011). In order to investigate the efficiency of the various enzymatic protocols, we compared them by using the same solution of ds-DNA that was previously split into different aliquots. After incubation the digestion mixtures were filtered by ultracentrifuge filter (3 kDa), the filtrates were lyophilized and resolubilized in ddH_2O before being injected into the HPLC-UV system. From the analysis it was found that the efficiency of the enzymatic protocols in releasing the single nucleosides varies among protocols. Protocols A and C exhibited similar efficiencies while protocol B reached only 50%. In our two-steps development of the enzymatic digestion protocol we first sough to find which protocol lead to the complete liberation of the unmodified nucleosides. Protocols A and C were found to give the same result (Figure S12) for the digestion of the same DNA samples, while Protocol B reached only up to ∼50% in respect to A or C. When other protocols liberate the same amount of unmodified nucleosides, then they can be further considered also for their efficiency in liberation of the other modified nucleosides (i.e., cyclonucleosides). In fact, we evaluated the protocols A and C based on their ability to liberate also the lesions. This evaluation showed that Protocol A was predominant over Protocol C (**Figure 5**). The new digestion protocol was designed based on the enzymatic combination of benzonase and P1 nucleases. Benzonase was successfully used in the quantification of 5-met-Cyt and 8-oxo-dG (Quinlivan and Gregory, 2008; Cui et al., 2013), however the choice of the other enzyme to couple and the exact steps and duration of the treatment required to be determined. The optimization of the enzymatic protocol was performed in two phases. Initially, ds-DNA was incubated with different amount of benzonase, DNAse I, alkaline phosphatase, and phoshodiesterase I in 20 mM Tris-HCl buffer at pH 8 containing 20 mM $MgCl_2$. It was found that the presence of 20 mM NaCl increases the reactivity of the enzymes and the HPLC-UV analysis showed that the digestion was complete after 21 h incubation at 37°C with 2 U of benzonase, 2 U DNAse, 2 U alkaline phosphatase, and 2 mU phoshodiesterase I. **Figure 4** summarize the protocol steps in a flow diagram (see also Figure S12 in Supplementary Material for the relative efficiency of the four protocols).

Next, DNA solution (0.5 mg/mL) flushed with Ar, irradiated in a Gammacell ^{60}Co with 60 Gy (4.1 Gy/min) of irradiation dose at ambient temperature, was split in different aliquots of 50 μL each, and incubated according to the described protocol D. For comparison, some of the ds-DNA aliquots were digested according to Protocols A and C. Identical analytical results were achieved for the normal nucleosides, as quantified after the HPLC-UV analysis. On the other hand, the LC-MS/MS quantification of the lesions in the above samples revealed that the protocol D is much less efficient on the liberation of the purine 5′,8-cyclo-2′-deoxynucleosides compared to protocol A,

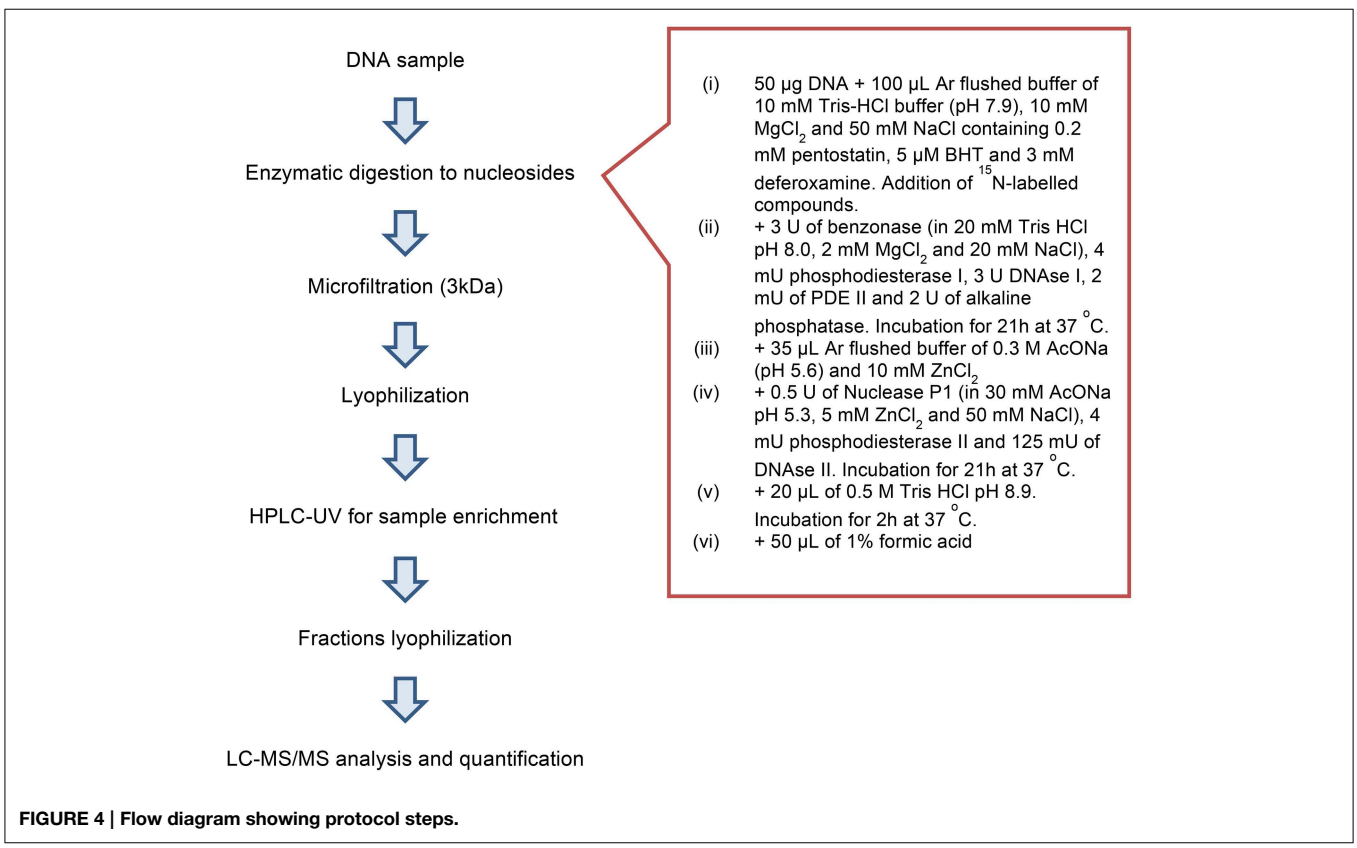

FIGURE 4 | Flow diagram showing protocol steps.

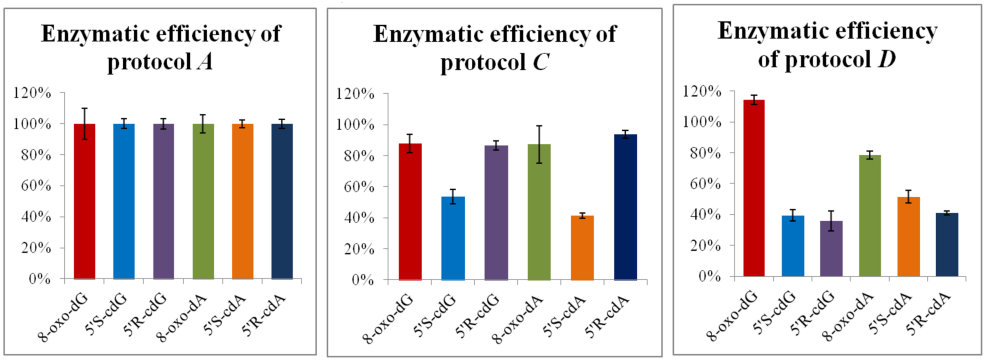

FIGURE 5 | Digestion efficiency of protocols A, C, and D based on the LC-MS/MS analysis. The values represent the mean of $n = 3$ independent experiments. The values recorded using Protocol A was employed as 100%.

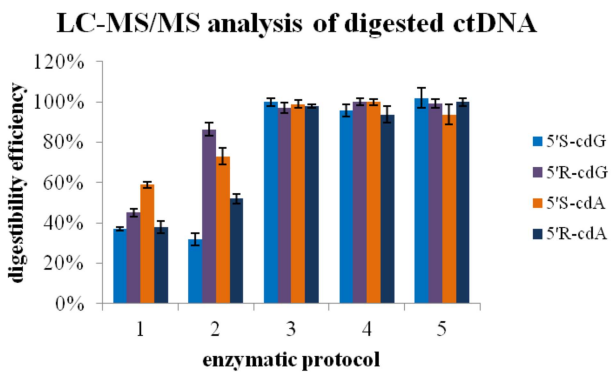

FIGURE 6 | Enzymatic protocol vs. digestibility efficiency 1 Application of Protocol D 2 Protocol D and then second digestion with 20 mU PDE II (pH 5.6) 3 Protocol D and then second digestion with 1U nuclease P1 and 20 mU PDE II (pH 5.6) 4 Protocol D and then second digestion with 1U nuclease P1 5 Protocol D, then 2nd digestion with 1U nuclease P1 (pH 5.6) and final third digestion with alkaline phosphatase and PDE I (pH 8.9). The values recorded using Protocol A was employed as 100%.

even after increment of the enzyme units and the incubation times (**Figure 5**). Considering the results for 8-oxo-dG, any of the protocols A, C, or D gave the same value.

Stability studies of the lesions in the buffer used during the enzymatic digestion with protocol A showed that special precautions are necessary for keeping the recovery close to 90% (ESCODD, 2002). Particularly, the combination of deferoxamine, BHT, inert atmosphere, and argon-flushed buffers is used as described elsewhere (Taghizadeh et al., 2008; Thornalley et al., 2010). Interestingly, the control samples of the calf thymus DNA, that were not exposed to γ-rays, were found to contain all four cyclopurines and the two 8-oxo lesions (see Table S4 in Supplementary Material) (Cui et al., 2013; Guerrero et al., 2013).

In order to identify the enzyme that can cleave the phosphodiester bond in the remaining DNA fragments, after treatment according to protocol D (**Figure 6**; ep1), the digestion mixture was split to different aliquots and a buffer of 300 mM AcONa pH 5.3 containing 10 mM $ZnCl_2$ was added (until final pH 5.8) together with 20 mU phosphodiesterase II (**Figure 6**; ep2). The same procedure was followed also with a combination of 20 mU phosphodiesterase II and 1 U nuclease P1 (**Figure 6**; ep3), and by using only 1 U of nuclease P1 (**Figure 6**; ep4). Finally, aliquots were treated with a combination of phosphodiesterase II, 1 U nuclease P1, DNase II according to protocol E (**Figure 6**; ep5).

Studies on the analytical recoveries were conducted by splitting a calf thymus DNA solution in multiple aliquots, spiking half of them with the lesions before being digested according to the enzymatic protocol E, and comparing the added amount with calculated by the LC-MS/MS system, after subtraction of the pre-existed in DNA amount of lesions. The calculated recoveries for 5′*R*-cdG, 5′*S*-cdG, 5′*R*-cdA, 5′*R*-cdA, 8-oxo-dG, and 8-oxo-dA were found 104, 95, 96, 90, 90, 113% respectively and the coefficients of variation as 2–5%. No significant loss was recorded during the sample workup, storage, and until the LC-MS/MS analysis.

In this work all the published digestion protocols have been applied to the same aliquots containing DNA irradiated with 60 Gy irradiation dose (γ-rays). Using this sampling, it was found surprisingly that the efficiency of the digestion protocols for the release of the single unmodified nucleosides is dissimilar in the case of Protocol B (Figure S12 in Supplementary Material). Additionally, when nuclease P1 was replaced by benzonase (Protocol D) the efficiency of the lesion release could be calculated as 30–60% (**Figure 6**). In order to identify the enzyme that can catalyze the hydrolysis of remaining DNA fragments containing the lesions, nuclease P1, and phosphodiesterase II were used either separately or together in the first digestion aliquots. In agreement with previous studies (Romieu et al., 1998) the LC-MS/MS analysis revealed that only nuclease P1 is able to lead to a complete digestion. Moreover, a subsequent activation of alkaline phosphatase by changing pH to basic values was found not to be necessary. The distortion that the purine 5′,8-cyclo-2′-deoxynucleosides cause to the active sites of phoshodiesterases can likely inhibit the formation of the necessary interactions for the hydrolysis of nucleotidyl-enzyme intermediate by the threonine active-site. On the contrary, the zinc-finger in the active site of nuclease P1, activated by a water molecule, was found to promote the hydrolysis at long incubation times.

Noteworthly, nuclease P1 is known to hydrolyse native DNA at much lower rate than the heat-denaturated DNA (Fujimoto et al., 1974) and it is much more expensive than benzonase, which is also more stable and known to hydrolyse fast both single and double stranded DNA. The nuclease P1 buffer used, in terms of zinc cation concentration, remained unaltered in respect to the ones reported elsewhere (Romieu et al., 1998; Wang et al., 2011), since our new protocol employs an off-line HPLC clean-up that eliminates the problems related to the mass detector deriving from the presence of non-volatile ions in the samples. In agreement to our results, recently it has been reported that the bulky spiroiminodihydantoin 2′-deoxynucleoside lesions challenge the hydrolytic activity of the 3′-exo and 5′-exo phosphodiesterases, and nuclease P1 quantitatively hydrolyzes the phosphodiester bond between the modified (lesion) and the normal nucleoside (Chen et al., 2013).

Conclusions

The use of purine 5′,8-cyclonucleosides as marker of DNA damage and reporter of DNA molecular asset at the moment of the HO$^{\bullet}$ insult is increasingly appreciated in free radical research, together with the advantage that cyclopurine markers do not suffer the stability problems and artifactual oxidative process of the most known 8-oxo-dG. In this paper we applied a step-wise approach for the development, optimization and validation of a new analytical procedure allowing the reproducible and quantitative determination of cdA, cdG and the two 8-oxo-lesions. Under the actual form, the procedure offers important ameliorations to apply extensively the protocol to the affirmation of cyclopurine biomarkers in different health conditions. The role of the zinc finger nuclease P1 as the only suitable enzyme, from those tested, for the quantitative liberation of the single nucleoside lesions was assessed. Moreover, we reduced by ∼10 fold the cost of the analysis per sample with the introduction of the nuclease benzonase.

Acknowledgments

This work was supported by the Ministero dell'Istruzione, dell'Università della Ricerca (PRIN 2009K3RH7N_002) and Marie Curie Intra-European Fellowship (CYCLOGUO–298555). The sponsorship of the COST Action CM1201 "Biomimetic Radical Chemistry" is gratefully acknowledged. The authors thank Dr. Gabriele Grossi and his group for the technical help and also Prof. Pasquale Chieco for the CRBA agreement of collaboration and the use of analytical facilities.

Supplementary Material

The Supplementary Material for this article can be found online at: http://journal.frontiersin.org/article/10.3389/fchem.2015.00047

References

Aydogan, B., Marshall, D. T., Swarts, S. G., Turner, J. E., Boone, A. J., Richards, N. G., et al. (2002). Site-specific OH attack to the sugar moiety of DNA: a comparison of experimental data and computational simulation. *Radiat. Res.* 157, 38–44. doi: 10.1667/0033-7587(2002)157[0038:SSOATT]2.0.CO;2

Belmadoui, N., Boussicault, F., Guerra, M., Ravanat, J.-L., Chatgilialoglu, C., and Cadet, J. (2010). Radiation-induced formation of purine 5′,8-cyclonucleosides in isolated and cellular DNA: high stereospecificity and modulating effect of oxygen. *Org. Biomol. Chem.* 8, 3211–3219. doi: 10.1039/c004531d

Boussicault, F., Kaloudis, P., Caminal, C., Mulazzani, Q. G., and Chatgilialoglu, C. (2008). The fate of C5′ radicals of purine nucleosides under oxidative conditions. *J. Am. Chem. Soc.* 130, 8377–8385. doi: 10.1021/ja800763j

Chatgilialoglu, C., Bazzanini, R., Jimenez, L. B., and Miranda, M. A. (2007). (5′S)- and (5′R)-5′,8-cyclo-2′-deoxyguanosine: mechanistic insights on the 2′-deoxyguanosin-5′-yl radical cyclization. *Chem. Res. Toxicol.* 20, 1820–1824. doi: 10.1021/tx700282x

Chatgilialoglu, C., Ferreri, C., and Terzidis, M. A. (2011). Purine 5′,8-cyclonucleoside lesions: chemistry and biology. *Chem. Soc. Rev.* 40, 1368–1382. doi: 10.1039/c0cs00061b

Chen, X., Fleming, A. M., Muller, J. G., and Burrows, C. J. (2013). Endonuclease and exonuclease activities on oligodeoxynucleotides containing spiroiminodihydantoin depend on the sequence context and the lesion stereochemistry. *New J. Chem.* 37, 3440–3449. doi: 10.1039/c3nj00418j

Cui, L., Ye, W., Prestwich, E. G., Wishnok, J. S., Taghizadeh, K., Dedon, P. C., et al. (2013). Comparative analysis of four oxidized guanine lesions from reactions of DNA with peroxynitrite, singlet oxygen, and γ-radiation. *Chem. Res. Toxicol.* 26, 195–202. doi: 10.1021/tx300294d

Culp, J. S., Blytt, H. J., Hermodson, M., and Butler, L. G. (1985). Amino acid sequence of the active site peptide of bovine intestinal 5′-nucleotide phosphodiesterase and identification of the active site residue as threonine. *J. Biol. Chem.* 260, 8320–8324.

Cummins, J. H., and Potter, B. V. (1987). On the mechanism of action of bovine intestinal mucosa 5′-nucleotide phosphodiesterase. Stereochemical evidence for a nucleotidyl-enzyme intermediate. *Eur. J. Biochem.* 162, 123–128. doi: 10.1111/j.1432-1033.1987.tb10551.x

Das, R. S., Samaraweera, M., Morton, M., Gascón, J. A., and Basu, A. K. (2012). Stability of N-glycosidic bond of (5′S)-8,5′-cyclo-2′-deoxyguanosine. *Chem. Res. Toxicol.* 25, 2451–2461. doi: 10.1021/tx300302a

European Standards Committee on Oxidative DNA Damage (ESCODD). (2002). Comparative analysis of baseline 8-oxo-7,8-dihydroguanine in mammalian cell DNA, by different methods in different laboratories: an approach to consensus. *Carcinogenesis* 23, 2129–2133. doi: 10.1093/carcin/23.12.2129

Fujimoto, M., Kuninaka, A., and Yoshino, H. (1974). Substrate specificity of nuclease P1. *Agric. Biol. Chem.* 39, 1991–1997. doi: 10.1271/bbb1961.39.1991

Fujimoto, M., Kuninaka, A., and Yoshino, H. (1975). Some physical and chemical properties of nuclease P1. *Agric. Biol. Chem.* 39, 1991–1997. doi: 10.1271/bbb1961.39.1991

Guerrero, C., Wang, J., and Wang, Y. (2013). Induction of 8,5′-Cyclo-2′-deoxyadenosine and 8,5′-Cyclo-2′-deoxyguanosine in isolated DNA by fenton-type reagents. *Chem. Res. Toxicol.* 26, 1361–1366. doi: 10.1021/tx400221w

Jaruga, P., Theruvathu, J., Dizdaroglu, M., and Brooks, P. J. (2004). Complete release of (5′S)-8,5′-cyclo-2′-deoxyadenosine from dinucleotides, oligodeoxynucleotides and DNA, and direct comparison of its levels in cellular DNA with other oxidatively induced DNA lesions. *Nucl. Acids Res.* 32:e87. doi: 10.1093/nar/gnh087

Jimenez, L. B., Encinas, S., Miranda, M. A., Navacchia, M. L., and Chatgilialoglu, C. (2004). The photochemistry of 8-bromo-2′-deoxyadenosine. A direct entry to cyclopurine lesions. *Photochem. Photobiol. Sci.* 3, 1042–1046. doi: 10.1039/b410939b

Kropachev, K., Ding, S., Terzidis, M. A., Masi, A., Liu, Z., Cai, Y., et al. (2014). Structural basis for the recognition of diastereomeric 5′,8-cyclo-2′-deoxypurine lesions by the human nucleotide excision repair system. *Nucl. Acids Res.* 42, 5020–5032. doi: 10.1093/nar/gku162

Mitra, D., Luo, X., Morgan, A., Wang, J., Hoang, M. P., Lo, J., et al. (2012). An ultraviolet-radiation-independent pathway to melanoma carcinogenesis in the red hair/fair skin background. *Nature* 491, 449–453. doi: 10.1038/nature11624

Münzel, M., Szeibert, C., Glas, A. F., Globisch, D., and Carell, T. (2011). Discovery and synthesis of new UV-induced intrastrand C(4-8)G and G(8-4)C photolesions. *J. Am. Chem. Soc.* 133, 5186–5189. doi: 10.1021/ja111304f

Quinlivan, E. P., and Gregory, J. F. (2008). DNA digestion to deoxyribonucleoside: a simplified one-step procedure. *Anal. Biochem.* 373, 383–385. doi: 10.1016/j.ab.2007.09.031

Romier, C., Dominguez, R., Lahm, A., Dahl, O., and Suck, D. (1998). Recognition of single-stranded DNA by nuclease P1: high resolution crystal structures of complexes with substrate analogs. *Proteins* 32, 414–424.

Romieu, A., Gasparutto, D., and Cadet, J. (1999). Synthesis and characterization of oligonucleotides containing 5′,8-cyclopurine 2′-deoxyribonucleosides: (5′R)-5′,8-cyclo-2′-deoxyadenosine, (5′S)-5′,8-cyclo-2′-deoxyguanosine, and (5′R)-5′,8-cyclo-2′-deoxyguanosine. *Chem. Res. Toxicol.* 1, 412–421. doi: 10.1021/tx9802668

Romieu, A., Gasparutto, D., Molko, D., and Cadet, J. (1998). Site-specific introduction of (5′S)-5′,8-cyclo-2′-deoxyadenosine into oligodeoxyribonucleotides. *J. Org. Chem.* 63, 5245–5249. doi: 10.1021/jo980083q

Taghizadeh, K., McFaline, J. L., Pang, B., Sullivan, M., Dong, M., Plummer, E., et al. (2008). Quantification of DNA damage products resulting from deamination, oxidation and reaction with products of lipid peroxidation by liquid chromatography isotope dilution tandem mass spectrometry. *Nat. Protoc.* 3, 1287–1298. doi: 10.1038/nprot.2008.119

Terzidis, M. A., and Chatgilialoglu, C. (2013). Radical cascade protocol for the synthesis of (5′S)- and (5′R)-5′,8-cyclo-2′-deoxyguanosine derivatives. *Aust. J. Chem.* 66, 330–335. doi: 10.1071/CH12494

Thornalley, P. J., Waris, S., Fleming, T., Santarius, T., Larkin, S. J., Winklhofer-Roob, B. M., et al. (2010). Imidazopurinones are markers of physiological genomic damage linked to DNA instability and glyoxalase 1-associated tumour multidrug resistance. *Nucl. Acids Res.* 38, 5432–5442. doi: 10.1093/nar/gkq306

Volbeda, A., Lahm, A., Sakiyama, F., and Suck, D. (1991). Crystal structure of Penicillium citrinum P1 nuclease at 2.8 A resolution. *EMBO J.* 10, 1607–1618.

Wang, J., Clauson, C. L., Robbins, P. D., Niedernhofer, L. J., and Wang, Y. (2012). The oxidative DNA lesions 8,5′-cyclopurines accumulate with aging in a tissue-specific manner. *Aging Cell* 11, 714–716. doi: 10.1111/j.1474-9726.2012.00828.x

Wang, J., Yuan, B., Guerrero, C., Bahde, R., Gupta, S., and Wang, Y. (2011). Quantification of oxidative DNA lesions in tissues of Long-Evans Cinnamon rats by capillary high-performance liquid chromatography-tandemmass spectrometry coupled with stable isotope-dilution method. *Anal. Chem.* 83, 2201–2209. doi: 10.1021/ac103099s

You, C., Dai, X., Yuan, B., Wang, J., Wang, J., Brooks, P. J., et al. (2012). A quantitative assay for assessing the effects of DNA lesions on transcription. *Nat. Chem. Biol.* 8, 817–822. doi: 10.1038/nchembio.1046

Conflict of Interest Statement: The authors declare that the research was conducted in the absence of any commercial or financial relationships that could be construed as a potential conflict of interest.

Copyright © 2015 Terzidis and Chatgilialoglu. This is an open-access article distributed under the terms of the Creative Commons Attribution License (CC BY). The use, distribution or reproduction in other forums is permitted, provided the original author(s) or licensor are credited and that the original publication in this journal is cited, in accordance with accepted academic practice. No use, distribution or reproduction is permitted which does not comply with these terms.

frontiers in Chemistry

ORIGINAL RESEARCH
published: 20 March 2015
doi: 10.3389/fchem.2015.00018

Radiation-induced formation of purine lesions in single and double stranded DNA: revised quantification

Michael A. Terzidis[1], *Carla Ferreri*[1] and *Chryssostomos Chatgilialoglu*[1,2]*

[1] Istituto per la Sintesi Organica e la Fotoreattività, Consiglio Nazionale delle Ricerche, Bologna, Italy, [2] Institute of Nanoscience and Nanotechnology, National Centre for Scientific Research "Demokritos", Athens, Greece

The formation of oxidative lesions arising from double stranded DNA damage is of major significance to chemical biology from the perspective of application to human health. The quantification of purine lesions arising from γ-radiation-induced hydroxyl radicals (HO•) has been the subject of numerous studies, with discrepancies on the measured 5′,8-cyclo-2′-deoxyadenosine (cdA) and 5′,8-cyclo-2′-deoxyguanosine (cdG) lesions reported by different groups. Here we applied an ameliorative protocol for the analysis of DNA damage with quantitative determination of these lesions via isotope dilution liquid chromatography coupled with tandem mass spectrometry. Tandem-type purine lesions were quantified along with 7,8-dihydro-8-oxo-2′-deoxyguanosine (8-oxo-dG) and 7,8-dihydro-8-oxo-2′-deoxyadenosine (8-oxo-dA) in single and double stranded DNA, generated during DNA exposure to diffusible HO• radicals in the absence or presence of physiological levels of oxygen. The cdA and cdG lesions in absence of oxygen were found ∼2 times higher in single than double stranded DNA, with 5′*R* being ∼6.5 and ∼1.5 times more predominant than 5′*S* in cdG and cdA, respectively. Interestingly, in the presence of 5% molecular oxygen the R/S ratios are retained with substantially decreased yields for cdA and cdG, whereas 8-oxo-dA and 8-oxo-dG remain nearly constant. The overall lesion formation follows the order: 8-oxo-dG >> 8-oxo-dA > 5′*R*-cdG > 5′*R*-cdA > 5′*S*-cdA > 5′*S*-cdG. By this method, there was a conclusive evaluation of radiation-induced DNA purine lesions.

Keywords: gamma radiation, free radicals, DNA damage, cyclopurines, 8-oxo-dG, LC-MS/MS

OPEN ACCESS

Edited by:
Antonio Monari, Université de Lorraine, France

Reviewed by:
Andrew Kellett, Dublin City University, Ireland
Thanasis Gimisis, National and Kapodistrian University of Athens, Greece

***Correspondence:**
Chryssostomos Chatgilialoglu, Institute of Nanoscience and Nanotechnology, National Centre for Scientific Research "Demokritos", 15341 Agia Paraskevi, Athens, Greece
c.chatgilialoglu@inn.demokritos.gr; chrys@isof.cnr.it

Specialty section:
This article was submitted to Chemical Biology, a section of the journal Frontiers in Chemistry

Received: *02 January 2015*
Paper pending published: *09 February 2015*
Accepted: *25 February 2015*
Published: *20 March 2015*

Citation:
Terzidis MA, Ferreri C and Chatgilialoglu C (2015) Radiation-induced formation of purine lesions in single and double stranded DNA: revised quantification. Front. Chem. 3:18. doi: 10.3389/fchem.2015.00018

Introduction

Genetic information of all living organisms is stored in DNA, a polymer consisting of 2′-deoxynucleosides. Reactive species, resulting from metabolic reactions, stresses, environmental conditions, presence of chemicals, etc., can alter the integrity of this biopolymer. Among highly reactive species, the hydroxyl radicals (HO•) can lead to nucleobase modifications and to strand breaks. The H5′ of sugars in DNA have been found quite vulnerable with a 55% probability of abstraction by HO•, in respect to the rest of the sugar hydrogen atoms (Aydogan et al., 2002). This fact leads to the generation of peculiar lesions containing a carbon-carbon bond between the sugar and the purine, rather than to abasic sites (Chatgilialoglu et al., 2011a). 5′,8-Cyclo-2′-deoxyadenosine (cdA) and 5′,8-cyclo-2′-deoxyguanosine (cdG), in their 5′*S* and 5′*R* diastereomeric forms (**Figure 1**), have been identified among other DNA lesions in

enzymatically digested cellular DNA of mammals (Chatgilialoglu et al., 2011a). Moreover it has been recently reported that aging causes accumulation of the cyclopurines in tissues, aging liver holding the first place in aging accumulated cyclopurines, followed by the kidney, while lower levels were found in the brain (Wang et al., 2011, 2012). It is worth noting that the cyclopurine lesions have been used in a recent study as reliable oxidative stress biomarkers in animal models focusing on the liver injury pathophysiology in Wilson's disease and pigmentation (Mitra et al., 2012; You et al., 2012). As matter of fact, oxidative artifacts during work-up of biological DNA samples are reported in the evaluation of 8-oxo-dG lesions, whereas cyclopurines are "pure" radical-derived products, and cannot derive from accidental oxidation of the material.

The repair efficiency of cyclopurine lesions has recently been studied in some aspects and more information is expected in the near future. These lesions are repaired by Nucleotide Excision Repair (NER) and not by Base Excision Repair (BER). HeLa cell extracts have been used in identical DNA sequences containing the cdA and cdG lesions giving a direct comparison of the relative NER efficiencies that was missing (Kropachev et al., 2014). Interestingly, the study revealed a higher repair efficiency, by a factor of ∼2, for the 5′*R* over the 5′*S* cyclopurines, however the excision efficiency of the cdA and cdG lesions was found similar. In the same vein, extensive *in silico* analysis confirmed the correlation of the stacking impairment of the stereoisomer with their relative NER excision efficiency. Evidence was recently provided that both 5′*R*-cdA and 5′*S*-cdA in a CAG repeat tract causes CTG repeat deletion exclusively during DNA lagging strand maturation and BER activity (Xu et al., 2014). The latter study indicates that accumulation of cyclopurine lesions in the human genome can lead to trinucleotide repeat instability via a unique lesion bypass by pol β.

Increased levels of cdA and cdG are linked to NER mechanism deficiency and mutagenesis. Particularly, 5′*S*-cdG results in strong inhibition and block of the transcription in both *in vitro* and in mammalian cells as found by a competitive transcription and adduct bypass assay by a recent study (You et al., 2012).

Attempts to accurately determine the level of these lesions in DNA by enzymatic digestion followed by chromatographic methods coupled to mass spectrometric (MS) analyses are numerous. Results reported for irradiated samples of calf thymus DNA have been critically reviewed by us in 2011, underlining the need of further research for the potential involvement of these lesions in human health (Chatgilialoglu et al., 2011a). A detailed protocol revision for the quantification of purine lesions in DNA has been recently provided (Terzidis and Chatgilialoglu, in preparation). The objectives of this work were to apply our protocol based on the stable isotope-dilution tandem mass spectrometry technique using triple quadrupole for the quantification of $HO^{\bullet}$ radical induced cyclopurine and 8-oxopurine lesions within single- and double-stranded DNA in gamma-irradiated aqueous solutions.

Materials and Methods

Chemicals

All the salts and solvents, activated calf thymus DNA, nuclease P1 from Penicillium citrinum, phosphodiesterase II, phosphodiesterase I from Crotalus Adamanteus venom, DNAse I, DNAse II, alkaline phosphatase from bovine intestinal mucosa, erythro-9-(2-hydroxy-3-nonyl)adenine hydrochoride (EHNA), benzonase 99%, deferoxamine mesylate salt, BHT and pentostatin, were obtained from Sigma (Taufkirchen, Germany and Milan, Italy) while the 3 and 100 kDa cut-off filters were purchased from Millipore (Bedford, USA). Distilled and deionized water (ddH_2O) was purified by a Milli-Q system (Millipore, Bedford,

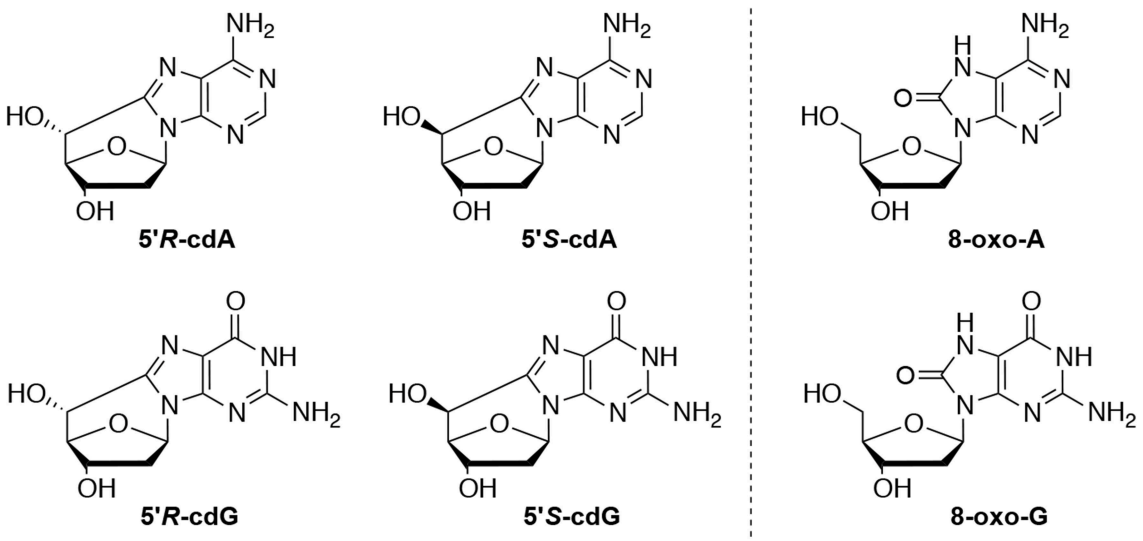

FIGURE 1 | Left: 5′,8-Cyclo-2′-deoxyadenosine (cdA) and 5′,8-cyclo-2′-deoxyguanosine (cdG) lesions; **Right:** 7,8-dihydro-8-oxo-2′-deoxyguanosine (8-oxo-dG) and 7,8-dihydro-8-oxo-2′-deoxyadenosine (8-oxo-dA) lesions.

USA). Synthesis of reference compounds and internal standards was based on previously reported protocols (Terzidis and Chatgilialoglu, in preparation).

γ-Radiolysis Experiments

Calf thymus DNA (1 mg) was dissolved in ddH_2O (1 mL) gently rocking overnight at 4°C. Next, the solution was transferred in a microspin filter (100 kDa) and centrifuged at ∼9000 g for 2 min. To the concentrated DNA solution, 1 mL of ddH_2O was added and the mixture was centrifuged again. The previous procedure was repeated for three times. Finally, an extra volume of ddH_2O was added and the concentration of the final DNA solution was estimated according to its absorbance at 260 nm. In a typical gamma irradiation experiment, 200 μL of the desalinated ctDNA solution (0.5 mg/mL) were placed in a glass vial of 2 mL, flushed with N_2O or N_2O/O_2 95:5 for 10 min. The solution was exposed to gamma rays in a ^{60}Co Gammacell apparatus (dose rate 4.1 Gy/min) and the irradiation dose increased from 0 to 20, 40, and 60 Gy. In the case of the experiments with the single stranded DNA the samples were heated up to 92°C for 2 min and were cooled down rapidly in ice water prior to irradiation. All the irradiation experiments were performed in triplicates.

Enzymatic Digestion to Nucleosides

Materials and methods are described in detail elsewhere (Terzidis and Chatgilialoglu, in preparation). **Figure 2** summarizes the protocol as a flow diagram, the key step being the enzymatic digestion to obtain nucleosides in the presence of antioxidants, inert atmosphere, an efficient biocompatible metal chelator and the ^{15}N-labeled compounds. In summary, the necessary steps for an efficient digestion are:

(i) in 50 μg DNA sample
(ii) add 100 μL Ar flushed buffer of 10 mM Tris-HCl buffer (pH 7.9), 10 mM $MgCl_2$ and 50 mM NaCl containing 0.2 mM pentostatin, 5 μM BHT and 3 mM deferoxamine
(iii) add the ^{15}N-labeled compounds
(iv) add a gently mixed cocktail of enzymes containing 3 U of benzonase (in 20 mM Tris HCl pH 8.0, 2 mM $MgCl_2$ and 20 mM NaCl), 4 mU phosphodiesterase I, 3 U DNAse I, 2 mU of PDE II and 2 U of alkaline phosphatase.
(v) Incubate for 21 h at 37°C
(vi) add 35 μL Ar flushed buffer of 0.3 M AcONa (pH 5.6) and 10 mM ZnCl
(vii) add a gently mixed cocktail of enzymes containing 0.5 U of Nuclease P1 (in 30 mM AcONa pH 5.3, 5 mM $ZnCl_2$ and 50 mM NaCl), 4 mU phosphodiesterase II and 125 mU of DNAse II.
(viii) Incubate for 21 h at 37°C
(ix) add 20 μL of 0.5 M Tris HCl pH 8.9 and incubate for 2 h at 37°C (this step is optional)
(x) quench the basic solution with 50 μL of 1% formic acid (final pH ∼ 7).

This procedure has been tested with purine cyclonucleosides to exclude the occurrence of any degradative process.

LC-MS/MS Analysis and Quantification

Isotope Dilution Tandem Mass Spectrometry Quantification

An LC-MS/MS system (LC, Perkin Elmer Inc., USA; triple quadrupole mass spectrometer Q-Trap 4000, AB Sciex Inc., Canada) was employed for the quantification of the lesions in the enzymatically digested DNA samples, while for the unmodified nucleosides an HPLC-UV (Agilent 1100 series, Agilent Technologies, USA) was used, as described elsewhere (Terzidis and Chatgilialoglu, in preparation). Briefly, the DNA samples, spiked with the ^{15}N-labeled nucleosides and after being enzymatically digested, were injected in the HPLC-UV system loaded with a 4.6 mm x 150 mm Luna C18 (2) 100 Å column (5 μ min particle size, Phenomenex). During the analysis the fractions in the

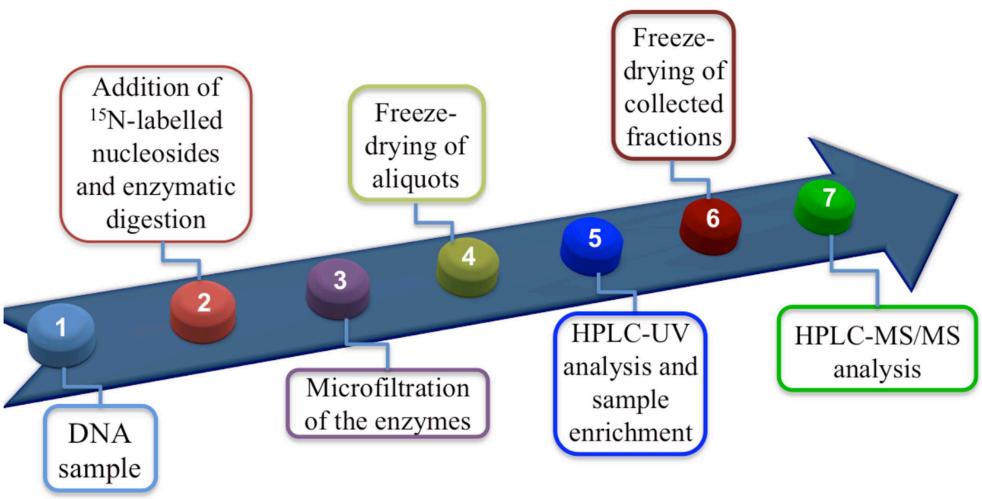

FIGURE 2 | Flow diagram showing protocol steps.

time windows where the lesions eluted were collected and freeze-dried. The unmodified nucleosides were quantified based on their absorption at 260 nm against their response calibration curves at the same wavelength. The collected fractions were subsequently injected to the LC-MS/MS system loaded with a 2 × 150 mm Luna C18 (2) 100 Å column (3 μ min particle size, Phenomenex) working on the multiple reaction monitoring (MRM) mode. A flow diagram showing the protocol for the quantification of the lesions is reported in **Figure 2**. All six lesions were found and quantified independently in all DNA samples before irradiation (control experiments). Thus, values of the control experiments were subtracted from the values recorded after the irradiation of the samples with the appropriate dose giving 0 lesions/10^6 nucleosides (radiation induced) at 0 Gy of irradiation.

Results

Radiolysis of neutral water leads to e^-_{aq}, $HO^\bullet$ and $H^\bullet$ as shown in eq 1. The values in parentheses represent the radiation chemical yields (G) in units of μmol J^{-1}. In N_2O-saturated solution (~0.02 m of N_2O), e^-_{aq} are efficiently transformed into $HO^\bullet$ radical via Reaction 2 ($k_2 = 9.1 \times 10^9$ M^{-1} s^{-1}), with $G(HO^\bullet) = 0.55$ μmol J^{-1}, i.e., $HO^\bullet$ radicals and H atoms account for 90 and 10%, respectively, of the reactive species (Buxton et al., 1988). The rate constants for the reactions of $HO^\bullet$ radicals and H atoms with DNA (Reactions 3 and 4) have been estimated to be ca. 2.5×10^8 M^{-1} s^{-1} and 6×10^7 M^{-1} s^{-1} per base unit, respectively (Buxton et al., 1988).

$$H_2O \rightsquigarrow e^-_{aq}(0.27), HO^\bullet(0.28), H^\bullet(0.062) \quad (1)$$

$$e^-_{aq} + N_2O + H_2O \rightarrow HO^\bullet + N_2 + HO^- \quad (2)$$

$$HO^\bullet + DNA \rightarrow \text{radical product} \quad (3)$$

$$H^\bullet + DNA \rightarrow \text{radical product} \quad (4)$$

The reactions of $HO^\bullet$ radicals with DNA were carried out using single- and double-stranded DNA. For this purpose 200 μL of N_2O-saturated aqueous solutions containing calf thymus DNA (0.5 mg/mL) at natural pH were irradiated under steady-state conditions with a dose rate of 4.1 Gy min^{-1}, followed by enzymatic DNA digestion optimized by us and LC-MS/MS analysis (see above). Both 5′*R* and 5′*S* diastereomers of cdA and cdG were found to be generated linearly with the applied dose within the range 0–60 Gy. **Figures 3A,B** (blue symbols) show 5′*R*-cdG and 5′*S*-cdG, respectively, in ss-DNA (open circles) and ds-DNA (closed circles). In addition the formation of 8-oxo-7,8-dihydro-2′-deoxyguanosine (8-oxo-dG) and 8-oxo-7,8-dihydro-2′-deoxyadenosine (8-oxo-dA) was also measured. The levels of DNA lesions per Gy in the absence of oxygen are reported in **Table 1** (For more details see Figures S1, S2 in Supplementary Material).

The reactions of $HO^\bullet$ radicals with ss-DNA or ds-DNA were also carried out in the presence of molecular oxygen. In particular, 200 μL of N_2O(95%)/O_2(5%)-saturated aqueous solutions of calf thymus DNA (0.5 mg/mL) were irradiated under stationary state conditions with a dose rate of 4.1 Gy min^{-1}. **Figures 3A,B**

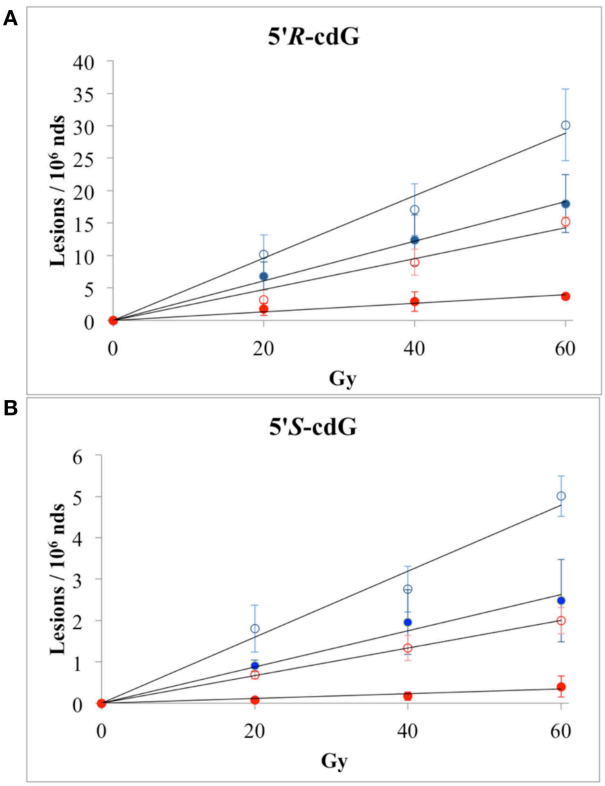

FIGURE 3 | Radiation-induced formation of 5′*R*-cdG (A) and 5′*S*-cdG (B) of ss-DNA (open circles) or ds-DNA (closed circles); (○●) N_2O-saturated aqueous solutions; (○●) N_2O (95%)/O_2(5%)-saturated aqueous solutions. The values represent the mean of $n = 3$ independent experiments.

(red symbols) show 5′*R*-cdG and 5′*S*-cdG, respectively, in ss-DNA (open circles) and ds-DNA (closed circles). The levels of DNA lesions per Gy in the presence of oxygen are also reported in **Table 1** (For more details see Figures S3, S4 in Supplementary Material). The 5% of oxygen-saturated solution corresponds to 6.7×10^{-5} M, which is the typical concentration of well-oxygenated tissues (Battino et al., 1983). Under our experimental conditions, e^-_{aq} are still converted into $HO^\bullet$ radical via Reaction 2, although Reaction 5 is quite fast ($k_5 = 1.9 \times 10^{10}$ M^{-1} s^{-1}) due the large difference in concentration of the two gases and $H^\bullet$ are efficiently converted into $O_2^{-\bullet}$ via Reaction 6 ($k_6 = 2 \times 10^{10}$ M^{-1} s^{-1}), the $pK_a(HOO^\bullet)$ being 4.8 (Buxton et al., 1988). Since $O_2^{-\bullet}$ does not react with DNA, these are ideal conditions for studying the reaction of $HO^\bullet$ radicals with DNA in the presence of oxygen.

$$e^-_{aq} + O_2 \rightarrow O_2^{-\bullet} \quad (5)$$

$$H^\bullet + O_2 \rightarrow HOO^\bullet \rightleftharpoons O_2^{-\bullet} + H^+ \quad (6)$$

In all cases, the formation of the 5′*R* and 5′*S* diastereomers of both cdG and cdA, as well as the 8-oxo-dG and 8-oxo-dA, was found to increase with the dose of γ-rays within the dose-range 0–60 Gy. The levels of lesions per Gy in the presence of oxygen are also reported in **Table 1**.

TABLE 1 | Lesions measured from irradiated sample of calf thymus DNA by LC-MS/MS.

Substrate[a]	Conditions[b]	Lesion	Lesions/10^6Nu/Gy	5′R/5′S
ss-DNA	N_2O, 0–60 Gy	cdG	0.56	6.0
		cdA	0.48	1.7
		8-oxo-dG	49.3	
		8-oxo-dA	4.29	
	N_2O:O_2 (95:5), 0–60 Gy	cdG	0.24	6.5
		cdA	0.21	1.7
		8-oxo-dG	57.0	
		8-oxo-dA	3.61	
ds-DNA	N_2O, 0–60 Gy	cdG	0.35	7.0
		cdA	0.23	1.6
		8-oxo-dG	20.2	
		8-oxo-dA	2.80	
	N_2O:O_2 (95:5), 0–60 Gy	cdG	0.08	7.0
		cdA	0.08	2.2
		8-oxo-dG	22.4	
		8-oxo-dA	2.37	

[a] *Calf thymus DNA.*
[b] *Used gas and irradiation dose.*

Discussion

Many efforts have been devoted during the last two decades to the identification and measurement of cdA and cdG lesions in DNA samples (see **Figure 1**). These lesions are the products of the intramolecular attack of C5′ radical to the purine moiety. Both lesions have two diastereomeric forms (5′*R* and 5′*S*), for the configuration of the C5′ position. The order of reactivity of HO• radical toward the various C–H bonds of the 2-deoxyribose moiety of DNA is expected to parallel the exposure to solvent of the 2-deoxyribose hydrogen atoms (i.e., H5′ > H4′ > H3′ ≈ H2′ ≈ H1′) (Chan et al., 2010). The yield of cdG was found to be equal or higher than that of cdA, the ratio of formation between cdG and cdA varying from 1 to 1.5 in all cases. The 5′*R* diastereomer is formed predominantly leading to 5′*R*/5′*S* ratio of ∼6.5:1.0 for cdG and ∼1.7:1.0 for cdA. It is worth mentioning that 5′*R*/5′*S* ratios of 8.3:1 for cdG and 6:1 for cdA were obtained in water upon irradiation of free nucleosides (Chatgilialoglu et al., 2007; Boussicault et al., 2008), indicating that the 5′*R*-diastereomer is always predominant in aqueous solution independently of the molecular complexity. On the other hand, the formation of 8-oxo-dG was about 90- and 60-fold higher than cdG in ss- and ds-DNA, respectively, in the absence of oxygen, whereas the formation of 8-oxo-dA was about 10-fold higher in both ss- and ds-DNA. The formation of both cdG and cdA decreases substantially in the presence of oxygen, indicating competition paths for C5′ radical between cyclization and addition to oxygen (**Figure 4**). Moreover, the 5′*R*/5′*S* ratio is similar for both cdG and cdA as observed in the absence of oxygen.

Experimental data on the reaction of HO• radical with simple nucleosides like 2′-deoxyadenosine and 2′-deoxyguanosine indicated that ca. 10% of H-atom abstraction occurs at the H5′ position affording purine 5′,8-cyclonucleosides (Chatgilialoglu et al., 2007; Boussicault et al., 2008). Rate constants (k_c) of 1.6×10^5 s^{-1} and 6.9×10^5 s^{-1} for the cyclization of 2′-deoxyadenosin-5′-yl and 2′-deoxyguanosin-5′-yl radicals (1→2) were also reported at room temperature (cf., **Figure 4**) (Chatgilialoglu et al., 2003, 2011b). The analogous cyclization rates in ss-DNA or ds-DNA are unknown. With the due precaution and reasonable assumptions, the rate constants of cyclization in ss-DNA or ds-DNA can be estimated from the data of **Table 1**. Assuming that in **Figure 4** the radical 1 is converted quantitatively to cdA and cdG in the absence of oxygen, and that decreased formation of purine 5′,8-cyclonucleosides in the presence of oxygen is mainly due to products deriving from the peroxyl radical 3, the rate constant of unimolecular path can be estimated by applying the free-radical clock methodology (Newcomb, 1993). Using $[O_2] = 6.7 \times 10^{-5}$ M and $k(O_2) = 1 \times 10^9$ M^{-1} s^{-1}, we estimated k_c to be ca. 5×10^4 s^{-1} for both 2′-deoxyadenosin-5′-yl and 2′-deoxyguanosin-5′-yl radicals in ss-DNA and about halved ($2–3 \times 10^4$ s^{-1}) in ds-DNA. We suggest that (i) these values represent the mean rate constant for cyclization obtained along the DNA sequence, and (ii) local conformations due to the supramolecular organization of DNA can give different contribution to these values, but overall they reduce substantially the cyclization rates of the two radicals.

It is worth pointing out that the data reported in the literature so far on the radiation-induced formation of purine 5′,8-cyclonucleosides in DNA give a quite confusing scenario. All data were compared in a review article (Chatgilialoglu et al., 2011a) evidencing the discrepancies including the latest one (Belmadoui et al., 2010). In **Table 1**, in N_2O-saturated solution experiments the level of lesions/10^6 nucleosides/Gy was found to be 0.23 for cdA, and 0.35 for cdG in ds-DNA, whereas the values of similar

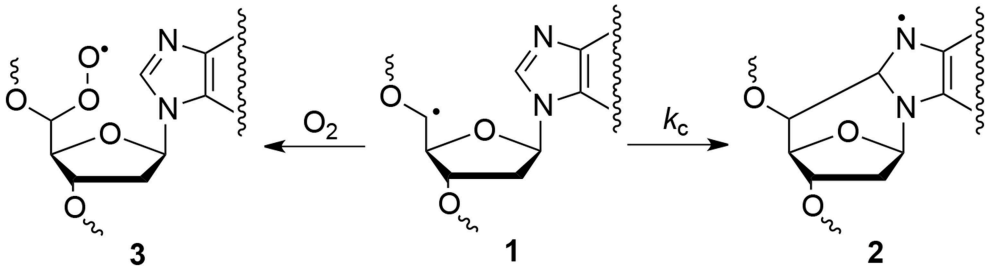

FIGURE 4 | Partition of C5′ radical 1 between cyclization reaction to give 2 and molecular oxygen addition to give 3.

experiments were reported by one of us and others to be 14.2 and 20.1 (Belmadoui et al., 2010), which is a ∼60-fold excess for both cdA and cdG. It is also worth mentioning that the 8-oxo-dA and 8-oxo-dG formation corresponds to a ∼3-fold excess. These discrepancies are likely derived from the analytical steps required after the reaction, which involve the enzymatic DNA digestion and the mass spectrometry assay. Indeed, the former quantification of 5′*R* and 5′*S* diastereomers of cdA and cdG was achieved by external calibration, whereas in the present work we employed HPLC coupled with tandem mass spectrometry (LC-MS/MS) with quantification given by the isotope-dilution technique.

Conclusions

The use of purine 5′,8-cyclonucleosides as marker of DNA damage and reporter of DNA structures at the moment of the HO• insult is increasingly appreciated in free radical research, together with the advantage that cyclopurine markers do not suffer the stability problems and artifactual oxidative process of the most known 8-oxo-dG. In this paper we applied the new analytical protocol to investigate the efficacy of the HO• generated by water radiolysis to form the cdA and cdG lesions in single and double stranded DNA in the presence and absence of molecular oxygen. All together our findings suggest that cdA and cdG formation depends on the dose of irradiation and the DNA secondary structure (single or double stranded), with the lesions following the order 5′*R*-cdG > 5′*R*-cdA > 5′*S*-cdA > 5′*S*-cdG. Particularly, in absence of oxygen the HO• insult causes ∼2 times more production of cdA and cdG in single than in double stranded DNA, with the 5′*R* diastereoisomer always more predominant than 5′*S*. Interestingly, the presence of molecular oxygen showed no influence on the cyclopurines diastereomeric ratios, but remarkably reduced their formation yields.

Acknowledgments

This work was supported by the Marie Curie Intra-European Fellowship (CYCLOGUO–298555). The sponsorship of the COST Action CM1201 "Biomimetic Radical Chemistry" is gratefully acknowledged. The authors thank Dr. Gabriele Grossi and Prof. Pasquale Chieco for the CRBA agreement of collaboration and the use of analytical facilities.

Supplementary Material

The Supplementary Material for this article can be found online at: http://www.frontiersin.org/journal/10.3389/fchem.2015.00018/abstract

References

Aydogan, B., Marshall, D. T., Swarts, S. G., Turner, J. E., Boone, A. J., Richards, N. G., et al. (2002). Site-specific OH attack to the sugar moiety of DNA: a comparison of experimental data and computational simulation. *Radiat. Res.* 157, 38–44. doi: 10.1667/0033-7587(2002)157[0038:SSOATT]2.0.CO;2

Battino, R., Rettich, T. R., and Tominaga, T. (1983). The solubility of oxygen and ozone in liquids. *J. Phys. Chem. Ref. Data* 12, 163–178. doi: 10.1063/1.555680

Belmadoui, N., Boussicault, F., Guerra, M., Ravanat, J.-L., Chatgilialoglu, C., and Cadet, J. (2010). Radiation-induced formation of purine 5′,8-cyclonucleosides in isolated and cellular DNA: high stereospecificity and modulating effect of oxygen. *Org. Biomol. Chem.* 8, 3211–3219. doi: 10.1039/C004531D

Boussicault, F., Kaloudis, P., Caminal, C., Mulazzani, Q. G., and Chatgilialoglu, C. (2008). The fate of C5′ radicals of purine nucleosides under oxidative conditions. *J. Am. Chem. Soc.* 130, 8377–8385. doi: 10.1021/ja800763j

Buxton, G. V., Greenstock, C. L., Helman, W. P., and Ross, A. B. (1988). Critical review of rate constants for hydrated electrons, hydrogen atoms and hydroxyl radicals (OH/O–) in aqueous solution. *J. Phys. Chem. Ref. Data* 17, 513–886. doi: 10.1063/1.555805

Chan, W., Chen, B., Wang, L., Taghizadeh, K., Demott, M. S., and Dedon, P. C. (2010). Quantification of the 2-deoxyribonolactone and nucleoside 5'-aldehyde products of 2-deoxyribose oxidation in DNA and cells by isotope-dilution gas chromatography mass spectrometry: differential effects of γ-radiation and Fe2+-EDTA. *J. Am. Chem. Soc.* 132, 6145–6153. doi: 10.1021/ja910928n

Chatgilialoglu, C., Bazzanini, R., Jimenez, L. B., and Miranda, M. A. (2007). (5′S)- and (5′R)-5′,8-cyclo-2′-deoxyguanosine: mechanistic insights on the 2′-deoxyguanosin-5′-yl radical cyclization. *Chem. Res. Toxicol.* 20, 1820–1824. doi: 10.1021/tx700282x

Chatgilialoglu, C., D'Angelantonio, M., Kciuk, G., and Bobrowski,K. (2011b). New insights into the reaction paths of hydroxyl radicals with 2′-deoxyguanosine. *Chem. Res. Toxicol.* 24, 2200–2206. doi: 10.1021/tx2003245

Chatgilialoglu, C., Ferreri, C., and Terzidis, M. A. (2011a). Purine 5′,8-cyclonucleoside lesions: chemistry and biology. *Chem. Soc. Rev.* 40, 1368–1382. doi: 10.1039/c0cs00061b

Chatgilialoglu, C., Guerra, M., and Mulazzani, Q. G. (2003). Model studies of DNA C5′ radicals: selective generation and reactivity of 2′-deoxyadenosin-5′-yl radical. *J. Am. Chem. Soc.* 125, 3939–3948. doi: 10.1021/ja029374d

Kropachev, K., Ding, S., Terzidis, M. A., Masi, A., Liu, Z., Cai, Y., et al. (2014). Structural basis for the recognition of diastereomeric 5′,8-cyclo-2′-deoxypurine lesions by the human nucleotide excision repair system. *Nucl. Acids Res.* 42, 5020–5032. doi: 10.1093/nar/gku162

Mitra, D., Luo, X., Morgan, A., Wang, J., Hoang, M. P., Lo, J., et al. (2012). An ultraviolet-radiation-independent pathway to melanoma carcinogenesis in the red hair/fair skin background. *Nature* 491, 449–453. doi: 10.1038/nature 11624

Newcomb, M. (1993). Competition methods and scales for alkyl radical reaction kinetics. *Tetrahedron* 49, 1151–1176. doi: 10.1016/S0040-4020(01)85808-7

Wang, J., Clauson, C. L., Robbins, P. D., Niedernhofer, L. J., and Wang, Y. (2012). The oxidative DNA lesions 8,5′-cyclopurines accumulate with aging in a tissue-specific manner. *Aging Cell* 11, 714–716. doi: 10.1111/j.1474-9726.2012.00828.x

Wang, J., Yuan, B., Guerrero, C., Bahde, R., Gupta, S., and Wang, Y. (2011). Quantification of oxidative DNA lesions in tissues of Long-Evans Cinnamon rats by capillary high-performance liquid chromatography-tandem mass spectrometry coupled with stable isotope-dilution method. *Anal. Chem.* 83, 2201–2209. doi: 10.1021/ac103099s

Xu, M., Lai, Y., Jiang, Z., Terzidis, M. A., Masi, A., Chatgilialoglu, C., et al. (2014). A 5′, 8-cyclo-2′-deoxypurine lesion induces trinucleotide repeat deletion via a unique lesion bypass by DNA polymerase β. *Nucleic Acids Res.* 42, 13749–13763. doi: 10.1093/nar/gku1239

You, C., Dai, X., Yuan, B., Wang, J., Wang, J., Brooks, P. J., et al. (2012). A quantitative assay for assessing the effects of DNA lesions on transcription. *Nat. Chem. Biol.* 8, 817–822. doi: 10.1038/nchembio.1046

Conflict of Interest Statement: The authors declare that the research was conducted in the absence of any commercial or financial relationships that could be construed as a potential conflict of interest.

Copyright © 2015 Terzidis, Ferreri and Chatgilialoglu. This is an open-access article distributed under the terms of the Creative Commons Attribution License (CC BY). The use, distribution or reproduction in other forums is permitted, provided the original author(s) or licensor are credited and that the original publication in this journal is cited, in accordance with accepted academic practice. No use, distribution or reproduction is permitted which does not comply with these terms.

frontiers in Chemistry

ORIGINAL RESEARCH
published: 27 March 2015
doi: 10.3389/fchem.2015.00022

The association constant of 5′,8-cyclo-2′-deoxyguanosine with cytidine

Amedeo Capobianco[1], Tonino Caruso[1], Sandra Fusco[1], Michael A. Terzidis[2], Annalisa Masi[2], Chryssostomos Chatgilialoglu[2,3] and Andrea Peluso[1]**

[1] *Dipartimento di Chimica e Biologia, Università di Salerno, Fisciano, Salerno, Italy,* [2] *Istituto per la Sintesi Organica e la Fotoreattività, Consiglio Nazionale delle Ricerche, Bologna, Italy,* [3] *Institute of Nanoscience and Nanotechnology, National Center for Scientific Research "Demokritos," Athens, Greece*

OPEN ACCESS

Edited by:
Elise Dumont, Ecole Normale Supérieure de Lyon, France

Reviewed by:
Célia Fonseca Guerra, VU University Amsterdam, Netherlands
Jean-Luc Ravanat, CEA Grenoble, France

***Correspondence:**
Chryssostomos Chatgilialoglu, Institute of Nanoscience and Nanotechnology, National Center for Scientific Research "Demokritos," 15341 Agia Paraskevi, Athens, Greece
c.chatgilialoglu@inn.demokritos.gr; chrys@isof.cnr.it;
Andrea Peluso, Dipartimento di Chimica e Biologia, Università di Salerno, I-84084 Fisciano, Salerno, Italy; apeluso@unisa.it

Specialty section:
This article was submitted to Chemical Biology, a section of the journal Frontiers in Chemistry

Received: *18 January 2015*
Paper pending published: *03 February 2015*
Accepted: *06 March 2015*
Published: *27 March 2015*

Citation:
Capobianco A, Caruso T, Fusco S, Terzidis MA, Masi A, Chatgilialoglu C and Peluso A (2015) The association constant of 5′,8-cyclo-2′-deoxyguanosine with cytidine. Front. Chem. 3:22. doi: 10.3389/fchem.2015.00022

The association of 5′,8-cyclo-2′-deoxyguanosine (cdG), a DNA tandem lesion, with its complementary base cytosine has been studied by voltammetry and NMR in chloroform, using properly silylated derivatives of the two nucleobases for increasing their solubilities. Both voltammetric data and NMR titrations indicated that the Watson-Crick complex of cytidine with cdG is weaker than that with guanosine, the difference being approximately of one order of magnitude between the two association constants.

Keywords: DNA damage, cyclopurines, voltammetry, NMR, Watson-Crick complex

Introduction

The level of distortion in DNA double helix is highly evaluated for the recognition and the repair of DNA lesions in cells. Among the various lesions that can be produced as consequence of metabolic processes and other external factors (oxidizing agents, drugs, ionizing, and non-ionizing irradiation, etc.) are the 5′,8-cyclo-2′-deoxypurines (cdP) where the base is covalently connected with the sugar with an extra carbon-carbon bond apart from the usual glycosidic bond (Chatgilialoglu et al., 2011). Both cdA and cdG lesions exist as 5′*R*- and 5′*S*-diastereomers. The structural changes that a C5′–C8 bond causes compared to natural purine nucleosides and the consequential distortion at the local DNA sequence, have been found efficient enough for the selective activation of the complex nucleotide excision repair (NER) apparatus in cells for restoring the damage. By the direct comparison of all four cdP lesions in NER efficiency studies, it has been reported that cdA and cdG are excised with similar yields while the configuration of the C5′ influences the repair yield with the 5′*R* lesions being 2 times more efficiently repaired (Kropachev et al., 2014).

The cdP are lesions observed among the DNA modifications and identified in mammalian cellular DNA *in vivo* (Chatgilialoglu et al., 2011). Recent studies reported cyclopurine lesions as reliable oxidative stress biomarkers in animal models (Wang et al., 2011; Mitra et al., 2012).

NMR studies integrated by molecular dynamics simulations have shown that replacing a deoxyguanosine (dG) with a 5′*S*-cdG in a B-DNA dodecamer results in perturbations of the helical twist and base pair stacking at the lesion sites (Huang et al., 2011). A similar behavior was observed in duplexes containing 5′*S*-cdA in place of dA (Zaliznyak et al., 2012). In both cases thermodynamic destabilization of the damaged duplexes was observed, as testified by the lowering of the melting point of the modified sequence with respect to unmodified DNA, amounting e.g., to 9°C for a double stranded dodecamer containing a single 5′*S*-cdG (Huang et al., 2011).

Molecular dynamics simulations highlighted that both the 5′*R*-cdA and 5′*R*-cdG lesions are significantly more distorting than the respective 5′*S* diastereomers, thus the different efficiency of NER

was traced back to the larger stacking impairment induced by 5′*R* isomers (Kropachev et al., 2014). However, the same lowering of melting temperature was observed for modified 17-mers double stranded oligonucleotides containing cdG and differing only for the absolute configuration at the 5′ carbon.

It is worth mentioning that the bulkiness of a lipophilic derivative of 5′*S*-cdG did not inhibit the self-assembly of the lesions in G-quartets as revealed by NMR experiments. However, the type of the supra-molecular organization was identified as all-*anti*-G-quadruplex, realizing the first exception to the all *syn* conformation as a critical factor for a G_4 self-assembly in non-aqueous medium (Pieraccini et al., 2014).

Due to their multidisciplinary importance, further exploration of the purine 5′,8-cyclonucleoside behavior in respect with its complementary base was investigated herein. Particularly, the lack of correlation of the melting temperatures with the extent of chain distortion and NER efficiencies indicated the existence of additional effects, such as the interaction of cdG with its complementary nucleoside, that may play a role in the thermodynamic destabilization of helices containing cyclopurines (Pande et al., 2012). Differential pulse voltammetry revealed to be a very powerful technique for investigating inter-base interactions between complementary nucleobases (Caruso et al., 2005, 2007; Capobianco et al., 2009, 2013a), and oligonucleotides (Capobianco et al., 2013b; Capobianco and Peluso, 2014) thus, aiming at investigating the peculiar interaction between cdG and cytidine, we have carried out a voltammetric and NMR study of lipophilic derivatives of the 5′*S*-cdG or 5′*R*-cdG with 2′-deoxycytidine in chloroform, a solvent in which the nucleosides mainly form H-bond complexes, mimicking the hydrophobic core of DNA (Kyogoku et al., 1967; Williams et al., 1987).

Materials and Methods

To increase solubility in $CHCl_3$ and prevent interference of hydrogen bonding by ribose hydroxyls, 2′-deoxycytidine was derivatized with tert-butyldimethylsilyl groups on the 2-deoxyribose unit to yield 3′,5′-bis-*O*-(*tert*-butyldimethylsilyl)-2′-deoxycytidine (dC′, **Scheme I**) (Caruso et al., 2005). (5′*S*)- and (5′*R*)-3′,5′-bis-*O*-(*tert*-butyldimethylsilyl)-5′,8-cyclo-2′-deoxyguanosine (*S*cdG′, *R*cdG′) were prepared by following the reported procedure (Terzidis and Chatgilialoglu, 2013).

^{1}H-NMR spectra were recorded in $CDCl_3$ by Bruker Advance 600 MHz. Differential pulse and cyclic voltammetry measurements were performed at room temperature in chloroform (Spectroscopic grade, Sigma-Aldrich), scan rate = 100 mV/s, by Autolab PGSTAT 302N potentiostat-galvanostat. A three-electrode cell configuration was adopted, Pt bars have been employed for quasi-reference and counter electrodes and a glassy carbon electrode (Metrohm) was used as working electrode; a positive feedback was applied to compensate for ohmic drop. The potential of the quasi-reference electrode was calibrated against the ferrocenium/ferrocene couple (Fc^+/Fc) (Capobianco et al., 2009; Bard and Faulkner, 2001). Tetrabutylammonium perchlorate (electrochemical grade, Sigma-Aldrich) 0.02 M was used as the supporting electrolyte. Solutions were deaerated by bubbling nitrogen before each experiment.

Results and Discussion

The differential pulse voltammogram of a 1.0 mM solution of *S*cdG' (see **Scheme I**) in chloroform is reported in **Figure 1** (red curve); an irreversible oxidation peak is observed at 0.95 V vs. Fc^+/Fc, a potential very close to the one (0.91 V) observed for the oxidation of dG' (Caruso et al., 2005) thus indicating that the formation of the C8–C5′ covalent bond does not constitute a severe perturbation of the π system of guanine, as expected.

The voltammogram of an equimolar solution of *S*cdG' and dC' (**Figure 1**, black curve) exhibits two voltammetric signals, one occurring at the same potential observed for solutions containing only 5′,8-cyclo-2′-deoxyguanosine, which can be safely assigned to the fraction of free *S*cdG' in solution, the other peaked at 0.77 V. Since dC' oxidation does not show any signal in the allowed potential window in chloroform, the lower potential peak is assigned to the 1:1 *S*cdG':dC' H-bond complex, in analogy with the case of guanosine and cytidine nucleosides (Caruso et al., 2005). Indistinguishable results were obtained for the *R* diastereoisomer and its 1:1 complex with dC'.

The stabilization of *S*cdG'$^{+\cdot}$ (or *R*cdG'$^{+\cdot}$) radical cation by cytidine in chloroform amounts to 0.18 eV, a value considerably lower than that observed for the pairing of dG' with dC' (0.34 eV) and even smaller than the oxidation potential shift of adenosine due to the formation of adenosine:thymidine complexes in chloroform (0.28 eV) (Caruso et al., 2005, 2007).

SCHEME I

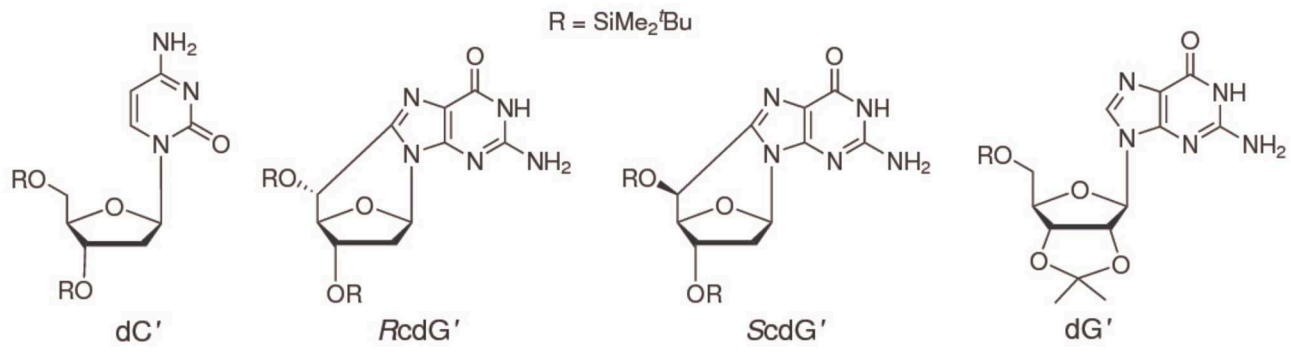

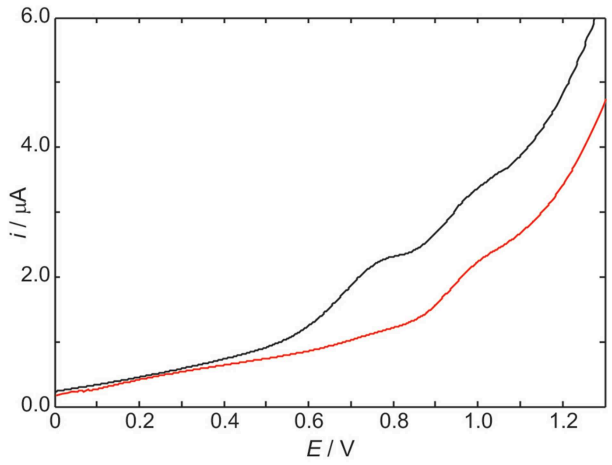

FIGURE 1 | Differential pulse voltammograms in $CHCl_3$ 20 mM TBAP of 1.0 mM ScdG' (red curve) and 1.0 mM ScdG': 1.0 mM dC' (black curve). Scan rate, 100 mV/s.

The above result has relevant consequences on binding energies. Consider A and B species forming the AB complex; the association and oxidation Gibbs free energies are defined as:

$$\triangle G^{ass}_{A\ldots B} = G_{AB} - G_A - G_B \tag{1}$$

and

$$\triangle G^{ox}_{A} = G_{A+} - G_A \tag{2}$$

By using Equations (1, 2), and assuming that A monomer holds the whole positive charge in the singly ionized complex $\{AB\}^+$ we have:

$$\begin{aligned} \triangle G^{ox}_{A} \;-\; \triangle G^{ox}_{AB} &= \triangle G^{ass}_{A\ldots B} \;-\; \triangle G^{ass}_{A+\ldots B} \;=\; \triangle H^{ass}_{A\ldots B} \\ &- \triangle H^{ass}_{A+\ldots B} \;-\; T\left(\triangle S^{ass}_{A\ldots B} \;-\; \triangle S^{ass}_{A+\ldots B}\right) \end{aligned} \tag{3}$$

Since

$$\triangle H^{ass}_{A\ldots B} \;\approx\; \triangle E^{ass}_{A\ldots B} \;=\; E^{bind}_{A\ldots B} \tag{4}$$

where $E^{bind}_{A\ldots B}$ is the binding energy in the AB complex, if we make the reasonable approximation:

$$\triangle S^{ass}_{A\ldots B} \;\approx\; \triangle S^{ass}_{A+\ldots B} \tag{5}$$

then Equation (3) becomes:

$$\triangle G^{ox}_{A} \;-\; \triangle G^{ox}_{AB} \;\approx\; E^{bind}_{A\ldots B} \;-\; E^{bind}_{A+\ldots B} \tag{6}$$

Application of Equation (6) in which B is dC' and A is dG', ScdG' or RcdG' shows that cdG':dC' and dG':dC' complexes are characterized by different interaction energies both in the neutral and in the charged state. To evaluate the binding energy of the ScdG':dC' complex, we have thus resorted to NMR titration experiments.

In **Figure 2** the most interesting region of the NMR spectra of solutions containing dC' and ScdG' in different ratios is reported. As the concentration of dC' increases, the imino N1–H proton shift of ScdG' increases from 11.5 ppm to 13.7 ppm, indicating that the Watson-Crick complex, which is by far the most stable motif for G:C association (Abo-Riziq et al., 2005) is actually established in $CHCl_3$, as also observed in modified DNA (Huang et al., 2011).

The determination of the association equilibrium constant for the ScdG':dC' Watson-Crick complex is not an easy task since many competitive processes may occur in solution. It is indeed well-known that guanosine self-associates in non-protic solvents, leading to at least four different dimeric complexes, see **Figure 3**, each of which is characterized by a different self-association constant. Moreover, hetero-association between guanine and cytosine is accompanied by additional, more intricate hydrogen-bonded complexes, such as trimers (cytosine:guanine$_2$) and tetramers [(cytosine:guanine)]$_2$ in weakly polar solvents (Williams et al., 1989; Sartorius and Schneider, 1996). Because of that, use of non-linear least-squares fits, explicitly considering the formation of self-association dimers GG and CC, in addition to the G-C base pair, are needed to obtain reliable association constants (Sartorius and Schneider, 1996) whereas more conventional treatment have only allowed to obtain rough estimates of both the self-association constant of guanine and the hetero-association constant with cytosine (Kyogoku et al., 1969).

It was therefore necessary to determine the self-association constant of cycloguanosine in $CDCl_3$ first in order to obtain a reliable estimate of the hetero-association constant of cycloguanosine with cytidine.

By following the chemical shift of the imino proton at increasing concentrations of cycloguanosine and using the standard equation (hereafter we further simplify notation, by indicating dC' as C and ScdG' as G in the following equations):

$$\delta_{obs} = \delta_G \;+\; \frac{\delta_{G2} - \delta_G}{4k_D[G]_0}\left(4k_D[G]_0 + 1 - \sqrt{8k_D[G]_0 + 1}\right) \tag{7}$$

where k_D is the dimerization constant, δ_G, δ_{G2} the shifts of the imino protons in G and G_2, respectively and $[G]_0$ is the analytical concentration of cycloguanosine (Davies et al., 1996), we have obtained $k_D \;\approx\; 10^3$ at 25°C.

The 1:1 model for the G:C association should be reliable only in the presence of an excess of cytidine, because in that case both the self-association of cycloguanosine and the formation of trimers and tetramers are disfavored. Moreover self-association of cytidine does not constitute a problem, because it is known to be negligible in chloroform (Kyogoku et al., 1969; Sartorius and Schneider, 1996).

The observed chemical shift of the imino proton when the simultaneous equilibria for the self and the hetero-association are considered, is given by:

$$\delta_{obs} = (1 - \alpha - 2\beta)\,\delta_G + \alpha\delta_{GC} + 2\beta\delta_{G2} \tag{8}$$

where α and β are the hetero and self- association degrees, respectively and are related by:

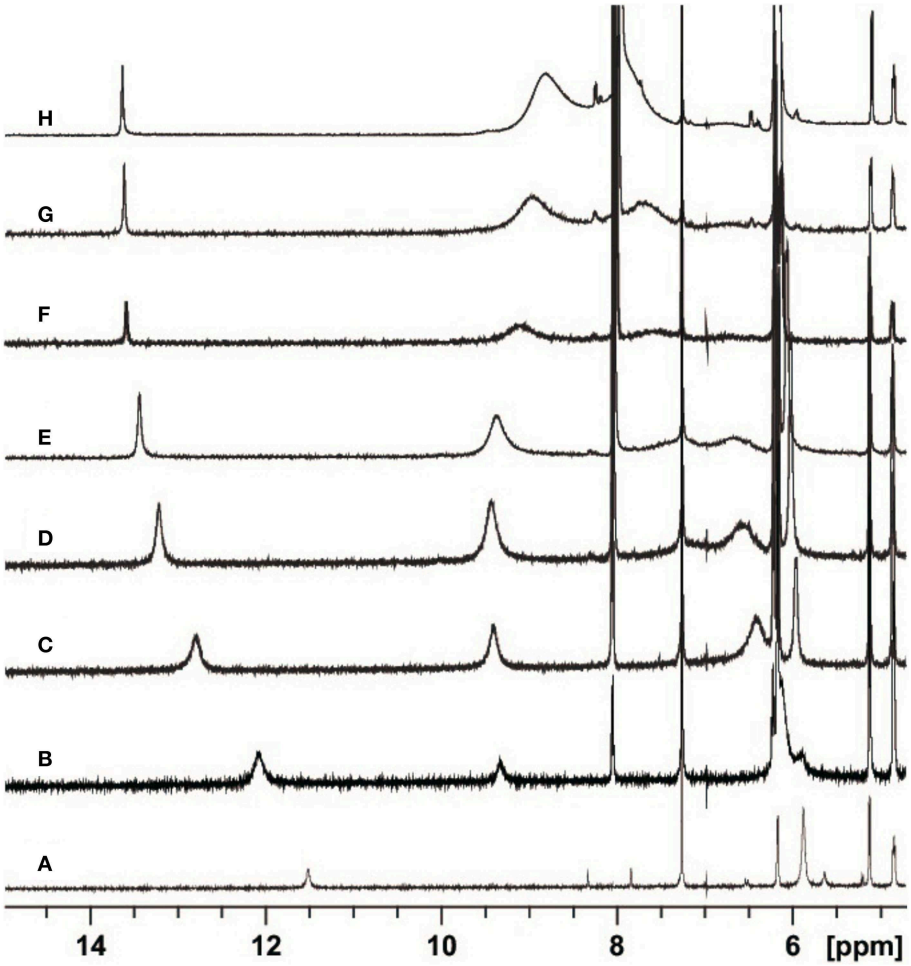

FIGURE 2 | Partial H-NMR (600 MHz) spectra of 3.6 mM ScdG' at *T* = 22 C in the presence of 0 (A), 1.7 (B), 4.7 (C), 8.7 (D), 13.0 (E), 25.0 (F), 36.7 (G), and 68.3 (H) mM dC' in $CDCl_3$.

$$\beta = \frac{\alpha^2 [G]_0 k_D}{k_A^2 ([C]_0 - \alpha [G]_0)^2} \tag{9}$$

k_A being the hetero-association constant. In the case of a large excess of cytidine, α may be approximated as:

$$\alpha = \frac{[C]_0 + [G]_0 + k_A^{-1} - \sqrt{\left([C]_0 + [G]_0 + k_A^{-1}\right)^2 - 4[G]_0 \left(1 - \frac{2k_D}{k_A^2 [C]_0}\right)[C]_0}}{2[G]_0 \left(1 - \frac{2k_D}{k_A^2 [C]_0}\right)[C]_0} \tag{10}$$

Equations (8–10) have been used to fit the NMR data of **Figure 4**, yielding $k_A = 1.4 \cdot 10^3\ M^{-1}$ at 22°C.

A slightly lower estimate, $k_A = 7 \cdot 10^2\ M^{-1}$ was obtained by fitting all the points of **Figure 4** and neglecting the self-association constant of cycloguanosine according to the well-known equation:

$$\delta_{obs} = \delta_G + \frac{\delta_{GC} - \delta_G}{2[G]_0} \left([C]_0 + [G]_0 + k_A^{-1} - \sqrt{\left([C]_0 + [G]_0 + k_A^{-1}\right)^2 - 4[G]_0 [C]_0} \right) \tag{11}$$

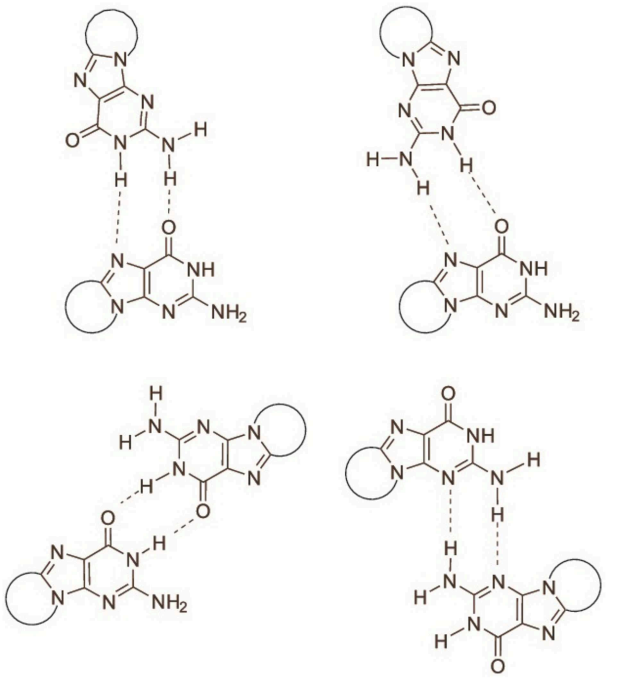

FIGURE 3 | Association modes of 5′,8-cyclo-2′-deoxyguanosine dimers.

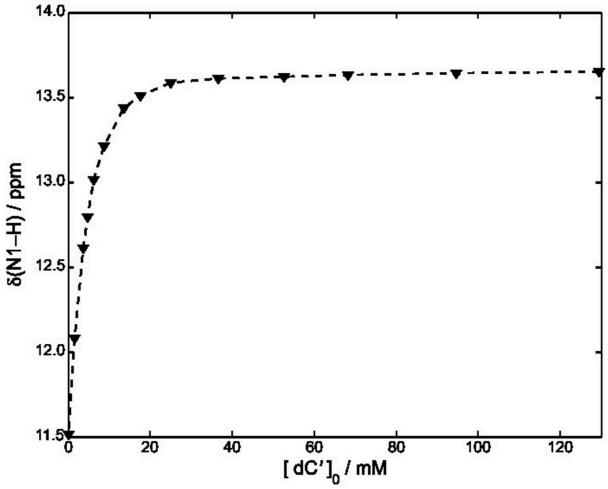

FIGURE 4 | Plot of δ (N1–H) vs. [dC'] in $CDCl_3$ at 22°C. The concentration of ScdG' was maintained constant at 3.6 mM. The dashed curve has been obtained by using Equation (11) and fitting all the experimental points.

We have also considered a further fitting model, by using only the points for which $\left[dC'\right]_0 > 10\left[ScdG'\right]_0$ (Fielding, 2000) in conjunction with the NMR version of the Benesi-Hildenbrand equation (Mathur et al., 1963). A similar value was obtained for the hetero-association constant, namely $k_A = 1 \cdot 10^3 M^{-1}$.

Independent of the adopted approximation, k_A is estimated to be one order of magnitude less than that obtained for the hetero-association of guanosine and cytidine in chloroform ($2.1 \cdot 10^4$ M^{-1}), Caruso et al. (2007) thus showing that the interaction of dC' with *S*cdG' is weaker than that with dG'. Moreover the equilibrium constant for the formation of the Watson-Crick complex appears to be slightly lower than that for the homo-association of guanosine in chloroform thus confirming that all the equilibria must be considered.

Conclusions

The interactions of *S*cdG' and *R*cdG', two important DNA tandem lesions (**Scheme I**), with their complementary base have been studied by NMR spectroscopy and differential pulse voltammetry in chloroform solution, a solvent where guanosine and cytidine are known to form the Watson-Crick hydrogen bonded complex. The oxidation potentials of *S*cdG' and *R*cdG' are almost the same as the undamaged nucleoside, whereas the oxidation potentials of their Watson-Crick complexes with cytidine are significantly higher (0.16 eV) than that of dG':dC'. Those somewhat intriguing results suggest that the interaction energies of the damaged nucleosides with their complementary one differ from that of guanosine. In line with that expectation, the equilibrium association constant for the *S*cdG':dC' complex, determined by NMR titrations in different ways, both by explicitly considering the existence of the simultaneous cdG' self-association equilibrium and by working in conditions of large cytosine excess, is found to be ca. 10^3 M^{-1}, about one order of magnitude less than its counterpart for undamaged nucleobase. No significant changes with respect to dG':dG' have been found for the self-association *S*cdG':*S*cdG' equilibrium constant, obtained under the simplified assumptions that either all self-association modes possess the same equilibrium constant or that one association mode is predominant over all the others. In summary the results reported here, although far from being exhaustive, suggest that other factors besides helical distortions are effective for thermodynamic destabilization of DNA tracts containing cycloguanosine.

Acknowledgments

Financial support from the Ministero dell'Istruzione, dell'Università e della Ricerca [PRIN-2009K3RH7N] and Marie Curie Intra-European Fellowship [CYCLOGUO298555] is gratefully acknowledged. The sponsorship of the COST Action CM1201 "Biomimetic Radical Chemistry" is gratefully acknowledged.

References

Abo-Riziq, A., Grace, L., Nir, E., Kabelac, M., Hobza, P., and de Vries, M. S. (2005). Photochemical selectivity in guanine–cytosine base-pair structures. *Proc. Natl. Acad. Sci. U.S.A.* 102, 20–23. doi: 10.1073/pnas.0408574102

Bard, A. J., and Faulkner, L. R. (2001). *Electrochemical Methods: Fundamentals and Applications, 2nd Edn*. New York, NY: John Wiley and Sons, Inc.

Capobianco, A., Caruso, T., Celentano, M., La Rocca, M. V., and Peluso, A. (2013a). Proton transfer in oxidized adenosine self-aggregates. *J. Chem. Phys.* 139, 145101. doi: 10.1063/1.4823495

Capobianco, A., Caruso, T., Celentano, M., D'Ursi, A. M., Scrima, M., and Peluso, A. (2013b). Stacking interactions between adenines in oxidized oligonucleotides. *J. Phys. Chem. B*. 117, 8947–8953. doi: 10.1021/jp404133a

Capobianco, A., Carotenuto, M., Caruso, T., and Peluso, A. (2009). The charge-transfer band of an oxidized Watson–Crick Guanosine–cytidine complex. *Angew. Chem. Int. Ed Engl.* 48, 9526–9528. doi: 10.1002/anie.200904305

Capobianco, A., and Peluso, A. (2014). The oxidation potential of AA steps in single strand DNA oligomers. *RSC Adv.* 4, 47887–47893. doi: 10.1039/C4RA09270H

Caruso, T., Capobianco, A., and Peluso, A. (2007). The oxidation potential of adenosine and adenosine-thymidine base pair in chloroform solution. *J. Am. Chem. Soc.* 129, 15347–15353. doi: 10.1021/ja076181n

Caruso, T., Carotenuto, M., Vasca, E., and Peluso, A. (2005). Direct experimental observation of the effect of the base pairing on the oxidation potential of guanine. *J. Am. Chem. Soc.* 127, 15040–15041. doi: 10.1021/ja055130s

Chatgilialoglu, C., Ferreri, C., and Terzidis, M. A. (2011). Purine 5′,8-cyclonucleoside lesions: chemistry and biology. *Chem. Soc. Rev.* 40, 1368–1382. doi: 10.1039/c0cs00061b

Davies, D. B., Djimant, L. N., and Veselkov, A. N. (1996). ^{1} H NMR investigation of self-association of aromatic drug molecules in aqueous solution. Structural and thermodynamical analysis. *J. Chem. Soc. Faraday Trans*. 92, 383–390. doi: 10.1039/FT9969200383

Fielding, L. (2000). Determination of association constants (K_a) from solution NMR data. *Tetrahedron* 56, 6151–6170. doi: 10.1016/S0040-4020(00)00492-0

Huang, H., Das, R. S., Basu, A. K., and Stone, M. P. (2011). Structure of (5′S)-8,5′-Cyclo-2′-deoxyguanosine in DNA. *J. Am. Chem. Soc.* 133, 20357–20368. doi: 10.1021/ja207407n

Kropachev, K., Ding, S., Terzidis, M. A., Masi, A., Liu, Z., Cai, Y., et al. (2014). Structural basis for the recognition of diastereomeric 5′,8-cyclo-2′-deoxypurine lesions by the human nucleotide excision repair system. *Nucleic Acids Res.* 42, 5020–5032. doi: 10.1093/nar/gku162

Kyogoku, Y., Lord, R. C., and Rich, A. (1967). The effect of substituents on the hydrogen bonding of adenine and uracil derivatives. *Proc. Natl. Acad. Sci. U.S.A.* 57, 250–257.

Kyogoku, Y., Lord, R. C., and Rich, A. (1969). An infrared study of the hydrogen-bonding specificity of hypoxanthine and other nucleic acid derivatives. *Biochim. Biophys. Acta* 179, 10–17.

Mathur, R., Becker, E. D., Bradley, R. B., and Li, N. C. (1963). Proton magnetic resonance studies of hydrogen bonding of benzenethiol with several hydrogen acceptors. *J. Phys. Chem.* 67, 2190–2194. doi: 10.1021/j100804a052

Mitra, D., Luo, X., Morgan, A., Wang, J., Hoang, M. P., Lo, J., et al. (2012). An ultraviolet-radiation-independent pathway to melanoma carcinogenesis in the red hair/fair skin background. *Nature* 491, 449–453. doi: 10.1038/nature11624

Pande, P., Das, R. S., Sheppard, C., Kow, Y. W., and Basu, A. K. (2012). Repair efficiency of (5′S)-8,5′-cyclo-2′-deoxyguanosine and (5′S)-8,5′-cyclo-2′-deoxyadenosine depends on the complementary base. *DNA Repair* 11, 926–931. doi: 10.1016/j.dnarep.2012.09.002

Pieraccini, S., Terzidis, M. A., Baldassarri, E. J., Fragneto, G., Mariani, P., Masiero, S., et al. (2014). A lipophilic "fully-anti" dodecamer from mutagenic (5′S)-5′,8-cyclo-2′-deoxyguanosine. *Chem. Commun. (Camb).* 50, 10722–10725. doi: 10.1039/c4cc04275a

Sartorius, J., and Schneider, H. J. (1996). A general scheme based on empirical increments for the prediction of hydrogen-bond associations of nucleobases and of synthetic host–guest complexes. *Chem. Eur. J.* 2, 1446–1452. doi: 10.1002/chem.19960021118

Terzidis, M. A., and Chatgilialoglu, C. (2013). Radical cascade protocol for the synthesis of (5′S)- and (5′R)-5′,8-cyclo-2′-deoxyguanosine derivatives. *Aust. J. Chem.* 66, 330–335. doi: 10.1071/CH12494

Wang, J., Yuan, B., Guerrero, C., Bahde, R., Gupta, S., and Wang, Y. (2011). Quantification of oxidative DNA lesions in tissues of Long-Evans Cinnamon rats by capillary high-performance liquid chromatography-tandem mass spectrometry coupled with stable isotope-dilution method. *Anal. Chem.* 83, 2201–2209. doi: 10.1021/ac103099s

Williams, L. D., Chawla, B., Shaw, R., Gross, P. M., and Carolina, N. (1987). The hydrogen bonding of cytosine with guanine: calorimetric and 1H-NMR analysis of the molecular interactions of nucleic acid bases. *Biopolymers* 26, 591–603. doi: 10.1002/bip.360260411

Williams, N. G., Williams, L. D., and Shaw, B. R. (1989). Dimers, trimers, and tetramers of cytosine with guanine. *J. Am. Chem. Soc.* 111, 7205–7209. doi: 10.1021/ja00200a046

Zaliznyak, T., Lukin, M., and de los Santos, C. (2012). Structure and stability of duplex DNA containing (5′S)-5′,8-cyclo-2′-deoxyadenosine: an oxidatively generated lesion repaired by NER. *Chem. Res. Toxicol.* 25, 2103–2111. doi: 10.1021/tx300193k

Conflict of Interest Statement: The authors declare that the research was conducted in the absence of any commercial or financial relationships that could be construed as a potential conflict of interest.

Copyright © 2015 Capobianco, Caruso, Fusco, Terzidis, Masi, Chatgilialoglu and Peluso. This is an open-access article distributed under the terms of the Creative Commons Attribution License (CC BY). The use, distribution or reproduction in other forums is permitted, provided the original author(s) or licensor are credited and that the original publication in this journal is cited, in accordance with accepted academic practice. No use, distribution or reproduction is permitted which does not comply with these terms.

frontiers in Chemistry

ORIGINAL RESEARCH
published: 06 March 2015
doi: 10.3389/fchem.2015.00013

Mutagenic effects induced by the attack of NO_2 radical to the guanine-cytosine base pair

José P. Cerón-Carrasco[1], Alberto Requena[1], José Zúñiga[1] and Denis Jacquemin[2,3]*

[1] Departamento de Química Física, Universidad de Murcia, Murcia, Spain, [2] Chimie et Interdisciplinarité, Synthèse, Analyse, Modélisation, UMR Centre National de la Recherche Scientifique, Université de Nantes, Nantes, France, [3] Institut Universitaire de France, Paris, France

We investigate the attack of the nitrogen dioxide radical ($NO_2^\bullet$) to the guanine—cytosine (GC) base pair and the subsequent tautomeric reactions able to induce mutations, by means of density functional theory (DFT) calculations. The conducted simulations allow us to identify the most reactive sites of the GC base pair. Indeed, the computed relative energies demonstrate that the addition of the $NO_2^\bullet$ radical to the C8 position of the guanine base forms to the most stable adduct. Although the initial adducts might evolve to non-canonical structures via inter-base hydrogen bonds rearrangements, the probability for the proton exchange to occur lies in the same range as that observed for undamaged DNA. As a result, tautomeric errors in NO_2-attacked DNA arises at the same rate as in canonical DNA, with no macroscopic impact on the overall stability of DNA. The potential mutagenic effects of the GC–$NO_2^\bullet$ radical adducts likely involve side reactions, e.g., the GC deprotonation to the solvent, rather than proton exchange between guanine and cytosine basis.

Keywords: guanine–cytosine, NO_2 radical, induced mutation, proton transfer reaction, tautomeric equilibria, rare tautomers, computational chemistry, density functional theory

OPEN ACCESS

Edited by:
Antonio Monari, Université de Lorraine, France

Reviewed by:
Nino Russo, Università della Calabria, Italy
Leif Axel Eriksson, University of Gothenburg, Sweden

****Correspondence:***
José P. Cerón-Carrasco, Departamento de Química Física, Universidad de Murcia, 30100 Murcia, Spain
jpceron@um.es

Specialty section:
This article was submitted to Chemical Biology, a section of the journal Frontiers in Chemistry

Received: *08 January 2015*
Accepted: *16 February 2015*
Published: *06 March 2015*

Citation:
Cerón-Carrasco JP, Requena A, Zúñiga J and Jacquemin D (2015) Mutagenic effects induced by the attack of NO_2 radical to the guanine-cytosine base pair. Front. Chem. 3:13. doi: 10.3389/fchem.2015.00013

1. Introduction

Free radicals are naturally present in the biological medium as intermediates of the cellular metabolism. Although necessary to keep the normal biochemical activity, these highly reactive species tend to react, when present in excess, with a wide panel of biomolecules including DNA (Cadet et al., 2010). Accordingly, free-radical-induced DNA damage (mutations) might eventually initiate degenerative diseases, cardiovascular problems and cancers (von Sonntag, 2009). The reactive nitrogen oxide species (RNOS) family is a representative example of the double role played by free radicals (Lonkar and Dedon, 2011). Indeed, it has been established that mammalians cells endogenously produce RNOS as critical biological mediators (Ignarro, 1990). However, intracellular amounts of RNOS can overpass the tolerable limit by exposure to external chemical agents, such as cigarette smoke or air pollution (Pacher et al., 2007), and physical agents like high-energy radiations (Douki and Cadet, 2008).

One of the most important RNOS is the nitrogen dioxide radical, which is mainly present under its monomer $NO_2^\bullet$ form in physiological conditions (Augusto et al., 2002). Like any free radical, $NO_2^\bullet$ might react by electron transfer, hydrogen atom abstraction and/or radical addition to unsaturated bonds (Galano, 2007; Cerón-Carrasco et al., 2010). As for a reaction with DNA is concerned, the latter mechanism involves the addition of the radical

to one of the unsaturated bonds of the guanine–cytosine (GC) base pair. There are, in particular, five possible reactive positions in the GC pair: C4, C5, and C8 in the guanine [C4(G), C5(G), and C8(G)] and C5 and C6 in the cytosine [C5(C) and C6(C)]. The atomic numbering is shown in **Figure 1**. Previous experimental and theoretical evidences indicated that C8(G) is the most reactive site for $OH^{\bullet}$ radical attack (Fortini et al., 2003; Shukla et al., 2004; Jena and Mishra, 2005; Shukla and Mishra, 2007; Zhang and Eriksson, 2007; Bergeron et al., 2010; Cerón-Carrasco and Jacquemin, 2012). Agnihotri and Mishra have also shown that $NO_2^{\bullet}$ quickly reacts with the guanine radical cation ($G^{\bullet+}$) at this same position (Agnihotri and Mishra, 2009, 2010, 2011), which might lead to DNA damage through the formation of an intermediate 8-nitroguanine structure (Misiaszek et al., 2005). The reaction of $NO_2^{\bullet}$ radical with the undamaged (neutral and closed-shell) GC pair has been, however, much less explored, so additional work is required to understand the biological action of such radical once inside the cellular medium.

In this work, we use an state-of-the-art theoretical approach within the density functional theory (DFT) framework to investigate the possible mutagenic effects induced by the $NO_2^{\bullet}$ radical. In particular, we study the formation of non-canonical Watson and Crick structures arising from activation of the tautomeric equilibria in the GC base pair. These equilibria involve proton transfer (PT) between the guanine and cytosine basis yielding the so-called rare tautomeric forms that have been proposed as a plausible source of genetic errors (Löwdin, 1963; Florián and Leszczyński, 1996; Dannenberg and Tomasz, 2000; Gorb et al., 2004; Kumar and Sevilla, 2010; Villani, 2010a; Jacquemin et al., 2014). In undamaged DNA, GC base pairs naturally exchange the position of the H1, H4 and H4′ protons (see **Figure 1**), eventually disrupting the standard hydrogen-bond pattern that maintain the double helix bounded and thus inducing genetic errors during the cell replication (Villani, 2010b). Consequently, the tautomeric equilibria can be altered by external agents facilitating PT reactions (Khanduri et al., 2011). The main goal of this contribution is therefore to determine whether $NO_2^{\bullet}$ radical contributes to the mutagenic processes by shifting PT mechanism toward rare-tautomeric GC structures.

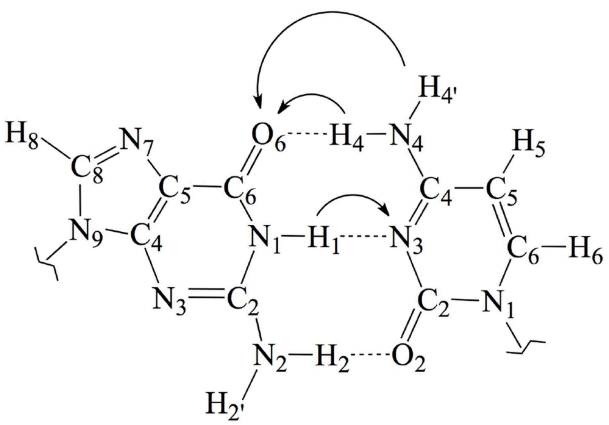

FIGURE 1 | Chemical structure and atomic numbering of the canonical GC base pair. Both N9 in G and N1 in C are the connections to the lateral backbone in DNA. In an isolated GC base pair, these positions are occupied by two hydrogen atoms. Arrows show the possible displacements of the protons H1, H4, and H4′ during the tautomeric reactions.

2. Methods

Since all the structures under study correspond to radical forms, the bullet superscript is hereafter omitted in the text in order to lighten the notation. We employ two different chemical models. In an early stage, a single GC base pair is used to determine the relative stabilities of all possible GC–radical adducts. More specifically, the NO_2 radical is added to all possible reactive sites of the GC base pair through the two possible binding modes, e.g., ONO–CX and O_2N–CX, where CX stands for the attacked carbons: C4(G), C5(G), C8(G), C5(C), and C6(C). The resulting adducts are next fully solvated with eleven water molecules, as illustrated in **Figure 2**, in order to mimic the solvent effects of a single solvated GC pair (Kumar et al., 2008). All these structures are optimized without symmetry constraints at the M06-2X/6-311G(d,p) level (Zhao and Truhlar, 2008a,b). The vibrational frequencies are computed at the same level of theory to confirm the absence of imaginary frequencies so that real minima are obtained. The total energies of all stationary points are then improved using the same exchange-correlation functional with the more extended atomic basis set, 6-311++G(d,p). Also, the well-known polarisable continuum model (PCM) is additionally used to account for solvent effects beyond the explicitly-treated first hydration shell (Tomasi et al., 1999, 2005).

The isolated GC–radical adducts might form indeed overdistorted structures compared to real DNA, since the stacking effect is neglected. Consequently, the single base pair model is next refined by sandwiching the most stable adduct into at double-stranded B-form trimer d(5′-GGG-3′)d(3′-CCC-5′), as shown in **Figure 3**. This model includes both nucleotides moieties and sugar-phosphate backbone chains (Chen et al., 2009, 2011; Cerón-Carrasco et al., 2011). Since phosphates are negatively charged at physiological pH, the neutrality of the systems can be ensured by either adding counterions, e.g., Na^+ or K^+, or protonating the phosphate groups. Since the backbone does not significantly affect PT reactions in DNA (Close and Øhman, 2008;

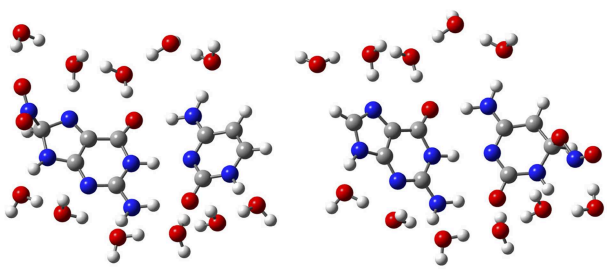

FIGURE 2 | Chemical structure for two of the single GC–radical adduct models: O_2N–C8(G) and ONO–C6(C).

Chen et al., 2009), we go for the latter procedure to have a neutral system and consequently facilitate the convergence of the calculations. The GC-radical adduct is therefore located between two GC base pairs, which correctly mimic the π-stacking interactions in real DNA (Chen et al., 2009). We should underline that the stacked DNA model includes five water molecules in the vicinity of N3(G), O6(G), N7(G), O2(C), and N4(C) atoms (see atomic numbering in 1), and not eleven as in the single GC–radical adduct. These five sites correspond to the solvent exposed heteroatoms in DNA, so five water molecules are enough to provide a suitable representation of the hydrogen-bonds network formed between the base pair and the first hydration shell of the stacked structure (Schneider and Berman, 1995; Auffinger and Westhof, 2000; Makarov et al., 2002).

Due to the size of the DNA fragment (ca. 200 atoms), we use the hybrid ONIOM approach (Dapprich et al., 1999), which allows us to split the system into different regions, called layers. In this system, the layer of interest (defined as high layer) is the central GC–NO_2 radical adduct plus the five explicit water molecules. This layer is treated at the same level that the isolated model, i.e., by using M06-2X/6-311G(d,p) for the optimization and PCM-M06-2X/6-31++G(d,p) for single-point energy calculations (Vreven et al., 2001; Mo et al., 2004). The two border GC base pairs that confine the central GC-radical adduct form the medium layer, which is described at the less demanding M06-2X/6-31G(d) level, while the lateral sugar-phosphate backbone (low layer) is simulated with the semiempirical PM6 method (Stewart, 2007). In this computation protocol, only the high layer is optimized whereas the rest of the system is frozen in the space. Such partial optimization procedure retains the characteristic double helix form of DNA while allowing relaxation of the central base pairs during the proton transfer reaction. Analytic calculations of the vibrational frequencies confirm the nature of the obtained structures to be minima (no imaginary frequencies) or transition states (a single imaginary frequency corresponding to the stretching of the transferred protons). All calculations are carried out with Gaussian09 (Frisch et al., 2009).

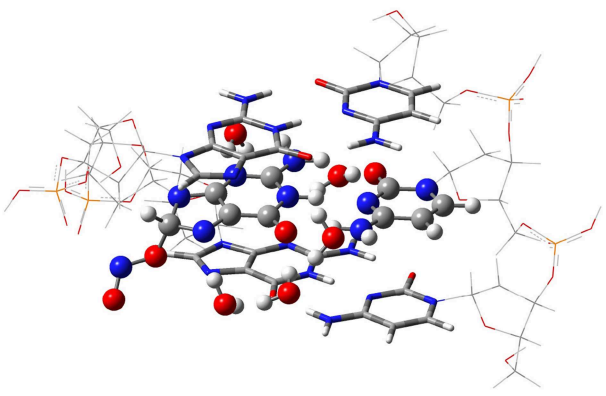

FIGURE 3 | The ONIOM model for the DNA-embedded GC-radical adduct. The high layer for the ONO-C8(G) adduct is represented as ball and sticks whereas the confining base pair of the medium layer are shown as tube, and the lateral back-bone placed in the low layer are displayed as wireframe.

3. Results and Discussion

Although previous experimental and theoretical evidences suggest that the C8(G) is the preferred site for adding radicals to the GC base pair (Kumar et al., 2011), we have calculated the relative stabilities of all possible GC–radical adducts to provide an accurate picture of the NO_2 radical reactivity. The relative energies obtained for the located adducts are listed in **Table 1**, with the reference value being taken as the most stable GC–radical adduct: ONO–C8(G). As observed, there are two main radical-attacking sites: C8(G) and C6(C). It wasn't possible to optimize GC-radical adduct at other positions, with the only exception of ONO–C5(C) at a significantly higher energy (11.76 kcal.mol^{-1}). This finding is consistent with previous results obtained by Zhang and Eriksson using DFT calculations to determine the reactivity of the OH radical with the neutral closed-shell GC base pair (Zhang and Eriksson, 2007). These authors concluded that the two most stable binding sites for the GC–OH mutation are C8(G) and C6(C) (Zhang and Eriksson, 2007). In contrast, there are two possible binding modes (O_2N– and ONO–) in the present case. Inspection of **Table 1** reveals that the attack of the NO_2 radical could proceed equally through the nitrogen or the oxygen atom. This is a remarkable result: the binding mode does not significantly affect the final stability of the generated adduct since the reported difference is negligible (<0.40 kcal.mol^{-1}).

Aiming to characterize better the structural changes induced by the radical, we also include in **Table 1** the interbase distances and the partial atomic charges of the protons involved in the intramolecular hydrogen bonds. Although there are slight differences (ca. 0.1 Å) in the interbase separation, adding the NO_2 radical does significantly alter the GC geometry. The structures of the two most stable GC–radical adducts, namely O_2N–C8(G) and ONO–C8(G), are shown in **Figure 4**. The side views show a clear bent structure as a result of the radial addition. Such departure from planarity can be quantified through the dihedral angle formed by C6(G)C2(G)C2(C)C4(C) (see atomic numbering in **Figure 1**), which has a value of around 1° for undamaged GC, but close to 10° in both GC–radical adducts. This is a logical consequence of the selected model, which mimics the reactivity of a single GC base pair in solution but does not reproduce the DNA environment, and in particular the π-stacking constrain.

More intriguing are the results shown in **Table 1** for the atomic charges. As observed, the O_2N– biding mode results in larger (more positive) atomic charges for the

TABLE 1 | Relative energy (ΔE/kcal.mol^{-1}), theoretical interbase bond distances (in Å) and Mulliken atomic charges (in |e|) for the single GC–radical adducts.

Adduct	ΔE	Distance			Charge		
		O_6–N_4	N_1–N_3	N_2–O_2	H_4	H_1	H_2
ONO–C8(G)	0.00	2.908	2.907	2.839	0.34	0.49	0.38
O_2N–C8(G)	0.15	2.894	2.890	2.838	0.38	0.56	0.36
O_2N–C6(C)	7.69	2.843	2.912	2.891	0.41	0.57	0.35
ONO–C6(C)	8.08	2.859	2.920	2.878	0.34	0.47	0.32
ONO–C5(C)	11.76	2.871	2.935	2.876	0.34	0.52	0.35

transferred proton during the tautomeric reaction, e.g., H4 and H1, compared to its ONO– counterpart. Although limited, these changes might affect the stability of the induced mutation since the atomic charges are directly related to the proton acidity and, consequently, to the tendency of forming tautomers.

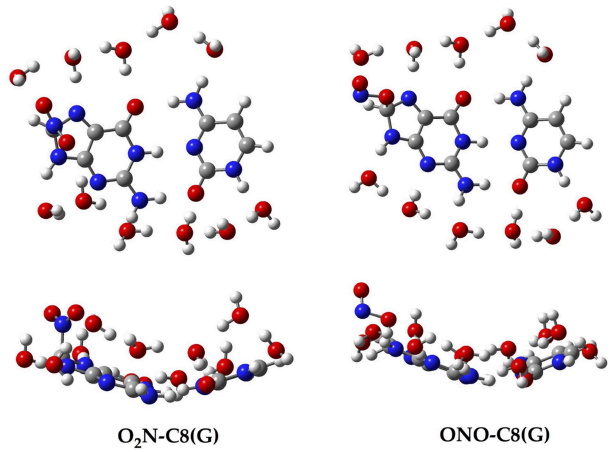

FIGURE 4 | Top and side views of the optimized structure for the O_2N–C8(G) and ONO–C8(G) adducts.

The single GC base pair model provides the first clues for the attack of the NO_2 radical to DNA, but the more refined model is required for biological analysis because (i) bend structures imply energetic penalties once inside DNA due to the π-stacking interactions; and (ii) the location of the radical could be modified by the chemical environment of DNA, e.g., by the interaction with other base pairs and/or later sugar-phosphate backbone. Consequently, the two most stable adducts, O_2N–C8(G) and ONO–C8(G), are "docked" into the DNA fragment shown in **Figure 3**. In contrast with the single GC model in which both binding modes are practically isoenergetic, the ONO–C8(G) adduct is now 3.23 kcal.mol^{-1} more stable than the O_2N–C8(G) adduct in DNA, which confirms the importance of accounting for all key interactions.

In addition to the optimal geometry of the canonical GC–radical adducts, we have computed the energetic profiles corresponding both to the transfer of protons H1 and H4, directly exchanged between the basis, and to the tautomeric equilibria arising from the movement of the H4′ (see **Figure 1**). The latter equilibrium implies a water-assisted mechanism in which the surrounding water molecules catalyze the process by accepting and donating protons (see Ref. Jacquemin et al., 2014 for details).

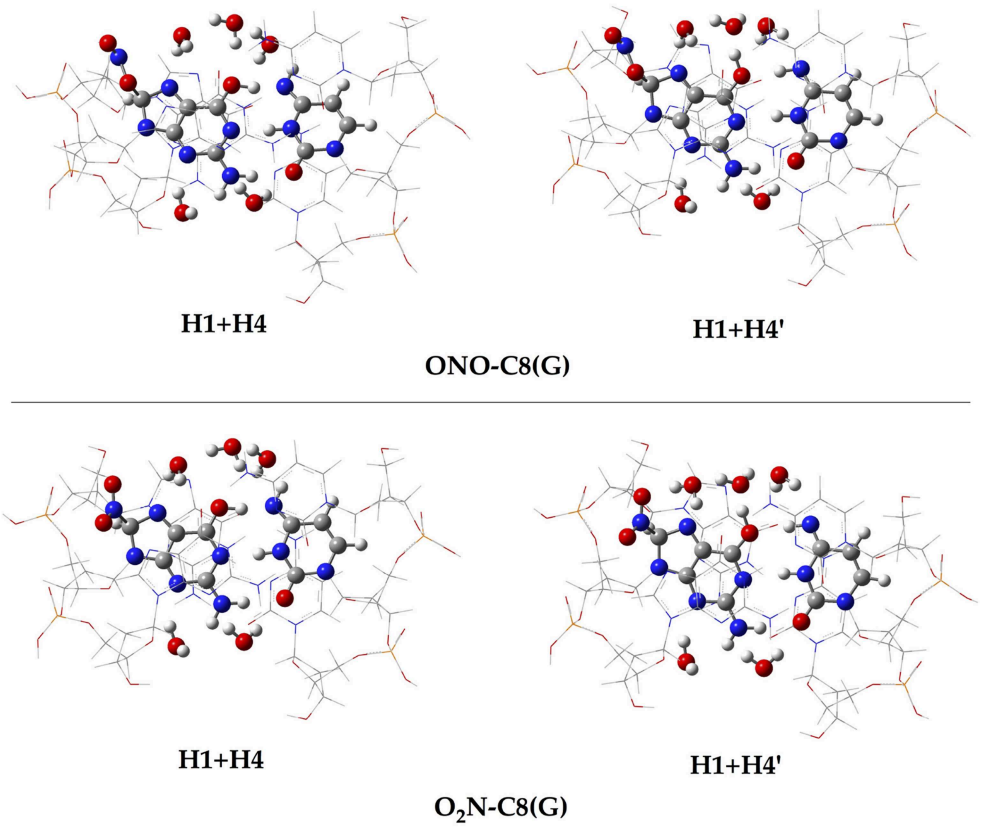

FIGURE 5 | Chemical structures of the canonical rare tautomeric form optimized for the O_2N–C8(G) and ONO–C8(G) adducts: H1+H4 and H1+H4′. For the sake of clarity only the central GC–radical adduct and the surrounding water molecules are displayed as balls and sticks, while the rest of the system is shown has wireframe.

The optimized rare tautomeric structures are shown in **Figure 5**, and their relative energies and equilibrium constant are given in **Table 2**. We should note that all the attempts tried to optimize products arising from a single-PT reaction, that is, to optimize rare tautomers where only one proton (H1, H4 or H4′) is shifted from its position, failed as the geometry optimization quickly restored the original canonical structure. However, we were able to localize the products for H1+H4 and H1+H4′ double-PT with both O_2N–C8(G) and ONO–C8(G) adducts, which structures are shown in **Figure 5**. As discussed above, the O_2N–C8(G) binding mode results in more acidic H4 and H1 protons, compared to the ONO–C8(G) adduct, eventually favouring the tautomeric equilibria by ca. 3 kcal.mol^{-1}. The associated equilibrium constants (K_{eq}) can be estimated from the relative energies obtained using the expression

$$K_{eq} = e^{-\Delta E/RT} \quad (1)$$

where R is the ideal gas constant and T is the temperature (298.15 K). K_{eq} provides a measure of the mutation frequency, which can be directly compared to the computed value for the radical-free DNA. Taking the undamaged-DNA as a reference for the impact of H1+H4 and H1+H4′ reactions, one notices that the latter is unlikely to occur due to the low K_{eq} values, which are of the order of 10^{-16} and 10^{-13} for the O_2N–C8(G) and ONO–C8(G) adducts, respectively. However, the energies listed in **Table 2** hint that the O_2N–C8(G) adduct stabilizes the H1+H4 mutation by ca. 2 kcal.mol^{-1}, slightly shifting the equilibrium toward the rare tautomeric form ($K_{eq} = 7.27 \times 10^{-08}$). Despite of such a difference, all rare tautomers are in the range of observed frequency for the spontaneous mutation, experimentally measured as ranging from 10^{-8} to 10^{-10} (Topal and Fresco, 1976). Interestingly, there is a certain dissimilarity between NO_2 and OH. The latter clearly shifts the PT reactions toward the rare tautomeric forms of the GC base pair, and its degenerative effects are therefore governed by the transition states along the PT reactions, which in turn determines their lifetimes (Zhang and Eriksson, 2007; Cerón-Carrasco and Jacquemin, 2012). In contrast, NO_2 does not affect the PT reactions, so it is not necessary to compute the transition states to conclude that they make no impact in the global mutation when present in DNA during cell replication.

Since the canonical O2N-C8(G) and ONO-C8(G) adducts are shown to be the most stable structures at an early stage of the radical attack, we decided to compute the spin densities surfaces for both forms to determine the localisation of the unpaired electron. Such calculations were performed by single-point full QM calculations at the M06-2X/6-311G(d,p) level. As illustrated in **Figure 6**, the spin density is distributed in the guanine as well as in the radical, in agreement with previous results obtained for the OH radical (Cerón-Carrasco and Jacquemin, 2012). This finding indicates that the subsequent mutagenic steps will be take place at this region rather than at further sugar-phosphate backbones moieties or at other DNA basis. It becomes therefore necessary to perform additional dynamics calculations with larger models (Loos et al., 2009; Ambrosek et al., 2010; Cauët et al., 2010; Dupont et al., 2011; Garrec et al., 2012; Cerón-Carrasco et al., 2013; Dupont et al., 2013; Patel et al., 2013) for the O_2N–C8(G) and ONO–C8(G) adducts to further investigate the damage mechanism initiated by GC-NO_2 structures. Our results indicate that such adducts should evolve by side mechanisms different than PT between guanine an cytosine, e.g., deprotonation to the solvent (Agnihotri and Mishra, 2011).

TABLE 2 | Relative energy (ΔE/kcal.mol^{-1}) and equilibrium constants (K_{eq}) at 298 K calculated for the H1+H4 and H1+H4′ tautomeric equilibria of undamaged-DNA, O_2N–C8(G) and ONO–C8(G) adducts.

Adduct	Undamaged-DNA		ONO–C8(G)		O_2N–C8(G)	
	ΔE	K_{eq}	ΔE	K_{eq}	ΔE	K_{eq}
Canonic	0.00		0.00		0.00	
H1+H4	11.23	5.75×10^{-09}	12.96	3.11×10^{-10}	9.73	7.27×10^{-08}
H1+H4′	17.37	1.80×10^{-13}	20.71	6.50×10^{-16}	17.48	1.52×10^{-13}

4. Concluding Remarks

We have performed theoretical calculations to determine the reaction mechanism between the NO_2 radical and the neutral closed-shell guanine–cytosine base pair. The reported data demonstrate that the carbon C8 of the guanine moiety is the preferential site to form the GC-radical adduct. The NO_2 radical equally reacts with the single GC base pair through either its nitrogen or its oxygen atom, with the latter yielding the most

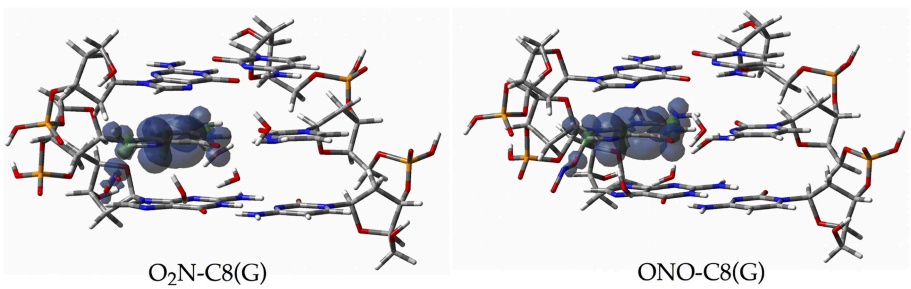

FIGURE 6 | Spin density distributions of the canonical radical adducts (isovalue = 0.002 a.u.) computed at M06-2X/6-311G(d,p) level for the three base pairs DNA fragment.

stable adduct when a more realistic DNA-embedded model is used. This finding confirms the importance of using a well-balanced chemical model to obtain valuable conclusions. For the radical addition to DNA, the π-stacking interaction not only constrain the planarity of the attacked base pair, but also accommodates better the ONO– binding mode compared to its O_2N– counterpart. We have assessed the possible evolution of these adducts through proton transfer reactions between guanine and cytosine basis, which is one of the sources of genetic errors in DNA. The associated equilibrium constants lie in the same range as the one observed for spontaneous mutation. We conclude that the initial ONO–C8(G) does not promote rare tautomeric forms by proton exchange, at least not at a rate larger than that in undamaged DNA. The NO_2-induced genetic damage is expectedly to be initiated by other side reactions.

Acknowledgments

JC acknowledges the support from the FP7 EU Marie Curie Actions through the Campus Mare Nostrum 37/38 CMN UMU Incoming Mobility Programme ACTion (U-IMPACT), and the support provided by Université de Nantes through its invited professor programme. DJ acknowledges the European Research Council (ERC) and the *Région des Pays de la Loire* for financial support in the framework of a Starting Grant (Marches - 278845) and a *recrutement sur poste stratégique*, respectively. This research work was partially supported by the Spanish Ministerio de Ciencia e Innovación under Projects CTQ2011-25872 and CONSOLIDER CSD2009-00038, and used resources of the CEN1 in Spain and the CINES and the CCIPL in France.

References

Agnihotri, N., and Mishra, P. C. (2009). Mutagenic product formation due to reaction of guanine radical cation with nitrogen dioxide. *J. Phys. Chem. B* 113, 3129–3138. doi: 10.1021/jp805942y

Agnihotri, N., and Mishra, P. C. (2010). Formation of 8-nitroguanine due to reaction between guanyl radicalnitrogen dioxide: catalytic role of hydration. *J. Phys. Chem. B* 114, 7391–7404. doi: 10.1021/jp9122437

Agnihotri, N., and Mishra, P. C. (2011). Reactivities of radicals of adenineguanine towards reactive oxygen speciesreactive nitrogen oxide species: $OH^{\bullet}NO_2^{\bullet}$. *Chem. Phys. Lett.* 503, 305–309. doi: 10.1016/j.cplett.2011.01.042

Ambrosek, D., Loos, P. F., Assfeld, X., and Daniel, C. (2010). A theoretical study of Ru(II) polypyridyl DNA intercalators structureelectronic absorption spectroscopy of $[Ru(phen)_2(dppz)]^{2+}$ $[Ru(tap)_2(dppz)]^{2+}$ complexes intercalated in guanine−cytosine base pairs. *J. Inorg. Biochem.* 104, 893–901. doi: 10.1016/j.jinorgbio.2010.04.002

Auffinger, P., and Westhof, E. (2000). Waterion binding around RNADNA (c,g) oligomers. *J. Mol. Biol.* 300, 1113–1131. doi: 10.1006/jmbi.2000.3894

Augusto, O., Bonini, M. G., Amanso, A. M., Linares, E., Santos, C. C., and De Menezes, S. L. (2002). Nitrogen dioxidecarbonate radical anion: Two emerging radicals in biology. *Free Radic. Biol. Med.* 32, 841–859. doi: 10.1016/S0891-5849(02)00786-4

Bergeron, F., Auvré, F., Radicella, J. P., and Ravanat, J. L. (2010). HO radicals induce an unexpected high proportion of tandem base lesions refractory to repair by DNA glycosylases. *Proc. Natl. Acad. Sci. U.S.A.* 107, 5528–5533. doi: 10.1073/pnas.1000193107

Cadet, J., Douki, T., and Ravanat, J. L. (2010). Oxidatively generated base damage to cellular DNA. *Free Radic. Biol. Med.* 49, 9–21. doi: 10.1016/j.freeradbiomed.2010.03.025

Cauët, E., Valiev, M., and Weare, J. H. (2010). Vertical ionization potentials of nucleobases in a fully solvated DNA environment. *J. Phys. Chem. B* 114, 5886–5894. doi: 10.1021/jp9120723

Cerón-Carrasco, J. P., and Jacquemin, D. (2012). Interplay between hydroxyl radical attackh–bond stability in guanine–cytosine. *RSC Adv.* 2, 11867–11875. doi: 10.1039/c2ra22389a

Cerón-Carrasco, J. P., Bastida, A., Zúñiga, J., Requena, A., and Miguel, B. (2010). A theoretical study of the reaction of β-carotene with the nitrogen dioxide radical in solution. *J. Phys. Chem. B* 114, 4366–4372. doi: 10.1021/jp911846h

Cerón-Carrasco, J. P., Zúñiga, J., Requena, A., Perpète, E. A., Michaux, C., and Jacquemin, D. (2011). Combined effect of stackingsolvation on the spontaneous mutation in DNA. *Phys. Chem. Chem. Phys.* 13, 14584–14589. doi: 10.1039/c1cp20946a

Cerón-Carrasco, J. P., Jacquemin, D., and Dumont, E. (2013). Impact of DNA environment on the intrastrand cross-link lesions: Hydrogen atom release as the last step of formation of G[8-5m]T. *J. Phys. Chem. B* 117, 16397–16404. doi: 10.1021/jp408947u

Chen, H. Y., Kao, C. L., and Hsu, S. C. N. (2009). Proton transfer in guanine-cytosine radical anion embedded in B-form DNA. *J. Am. Chem. Soc.* 131, 15930–15938. doi: 10.1021/ja906899p

Chen, H. Y., Yeh, S. W., Hsu, S. C. N., Kao, C. L., and Dong, T. Y. (2011). Effect of nucleobase sequence on the proton transfer reactionstability of the guanine–cytosine base pair radical anion. *Phys. Chem. Chem. Phys.* 13, 2674–2681. doi: 10.1039/c0cp01419b

Close, D. M., and Øhman, K. T. (2008). Ionization energies of the nucleotides. *J. Phys. Chem. A* 112, 11207–11212. doi: 10.1021/jp805308p

Dannenberg, J. J., and Tomasz, M. (2000). Hydrogen-bond acid/base catalysis: a density functional theory study of protonated guanine-(substituted) cytosine base pairs as models for nucleophilic attack on mitomycin in DNA. *J. Am. Chem. Soc.* 122, 2062–2068. doi: 10.1021/ja993145i

Dapprich, S, Komáromi, I., Byun, K. S., Morokuma, K., and Frisch, M. J. (1999). A new ONIOM implementation in Gaussian 98. part 1. The calculation of energies, gradientsvibrational frequencieselectric field derivatives. *J. Mol. Struct.* 462, 1–21. doi: 10.1016/S0166-1280(98)00475-8

Douki, T., and Cadet, J. (2008). *Radiation Chemistry: From Basics to Applications in Materiallife Sciences.* Les Ulis: edp Sciences.

Dupont, C., Patel, C., and Dumont, E. (2011). Improved DFT description of intrastrand cross-link formation by inclusion of London dispersion corrections. *J. Phys. Chem. B* 115, 15138–15144. doi: 10.1021/jp209074q

Dupont, C., Patel, C., Ravanat, J. L., and Dumont, E. (2013). Addressing the competitive formation of tandem DNA lesions by a nucleobase peroxyl radical: a DFT-D screening. *Org. Biomol. Chem.* 11, 3038–3045. doi: 10.1039/c3ob40280k

Florián, J., and Leszczyński, J. (1996). Spontaneous DNA mutations induced by proton transfer in the guanine·cytosine base pairs: An energetic perspective. *J. Am. Chem. Soc.* 118, 3010–3017. doi: 10.1021/ja951983g

Fortini, P., Pascucci, B., Parlanti, E., D'Errico, M., Simonelli, V., and Dogliotti, E. (2003). 8-oxoguanine DNA damage: At the crossroad of alternative repair pathways. *Mutat. Res.* 531, 127–139. doi: 10.1016/j.mrfmmm.2003.07.004

Frisch, M., J., Trucks, G. W., Schlegel, H. B., Scuseria, G. E., Robb, M. A., Cheeseman, J. R., et al. (2009). *Gaussian 09 Revision D.01*. Wallingford CT: Gaussian Inc.

Galano, A. (2007). Relative antioxidant efficiency of a large series of carotenoids in terms of one electron transfer reactions. *J. Phys. Chem. B* 111, 12898–12908. doi: 10.1021/jp074358u

Garrec, J., Patel, C., Rothlisberger, U., and Dumont, E. (2012). Insights into intrastrand cross-link lesions of DNA from QM/MM molecular dynamics simulations. *J. Am. Chem. Soc.* 134, 2111–2119. doi: 10.1021/ja2084042

Gorb, L., Podolyan, Y., Dziekonski, P., Sokalski. W. A., and Leszczyński, J. (2004). Double-proton transfer adenine-thymineguanine-cytosine base pairs. A post-hartree-fock ab initio study. *J. Am. Chem. Soc.* 126, 10119–10129. doi: 10.1021/ja049155n

Ignarro, L. J. (1990). Biosynthesismetabolism of endothelium-derived nitric oxide. *Annu. Rev. Pharmacol. Toxicol.* 30, 535–560. doi: 10.1146/annurev.pa.30.040190.002535

Jacquemin, D., Zúñiga, J., Requena, A., and Cerón-Carrasco, J. P. (2014). Assessing the importance of proton transfer reactions in DNA. *Acc. Chem. Res.* 47, 2467–2474. doi: 10.1021/ar500148c

Jena, N. R., and Mishra, P. C. (2005). Mechanisms of formation of 8-oxoguanine due to reactions of onetwo $OH^{\bullet}$ radicalsthe H_2O_2 molecule with guanine: a quantum computational study. *J. Phys. Chem. B* 109, 1405–14218. doi: 10.1021/jp050646j

Khanduri, D., Adhikary, A., and Sevilla, M. D. (2011). Highly oxidizing excited states of one-electron-oxidized guanine in DNA: wavelengthpH dependence. *J. Am. Chem. Soc.* 133, 4527–4537. doi: 10.1021/ja110499a

Kumar, A., and Sevilla, M. D. (2010). Proton-coupled electron transfer in DNA on formation of radiation-produced ion radicals. *Chem. Rev.* 110, 7002–7023. doi: 10.1021/cr100023g

Kumar, A., and Sevilla, M., and Suhai, S. (2008). Microhydration of the guanine-cytosine (GC) base pair in the neutralanionic radical states: a density functional study. *J. Phys. Chem. B* 112, 5189–5198. doi: 10.1021/jp710957p

Kumar, A., Pottiboyina, V., and Sevilla, M. D. (2011). Hydroxyl radical ($OH^{\bullet}$) reaction with guanine in an aqueous environment: a DFT study. *J. Phys. Chem. B* 115, 15129–15137. doi: 10.1021/jp208841q

Löwdin, P. O. (1963). Proton tunneling in DNAits biological implications. *Rev. Mod. Phys.* 35, 724–732. doi: 10.1103/RevModPhys.35.724

Lonkar, P., and Dedon, P. C. (2011). Reactive speciesDNA damage in chronic inflammation: reconciling chemical mechanismsbiological fates. *Int. J. Cancer* 128, 1999–2009. doi: 10.1002/ijc.25815

Loos, P. F., Dumont, E., Laurent, A. D., and Assfeld, X. (2009). Important effects of neighbouring nucleotides on electron induced DNA single-strand breaks. *Chem. Phys. Lett.* 475, 120–123. doi: 10.1016/j.cplett.2009.05.041

Makarov, V., Pettitt, B., and Feig, M. (2002). Solvationhydration of proteinsnucleic acids: a theoretical view of simulationexperiment. *Acc. Chem. Res.* 35, 376–384. doi: 10.1021/ar0100273

Misiaszek, R., Crean, C., Geacintov, N. E., and Shafirovich, V. (2005). Combination of nitrogen dioxide radicals with 8-oxo-7,8-dihydroguanineguanine radicals in DNA: a oxidation and nitration end-products. *J. Am. Chem. Soc.* 127, 2191–2200. doi: 10.1021/ja044390r

Mo, S. J., Vreven, M., Mennucci, B., Morokuma, K., and Tomasi, J. (2004). Theoretical study of the sn2 reaction of Cl^{-} (H_2O)+CH_3Cl using our own n-layered integrated molecular orbitalmolecular mechanics polarizable continuum model method (ONIOM–PCM). *Theor. Chem. Acc.* 111, 154–161. doi: 10.1007/s00214-003-0519-2

Pacher, P., Beckman, J. S., and Liaudet, L. (2007). Nitric oxideperoxynitrite in healthdisease. *Physiol. Rev.* 87, 315–424. doi: 10.1152/physrev.00029.2006

Patel, C., Garrec, J., Dupont, C., and Dumont, E. (2013). What singles out the G[8-5]C intrastrand DNA cross-link? Mechanisticstructural insights from quantum mechanics/molecular mechanics simulations. *Biochemistry* 52, 425–431. doi: 10.1021/bi301198h

Schneider, B., and Berman, H. M. (1995). Hydration of the DNAA bases is local. *Biophys. J.* 69, 2661–2669. doi: 10.1016/S0006-3495(95)80136-0

Shukla, L. I., Adhikary, A., Pazdro, R., Becker, D., and Sevilla, M. D. (2004). Formation of 8-oxo-7,8-dihydroguanine-radicals in γ-irradiated DNA by multiple one-electron oxidations. *Nucleic Acids Res.* 32, 6565–6574. doi: 10.1093/nar/gkh989

Shukla, P. K., and Mishra, P. C. (2007). H_2O_3 as a reactive oxygen species: formation of 8-oxoguanine from its reaction with guanine. *J. Phys. Chem. B* 111, 4603–4615. doi: 10.1021/jp070399e

Stewart, J. J. P. (2007). Optimization of parameters for semiempirical methods v: modification of NDDO approximationsapplication to 70 elements. *J. Mol. Model.* 13, 1173–1213. doi: 10.1007/s00894-007-0233-4

Tomasi, J., Mennucci, M., and Cances, E. (1999). The IEF version of the PCM solvation method: An overview of a new method addressed to study molecular solutes at the QM ab initio level. *J. Mol. Struct.* 464, 211–226. doi: 10.1016/S0166-1280(98)00553-3

Tomasi, J., Mennucci, B., and Cammi, R. (2005). Quantum mechanical continuum solvation models. *Chem. Rev.* 105, 2999–3093. doi: 10.1021/cr9904009

Topal, M. D., and Fresco, J. R. (1976). Complementary base pairingthe origin of substitution mutations. *Nature* 263, 285–289. doi: 10.1038/263285a0

Villani, G. (2010a). Theoretical investigation of hydrogen atom transfer in the adenine−thymine base pairits coupling with the electronic rearrangement. Concerted vs. stepwise mechanism. *Phys. Chem. Chem. Phys.* 12, 2664–2669. doi: 10.1039/b917672a

Villani G. (2010b). Theoretical investigation of hydrogen atom transfer in the cytosine-guanine base pairits coupling with electronic rearrangement. concerted vs. stepwise mechanism. *J. Phys. Chem. B* 114, 9653–9662. doi: 10.1021/jp102457s

von Sonntag, C. (2009). *Free-Radical-Induced DNA DamageIts Repair*. Berlin; Heidelberg: Springer-Verlag.

Vreven, T., Mennucci, B., da Silva, C. O., Morokuma, K., and Tomasi, J. (2001). The ONIOM-PCM method: combining the hybrid molecular orbital methodthe polarizable continuum model for solvation. Application to the geometryproperties of a merocyanine in solution. *J. Chem. Phys.* 115, 62–72. doi: 10.1063/1.1376127

Zhang, R. B., and Eriksson, L. A. (2007). Effects of oh radical addition on proton transfer in the guanine–cytosine base pair. *J. Phys. Chem. B* 111, 6571–6576. doi: 10.1021/jp071772l

Zhao, Y., and Truhlar, D. G. (2008a). Density functionals with broad applicability in chemistry. *Acc. Chem. Res.* 41, 157–167. doi: 10.1021/ar700111a

Zhao, Y., and Truhlar, D. G. (2008b). The M06 suite of density functionals for main group thermochemistry, thermochemical kinetics, noncovalent interactions, excited states,transition elements: Two new functionalssystematic testing of four mM6-class functionals12 other functionals. *Theor. Chem. Acc.* 120, 215–241. doi: 10.1007/s00214-007-0310-x

Conflict of Interest Statement: The authors declare that the research was conducted in the absence of any commercial or financial relationships that could be construed as a potential conflict of interest.

Copyright © 2015 Cerón-Carrasco, Requena, Zúñiga and Jacquemin. This is an open-access article distributed under the terms of the Creative Commons Attribution License (CC BY). The use, distribution or reproduction in other forums is permitted, provided the original author(s) or licensor are credited and that the original publication in this journal is cited, in accordance with accepted academic practice. No use, distribution or reproduction is permitted which does not comply with these terms.

frontiers in Chemistry

ORIGINAL RESEARCH
published: 21 April 2015
doi: 10.3389/fchem.2015.00028

DNA oxidation profiles of copper phenanthrene chemical nucleases

Zara Molphy[1], *Creina Slator*[1], *Chryssostomos Chatgilialoglu*[2,3] *and Andrew Kellett*[1]*

[1] School of Chemical Sciences, National Institute for Cellular Biotechnology, Dublin City University, Dublin, Ireland, [2] Istituto per la Sintesi Organica e la Fotoreattività, Consiglio Nazionale delle Ricerche, Bologna, Italy, [3] Institute of Nanoscience and Nanotechnology, National Center for Scientific Research "Demokritos," Athens, Greece

The deleterious effects of metal-catalyzed reactive oxygen species (ROS) in biological systems can be seen in a wide variety of pathological conditions including cancer, cardiovascular disease, aging, and neurodegenerative disorder. On the other hand however, targeted ROS production in the vicinity of nucleic acids—as demonstrated by metal-activated bleomycin—has paved the way for ROS-active chemotherapeutic drug development. Herein we report mechanistic investigations into the oxidative nuclease activity and redox properties of copper(II) developmental therapeutics $[Cu(DPQ)(phen)]^{2+}$ (Cu-DPQ-Phen), $[Cu(DPPZ)(phen)]^{2+}$ (Cu-DPPZ-Phen), and $[\{Cu(phen)_2\}_2(\mu\text{-terph})](terph)$ (Cu-Terph), with results being compared directly to Sigman's reagent $[Cu(phen)_2]^{2+}$ throughout (phen = 1,10-phenanthroline; DPQ = dipyridoquinoxaline; DPPZ = dipyridophenazine; Terph = terephthalate). Oxidative DNA damage was identified at the minor groove through use of surface bound recognition elements of methyl green, netropsin, and $[Co(NH_3)_6]Cl_3$ that functioned to control complex accessibility at selected regions. ROS-specific scavengers and stabilizers were employed to identify the cleavage process, the results of which infer hydrogen peroxide produced metal-hydroxo or free hydroxyl radicals (•OH) as the predominant species. The extent of DNA damage owing to these radicals was then quantified through 8-oxo-2′-deoxyguanosine (8-oxo-dG) lesion detection under ELISA protocol with the overall trend following Cu-DPQ-Phen > Cu-Terph > Cu-Phen > Cu-DPPZ. Finally, the effects of oxidative damage on DNA replication processes were investigated using the polymerase chain reaction (PCR) where amplification of 120 base pair DNA sequences of varying base content were inhibited—particularly along A-T rich chains—through oxidative damage of template strands.

Keywords: copper, phenazine, chemical nuclease, hydroxyl radical, DNA damage, 8-oxo-dG

OPEN ACCESS

Edited by:
Youla S. Tsantrizos, McGill University, Canada

Reviewed by:
Martin Schmeing, McGill University, Canada
John Brazier, University of Reading, UK

***Correspondence:**
Andrew Kellett, School of Chemical Sciences, National Institute for Cellular Biotechnology, Dublin City University, Glasnevin, Dublin 9, Ireland
andrew.kellett@dcu.ie

Specialty section:
This article was submitted to Chemical Biology, a section of the journal Frontiers in Chemistry

Received: *22 January 2015*
Accepted: *30 March 2015*
Published: *21 April 2015*

Citation:
Molphy Z, Slator C, Chatgilialoglu C and Kellett A (2015) DNA oxidation profiles of copper phenanthrene chemical nucleases. Front. Chem. 3:28. doi: 10.3389/fchem.2015.00028

Introduction

Oxygen radical generation is an inevitable consequence of aerobic existence and has been implicated in a wide variety of pathological conditions including cancer, cardiovascular disease, aging, and neurodegenerative disease (Cooke and Evans, 2007). Reactive oxygen species (ROS) are created in a variety of endogenous chemical and biological processes in the human body—predominantly through oxygen metabolism. The sequential reduction of molecular oxygen can generate reactive intermediates such as superoxide ($O_2^{\bullet-}$) and hydrogen peroxide (H_2O_2) that initiate a cascade of redox reactions toward the production of hydroxyl radicals (•OH) and related metal-oxo species

(Kellett et al., 2012). Molecular targets of ROS include proteins, lipids, and nucleic acids—the deleterious effects of which include base and deoxyribose modifications that ultimately precipitate single or double strand breaks. To counteract this, the majority of cells possess defense mechanisms such as base excision repair (BER)—*e.g.,* 8-oxoguanine glycosylase (OGG1) (Xu et al., 2014)—and nucleotide excision repair (NER) pathways that prevents genome instability to ultimately limit cytotoxicity, the accumulation of deleterious mutations, and maintain genome integrity. Two major $^{\bullet}$OH induced DNA lesions are 8-oxoguanine (8-oxo-dG), a mutagenic lesion that induces G → T transversions widely seen in mutated oncogenes and tumor suppressor genes, and the poorly mutagenic thymine glycol (Basu et al., 1989; Chatgilialoglu and O'Neill, 2001). Recent evidence suggests $^{\bullet}$OH attacks occur primarily at base moieties and account for the majority of total hydrogen atom abstraction on DNA alone (Chatgilialoglu et al., 2011). Thus, 8-oxo-dG has been subjected to intensive investigation due to its prominence as a biomarker within ROS-mediated disease pathology, and its ease of detection in bodily fluids and tissue samples has allowed a variety of detection methods to accurately assess 8-oxo-dG lesions including high-pressure liquid chromatography (HPLC), gas chromatography (GC), mass spectrometry (MS), and the enzyme linked immunosorbent assay (ELISA).

In addition to the induction of endogenous DNA damage, exogenous sources including UV light, ionizing radiation, environmental agents, pharmaceuticals, and industrial chemicals can also initiate ROS production (Klaunig et al., 2010). Indeed the clinical antineoplastic agent bleomycin (BLM) is a redox active agent capable of DNA oxidative cleavage in the presence of Fe(II) (and Cu(I)), molecular oxygen, and endogenous one electron reductants (Stubbe and Kozarich, 1987; Burger, 1998; Chen et al., 2008). Bleomycin can abstract hydrogen atoms from deoxyribose in the DNA backbone, specifically from C4′ position (Breen and Murphy, 1995). The active form of Fe(II)-BLM is a ternary, high-valence Fe(III)-O$^{\bullet}$ species (Rodriguez and Hecht, 1982; Pratviel and Bernadou, 1989; Gajewski et al., 1991) that undergoes an electron reduction by biological reductants (*e.g., L*-ascorbate) or by another molecule of Fe(II)-BLM (Burger et al., 1981; Natrajan et al., 1990). Fe(II)-BLM can form 8-oxo-dG and other base propenals, however these are known to occur in small amounts; the formation of such DNA degradation products results from $^{\bullet}$OH oxidative damage—a side product only of the ferryl-oxo species—that does not functionally contribute to biological systems or participate in the nuclease activity of activated Fe(II)-BLM (Rodriguez and Hecht, 1982).

Our group have recently investigated a range of $[Cu(phen)_2]^{2+}$ (Cu-Phen) (Phen = 1,10-phenanthroline) type systems as potential lead compounds for therapeutic and biochemical application (Kellett et al., 2011; Prisecaru et al., 2012, 2013; Molphy et al., 2014). $[Cu(phen)_2]^{2+}$, originally reported by Sigman et al. (1979), is believed to cleave DNA through a variety of copper bound oxidants including Cu^{3+}-OH and Cu^{+}-OOH with the possibility of free $^{\bullet}$OH playing a role in the overall process (Marshall et al., 1981; Johnson and Nazhat, 1987). Recent work on the development of bis-chelate Cu^{2+} phenanthroline-phenazine cationic complexes of $[Cu(DPQ)(phen)]^{2+}$ (Cu-DPQ-Phen) and $[Cu(DPPZ)(phen)]^{2+}$ (Cu-DPPZ-Phen) (DPQ = dipyridoquinoxaline; DPPZ = dipyridophenazine) have demonstrated how extension of the ligated phenazine ligand influences DNA recognition and oxidative degradation (Molphy et al., 2014). Indeed, when designer phenazine ligands (DPQ and DPPZ) are incorporated into the "copper bis-phen" chemical nuclease model, these agents display enhanced DNA recognition and intercalation among the highest reported on ctDNA (**Table 1**, $K_{app} \approx 3 \times 10^7$ M(bp)$^{-1}$). Since nuclearity is also established as an important factor in oxidative DNA cleavage (Li et al., 2005; van der Steen et al., 2010), we also reported the dinuclear complex, $[\{Cu(phen)_2\}_2(\mu\text{-terph})](terph)$ (Cu-Terph) (terph = terephtalate), which is capable of inducing oxidative DNA strand breaks in the absence of exogenous reductant (Kellett et al., 2011). Cu-Terph has promising *in vitro* cytoxicity toward human derived breast, prostate, colon, ovarian, and lung human cance cell lines, with comparable activity to mitoxantrone—a clinincal anthracene topoisomerase II inhibitor (Kellett et al., 2011; Prisecaru et al., 2012).

In this contribution we identify, using head-to-head analysis, the comparative oxidative DNA cleavage properties of DNA binding Cu^{2+} complexes Cu-Phen, Cu-DPQ-Phen, Cu-DPPZ-Phen, and Cu-Terph (**Scheme 1**) through a variety of biophysical and molecular biological methods. Additionally, we report these agents inhibit DNA polymerase activity—particularly at A-T rich sites—through oxidative degradation of template strands. To that end, we report (*i.*) oxidative DNA profiles in the presence

TABLE 1 | Summary of DNA binding properties of tested complexes toward calf thymus DNA (ctDNA) along with synthetic nucleic acid polymers poly[d(A-T)$_2$] and poly[d(G-C)$_2$].

Compound	C_{50}[a]	K_{app}M(bp)$^{-1}$[b]	Q (μM) poly[d(A-T)$_2$][c]	Q (μM) poly[d(G-C)$_2$][c]	ΔT_M(°C) poly[d(A-T)$_2$][d]	ΔT_M (°C) poly[d(G-C)$_2$][d]
Cu-Phen	179.21	0.67×10^6	13.34	7.96	−0.02 ± 0.29	06.64 ± 1.58
Cu-DPQ-Phen	3.93	30.45×10^6	8.34	3.97	0.60 ± 0.18	11.39 ± 1.10
Cu-DPPZ-Phen	4.63	25.85×10^6	11.60	10.12	0.50 ± 0.10	10.44 ± 1.10
Cu-Terph	39.36	0.30×10^6	8.6	10.3	NT	NT

[a] *C_{50} = concentration required to reduce 50% fluorescence of saturated bound ethidium bromide (12.6 μM) on ctDNA (10 μM).*
[b] *$K_{app} = K_e \times 12.6/C_{50}$ where, $K_e = 9.5 \times 10^6$ M(bp)$^{-1}$ (apparent binding constant on ctDNA).*
[c] *Fluorescence Quenching (Q) of limited bound Ethidium Bromide (5 μM) bound poly[d(A-T)$_2$] and poly[d(G-C)$_2$] by Cu^{2+} complexes.*
[d] *ΔT_M = difference in thermal melting (T_M) of drug-treated nucleotide at r = 0.1 compared with drug-untreated nucleotide.*
NT = not tested.

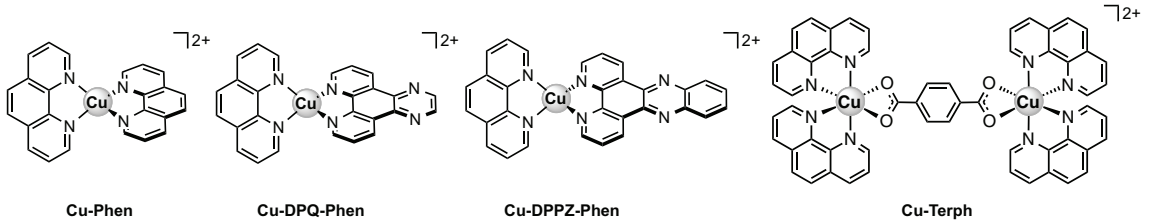

SCHEME 1 | Molecular structures of the copper(II) complex cations examined in this study.

of DNA recognition agents of netropsin, methyl green, and $[Co(NH_3)_6]Cl_3$, (*ii.*) DNA cleavage profiles in the presence of radical trapping and stabilizing co-factors, (*iii.*) quantitation of 8-oxo-dG lesions arising from complex treated superhelical plasmid DNA, and (*iv.*) DNA polymerase inhibition on DNA templates of differential A-T content. The DNA binding profiles for this series have previous been reported and are summarized in **Table 1** (Kellett et al., 2011; McCann et al., 2013; Prisecaru et al., 2013; Molphy et al., 2014); simple phenanthroline containing complexes (Cu-Phen and Cu-Terph) have moderate binding constants toward ctDNA while phenazine compounds (Cu-DPQ-Phen and Cu-DPPZ-Phen) can be considered as high-affinity dsDNA intercalators. Further, ethidium bromide fluorescence quenching on alternating duplex polymers—poly[d(A-T)$_2$] and poly[d(G-C)$_2$]—has shown complexes intercalate from both minor and major grooves. It has not been established, as yet, if chemical nuclease activity occurs preferentially at either or both recognition sites.

Materials and Methods

Preparation of the Complexes

Chemicals were purchased from Sigma-Aldrich Ireland and used without further purification.

DPQ and DPPZ ligands were initially generated through the Schiff base condensation reactions of 1,10-phenanthroline-5,6-dione with ethylenediamine and *o*-phenylenediamine respectively. The bis-phenanthroline complex $[Cu(phen)_2](NO_3)_2$ (Cu-Phen) was prepared by refluxing 1,10-phenanthroline with copper(II) nitrate in a 2:1 molar ratio in aqueous-ethanol (Prisecaru et al., 2013). The phenazine complexes $[Cu(DPQ)(Phen)](NO_3)_2$ (Cu-DPQ-Phen) and $[Cu(DPPZ)(Phen)](NO_3)_2$ (Cu-DPPZ-Phen) were prepared by treating the mono-phenanthroline complex $[Cu(Phen)](NO_3)_2$ with 1 molar equivalent of the corresponding phenazine ligand in ethanol (Molphy et al., 2014). The $[Cu_2(\mu\text{-terephthalate})(1,10\text{-phen})_4]^{2+}$ was prepared by ethanolic reflux of copper(II) terephthalate hydrate and 1,10-phenanthroline in a 1:2 ratio according to the reported method (Kellett et al., 2011).

DNA Cleavage Studies

DNA Cleavage in the Presence of Added Reductant

The ability of the complexes to oxidatively damage DNA in the presence of added reductant was determined using a method previously published by this laboratory with minor changes (Molphy et al., 2014). Reactions were carried out according to the following general procedure: in a total volume of 20 μL using 80 mM HEPES buffer (pH 7.2) with 25 mM NaCl, 1 mM Na-L-ascorbate, 400 ng superhelical pUC19 (NEB, N3041) and varying concentrations of test complex (250 nM, 500 nM, 1 μM and 2.5 μM). Complexes were initially prepared in DMF and further diluted in HEPES buffer (Fisher). Samples were incubated at 37°C for 30 min. Reactions were quenched by adding 6× loading buffer (Fermentas) containing 10 mM Tris-HCl, 0.03% bromophenol blue, 0.03% xylene cyanole FF, 60% glycerol, 60 mM EDTA and samples were loaded onto an agarose gel (1.2%) containing 8 μL EtBr. Electrophoresis was completed at 70 V for 2 h in 1× TAE buffer.

DNA Cleavage in the Presence of Non-Covalently Bound Recognition Elements

This protocol was adapted from a previously reported procedure (Tabassum et al., 2012). Briefly, 400 ng pUC19 was incubated with 25 mM NaCl, 1 mM Na-L-ascorbate, and 8, or 16 μM of either methyl green, netropsin or hexamine cobalt(III) chloride in 80 mM HEPES buffer (pH 7.2) for 45 min at 37°C. Sample tubes were then vortexed and varying concentrations of test complex were added (250 nM, 500 nM, 1 μM, and 2.5 μM). The reaction mixture was further incubated at 37°C for 30 min. The reaction was then quenched with 6× loading buffer and subjected to gel electrophoresis (prepared and stained as previously described).

DNA Oxidation with ROS Scavengers and Stabilizers

The presence of ROS specific scavengers was used to determine the effect on the DNA cleavage abilities of each copper complex. The procedure was adapted to the previously reported method (Zhou et al., 2014). Briefly, to a final volume of 20 μL, 80 mM HEPES (pH = 7.2), 25 mM NaCl, 1 mM Na-L-ascorbate, and 400 ng of pUC19 DNA were treated with drug concentrations of 250 nM, 500 nM, 1 μM, and 2.5 μM in the presence ROS scavengers / stablilisers; KI (10 mM), NaN_3(10 mM), DMSO (10%), and D_2O (77%). Reactions were incubated for 30 min at 37°C, quenched with DNA loading dye and loaded onto 1.2% agarose gel and run under conditions previously described.

HT Quantitation of 8-oxo-dG

Quantitation of 8-oxo-dG lesions present in 3000 ng pUC19 plasmid DNA pre-incubated with test complexes (10 and 20 μM) at 37°C for 30 min was achieved utilizing a high throughput

8-oxo-dG ELISA kit (Trevigen) and performed as per manufacturers guidelines. Samples of damaged DNA were examined in triplicate using a 96 well plate, pre-coated with 8-oxo-dG along with varying concentrations of a standard 8-oxo-dG (200, 100, 50, 25, 12.5, 6.25, and 3.13 nM). An 8-oxo-dG monoclonal antibody, which competitively binds to 8-oxo-dG immobilized to each well, was added to the plate with excess antibody being washed with PBST (1× PBS, 0.1% Tween 20). The concentration of 8-oxo-dG was determined based on antibody retention in each well using goat anti-mouse IgG-HRP conjugated antibody and colorimetric detection substrate TACS-Sapphire. Product formation was inversely proportional to 8-oxo-dG present in the DNA sample. Samples were determined using a Bio-Tek synergy HT multimode microplate reader at 450 nm and quantitation of 8-oxo-dG was extrapolated from the standard curve.

PCR Inhibition Studies

This protocol was adapted from a previously reported procedure (Sanchez-Cano et al., 2010). 400 ng pUC19 DNA was initially exposed to each test complex in the presence and absence of 1 mM added reductant at 37°C for 30 min (Figures S-2, S-3). 20 ng of damaged DNA template was removed and PCR reactions (35 cycles) were carried out with each varying G-C content primer set (Figure S-4) at optimum annealing temperatures and analyzed using gel electrophoresis. This investigation was replicated in the absence of added reductant (Figure S-5) and also at lower drug loading (250 nM, 500 nM, 1 μM, and 2.5 μM) with 1 mM reductant (Figure S-6).

Results and Discussion

DNA Cleavage in the Presence of Non-Covalently Bound Recognition Elements

We have previously shown that DNA oxidative cleavage by copper complexes is dependent on a range of factors including (but not limited to): plasmid DNA conformation and type, presence of competing metal chelating agents (*e.g.,*

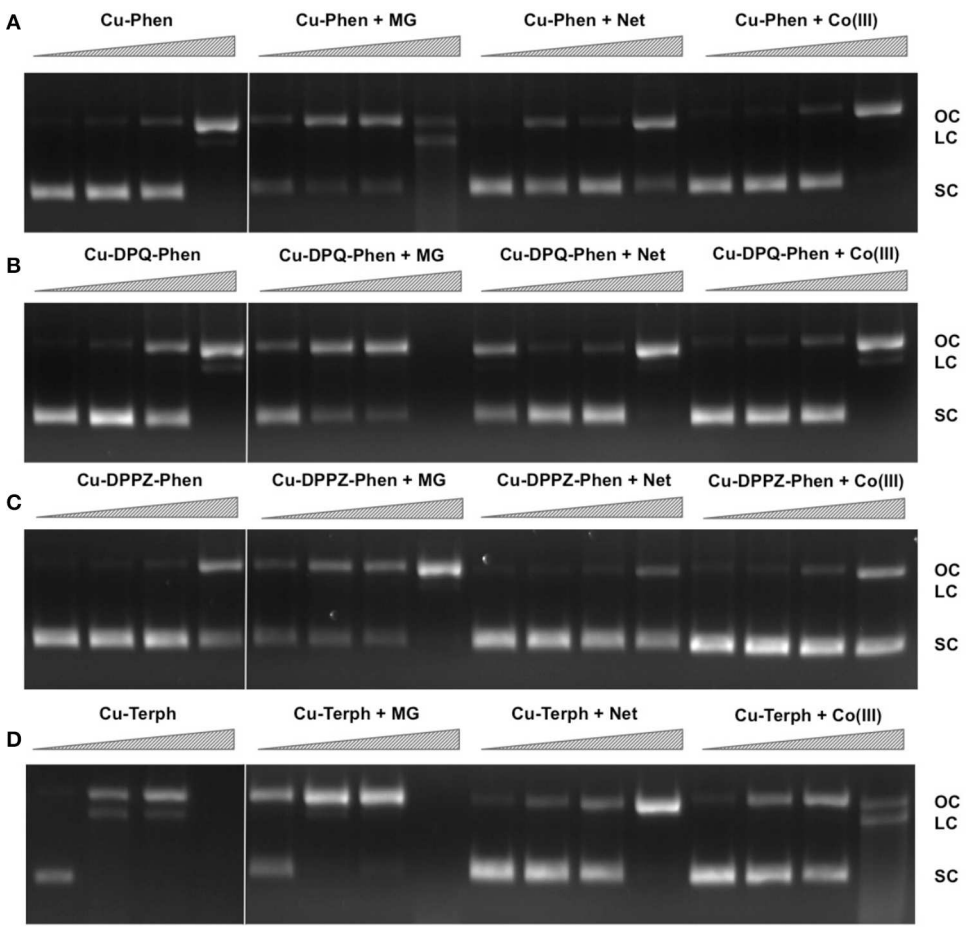

FIGURE 1 | Lane 1–4 (A–D) DNA cleavage reactions with 250 nM, 500 nM, 1.0 μM, and 2.5 μM test complex (A) Cu-Phen, (B) Cu-DPQ-Phen, (C) Cu-DPPZ-Phen, and (D) Cu-Terph, 400 ng superhelical pUC19 and 1 mM added Na-L-ascorbate incubated at 37°C for 30 min. Lanes 5–16 **(A–D)** DNA cleavage reactions in the presence of recognition elements, methyl green (MG), netropsin (Net), and $[Co(NH_3)_6]Cl_3$ (Co(III)), where 400 ng pUC19 was initially pre-treated with 8 μM of respective non-covalent binding control at 37° C for 45 min and then with 250 nM, 500 nM, 1 μM, and 2.5 μM test complex in the presence of 1 mM added Na-L-ascorbate at 37°C for 30 min.

EDTA), reaction/exposure time, and presence/concentration of exogenous reductant or oxidant. In the current work we examine chemical nuclease activity of supercoiled pUC19 plasmid DNA in the presence of 1 mM reductant (Na-L-ascorbate) using agarose gel electrophoresis. In order to ensure the copper(I) active species (i.e., the nuclease) was fully generated, each complex was initially reduced with 1 mM of added reductant prior to pUC19 titration. Relaxation of supercoiled (SC, FI) pUC19 DNA into open circular (OC, FII) and linear (LC, FIII) conformations was employed to qualitatively measure the cleavage efficiency of complexes over a concentration range of 250 nM, 500 nM, 1.0 μM, and 2.5 μM for 30 min at 37°C (**Figures 1A–D**, lanes 1–4). Complexes show concentration-dependent relaxation of FI (superhelical) to FII (open circular/nicked), while FIII (linear conformation) is evident at 2.5 μM Cu-DPQ-Phen exposure and with 500 nM of the dinuclear agent Cu-Terph. Complete digestion of SC DNA occurs only with the maximum tested concentration (2.5 μM) of Cu-Terph. The overall trend in chemical nuclease activity is Cu-Terph > Cu-DPQ-Phen > Cu-Phen > Cu-DPPZ-Phen. The activity profiles observed here are in good agreement with those previously reported by this group; Cu-Terph has previously displayed nicking at 1.0 μM on the plasmid pBR322 with complete digestion occurring thereafter (Prisecaru et al., 2012). We also established that both 2.5 and 5.0 μM of Cu-Phen induced nicking (OC) on both pBR322 (Prisecaru et al., 2012; McCann et al., 2013) with activity being impeded in the presence of EDTA (Prisecaru et al., 2013). The nuclease activity of both Cu-DPQ-Phen and Cu-DPPZ-Phen has been identified previously (Molphy et al., 2014), however, direct analysis with the current conditions cannot be made.

In an attempt to determine DNA cleavage site specificity, minor groove (netropsin, Net) and major groove (methyl green, MG) binders, along a surface electrostatic binding and condensing agent ($[Co(NH_3)_6]Cl_3$, Co(III)) were pre-incubated with pUC19 DNA prior to the addition of test complex (**Figures 1A–D**, lanes 5–16). In all cases, presence of the major groove binder MG enhanced chemical nuclease activity with greater nicking (OC) and linearization (LC) frequency compared with control experiments. Conversely, the minor groove binder Net impedes chemical nuclease activity as pUC19 is clearly protected from both OC and LC damage across all experiments. The cationic surface binding agent $[Co(NH_3)_6]^{3+}$ had no major impact on the chemical nuclease activity of Cu-Phen

TABLE 2 | Scavengers and stabilizers utilized within this study.

Scavenger[a]/Stabilizer[b]	ROS	References
NaN_3[a]	$^1O_2$	Franco et al., 2007
KI[a]	H_2O_2	Dunand et al., 2007; Steffens et al., 2012
DMSO[a]	$^{\bullet}OH$	Franco et al., 2007; Mazzer et al., 2007
D_2O[b]	$^1O_2$	Merkel et al., 1972; Xia et al., 2006

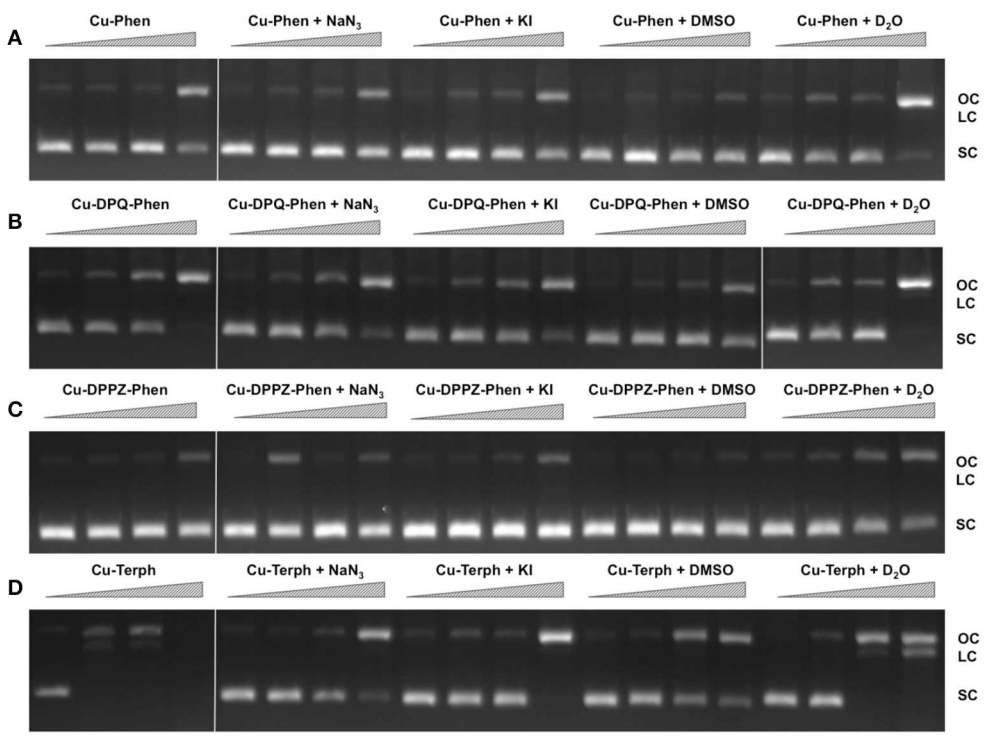

FIGURE 2 | DNA cleavage reactions in the presence of ROS scavengers. 400 ng of SC pUC19 was incubated for for 30 min at 37°C with 250 nM, 500 nM, 1 μM, and 2.5 μM of test complex **(A)** Cu-Phen, **(B)** Cu-DPQ-Phen, **(C)** Cu-DPPZ-Phen, and **(D)** Cu-Terph in the presence of 1 mM added Na-L-ascorbate for 30 min. Lanes 1–4 metal complex only, lanes 5–8, complex + 10 mM NaN_3; lanes 9–12, complex + 10 mM KI; lanes 13–16, complex + 10% DMSO; and lanes 17–20, complex + 77% D_2O.

and Cu-DPPZ-Phen but did reduce nicking by Cu-DPQ-Phen at 1 μM and was also effective in protecting pUC19 damage by Cu-Terph. Taken together, evidence here points toward the minor groove as the major site of DNA oxidation by this complex series; MG bound pUC19 primes the minor groove for chemical nuclease activity while titrated Net clearly diminishes this damage. Indeed this observation of minor groove targeting is consistent with previous analysis on the rapid cleavage of poly(dA-dT) by 2:1 phenanthroline-Cu^{+} mixtures (Sigman et al., 1979).

DNA Oxidation with ROS Scavengers and Stabilizers

In order to examine ROS species involved in DNA oxidation, activity was investigated in the presence of radical-specific scavengers and stabilizers (**Table 2**) with results shown in **Figure 2**. Before complex analysis, scavengers were confirmed to have no impact on pUC19 conformation (data not shown). Control experiments are in excellent agreement with those observed in **Figure 1** (lanes 1–4), however, a fraction of superhelical (FI) pUC19 was found to remain upon 2.5 μM exposure of Cu-Phen. Results here suggest that $^{\bullet}OH$ is the most prevalent radical species involved in strand scission as the presence of DMSO considerably impedes cleavage activity of all complexes. It is noteworthy DMSO had a major impact on cleavage activity of Cu-Terph as only the maximum tested concentrations (1.0 and 2.5 μM) contained nicked cleavage products. The presence of the H_2O_2 scavenger, KI, was also found to inhibit chemical nuclease activity of tested complexes—again most notably within Cu-Terph reactions—and this observation is consistent with previous trapping studies conducted on these model systems (Johnson and Nazhat, 1987; Prisecaru et al., 2013). It is interesting to note the catalase enzyme is a more effective scavenger of H_2O_2 compared with KI as previous work revealed complete inhibition of DNA oxidation by Cu-Phen, Cu-DPQ-Phen, and Cu-DPPZ-Phen complexes (Molphy et al., 2014).

The role of $^1O_2$ was next examined utilizing the NaN_3 scavenger (Franco et al., 2007) and D_2O as a $^1O_2$ stabilizer (Merkel et al., 1972; Xia et al., 2006). Nuclease activity by

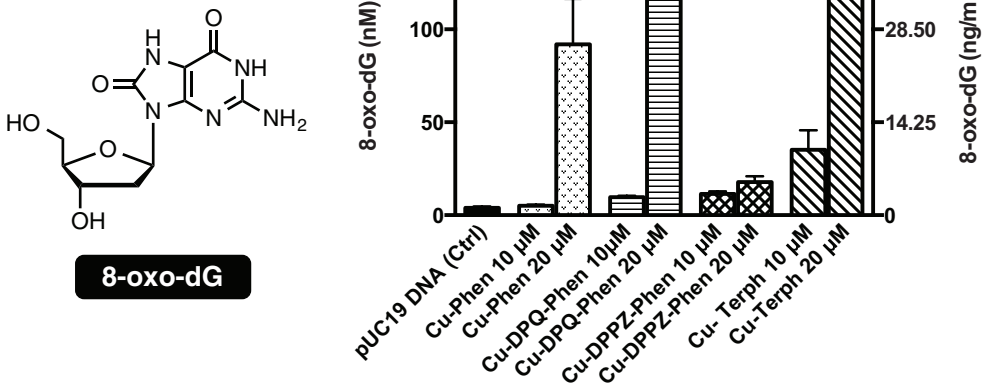

FIGURE 3 | Structure and quantification of 8-oxo-dG. Graph represents level of generated 8-oxo-dG as nM (left axis) and ng/mL (right axis). 3000 ng of SC pUC19 with 10 and 20 μM of test complexes Cu-Phen, Cu-DPQ-Phen, Cu-DPPZ-Phen, and Cu-Terph with 1 mM Na-L-ascorbate were incubated at 37°C for 30 min and followed by ELISA protocol.

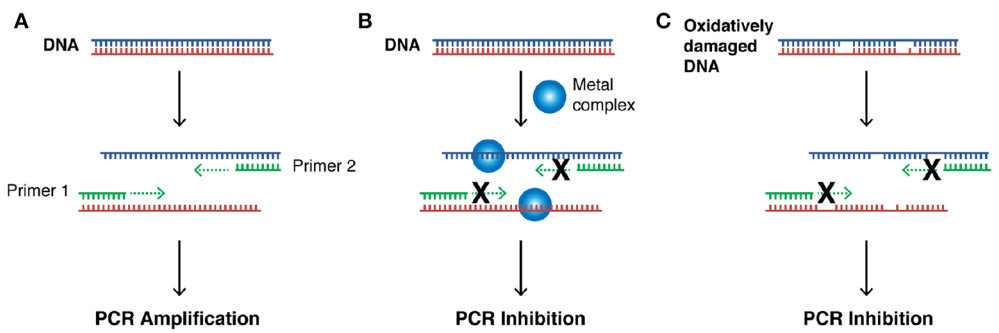

FIGURE 4 | (A) Illustration of steps involved in a successful PCR reaction (denaturation, primer annealing, primer extension, and template amplification), **(B)** the impact of a bound metal complex as physical block of the primer extension step, **(C)** inhibition of DNA amplification in the PCR cycle through the oxidative damage of template strand.

Cu-Phen, Cu-DPQ-Phen, and Cu-DPPZ-Phen complexes was only marginally inhibited by NaN_3 while no change in activity (relative to control) was observed in D_2O thus suggesting a limited role in DNA oxidation by $^1O_2$. NaN_3 did, however, impede activity by Cu-Terph but the role of $^1O_2$ in the scission process could not be verified as D_2O was also found to reduce activity, somewhat.

Quantitation of 8-oxo-dG

To examine if the oxidative DNA lesion, 8-oxo-dG, is formed during complex reactions with DNA, an HT 8-oxo-dG ELISA kit was employed for immunological detection and quantification. The complex series was investigated at 10 and 20 μM with 3000 ng of SC pUC19, with 8-oxo-dG being quantified in both nM and ng/mL (**Figure 3**). Nuclease activity was firstly confirmed at 10 μM and 20 μM (Figure S-1). Low numbers of lesions were detected in the untreated control (3.92 ± 0.79 nM) and the exposure of pUC19 to each of the complexes at 10 μM resulted in detectable increases in 8-oxo-dG (between 35.24 and 5.05 nM) with the trend following Cu-Terph > Cu-DPPZ-Phen > Cu-DPQ-Phen > Cu-Phen. Upon 20 μM complex exposure significant levels of 8-oxo-dG (between 129.22 and 17.77 nM) were produced with the trend changing toward Cu-DPQ-Phen > Cu-Terph > Cu-Phen > Cu-DPPZ-Phen. Given the $^{\bullet}OH$ radical is fundamental in the production of 8-oxo-dG, results here demonstrate DNA oxidation by copper phenanthrene complexes, particularly under extensive shearing conditions (Figure S-1), drive formation of 8-oxo-dG lesions.

PCR Inhibition Studies

Our next aim was to investigate how oxidative lesions—induced through complex exposure—can ultimately impact on *in vitro* DNA processing by the polymerase chain reaction (PCR) (**Figure 4**). During the normal PCR process, a DNA template is initially denatured through heating to more than 90°C to separate double stranded DNA into constituent single strands. The second step involves lowering the temperature (40–60°C) to allow specifically designed forward and reverse primers to anneal at targeted regions (for selective amplification) through complementary base pairing. At this point the temperature is increased again to allow Taq polymerase to attach at each priming site and extend to synthesize a new DNA strand. This thermal cycling process allows for a chain reaction to occur in which the selected DNA template is exponentially amplified creating millions of copies of the targeted sequence (**Figure 4A**). In our study 400 ng of pUC19 plasmid DNA was initially exposed to increasing concentrations (2.5, 5, 10, 20, 30, 40, and 50 μM) of test complexes in the absence and presence of exogenous reductant at 37°C for 30 min and used as a substrate for the PCR reaction along with specific primer sets to generate three 120 bp sequences of varying G·C content (35, 50, and 63%). PCR inhibition (up to 50 μM) was not achieved by any tested agent (Figure S-5) in the absence of added reductant indicating physical blocking of the PCR process (**Figure 4B**) does not occur. With added reductant, however, the pattern emerges as described in **Figure 4C**. In the high A·T amplification set (35% G·C), PCR was inhibited by 5.0 μM of the mono-nuclear complexes (Cu-Phen, Cu-DPQ-Phen and Cu-DPPZ-Phen). In the case of the di-nuclear agent (Cu-Terph), complete inhibition of template amplification was observed at all exposure levels (**Figure 5A**). Within the 50 and 63% G·C templates (**Figures 5B,C** respectively), the PCR reaction was impeded at 5.0 μM for both Cu-DPQ-Phen and Cu-Terph complexes whereas template DNA, oxidatively damaged by 5.0 μM

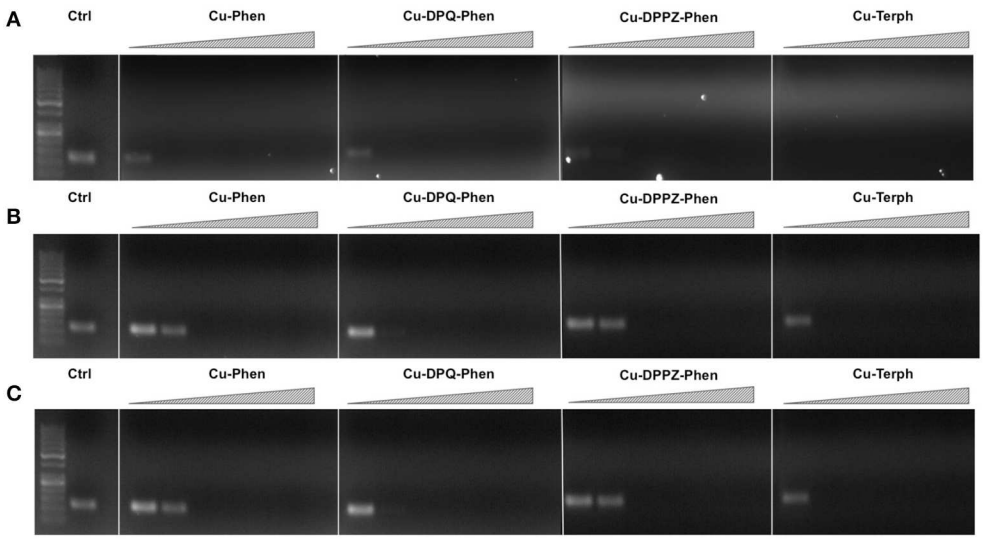

FIGURE 5 | 400 ng pUC19 DNA was initially exposed to 2.5, 5, 10, 20, 30, 40, and 50 μM of each test complex in the presence of 1 mM added reductant at 37°C for 30 min. 20 ng of damaged DNA template was removed and PCR reaction was carried out with each varying GC content primer set at optimum annealing temperatures and analyzed using gel electrophoresis. Panel **(A)** Lane 1, 50 bp DNA ladder, lane 2, 35 % GC control; lane 3–9, 35% GC + Cu-Phen; lane 10–16, 35% GC + Cu-DPQ-Phen; lane 17–23, 35% GC + Cu-DPPZ-Phen and lane 24–30, 35% GC + Cu-Terph. Panel **(B)** 50% GC, and Panel (C) 63% GC respectively. All duplex sequences generated were 120 base pairs.

of Cu-Phen and Cu-DPPZ-Phen, was still suitable for amplifying 120 base pair DNA sequences.

Conclusions

Mechanistic investigations into oxidative cleavage properties of the copper(II) complex series $[Cu(phen)_2]^{2+}$ (Cu-Phen) $[Cu(DPQ)(phen)]^{2+}$ (Cu-DPQ-Phen), $[Cu(DPPZ)(phen)]^{2+}$ (Cu-DPPZ-Phen), and $[\{Cu(phen)_2\}_2(\mu\text{-terph})](terph)$ (Cu-Terph) reveal chemical nuclease activity occurs primarily at the minor groove; titration of the major groove binder, methyl green, enhances DNA degradation—most likely by directing (priming) complex-DNA interactions to the minor groove—while the presence of the minor grove binder, netropsin, was found to significantly reduce oxidative damage on pUC19. It is also interesting to note that no correlation exists between chemical nuclease activity (**Figure 1**) and apparent DNA binding constant (**Table 1**). Instead, nuclearity has a more dramatic effect as evidenced by Cu-Terph mediated DNA damage. ROS-specific scavengers employed to identify the cleavage mechanism revealed metal-hydroxo or free hydroxyl radicals ($^{\bullet}OH$), and not $^1O_2$, as the predominant species generated; DMSO was found to limit DNA oxidation—most likely through the trapping of hydroxyl radicals $[(CH_3)_2SO + {}^{\bullet}OH \rightarrow CH_3SO_2H + CH_3]$ (Burkitt and Mason, 1991) —with sodium azide (NaN_3) having neglibile influence on all complexes except Cu-Terph. It is also likely that hydrogen peroxide (H_2O_2) is the key intermediary in $^{\bullet}OH$ production as the peroxide scavenger KI (Dunand et al., 2007; Steffens et al., 2012) was refractory to oxidative damage by tested agents. The generation of hydroxyl-based radicals was corroborated through identification of 8-oxo-2′-deoxyguanosine (8-oxo-dG) DNA lesions quantified under an ELISA protocol. 8-oxo-dG liberation followed the overall trend Cu-DPQ-Phen > Cu-Terph > Cu-Phen > Cu-DPPZ with higher lesion numbers detected under heavily sheared (damaged) plasmid conditions. Finally, oxidative damage by the complex series was found to inhibit the DNA replication process; polymerase chain reaction (PRC) reactions were impeded—particularly along A-T rich chains—through oxidative damage of template strands with the di-nuclear Cu-Terph, and mono-nuclear Cu-DPQ-Phen, being particularly potent oxidants to this process.

Acknowledgments

This work was supported by Irish Research Council (IRC) grants GOIPG/2013/826 and GOIPG/2014/1182. Sponsorship from COST Action CM1201: "Biomimetic Radical Chemistry" is gratefully acknowledged.

Supplementary Material

The Supplementary Material for this article can be found online at: http://journal.frontiersin.org/article/10.3389/fchem.2015.00028/abstract

References

Basu, A. K., Loechler, E. L., Leadon, S. A., and Essigmann, J. M. (1989). Genetic effects of thymine glycol: site-specific mutagenesis and molecular modeling studies. *Proc. Natl. Acad. Sci. U.S.A.* 86, 7677–7681. doi: 10.1073/pnas.86.20.7677

Breen, A. P., and Murphy, J. A. (1995). Reactions of oxyl radicals with DNA. *Free Radic. Biol. Med.* 18, 1033–1077. doi: 10.1016/0891-5849(94)00209-3

Burger, R. M. (1998). Cleavage of nucleic acids by Bleomycin. *Chem. Rev.* 98, 1153–1169. doi: 10.1021/cr960438a

Burger, R. M., Peisach, J., and Horwitz, S. B. (1981). Activated bleomycin. A transient complex of drug, iron, and oxygen that degrades DNA. *J. Biol. Chem.* 256, 11636–11644.

Burkitt, M. J., and Mason, R. P. (1991). Direct evidence for *in vivo* hydroxyl-radical generation in experimental iron overload: an ESR spin-trapping investigation. *Proc. Natl. Acad. Sci. U.S.A.* 88, 8440–8444. doi: 10.1073/pnas.88.19.8440

Chatgilialoglu, C., Ferreri, C., and Terzidis, M. A. (2011). Purine 5',8-cyclonucleoside lesions: chemistry and biology. *Chem. Soc. Rev.* 40, 1368–1382. doi: 10.1039/c0cs00061b

Chatgilialoglu, C., and O'Neill, P. (2001). Free radicals associated with DNA damage. *Exp. Gerontol.* 36, 1459–1471. doi: 10.1016/S0531-5565(01)00132-2

Chen, J., Ghorai, M. K., Kenney, G., and Stubbe, J. (2008). Mechanistic studies on bleomycin-mediated DNA damage: multiple binding modes can result in double-stranded DNA cleavage. *Nucleic Acids Res.* 36, 3781–3790. doi: 10.1093/nar/gkn302

Cooke, M. S., and Evans, M. D. (2007). 8-Oxo-deoxyguanosine: reduce, reuse, recycle? *Proc. Natl. Acad. Sci. U.S.A.* 104, 13535–13536. doi: 10.1073/pnas.0706878104

Dunand, C., Crèvecoeur, M., and Penel, C. (2007). Distribution of superoxide and hydrogen peroxide in Arabidopsis root and their influence on root development: possible interaction with peroxidases. *New Phytol.* 174, 332–341. doi: 10.1111/j.1469-8137.2007.01995.x

Franco, R., Panayiotidis, M. I., and Cidlowski, J. A. (2007). Glutathione depletion Is necessary for apoptosis in lymphoid cells independent of reactive oxygen species formation. *J. Biol. Chem.* 282, 30452–30465. doi: 10.1074/jbc.M703091200

Gajewski, E., Aruoma, O. I., Dizdaroglu, M., and Halliwell, B. (1991). Bleomycin-dependent damage to the bases in DNA is a minor side reaction. *Biochemistry* 30, 2444–2448. doi: 10.1021/bi00223a021

Johnson, G. R. A., and Nazhat, N. B. (1987). Kinetics and mechanism of the reaction of the bis(1,10-phenanthroline)copper(I) ion with hydrogen peroxide in aqueous solution. *J. Am. Chem. Soc.* 109, 1990–1994. doi: 10.1021/ja00241a015

Kellett, A., Howe, O., O'Connor, M., McCann, M., Creaven, B. S., McClean, S., et al. (2012). Radical-induced DNA damage by cytotoxic square-planar copper(II) complexes incorporating o-phthalate and 1,10-phenanthroline or 2,2'-dipyridyl. *Free Radic. Biol. Med.* 53, 564–576. doi: 10.1016/j.freeradbiomed.2012.05.034

Kellett, A., O'Connor, M., McCann, M., McNamara, M., Lynch, P., Rosair, G., et al. (2011). Bis-phenanthroline copper(II) phthalate complexes are potent *in vitro* antitumour agents with "self-activating" metallo-nuclease and DNA binding properties. *Dalton Trans.* 40, 1024–1027. doi: 10.1039/c0dt01607a

Klaunig, J. E., Kamendulis, L. M., and Hocevar, B. A. (2010). Oxidative stress and oxidative damage in carcinogenesis. *Toxicol. Pathol.* 38, 96–109. doi: 10.1177/0192623309356453

Li, L., Karlin, K. D., and Rokita, S. E. (2005). Changing selectivity of DNA oxidation from deoxyribose to guanine by ligand design and a new binuclear copper complex. *J. Am. Chem. Soc.* 127, 520–521. doi: 10.1021/ja044209e

Marshall, L. E., Graham, D. R., Reich, K. A., and Sigman, D. S. (1981). Cleavage of deoxyribonucleic acid by the 1,10-phenanthroline-cuprous complex. Hydrogen peroxide requirement and primary and secondary structure specificity. *Biochemistry* 20, 244–250. doi: 10.1021/bi00505a003

Mazzer, P. A., Maurmann, L., and Bose, R. N. (2007). Mechanisms of DNA damage and insight into mutations by chromium(VI) in the presence of glutathione. *J. Inorg. Biochem*. 101, 44–55. doi: 10.1016/j.jinorgbio.2006.08.008

McCann, M., McGinley, J., Ni, K., O'Connor, M., Kavanagh, K., McKee, V., et al. (2013). A new phenanthroline-oxazine ligand: synthesis, coordination chemistry and atypical DNA binding interaction. *Chem. Comm.* 49, 2341–2343. doi: 10.1039/c3cc38710k

Merkel, P. B., Nilsson, R., and Kearns, D. R. (1972). Deuterium effects on singlet oxygen lifetimes in solutions. New test of singlet oxygen reactions. *J. Am. Chem. Soc.* 94, 1030–1031. doi: 10.1021/ja00758a072

Molphy, Z., Prisecaru, A., Slator, C., Barron, N., McCann, M., Colleran, J., et al. (2014). Copper phenanthrene oxidative chemical nucleases. *Inorg. Chem.* 53, 5392–5404. doi: 10.1021/ic500914j

Natrajan, A., Hecht, S. M., and van der Marel, G. A. (1990). A study of oxygen- versus hydrogen peroxide-supported activation of iron. cntdot. bleomycin. *J. Am. Chem. Soc.* 112, 3997–4002. doi: 10.1021/ja00166a042

Pratviel, G., and Bernadou, J. (1989). Evidence for high-valent iron-oxo species active in the DNA breaks mediated by iron-bleomycin. *Biochem. Pharmacol.* 38, 133–140. doi: 10.1016/0006-2952(89)90159-7

Prisecaru, A., Devereux, M., Barron, N., McCann, M., Colleran, J., Casey, A., et al. (2012). Potent oxidative DNA cleavage by the di-copper cytotoxin: $[Cu_2(\mu\text{-terephthalate})(1,10\text{-phen})_4]^{2+}$. *Chem. Commun.* 48, 6906–6908. doi: 10.1039/c2cc31023f

Prisecaru, A., McKee, V., Howe, O., Rochford, G., McCann, M., Colleran, J., et al. (2013). Regulating Bioactivity of Cu2+ Bis-1,10-phenanthroline Artificial Metallonucleases with Sterically Functionalized Pendant Carboxylates. *J. Med. Chem.* 56, 8599–8615. doi: 10.1021/jm401465m

Rodriguez, L. O., and Hecht, S. M. (1982). Iron(II)-bleomycin. Biochemical and spectral properties in the presence of radical scavengers. *Biochem. Biophys. Res. Commun.* 164, 1470–1476. doi: 10.1016/0006-291X(82)91416-4

Sanchez-Cano, C., Huxley, M., Ducani, C., Hamad, A. E., Browning, M. J., Navarro-Ranninger, C., et al. (2010). Conjugation of testosterone modifies the interaction of mono-functional cationic platinum(II) complexes with DNA, causing significant alterations to the DNA helix. *Dalton Trans.* 39, 11365–11374. doi: 10.1039/c0dt00839g

Sigman, D. S., Graham, D. R., Aurora, V. D., and Stern, A. M. (1979). Oxygen-dependent cleavage of DNA by the 1,10-phenathroline cuporous complex. Inhibition of Escherichia coli DNA polymerase I. *J. Biol. Chem.* 254, 12269–12272.

Steffens, B., Kovalev, A., Gorb, S. N., and Sauter, M. (2012). Emerging roots alter epidermal cell fate through mechanical and reactive oxygen species signaling. *Plant Cell* 24, 3296–3306. doi: 10.1105/tpc.112.101790

Stubbe, J. A., and Kozarich, J. W. (1987). Mechanisms of bleomycin-induced DNA degradation. *Chem. Rev.* 87, 1107–1136. doi: 10.1021/cr00081a011

Tabassum, S., Al-Asbahy, W. M., Afzal, M., Arjmand, F., and Bagchi, V. (2012). Molecular drug design, synthesis and structure elucidation of a new specific target peptide based metallo drug for cancer chemotherapy as topoisomerase I inhibitor. *Dalton Trans.* 41, 4955–4964. doi: 10.1039/c2dt 12044e

van der Steen, S., de Hoog, P., van der Schilden, K., Gamez, P., Pitié, M., Kiss, R., et al. (2010). Novel heteronuclear ruthenium–copper coordination compounds as efficient DNA-cleaving agents. *Chem. Commun.* 46, 3568. doi: 10.1039/c000077a

Xia, Q., Chou, M. W., Yin, J. J., Howard, P. C., Yu, H., and Fu, P. P. (2006). Photoirradiation of representative polycyclic aromatic hydrocarbons and twelve isomeric methylbenz[α]anthracene with UVA light: formation of lipid peroxidation. *Toxicol. Ind. Health* 22, 147–156. doi: 10.1191/0748233706 th259oa

Xu, M., Lai, Y., Jiang, Z., Terzidis, M. A., Masi, A., Chatgilialoglu, C., et al. (2014). A 5', 8-cyclo-2'-deoxypurine lesion induces trinucleotide repeat deletion via a unique lesion bypass by DNA polymerase β. *Nucleic Acids Res.* 42, 13749–13763. doi: 10.1093/nar/gku1239

Zhou, W., Wang, X., Hu, M., Zhu, C., and Guo, Z. (2014). A mitochondrion-targeting copper complex exhibits potent cytotoxicity against cisplatin-resistant tumor cells through multiple mechanisms of action. *Chem. Sci.* 5, 2761–2770. doi: 10.1039/c4sc00384e

Conflict of Interest Statement: The authors declare that the research was conducted in the absence of any commercial or financial relationships that could be construed as a potential conflict of interest.

Copyright © 2015 Molphy, Slator, Chatgilialoglu and Kellett. This is an open-access article distributed under the terms of the Creative Commons Attribution License (CC BY). The use, distribution or reproduction in other forums is permitted, provided the original author(s) or licensor are credited and that the original publication in this journal is cited, in accordance with accepted academic practice. No use, distribution or reproduction is permitted which does not comply with these terms.

frontiers in Chemistry

ORIGINAL RESEARCH
published: 16 April 2015
doi: 10.3389/fchem.2015.00025

Flexibility of short ds-DNA intercalated by a dipyridophenazine ligand

Fuchao Jia[1,2], *Stéphane Despax*[1], *Jean-Pierre Münch*[1] *and Pascal Hébraud*[1]*

[1] *Institut de Physique et Chimie des Matériaux de Strasbourg/Centre National de la Recherche Scientifique, University of Strasbourg, Strasbourg, France,* [2] *Department of Physics, School of Science, Shangdong University, Zibo, China*

We use Förster Resonant Energy Transfer (FRET) in order to measure the increase of flexibility of short ds-DNA induced by the intercalation of dipyridophenazine (dppz) ligand in between DNA base pairs. By using a DNA double strand fluorescently labeled at its extremities, it is shown that the end-to-end length increase of DNA due to the intercalation of one dppz ligand is smaller than the DNA base pair interdistance. This may be explained either by a local bending of the DNA or by an increase of its flexibility. The persistence length of the formed DNA/ligand is evaluated. The described structure may have implications in the photophysical damages induced by the complexation of DNA by organometallic molecules.

Keywords: DNA intercalation, DNA flexibility, FRET, ruthenium compounds, dppz intercalator

OPEN ACCESS

Edited by:
Elise Dumont,
Ecole Normale Supérieure de Lyon, France

Reviewed by:
Xavier Assfeld,
Université de Lorraine, France
José Pedro Cerón-Carrasco,
Universidad de Murcia, Spain

***Correspondence:**
Pascal Hébraud,
Institut de Physique et Chimie des Matériaux de Strasbourg/Centre National de la Recherche Scientifique, University of Strasbourg, 23 rue du Loess, 67034 Strasbourg, France
pascal.hebraud@ipcms.unistra.fr

Specialty section:
This article was submitted to Chemical Biology, a section of the journal Frontiers in Chemistry

Received: *22 January 2015*
Paper pending published: *02 March 2015*
Accepted: *20 March 2015*
Published: *16 April 2015*

Citation:
Jia F, Despax S, Münch J-P and Hébraud P (2015) Flexibility of short ds-DNA intercalated by a dipyridophenazine ligand. Front. Chem. 3:25. doi: 10.3389/fchem.2015.00025

1. Introduction

Since the first observation of the molecular "light switch" effect of $Ru(bpy)_2dppz^{2+}$for DNA their interaction with DNA has been intensively studied (Friedman et al., 1990; Brennaman et al., 2002, 2004; Hu et al., 2009; Lim et al., 2009; Klajner et al., 2010; Sun et al., 2010; Song et al., 2012; Vidimar et al., 2012). $Ru(bpy)_2dppz^{2+}$is a highly sensitive spectroscopic reporter of double-helical DNA (Very et al., 2012). In aqueous solution, luminescence is detectable when $Ru(bpy)_2dppz^{2+}$intercalates into the nucleic acid structure (Batista and Martin, 2005). The emission properties (both in terms of intensity and spectral band) furthermore depend on the different helical forms of the polynucleotides, allowing the use of $Ru(bpy)_2dppz^{2+}$as a sensitive, non-radioactive, luminescent DNA probe in both heterogeneous and homogeneous assays. $Ru(phen)_2dppz^{2+}$ possesses similar properties. Both complexes $Ru(bpy)_2dppz^{2+}$and $Ru(phen)_2dppz^{2+}$ have served as "molecular light switch" for DNA, luminescing intensely in the presence of DNA but with no photoluminescence in aqueous solution and can be seen as unique reporters of nucleic acid structures (Song et al., 2012). The luminescent enhancement observed upon binding is attributed to the sensitivity of the excited state to quenching by water; the metal complex, upon intercalation into the DNA helix, is protected from the aqueous solvent, thereby preserving the luminescence (Friedman et al., 1990). Correlations between the extent of protection (depending upon the DNA conformation) and the luminescence parameters have been proven. Indeed, the strongest luminescent enhancement is observed for intercalation into DNA conformations which afford the greatest amount of overlap with access from the major groove, such as in triple helices. Differences are observed in the luminescent parameters between the two complexes which also correlate with the level of water protection. In the presence of nucleic acids, these two complexes exhibit biexponential decays in emission (Jenkins et al., 1992). Quenching studies are consistent with two intercalative binding modes for the dppz ligand in the major groove: one in which the metal-phenazine axis lies

along the DNA dyad axis and another where the metal-phenazine axis lies almost perpendicular to the DNA dyad axis.

Upon binding to mismatched DNA base pair, $Ru(bpy)_2dppz^{2+}$ exhibits significant luminescent enhancements compared to well-matched DNA (Lim et al., 2009). In the presence of a single base mismatch, large luminescent enhancements are evident when ruthenium binds to an oligonucleotide containing an abasic site. Titrations with hairpin oligonucleotides containing a variable mismatch site have revealed correlation between the level of luminescent enhancement and the thermodynamic destabilization associated with the mismatch (Lim et al., 2009). This correlation is reminiscent of that found earlier for a bulky rhodium complex that binds mismatched DNA sites through metalloinsertion, where the complex binds the DNA from the minor groove side, ejecting the mismatched bases into the major groove (Lim et al., 2009). The smaller size of the dppz ligand also allows the ruthenium complex to bind through classical intercalation between two consecutive well-matched base pairs. Intercalated complexes are also located in the minor groove, stabilized by extensive ancillary interactions (Erkkila et al., 1999). This discrepancy notwithstanding, the crystal structure attests the remarkable structural flexibility of DNA upon high-density ligand binding, and illustrates the nuanced binding geometries sampled by a non-covalently bound small molecule. It highlights the dominance of metalloinsertion as the preferred binding mode to destabilized regions of DNA.

2. Flexibility

Although it is well-known that the length of DNA increases approximately linearly with the number of intercalated $Ru(bpy)_2dppz^{2+}$ molecules into the DNA double strand (Vladescu et al., 2007), the induced dynamical changes of the DNA chain have not been studied. Here, we quantify the variation of double strand flexibility induced by the intercalation of $Ru(bpy)_2dppz^{2+}$ into a short dsDNA (15 base pair long). We use Fluorescence Resonance Energy Transfer (FRET) in order to monitor the average distance between the extremities of a 15 bp dsDNA modified with two fluorophores at its extremities: both ends of dsDNA are modified by two types of fluorophores: Alexa488 and Alexa568. When Alexa488 is excited, it can decay by transferring non-radiative energy to Alexa568, which then de-excites by emitting photons of lower energy than those emitted by Alexa488. The efficiency of this energy transfer can be quantified from the measurement of the intensities emitted at low and high energy. It depends *a priori* on the coupling efficiency (and therefore the distance) between the two fluorophores. We will show that the increase of the average distance between the DNA extremities is incompatible with the assumption of a rigid and straight DNA/$Ru(bpy)_2dppz^{2+}$ complex. Nevertheless, the observation is made difficult due to the strong quenching of the fluorophores induced by the intercalation of the $Ru(bpy)_2dppz^{2+}$. Thus, in this article, from the analysis of the evolution of the lifetime of the donor on one hand, and that of the acceptor on the other hand, we deduce the evolution of the efficiency of the energy transfer in the concentration of ligand. We analyze the evolution of the emitted intensity of the donor and the lifetime of its excited state, and those of the acceptor, taking into account the photophysical properties of the ruthenium complex. We then obtain the evolution of the dsDNA average length as a function of the $Ru(bpy)_2dppz^{2+}$ complexation.

3. Materials and Methods

15 base pair dsDNA are used to perform the experiment. The number of DNA base pairs is limited by the range over which the FRET can take place that is approximately 10 nm. Complementary strands were purchased from IBA (Germany company) with sequences GGA GAC CAG AGG CCT and CCT CTG GTC TCC GGA. The length of 15 base pairs is 5.1 nm. The extremity of the short double-stranded DNA (dsDNA) is labeled with different kinds of fluorophores. The first sequence is modified in three different ways. (1) 5′-end is labeled with Alexa488, (2) 3′-end is labeled with Alexa568, (3) 5′-end and 3′-end are labeled with Alexa488 and Alexa568, respectively (**Figure 1**). The Alexa fluorophore is chemically linked with DNA base. Titrations are performed by the addition of $Ru(bpy)_2dppz^{2+}$ to a solution of DNA at constant DNA concentration, equal to 1μM.

A pulsed laser of 495 nm wavelength with a repetition rate of 1 MHz is used to excite the fluorophore. The photon detector temporal resolution is 0.1 ns. The wavelength collected is at 517 nm and 600 nm with 2 nm spectral slit. The acquisition time is chosen so that the number of photons collected in the first channel is equal to 10^4. Under these experimental conditions, a

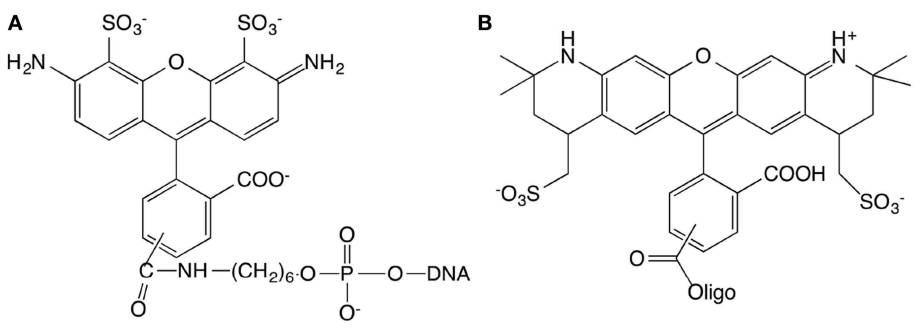

FIGURE 1 | Chemical structures of the Alexa488 (A) and Alexa568 (B) modified oligonucleotides.

measurement lasts between 10 and 120 min. All measurements are performed at constant room temperature (20°C).

The notations used in the analysis of the results are given in **Table 1**.

4. Analysis of the Emission at 517 nm

We now turn to the analysis of the intensity emitted at 517 nm. The most important factor we care in FRET process is the transfer efficiency, that relies on two assumptions. First, it is assumed that the presence of the acceptor neither changes nor adds any relaxation process except for the FRET process. Then, the number donor molecules excited by the laser is assumed to remain constant when the acceptor is present. The transfer efficiency is defined as the probability that an excited donor fluorophore comes back to its ground state by FRET process. This can be expressed as:

$$E = \kappa_T \tau^{DA} \tag{1}$$

where κ_T is the FRET transfer rate. κ_T is directly related to the distance r between the two fluorophores according to: $\kappa_T(r) = \frac{1}{\tau^D}\left(\frac{R_0}{r}\right)^6$, where R_0 is the Förster distance and τ^D the relaxation time of the donor fluorophore in the absence of the acceptor. τ^{DA} is the overall characteristic decay time of the donor molecule in the presence of the acceptor: it is directly measured as the decay time of the fluorophore emission at its maximum wavelength. According to the first assumption, the presence of the acceptor does not change any relaxation process except for the FRET process. We thus have:

TABLE 1 | List of notations used in the analysis of the fluorophore emission.

τ^D	relaxation time of the donor in the absence of the acceptor
τ^{DA}	relaxation time of the donor in the presence of the acceptor
τ^A	relaxation time of the acceptor
τ^A_{600}	decay time of the emission of the acceptor at 600 nm
κ_T, τ^F	Förster Resonant Energy Transfer rate, $\tau^F = \kappa_T^{-1}$
$D^*(t)$	number of excited donor molecules at time t
D^*_{02}	initial number of excited donor molecules in the presence of the acceptor
D^*_{01}	initial number of excited donor molecules in the absence of the acceptor
$A^*(t)$	number of excited acceptor molecules at time t
A^*_{02}	initial number of excited acceptor molecules in the presence of the donor
N^D_{517}	number of photons emitted at 517 nm by the donor in the absence of the acceptor
N^{DA}_{517}	number of photons emitted at 517 nm by the donor in the presence of the acceptor
N^D_{600}	number of photons emitted at 600 nm by the donor in the absence of the acceptor
N^{DA}_{600}	number of photons emitted at 600 nm by the donor in the presence of the acceptor
N^{AD}_{600}	number of photons emitted at 600 nm by the acceptor in the presence of the donor
N^{Ru}_{600}	number of photons emitted at 600 nm by the ruthenium compound

$$\frac{1}{\tau^{DA}} = \frac{1}{\tau^D} + \kappa_T \tag{2}$$

where τ^D is the characteristic decay time in the absence of acceptor, that can also be measured directly. Then the transfer efficiency may be rewritten as:

$$E = 1 - \frac{\tau^{DA}}{\tau^D} = \frac{1}{1 + \left(\frac{R_0}{r}\right)^6} \tag{3}$$

D^* being the number concentration of excited donor molecules, we have:

$$\frac{dD^*}{dt} = -\frac{D^*}{\tau^{DA}} \tag{4}$$

leading to:

$$D^*(t) = D^*_{02} e^{-\frac{t}{1/\tau^D + \kappa_T}} = D^*_{02} e^{-t/\tau^{DA}} \tag{5}$$

where D^* is the number of excited donors at time t, D^*_{02} is the initial population of excited donors in the presence of acceptor, τ^{DA} and τ^D are the lifetimes in the presence and absence of acceptor, respectively. Nevertheless, D^* cannot be measured directly: the emitted intensity is measured. But the donor emits photons both at 517 nm and at the maximum emission wavelength of this acceptor, at 600 nm (this is the cross-talk phenomenon).The number of photons emitted by the donor in the presence, N^{DA}_{517}, and in the absence,N^D_{517}, of the acceptor, at 517 can be expressed as the probability that their relaxation occurs through the emission of a photon at the corresponding wavelength:

$$N^D_{517} = D^*_{01} \frac{\tau^D}{\tau^D_{517}} \tag{6}$$

$$N^{DA}_{517} = D^*_{02} \frac{\tau^{DA}}{\tau^D_{517}} \tag{7}$$

where τ^D and τ^{DA} are the overall decay times in the absence and presence of the acceptor, τ^D_{517} and τ^D_{600} the characteristic decay times of photon emission at 517 nm and 600 nm by the donor. D^*_{01} and D^*_{02} are the initial number of excited donors by the laser in the absence and presence of acceptor. We thus have:

$$\frac{N^{DA}_{517}}{N^D_{517}} = \frac{D^*_{02}}{D^*_{01}} \frac{\tau^{DA}}{\tau^D} = \frac{\tau^{DA}}{\tau^D} \tag{8}$$

assuming that the number of donor molecules excited by the laser does not change when the acceptor fluorophore is present. This leads to a new expression of the transfer efficiency:

$$E = 1 - \frac{\tau^{DA}}{\tau^D} = 1 - \frac{N^{DA}_{517}}{N^D_{517}} \tag{9}$$

We first consider the interaction between $Ru(bpy)_2dppz^{2+}$and the fluorophores. The overall intensities and relaxation times of single labeled DNA molecules is observed to decrease slightly in the presence of $Ru(bpy)_2dppz^{2+}$, due to quenching. The inverse

of the intensity emitted by the donor fluorophore as well as its life time are represented in **Figure 2**. One observes that:

$$\frac{I_0}{I(C_{Ru})} = \frac{\tau_0}{\tau(C_{Ru})} = 1 + K_D C_{Ru} \tag{10}$$

where the subscript indicates that the measurement is performed at null $Ru(bpy)_2dppz^{2+}$concentration. This relation implies that $Ru(bpy)_2dppz^{2+}$dynamically quenches the emission of the donor fluorophore and defines the dynamical quenching constant . One finds $K_D = 0.3\ \mu\text{M}^{-1}$.

The transfer rate κ_T and the transfer efficiency E are separately computed from Equations 2, 9. The evolutions of $\tau^F = \frac{1}{\kappa_T}$ and E as a function of the ruthenium complex concentration are shown in **Figure 3**. On the whole, τ^F increases with the increase of the complex whereas the transfer efficiency decreases with increasing the $Ru(bpy)_2dppz^{2+}$concentration. In the range of studied concentrations, the evolution of τ^F and E with the $Ru(bpy)_2dppz^{2+}$concentration may be well-described by a linear behavior.

4.1. Dynamical Measurements of the Emission at 600 nm

The acceptor can be excited following two different mechanisms, either by direct excitation by the laser or by energy transfer from the donor fluorophore. τ^A is the overall relaxation time of the acceptor. The existence of FRET does not change the relaxation path of an excited acceptor, and τ^A is identical to the relaxation time of acceptor excited by the laser in the absence of donor. From the perspective of the acceptor, the FRET process can be determined by the following equations:

$$\frac{dA^*}{dt} = \kappa_T D^*(t) - \frac{1}{\tau^A} A^*(t) \tag{11}$$

where the first term represents the excitation through FRET and the second one the desexcitation of the acceptor. With the initial condition $A^*(0) = A^*_{02}$, the solution is:

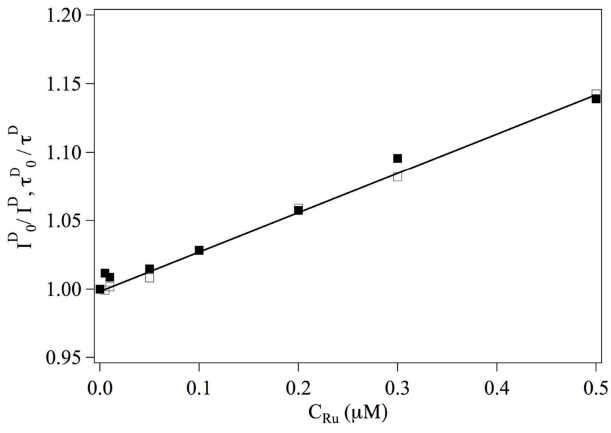

FIGURE 2 | Evolution of $\frac{I_0}{I(C_{Ru})}$ ■ and $\frac{\tau_0}{\tau(C_{Ru})}$ □ as a function of the ruthenium concentration. Continuous line is a adjustment fit of the data from which one gets $K_D = 0.3\ \mu\text{M}.^{-1}$.

$$A^*(t) = D^*_{02}\kappa_T \frac{1}{\tau^{A^{-1}} - \tau^{DA^{-1}}} e^{-t/\tau^{DA}} + \left(A^*_{02} - D^*_{02}\kappa_T \frac{1}{\tau^{A^{-1}} - \tau^{DA^{-1}}}\right) e^{-t/\tau^A} \tag{12}$$

where A^*_{02} is the number of acceptor molecules excited by the laser at time 0. This result states that the $A^*(t)$ should exhibit a two-time relaxation process, the first one equals to the relaxation time of the donor population in the presence of the acceptor, τ^{DA}, and the second one equals to the relaxation time of the acceptor, τ^A. Moreover, if $\frac{1}{\tau^{A^{-1}} - \tau^{DA^{-1}}} < 0$, the amplitude of the acceptor decay over τ^{DA} is negative.

The number of photons emitted by the acceptor, N^{DA}_{600} can be written as:

$$N^{AD}_{600} = \int_0^\infty \frac{1}{\tau^A_{600}} \left(D^*_{02}\kappa_T \frac{1}{\tau^{A^{-1}} - \tau^{DA^{-1}}} e^{-t/\tau^{DA}} + \frac{1}{\tau^A_{600}} (A^*_{02} - D^*_{02}\kappa_T) \frac{1}{\tau^{A^{-1}} - \tau^{DA^{-1}}} e^{-t/\tau^A} \right) dt \tag{13}$$

$$= A^*_{02} \frac{\tau^A}{\tau^A_{600}} + D^*_{02}\kappa_T \tau^{DA} \frac{\tau^A}{\tau^A_{600}} \tag{14}$$

Where τ^A_{600} is the characteristic time of photon emission at 600 nm by the acceptor, and $\tau^A = \tau^{AD}$, since the presence of the donor does not change the relaxation of the acceptor. Finally, using $E = \kappa_T \tau^{DA}$, we have:

$$N^{AD}_{600} = (A^*_{02} + D^*_{02}E) \frac{\tau^A}{\tau^A_{600}} \tag{15}$$

where A^*_{02} is the number of excited acceptor from the lasers excitation, and $D^*_{02}E$ is the number of acceptor molecules excited by the FRET process.

We now consider the emission at 600 nm of double labeled dsDNA bound with ruthenium complex, N_{600}. There are three contributions to this emission. (i) the contribution of the donor fluorophore, N^{DA}_{600}, the intensity emitted at 600 nm by the donor after a pulse, $I^{DA}_{600}(t)$,(ii) the contribution of the acceptor, N^{AD}_{600}, the intensity emitted at 600 nm by the acceptor after a pulse, $I^{AD}_{600}(t)$, and (iii) the emission of $Ru(bpy)_2dppz^{2+}$that is luminescent when intercalated between DNA base pairs, N^{Ru}_{600}

So the total number of photons emitted at 600 nm can be expressed as $N_{600} = N^{Ru}_{600} + N^{DA}_{600} + N^{AD}_{600}$, whose we are going to perform an analysis term by term.

The intensity of emission at 600 nm of bound $Ru(bpy)_2dppz^{2+}$has been measured when the ruthenium complex bound with non-labeled DNA. The contribution of the ruthenium complex is found to be smaller than 0.5% of the total observed intensity, so that we will neglect N^{Ru}_{600} in the subsequent analysis.

The emission of the donor fluorophore at 600 nm in the presence of the acceptor cannot be measured independently and will be obtained indirectly. The number of photons emitted by the donor at the two studied wavelengths with and without the acceptor are given by the probabilities that the relaxation

process occurs by the emission of a photon at the corresponding wavelength. We have (Equation 8):

$$\frac{N_{517}^{DA}}{N_{517}^{D}} = \frac{D_{02}^{*}}{D_{01}^{*}} \frac{\tau^{DA}}{\tau^{D}} \tag{16}$$

and similarly at 600 nm:

$$\frac{N_{600}^{DA}}{N_{600}^{D}} = \frac{D_{02}^{*}}{D_{01}^{*}} \frac{\tau^{DA}}{\tau^{D}} \tag{17}$$

We finally obtain the number of photons emitted by the donor in the presence of the acceptor, at 600 nm:

$$N_{600}^{DA} = N_{517}^{DA} \frac{N_{600}^{D}}{N_{517}^{D}} \tag{18}$$

The ratio $\frac{N_{600}^{D}}{N_{517}^{D}}$ does not depend on the ruthenium complex concentration, and is measured at the null ruthenium concentration. It is equal to 2.74%. N_{517}^{DA} is then measured directly from which N_{600}^{DA} can be calculated as a function of the ruthenium concentration. We can then obtain the emission of the acceptor in the presence of the donor fluorophore, at 600 nm: $N_{600}^{AD} = N_{600} - N_{600}^{DA} = \left(A_{02}^{*} + D_{02}^{*}E\right) \frac{\tau^{A}}{\tau_{600}^{A}}$. The efficiency is then computed:

$$E = \left(\frac{N_{600}^{AD}}{\tau^{A}} - \frac{A_{02}^{*}}{\tau_{600}^{A}} \right) \frac{\tau_{600}^{A}}{D_{02}^{*}} \tag{19}$$

We now determine the three ratios involved:

- $\frac{N_{600}^{AD}}{\tau^{A}}$: τ^{A} is the fluorescence lifetime of single labeled DNA with alexa568, and N_{600}^{AD} has been obtained in the previous paragraph.
- $\frac{A_{02}^{*}}{\tau_{600}^{A}}$ is obtained from the amplitude of the 2 relaxation modes of the intensity emitted at 600 nm by two labeled DNA. This intensity is $I_{600}(t)$:

$$I_{600}(t) = I_{600}^{AD}(t) + I_{600}^{DA}(t) \tag{20}$$

with

$$I_{600}^{DA}(t) = \frac{D_{02}^{*}}{\tau_{600}^{D}} e^{-t/\tau^{DA}} = \frac{N_{600}^{DA}}{\tau^{DA}} e^{-t/\tau^{DA}} \tag{21}$$

and

$$I_{600}^{AD}(t) = \alpha_1 e^{-t/\tau^{DA}} + \alpha_2 e^{-t/\tau^{A}} \tag{22}$$

which defines α_1 and α_2. They are obtained from the measurement of $I_{600}(t) = \left(\alpha_1 + \frac{N_{600}^{DA}}{\tau^{DA}}\right) e^{-t/\tau^{DA}} + \alpha_2 e^{-t/\tau^{A}}$. We thus obtain $\frac{A_{02}^{*}}{\tau_{600}^{A}} = \alpha_1 + \alpha_2$.

- $\frac{\tau_{600}^{A}}{D_{02}^{*}}$ does not depend on the ruthenium concentration. Its value can not be measured from measurements of $I_{600}(t)$ as it always appears under the form $\frac{D_{02}^{*}}{\tau_{600}^{A}\kappa_T}$. The evolution of the efficiency E as a function of the ruthenium concentration is thus obtained up to a constant multiplicative factor. In order to compare the evolution of $E(C_{Ru})$ with the efficiency obtained from measurement at 517 nm, we determine this multiplication factor at $C_{Ru} = 0$. The evolution of the FRET efficiency and of the transfer rate κ_T are plotted in **Figure 3●**.

5. Discussion

At the concentration under study, the fraction of DNA strand complexed by more than one ruthenium molecule may be neglected. We thus have a mixture of uncomplexed DNA and DNA strands complexed with one ruthenium molecule. Moreover this molecule may be intercalated at one or other of the 14 positions along the DNA double strand The intensities and lifetimes measured are thus average values of the intensities and lifetimes of these different complexes. The measured lifetime may be written as:

$$\bar{\tau} = (1 - \xi)\tau_0 + \frac{\xi}{14} \sum_{n=1}^{14} \tau_{1,n} \tag{23}$$

where ξ is the fraction of DNA strands complexed with one $Ru(bpy)_2dppz^{2+}$, τ_0 is the decay time of non-complexed DNA, $\tau_{1,n}$ is the decay time of DNA strand intercalated with $Ru(bpy)_2dppz^{2+}$ at the nth position. We moreover assume that all the intercalation positions are equiprobable. The decay time may be expressed as the consequence of the existence of two processes:

$$\frac{1}{\tau_0(C_{Ru})} = \frac{1}{\tau_0^{D}(C_{Ru})} + \frac{1}{\tau_0^{F}} \tag{24}$$

where τ_0^{D} is the donor decay time in the absence of the acceptor at concentration C_{Ru}, for a non-complexed dsDNA, and $\tau_0^{F} = \kappa_T^{-1}$

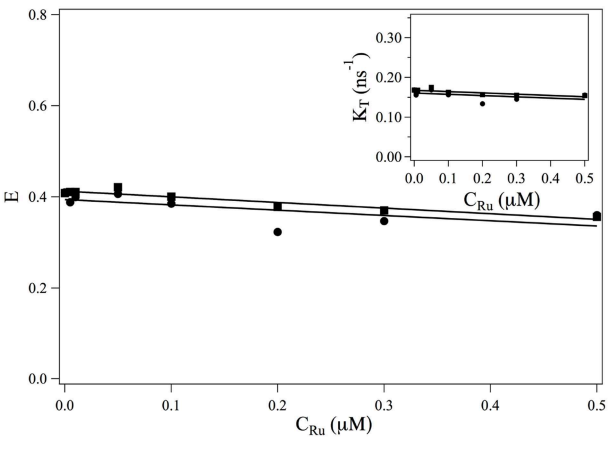

FIGURE 3 | Evolution of the FRET efficiency *E* and of $\kappa_T = 1/\tau_F$ (*insert*) as a function of the ruthenium concentration. ■: values obtained from the measurements at 517 nm (Equations 9, 2). ●: values obtained from the measurements at 600 nm (Equation 19) and $\kappa_T = E/\tau^{DA}$.

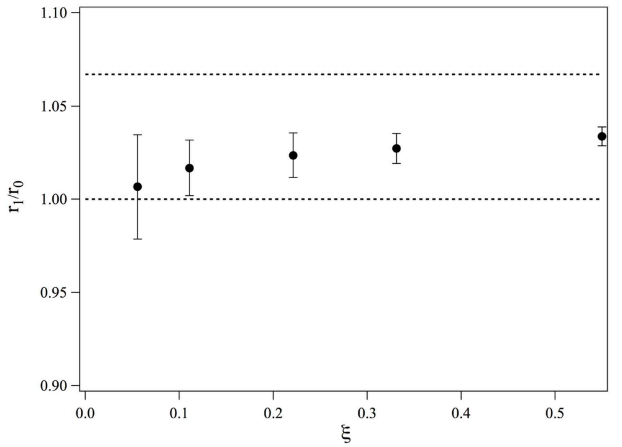

FIGURE 4 | Evolution of the average end-to-end distance of a 15-bp dsDNA bound to one molecule of *Ru(bpy)$_2$dppz^{2+}*, measured for different ratios of complexation.

is the inverse of the FRET rate in the absence of complexation. τ_0^F does not depend on the $Ru(bpy)_2dppz^{2+}$concentration and is measured at $C_{Ru} = 0$.

$$\frac{1}{\tau_{1,n}} = \frac{1}{\tau_{1,n}^D(C_{Ru})} + \frac{1}{\tau_{1,n}^F(C_{Ru})} \tag{25}$$

with similar notations. We have used the fact the $\tau_{1,n}^D(C_{Ru})$ does not depend on n, as the observed quenching is dynamic. We thus have:

$$\bar{\tau} = (1-\xi)\frac{\tau_0^F\tau_0^D(C_{Ru})}{\tau_0^F+\tau_0^D} + \frac{\xi}{14}\tau_1^D(C_{Ru})\sum_{n=1}^{14}\frac{1}{1+\left(\frac{R_0}{r_{1,n}}\right)^6} \tag{26}$$

where $r_{1,n}$ is the distance between the two fluorophores when the intercalation occurs at the *nth* position. It is known that the intercalation of the ruthenium compound induces a length increase of the DNA chain equal to the base pair distance. We moreover assume that the DNA double strand remains linear and rigid (Vladescu et al., 2007) Then, the length of the dsDNA, complexed with one $Ru(bpy)_2dppz^{2+}$does not depend on the intercalation position and we have $r_{1,n} = 16/15r_0$ where r_0 is the length of the 15 bp dsDNA chain. We now compute r_1 from thee experimental measurements. We can use Equation 26, recognizing that:

$$\left(\frac{r_1}{r_0}\right)^6 = \frac{\tau_1^F}{\tau_0^F} = \frac{\tau_1}{\tau_0^F\left(1-\frac{\tau_1}{\tau_n^D}\right)} \tag{27}$$

We obtain r_1/r_0. The values of r_1/r_0 are plotted in **Figure 4** as a function of ξ. At low ξ , the bound ruthenium fraction is too low and the measurement is not accurate, but for values of $\xi \geq 0.2$, r_1/r_0 saturates and its average value over the three highest complexation ratios is 1.028. This value is smaller than if the intercalation would have led to a length increase of a straight double strand, we would have: $r_{1,n}/r_0 = 16/15 = 1.067$. We thus conclude that the complexation induces a bending in the dsDNA. This bending may be static or dynamic, that is, due to an increase of flexibility of the DNA double strand at the intercalation. We define θ the bent angle induced by the intercalation, θ is of the order of 30°. It has been observed that short ds-DNA molecules are more flexible than worm-like chains of small lengths and whose persistence length would be equal to that of long DNA chains (Cloutier and Widom, 2005; Wiggins et al., 2006; Kahn, 2014; Le and Kim, 2014). This may also contribute to the increase of flexibility observed in our measurements.

As a conclusion, we have observed that the end-to-end distance increase of 15 bp dsDNA complexed with $Ru(bpy)_2dppz^{2+}$is smaller than that would be increase if the DNA would remain rigid upon complexation. We may thus conclude that DNA bends upon complexation. Nevertheless, our experiments cannot determine whether time average bending is due to a local dynamic flexibility or a static kink induced by the intercalation.

References

Batista, E. R., and Martin, R. L. (2005). On the excited states involved in the luminescent probe [ru(bpy)2dppz]2+. *J. Phys. Chem. A* 109, 3128–3133. doi: 10.1021/jp050673+

Brennaman, M. K., Alstrum-Acevedo, J. H., Fleming, C. N., Jang, P., Meyer, T. J., and Papanikolas, J. M. (2002). Turning the [ru(bpy)2dppz]2+ light-switch on and off with temperature. *J. Am. Chem. Soc.* 124, 15094–15098. doi: 10.1021/ja0279139

Brennaman, M. K., Meyer, T. J., and Papanikolas, J. M. (2004). [ru(bpy)2dppz]2+ light-switch mechanism in protic solvents as studied through temperature-dependent lifetime measurements†. *J. Phys. Chem. A* 108, 9938–9944. doi: 10.1021/jp0479670

Cloutier, T. E., and Widom, J. (2005). DNA twisting flexibility and the formation of sharply looped protein–dna complexes. *Proc. Natl. Acad. Sci. U.S.A.* 102, 3645–3650. doi: 10.1073/pnas.0409059102

Erkkila, K. E., Odom, D. T., and Barton, J. K. (1999). Recognition and reaction of metallointercalators with DNA. *Chem. Rev.* 99, 2777–2796. doi: 10.1021/cr9804341

Friedman, A. E., Chambron, J. C., Sauvage, J. P., Turro, N. J., and Barton, J. K. (1990). A molecular light switch for DNA: ru(bpy)2(dppz)2+. *J. Am. Chem. Soc.* 112, 4960–4962. doi: 10.1021/ja00168a052

Hu, L., Bian, Z., Li, H., Han, S., Yuan, Y., Gao, L., et al. (2009). [ru(bpy)2dppz]2+ electrochemiluminescence switch and its applications for dna interaction study and label-free atp aptasensor. *Anal. Chem.* 81, 9807–9811. doi: 10.1021/ac901925x

Jenkins, Y., Friedman, A. E., Turro, N. J., and Barton, J. K. (1992). Characterization of dipyridophenazine complexes of ruthenium(II): the light switch effect as a function of nucleic acid sequence and conformation. *Biochemistry* 31, 10809–10816. doi: 10.1021/bi00159a023

Kahn, J. D. (2014). DNA, flexibly flexible. *Biophys. J.* 107, 282–284. doi: 10.1016/j.bpj.2014.06.007

Klajner, M., Hébraud, P., Sirlin, C., Gaiddon, C., and Harlepp, S. (2010). DNA binding to an anticancer organo-ruthenium complex. *J. Phys. Chem. B* 114, 14041–14047. doi: 10.1021/jp10 44783

Le, T. T., and Kim, H. D. (2014). Probing the elastic limit of DNA bending. *Nucleic Acids Res.* 42, 10786–10794. doi: 10.1093/nar/gku735

Lim, M. H., Song, H., Olmon, E. D., Dervan, E. E., and Barton, J. K. (2009). Sensitivity of ru(bpy)2dppz2+ luminescence to DNA defects. *Inorg. Chem.* 48, 5392–5397. doi: 10.1021/ic900407n

Song, H., Kaiser, J. T., and Barton, J. K. (2012). Crystal structure of δ-$[ru(bpy)_2dppz]^{2+}$ bound to mismatched dna reveals side-by-side metalloinsertion and intercalation. *Nat. Chem.* 4, 615–620. doi: 10.1038/nchem.1375

Sun, Y., Collins, S. N., Joyce, L. E., and Turro, C. (2010). Unusual photophysical properties of a ruthenium(II) complex related to [ru(bpy)2(dppz)]2+. *Inorg. Chem.* 49, 4257–4262. doi: 10.1021/ic9025365

Very, T., Despax, S., Hébraud, P., Monari, A., and Assfeld, X. (2012). Spectral properties of polypyridyl ruthenium complexes intercalated in DNA: theoretical insights into the surrounding effects of [ru(dppz)(bpy)2]2+. *Phys. Chem. Chem. Phys.* 14, 12496–12504. doi: 10.1039/c2cp40935f

Vidimar, V., Meng, X., Klajner, M., Licona, C., Fetzer, L., Harlepp, S., et al. (2012). Induction of caspase 8 and reactive oxygen species by ruthenium-derived anticancer compounds with improved water solubility and cytotoxicity. *Biochem. Pharmacol.* 84, 1428–1436. doi: 10.1016/j.bcp.2012.08.022

Vladescu, I. D., McCauley, M. J., Nuñez, M. E., Rouzina, I., and Williams, M. C. (2007). Quantifying force-dependent and zero-force DNA intercalation by single-molecule stretching. *Nat. Methods* 4, 517–522. doi: 10.1038/nmeth1044

Wiggins, P. A., van der Heijden, T., Moreno-Herrero, F., Spakowitz, A., Phillips, R., Widom, J., et al. (2006). High flexibility of DNA on short length scales probed by atomic force microscopy. *Nat. Nanotechnol.* 1, 137–141. doi: 10.1038/nnano.2006.63

Conflict of Interest Statement: The authors declare that the research was conducted in the absence of any commercial or financial relationships that could be construed as a potential conflict of interest.

Copyright © 2015 Jia, Despax, Münch and Hébraud. This is an open-access article distributed under the terms of the Creative Commons Attribution License (CC BY). The use, distribution or reproduction in other forums is permitted, provided the original author(s) or licensor are credited and that the original publication in this journal is cited, in accordance with accepted academic practice. No use, distribution or reproduction is permitted which does not comply with these terms.

frontiers in Chemistry

ORIGINAL RESEARCH
published: 20 April 2015
doi: 10.3389/fchem.2015.00029

Deciphering the photochemical mechanisms describing the UV-induced processes occurring in solvated guanine monophosphate

Salvatore F. Altavilla[1], Javier Segarra-Martí[1], Artur Nenov[1], Irene Conti[1], Ivan Rivalta[2] and Marco Garavelli[1,2]**

[1] *Dipartimento di Chimica "G. Ciamician," Università di Bologna, Bologna, Italy,* [2] *École Normale Supérieure de Lyon, Centre National de la Recherche Scientifique, UMR 5182, Université de Lyon, Lyon, France*

OPEN ACCESS

Edited by:
Antonio Monari, Université de Lorraine, France

Reviewed by:
Michael Bearpark, Imperial College London, UK
Chantal Daniel, Centre National de la Recherche Scientifique, France

***Correspondence:**
Javier Segarra-Martí and Marco Garavelli, École Normale Supérieure de Lyon, Centre National de la Recherche Scientifique, UMR 5182, Université de Lyon, 46 Allée d'Italie, Lyon 69364, France
javier.segarra@unibo.it; marco.garavelli@unibo.it

Specialty section:
This article was submitted to Chemical Biology, a section of the journal Frontiers in Chemistry

Received: *22 January 2015*
Accepted: *30 March 2015*
Published: *20 April 2015*

Citation:
Altavilla SF, Segarra-Martí J, Nenov A, Conti I, Rivalta I and Garavelli M (2015) Deciphering the photochemical mechanisms describing the UV-induced processes occurring in solvated guanine monophosphate. Front. Chem. 3:29. doi: 10.3389/fchem.2015.00029

The photophysics and photochemistry of water-solvated guanine monophosphate (GMP) are here characterized by means of a multireference quantum-chemical/molecular mechanics theoretical approach (CASPT2//CASSCF/AMBER) in order to elucidate the main photo-processes occurring upon UV-light irradiation. The effect of the solvent and of the phosphate group on the energetics and structural features of this system are evaluated for the first time employing high-level *ab initio* methods and thoroughly compared to those *in vacuo* previously reported in the literature and to the experimental evidence to assess to which extent they influence the photoinduced mechanisms. Solvated electronic excitation energies of solvated GMP at the Franck-Condon (FC) region show a red shift for the $\pi\pi^*$ L_a and L_b states, whereas the energy of the oxygen lone-pair $n\pi^*$ state is blue-shifted. The main photoinduced decay route is promoted through a ring-puckering motion along the bright lowest-lying L_a state toward a conical intersection (CI) with the ground state, involving a very shallow stationary point along the minimum energy pathway in contrast to the barrierless profile found in gas-phase, the point being placed at the end of the minimum energy path (MEP) thus endorsing its ultrafast deactivation in accordance with time-resolved transient and photoelectron spectroscopy experiments. The role of the $n\pi^*$ state in the solvated system is severely diminished as the crossings with the initially populated L_a state and also with the L_b state are placed too high energetically to partake prominently in the deactivation photo-process. The proposed mechanism present in solvated and *in vacuo* DNA/RNA chromophores validates the intrinsic photostability mechanism through CI-mediated non-radiative processes accompanying the bright excited-state population toward the ground state and subsequent relaxation back to the FC region.

Keywords: DNA, purine, CASSCF/CASPT2, photochemistry, QM/MM, photostability, GMP, guanine

Introduction

The genomic material and the mechanisms that process the disposal of the excess energy attained upon UV-light irradiation are of paramount importance from both biomedical and biotechnological standpoints. The initially populated excited states and their fate along the

distinct deactivation routes present in the DNA/RNA double helix chains relate simultaneously to the intrinsic photostability of the genomic material (Callis, 1983; Crespo-Hernandez et al., 2004; Kohler, 2010), as well as to the damaging photo-reactions that ultimately yield mutations and single- and double-strand breaks that have been associated to increasingly featured diseases like skin cancer (Cadet et al., 2012; Noonan et al., 2012; Giussani et al., 2013b; Brash, 2015). Besides the biological relevance, the intricate photophysical properties of nucleobases can be also exploited to design optical photo-responsive nanomachines among a long list of prospective applications (Kamiya and Asanuma, 2014), yet it is their biological relevance that focuses our attention.

From a bio-physical and chemical point of view, fundamental knowledge on the deactivation processes, including the associated underlying molecular motions, are essential to rationalize the intrinsic photostability of the genomic material and to characterize the aforementioned routes leading to deleterious photochemical reactions (Markovitsi et al., 2010; Cadet et al., 2012). These different pathways increase in number and complexity as the size of the DNA/RNA single- or double-stranded chain enlarges, as the different de-excitation routes interact with one another yielding a ramification of complex photoinduced pathways that become extremely hard to discern, disentangle, and comprehend. This increasing degree of complexity arises partially due to the intermolecular interactions occurring from inter- and intra-strand conformations between the nucleobases compressing the DNA/RNA chains, related to their hydrogen-bonding motifs and π-stacking interactions, respectively. Extensive experimental work has been carried out recently in order to identify and separate the different contributions arising from these interactions, providing indicative fingerprints in the appearance of a long-lived spectroscopic signal originating from a π-stacking conformation within intra-strand sequences (Takaya et al., 2008; Su et al., 2012; Vayá et al., 2012; Chen et al., 2013, 2014; Chen and Kohler, 2014; Plasser et al., 2015) and to an ultrafast proton/hydrogen transfer stemming from a charge-transfer event in the hydrogen-bonding motifs responsible for the inter-strand interactions (Schwalb and Temps, 2007, 2008; Saurí et al., 2012). Given the abstruse nature of the photo-processes under study and their intrinsic difficulty, new development in methods and techniques are expected to play a crucial role on disentangling all the different deactivation channels (West et al., 2011, 2012; Krause et al., 2012; West and Moran, 2012; Fingerhut et al., 2013, 2014; Rivalta et al., 2014; Nenov et al., 2014a,b), even though the photophysical and photochemical studies on single nucleobases remain at the cornerstone of the field.

A proper characterization of the monomeric chromophores is therefore essential to understand the photoinduced events occurring in DNA/RNA from a bottom-up approach that can yield definitive answers regarding their role in photostability and photo-damage (Serrano-Andrés and Merchán, 2009). This avenue of research embodies the main efforts carried out by the research community over the last two decades (Kleinermanns et al., 2013; Giussani et al., 2013a; Barbatti et al., 2014; Chen et al., 2014; Mai et al., 2014), and even though plenty of advances have been made there is still no definitive consensus regarding the main deactivation routes present in the nucleobases (Crespo-Hernandez et al., 2004; Hudock et al., 2007; Barbatti et al., 2010; McFarland et al., 2014). Several decay paths have been identified both *in vacuo* (Giussani et al., 2013a) and in solution (Improta and Barone, 2014) and assigned to a number of processes, ranging from a barrierless deactivation through a ring-puckering motion of the bright $\pi\pi^*$ state (Merchán and Serrano-Andrés, 2003; Gustavsson et al., 2006; Merchán et al., 2006; Serrano-Andrés et al., 2006, 2008; Conti et al., 2009; Improta and Barone, 2014) to a long-lived signal arising due to a possible crossing with a dark $n\pi^*$ state (Hare et al., 2007), as well as an even longer-lived pathway widely attributed to the role of triplet states, specially prominent in non-canonical nucleobases with heavy-atom substitutions (Merchán et al., 2005; González-Luque et al., 2010; Martinez-Fernandez et al., 2012, 2014; Pollum et al., 2014).

In this study we turn out attention to water-solvated guanine monophosphate (GMP), one of the canonical DNA/RNA nucleobases. GMP has also been recently proposed to be an interesting compound for nanotechnological applications due to its outstanding capacity for self-assembly (Gupta et al., 2014), specially remarkable in its quadruplex form, which has even been located in DNA/RNA chains (Lam et al., 2013; Murat and Balasubramanian, 2014). Whereas, guanine *in vacuo* has been extensively studied at a high-level multireference *ab initio* level (Serrano-Andrés et al., 2008; Barbatti et al., 2010, 2011) as well as experimentally (Miannay et al., 2010; Chatterley et al., 2014), a lesser degree of scrutiny, mainly at a density functional theory level (Karunakaran et al., 2009; Parac et al., 2010; Santoro et al., 2010; Improta, 2014; Improta and Barone, 2014), has been considered on the effect of the phosphate group and the the solvent on the photoinduced processes occurring in this compound (Crespo-Hernandez et al., 2004). In the present work we propose a theoretical assessment of the deactivation routes embodying the main photophysical and photochemical features of GMP by employing high-level *ab initio* multireference perturbation theory methods coupled with a quantum-mechanical/molecular mechanics (QM/MM) approach, in order to ascertain the role of the environmental perturbations in these type of systems as they remain relatively unknown (Conti et al., 2010; Nachtigallová et al., 2010; Barbatti, 2014). Further knowledge on the environmental effects affecting the photo-processes occurring in the DNA/RNA chromophores upon UV-light irradiation will provide essential information that can be properly translated to water-solvated DNA/RNA systems such as those found in cells.

Computational Details

Sections MM Dynamics and Sampling and QM/MM Calculations describe the computational strategies and methodological details considered in the computations of the MM sampling dynamics and electronic structure QM/MM calculations carried out.

MM Dynamics and Sampling

MM simulations were performed for GMP in water to obtain a representative starting geometry to be employed for all subsequent computations and analyses. The MM dynamics

calculations were carried out using the Amber-11 suite of programs making use of the Parm99 force field (Case et al., 2005, 2011). Initially, a cubic solvent box comprising 700 water molecules of explicit TIP3P (Jorgensen et al., 1983) with one Na^+ counterion were considered. The entire system was then heated from 0 to 300 K for 1 ns at constant volume and constant pressure (1 atm), and then finally performing a production run for 100 ns recording the snapshots every 200 fs. To select the initial geometry we performed a cluster analysis based on a Root Mean Square (RMS) coordinate deviation analysis on the guanine moiety over all snapshots recorded along the MM dynamics run within a 2.0 Å difference using the MMTSB toolbox. We obtained three different clusters, denoted a, b, and c in **Figure 1**, with populations relating to the 93, 6, and 1% of the total number of structures obtained along the dynamics run, respectively. The selected initial structure was therefore chosen as the snapshot with the closest geometrical parameters to the centroid of the average structures obtained in cluster A, being the most representative.

QM/MM Calculations

QM/MM calculations were performed using the COBRAMM interface developed in our group (Altoé et al., 2007a,b). The cut between the QM and MM regions has been done so that it includes all guanine atoms in the QM region, placing the link atom between the N9 of guanine and the carbon of the sugar ring directly attached to the nucleobase (see **Figure 2**). The choice of the cut between the QM and MM regions is justified in terms of charge redistribution on the nucleobase and its π-system in order to better reflect the covalent link between guanine and the monophosphate group. A three-layer approach (high, medium, and low) was used throughout (Altoé et al., 2007a): guanine was included in the QM region (high layer, ball, and stick representation in **Figure 2**), whereas the medium layer comprises the movable MM atoms within a 10 Å radius surrounding the GMP moiety, the remainder of the MM system being kept frozen during all optimization procedures in the low layer. Equilibrium geometries and photoreaction paths (Garavelli, 2006) were determined by using fully unconstrained optimizations and minimum energy path (MEP) computations on the relevant potential energy hypersurfaces by employing the intrinsic reaction coordinate (IRC) and optimization algorithms as implemented in the Gaussian 09 program package (Frisch et al., 2009) interfaced with COBRAMM. CI optimizations were performed with the gradient projection algorithm of Bearpark et al. (1994) as implemented in COBRAMM at the QM/MM level. Further details can be found in Conti et al. (2015).

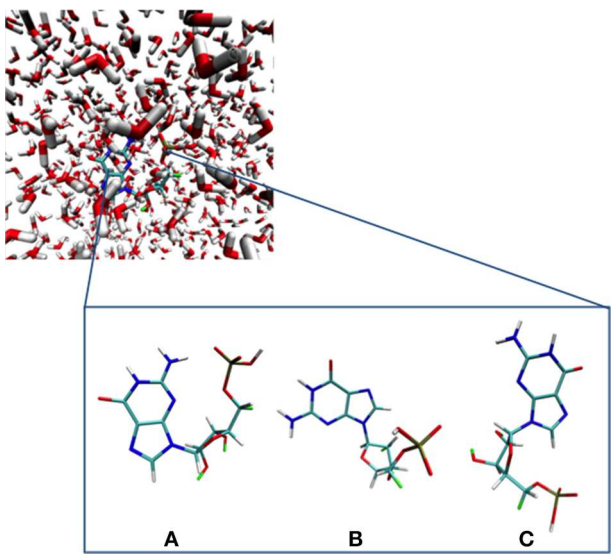

FIGURE 1 | GMP and its different main conformations along the MM dynamics run obtained through a RMS deviation cluster analysis. (A–C) depict the most important conformations extracted from the molecular dynamics simulation (see text).

Energies and gradients in the QM region were computed making use of the complete active space self-consistent field (CASSCF) and complete active space second-order perturbation theory (CASPT2) methods (Andersson et al., 1992; Roca-Sanjuán et al., 2012), as implemented in the MOLPRO-2010 (Werner et al., 2012a,b) and MOLCAS-7 (Aquilante et al., 2010, 2013) suite of programs, respectively. All gradient and non-adiabatic coupling calculations have been performed with the CASSCF implementation of the MOLPRO-2010 code. Subsequent CASPT2 calculations on the key structures obtained along the optimizations and MEPs have been carried out as implemented in the MOLCAS package in order to correct the energy values due to the lack of dynamic correlation present in the CASSCF method. This procedure is referred to as the CASSCF/CASPT2 protocol, and has been successfully employed over the years to tackle a variety of photoinduced phenomena from a theoretical standpoint (Garavelli, 2006; González-Ramírez et al., 2012; Segarra-Martí et al., 2012; Segarra-Martí and Coto, 2014). The active space selected comprised the full π space with the exception of the lowest occupied π orbital plus the three lone-pair orbitals to provide a proper description of the nπ* states, thus making 18 electrons in 13 orbitals. The removal of the lowest occupied π orbital is carried out due to its occupation number being very close to two and given that its removal does not affect the energy values obtained while speeding up the computations. An imaginary level shift of 0.2 a.u. was employed in the perturbation step to avoid intruder states. Two different basis sets were employed throughout: 6-31G* was used in order to map the hypersurfaces at the CASSCF level whereas atomic natural orbital (ANO) type (Pierloot et al., 1995) basis set with the large (ANO-L) primitive set C,N,O(14s9p4d3f)/H(8s4p3d) contracted to O[3s2p1d]/C[3s2p1d]/N[3s2p1d]/H[2s1p] (ANO-L 321/21 hereafter) was employed in order to refine the single-point CASPT2 energies.

Results and Discussion

The results are divided in three different sections: First, the main geometrical parameters of the ground-state Franck-Condon minimum of 9H-guanine both *in vacuo* and in solvated GMP are presented, together with its corresponding vertical spectra, drawing some conclusions on the influence the solvent and phosphate group have on the relative position of the excited states. Next,

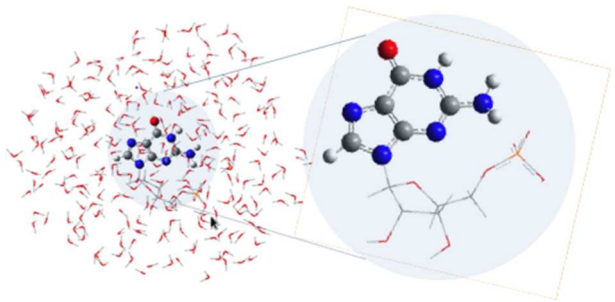

FIGURE 2 | GMP and the three different QM/MM partitions defined in the present study. The high layer treating the guanine moiety at the QM level (ball and stick representation), the medium layer encompassing the movable MM water molecules and the phosphate group enclosed within a 10 Å radius distance from GMP, and the low layer containing the remainder of the MM region that is kept frozen throughout the calculations (see text).

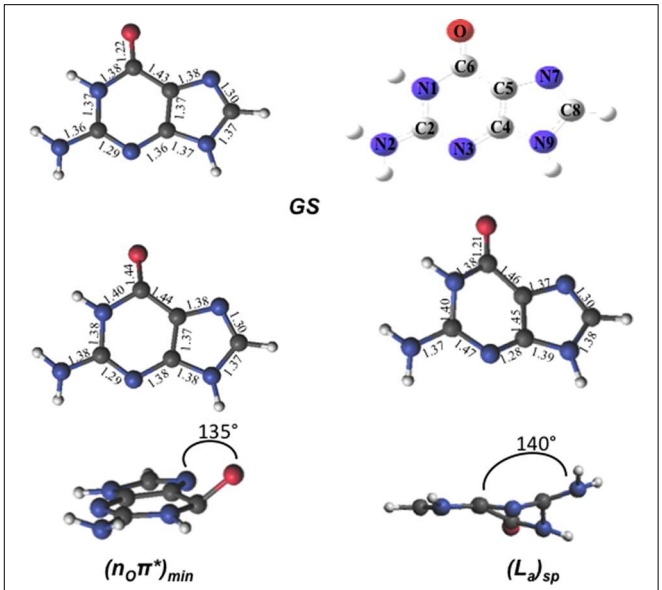

FIGURE 3 | Geometries and main geometrical parameters of the Franck-Condon structure and excited-state stationary points characterized in GMP for its lowest-lying excited states computed at the CASSCF/6-31G* level of theory.

the different minima and conical intersections describing the photo-process are presented. Finally, a rationale of the photoinduced mechanisms in GMP is drawn in conjunction with previous results and experimental data acquired from the literature, yielding concluding notes on the photophysical and photochemical decay channels featuring in GMP and leading to its intrinsic photostability.

UV Absorption at the Franck-Condon Region

The optimized FC structure of GMP in solution (**Figure 3**) shows a strong resemblance with the *in vacuo* 9H-Guanine CASSCF/6-31G* structure previously reported in the literature (Serrano-Andrés et al., 2008). **Table 1** presents the main geometrical parameters of both structures. As can be seen, bond lengths and dihedral angles are analogous giving rise to a planar structure. Small solvation effects are noticed in the GS structure mainly due to its relatively small dipole moment, providing slight shortenings in the C6-N1 bond distance in the presence of the solvent. A very shallow stationary point $(L_a)_{sp}$, not present in the gas phase, has been located at the end of the L_a MEP featuring a pronounced elongation of the C2-N3 and a shortening of the N3-C4 distances, similar to those featured by the conical intersections between the L_a and GS states both *in vacuo* and in solution. The two CIs located between the L_a and GS states do show pronounced differences due to the solvent, yielding large elongations in the C2-N3 bond compared to its *in vacuo* counterparts. This is mainly due to the large dipole moment featured by the L_a state, which makes it a more influenced state upon solvation. A similar behavior can be seen in the CIs between the L_a and L_b states, prompting large deviations in the C4-C5, C5-C6 and specially pronounced in the C6-O distance, where water-solvated GMP suffers an elongation of 0.15 Å. The $n_O\pi^*$ state minimum does not show significant differences highlighting the scarce role polar solvation has on these types of states. The CIs between $n_O\pi^*$ and the polar $\pi\pi^*$ L_a and L_b states are profoundly influenced by the solvent comparing them to their *in vacuo* counterparts, featuring large differences in the C4-C5 bond distance. These differences are mainly attributed to the polar character of the $\pi\pi^*$ L_a/L_b states than to the effects on the $n_O\pi^*$ state. Overall, it can be concluded that solvation has an important effect on the polar $\pi\pi^*$ L_a/L_b states, while being negligible for the $n_O\pi^*$ state. These states feature excitations that are prominently placed on the six-member ring of guanine featuring noticeable changes in the structure upon solvation, whereas the five-member ring remains relatively unchanged. A possible cause for this effect could lie on the presence of the phosphate group, which is tied to the five-ring member and could be shielding that molecular moiety from the surrounding water molecules thus mitigating its exposure as compared to the six-member ring and justifying why the latter suffers such pronounced changes upon solvation.

Table 2 contains the vertical excitation energies at the CASPT2 level computed in the present study, together with several other computations and experimental values reported in the literature. We have used Platt's nomenclature (Platt, 1949), where L_a represents the $\pi\pi^*$ excited state characterized by the largest contribution of the configuration HOMO (H) → LUMO (L) to the CASSCF wave function, whereas L_b depicts the $\pi\pi^*$ excited state with a predominance of H → L+1 and H-1 → L configurations. By inspection of **Table 2**, it can be readily seen that there is a qualitative difference in the relative order of the lowest-lying excited states *in vacuo* and in solution: both cases feature the $\pi\pi^*$ L_a state as the energetically lowest-lying excited state, at 4.93 and 4.77 eV respectively, but while *in vacuo* S_2 has $n_O\pi^*$ nature (5.54 eV, involving the oxygen lone pair of the purinic base), in solution S_2 isthe $\pi\pi^*$ L_b state, placed at 5.44 eV. This effect has been widely reported in the literature being related to a bathochromic effect (Nakayama et al., 2013), with the $n_O\pi^*$ featuring a dipole moment of 5.69 D (3.51 D *in vacuo*) being less stabilized than the $\pi\pi^*$ L_b state (7.96 D, 4.92 D *in vacuo*) as it can be also noticed by looking at their change in dipole moment. The solvent therefore

TABLE 1 | Bond distances (in Å) characterizing the key structures involved in the photoinduced events of GMP upon UV-light irradiation.

	N1-C2	C2-N2	C2-N3	N3-C4	C4-C5	C5-C6	C6-O	C6-N1	C5-N7	N7-C8	C8-N9	N9-C4
GS *in vacuo*[a]	1.37	1.38	1.31	1.36	1.39	1.44	1.21	1.41	1.38	1.30	1.38	1.37
GS in solution [b]	1.37	1.36	1.29	1.36	1.37	1.43	1.20	1.38	1.38	1.30	1.37	1.37
$(L_a)_{sp}$in solution[b]	1.40	1.37	1.47	1.28	1.45	1.46	1.21	1.38	1.37	1.30	1.38	1.39
$(L_a/GS)_{CI\text{-}1}$ *in vacuo*[a]	1.41	1.40	1.45	1.29	1.45	1.47	1.20	1.41	1.39	1.29	1.39	1.37
$(L_a/GS)_{CI\text{-}1}$ in solution[b]	1.37	1.38	1.50	1.24	1.48	1.47	1.23	1.37	1.37	1.30	1.38	1.42
$(L_a/GS)_{CI\text{-}2}$ *in vacuo*[a]	1.41	1.40	1.38	1.28	1.45	1.35	1.34	1.36	1.39	1.29	1.38	1.38
$(L_a/GS)_{CI\text{-}2}$ in solution[b]	1.42	1.36	1.49	1.27	1.48	1.48	1.21	1.39	1.38	1.30	1.39	1.39
$(L_b/L_a)_{CI}$*in vacuo*[a]	1.38	1.40	1.32	1.31	1.45	1.43	1.24	1.36	1.35	1.44	1.42	1.40
$(L_b/L_a)_{CI\text{-}1}$ in solution[b]	1.39	1.37	1.28	1.37	1.38	1.38	1.39	1.39	1.38	1.30	1.36	1.38
$(L_b/L_a)_{CI\text{-}2}$ in solution[b]	1.46	1.35	1.37	1.21	1.59	1.54	1.18	1.30	1.30	1.47	1.41	1.39
$(n_O)_{min}$ *in vacuo*[a]	1.38	1.38	1.28	1.37	1.36	1.44	1.38	1.41	1.36	1.30	1.37	1.36
$(n_O)_{min}$ in solution[b]	1.38	1.38	1.29	1.38	1.36	1.44	1.41	1.40	1.38	1.30	1.37	1.80
$(n_O/L_a)_{CI}$ *in vacuo*[a]	1.41	1.40	1.38	1.28	1.45	1.35	1.34	1.36	1.39	1.29	1.38	1.38
$(n_O/L_a)_{CI}$ in solution[b]	1.39	1.37	1.28	1.37	1.38	1.38	1.39	1.39	1.38	1.30	1.36	1.38
$(n_O/L_b)_{CI}$ in solution[b]	1.40	1.35	1.30	1.36	1.38	1.42	1.24	1.36	1.37	1.30	1.37	1.37

[a]*Values obtained at the CASSCF/6-31G* level of theory by Serrano-Andrés et al. (2008).*
[b]*Values computed in the present study.*

affects the absorption spectra prominently at the FC region by blue-shifting the $n_O\pi^*$ state by 0.23 and red-shifting the $\pi\pi^*$ L_b by 0.33 eV with respect to the gas-phase, a change comparable to those previously reported in other QM/MM studies in solution (Parac et al., 2010; Nakayama et al., 2013). It is worth noting that the oscillator strengths associated to the transitions to the L_a and L_b states are also affected by the effect of the solvent. Whereas, L_a features as the brightest lowest-lying excited state in the gas phase and the L_b state presents a slightly smaller oscillator strength (0.158 and 0.145 respectively), in solvent L_a and L_b present an inverse order in the values for the oscillator strength associated to their transitions (0.09 and 0.17 respectively), being in agreement with the experimental data reported by femtosecond broad-band transient spectroscopy (Karunakaran et al., 2009).

The effect of the basis set on the excitation energies has also been studied by employing both 6-31G* and ANO-L 321/21 basis sets. The 6-31G* CASPT2 computations report values of 4.77, 5.44, and 5.77 eV for the L_a, L_b, and $n_O\pi^*$ transitions, respectively, whereas the ANO-L yields absorption energy values of 4.50, 5.10, and 5.71 eV for the L_a, L_b, and $n_O\pi^*$ states respectively, consistent with those reported experimentally (Karunakaran et al., 2009), which place the absorption maximum of L_a at 4.50 eV. **Table 2** also reports several theoretical approaches found in the literature employing different methods to simulate solvated GMP. As can be seen, more sophisticated DFT/MRCI methods agree qualitatively with the values here reported at the CASPT2 level of theory, yielding values within 0.33 and 0.02 for the L_a and L_b states respectively with respect to the CASPT2/ANO-L values here obtained, and a slight energetic deviation is also found when comparing to the values computed at a TDDFT level. This small difference present in TDDFT results employing a polarization continuum model (PCM) (see **Table 2**) could also be due to the fact that (Karunakaran et al., 2009) used a methylated guanine to model the effect of the phosphate group whereas here the phosphate group is explicitly included even if just at the MM level. On overall we can conclude that the absorption values reported here at the CASPT2/ANO-L level are consistent with the experimental data and with the highest-level theoretical estimates present in the literature, thus highlighting the capabilities of the CASSCF/CASPT2 protocol to treat excited states in a balanced manner (Roos et al., 1996) and its usage for mapping photochemical reaction paths (Garavelli, 2006).

Excited-State Evolution

The excited-state evolution is here tracked by means of static approaches through excited-state optimizations and the characterization of the conical intersections representing the crossings among the energetically lowest-lying excited states, ultimate protagonists in the deactivation photo-process. Additionally, the MEPs connecting the initially accessed states and subsequent photoinduced events have been mapped making use of the IRC technique.

The lowest-lying excited state is the $\pi\pi^*$ L_a state, which is expected to be the main spectroscopic state due to its lowest-lying position and relatively large oscillator strength. This state is generally assumed to present an easily accessible CI along its relaxation pathway toward the ground-state characterized by a ring-puckering motion (see **Figure 4**) widely featured in the DNA/RNA nucleobases (Giussani et al., 2013a) *in vacuo*. This profile is slightly altered in the presence of polar environments as it has been previously reported for other purine nucleobases (Conti et al., 2010), where a shallow stationary point $(L_a)_{sp}$ arises along the MEP close to the CI with the ground state being placed at 1.15 eV vertically and adiabatically at 3.30 eV from the ground state (see **Figure 5**). Two different CIs have been characterized in the vicinity of this stationary point, one optimized directly in solvent corresponding to the minimum energy conical intersection (MECI) also reported by Serrano-Andrés

TABLE 2 | Vertical absorption energies (ΔE, in eV), oscillator strengths (*f*) and dipole moments (μ, in Debye) computed at the FC region, together with previous theoretical and experimental data.

States	ΔE	*f*	μ
9H-GUANINE *IN VACUO*[a]			
GS	0		5.81
$\pi\pi^*$ L_a	4.93	0.158	5.23
$n_O\pi^*$	5.54	0.002	3.51
$\pi\pi^*$ L_b	5.77	0.145	4.92
GMP IN SOLVENT (6-31G*)[b]			
GS	0		8.58
$\pi\pi^*$ L_a	4.77	0.09	8.97
$n_O\pi^*$	5.77	0.00	5.69
$\pi\pi^*$ L_b	5.44	0.17	7.96
GMP IN SOLVENT (ANO-L 321/21)[b]			
GS	0		8.88
$\pi\pi^*$ L_a	4.50	0.17	9.62
$n_O\pi^*$	5.71	0.00	5.64
$\pi\pi^*$ L_b	5.10	0.20	8.31
EXPERIMENT[c]			
$\pi\pi^*$ L_a	4.50	0.094	
$n_O\pi^*$			
$\pi\pi^*$ L_b	4.96	0.167	
9Me-GUANINE*5H2O (TDDFT/PCM)[c]			
$\pi\pi^*$ L_a	4.68	0.16	
$n_O\pi^*$	5.77		
$\pi\pi^*$ L_b	5.18	0.34	
9H-GUANINE (TDDFT/TZVP)[d]			
$\pi\pi^*$ L_a	4.93	0.158	
$n_O\pi^*$	5.36	0.106	
$\pi\pi^*$ L_b	5.28	0.117	
9H-GUANINE (DFT/MRCI/TZVP)[d]			
$\pi\pi^*$ L_a	4.83	0.22	
$n_O\pi^*$	5.32	0.001	
$\pi\pi^*$ L_b	5.08	0.368	

[a] *Values obtained at the CASSCF/6-31G* level of theory by Serrano-Andrés et al. (2008).*
[b] *Results obtained in the present study.*
[c] *Results obtained by Karunakaran et al. (2009).*
[d] *Results obtained by Parac et al. (2010).*

et al. (2008), and another relating to the CI found in the same study along the MEP *in vacuo*, which we have tentatively named $(L_a/GS)_{CI\text{-}1}$ and $(L_a/GS)_{CI\text{-}2}$ in the present study, respectively. Both CIs as well as the $(L_a)_{sp}$ present ring-puckering structures in the A6 cycle yielding slight bond-length alterations (C2-N3, N1-C2, N3-C4, and C4-C5) compared to the FC structure and featuring prominent N1-N-C2-N3 dihedral angle distortions at 133°, 132°, and 140° for the $(L_a/GS)_{CI\text{-}1}$, $(L_a/GS)_{CI\text{-}2}$, and $(L_a)_{sp}$ structures, respectively. These distortions are quantitatively different to those reported *in vacuo*, stressing out the importance of the solvent where the $(L_a/GS)_{CI\text{-}1}$ presents a ∼143° dihedral angle as compared to its 133° solvated counterpart, together with slightly pronounced bond-length differences as can be seen in **Table 1**. Both CIs here characterized present very similar structures (see **Figure 4**) and charge distributions very close to those found in the gas phase, presenting an inversion in their energetic order in solution being $(L_a/GS)_{CI\text{-}1}$ the energetically lowest-lying adiabatically at 3.31 eV, $(L_a/GS)_{CI\text{-}2}$ being placed 0.3 eV higher in energy and 3.60 eV adiabatically from the FC region.

Two different CIs connecting the $\pi\pi^*$ L_a and $\pi\pi^*$ L_b states have also been located. Direct CI optimization leads to $(L_b/L_a)_{CI\text{-}2}$, its geometry presenting a deformation near the N9-C8-N7 angle with respect to the ground state. The bond lengths suffer large distortions, observing a shortening of the N1-C6, C5-N7, C4-N3, N3-C2, C6-O, and C2-N bonds, and an increase in the length of the remaining bonds with respect to the FC region (see **Figure 4**). This CI is placed at 7.62 eV vertically from the FC region, which is higher in energy than both $\pi\pi^*$ L_a and $\pi\pi^*$ L_b vertical excitation energies, placed at 4.77 and 5.44 respectively, thus hinting toward a sloped CI profile preventing their non-adiabatic interaction. A second CI, $(L_b/L_a)_{CI\text{-}1}$, obtained along the L_b MEP computed within a 4in4 active space to avoid excessive wave function mixing, has been located being placed ∼5 eV adiabatically from the FC region. This CI presents geometrical similarities with its *in vacuo* counterpart and provide an accessible channel to funnel the initially populated $L_b$state down to L_a. Further attempts to optimize the L_b state toward a possible minimum have been fruitless due to the large wave function mixing and root flipping problems experienced along the optimization procedure, preventing us to obtain further information on this specific state.

As previously stated, $n_O\pi^*$ represents the third energetically wise excited state for the GMP in solvent. The optimized $n_O\pi^*$ minimum found in solvent is prominently characterized by an elongation of the C6-O bond distance with respect to the ground state. **Table 1** shows the main differences in bond lengths, where the C6-O bond is elongated in this minimum from 1.22 Å at the FC region to 1.41 Å. The minimum of this excited state in solvent is very similar to the one reported *in vacuo* (Serrano-Andrés et al., 2008), as would be expected given the small effects provided by the solvent on $n\pi^*$ excited states. Energetically it is placed 3.97 eV adiabatically and 2.67 eV vertically with respect to the ground state (see **Figure 6**), which constitutes a stabilization of 1.8 eV from its initial value at the FC region.

We have also located the CI between the states $n_O\pi^*$ and $\pi\pi^*$ L_a, $(n_O/L_a)_{CI}$, its geometry presenting a planar structure like the ground state, but showing an elongation of the C6-O bond and a shortening of the C6-C5 bond. We observe similarities between this geometry and that of the CI optimized *in vacuo*, as they both present the same kind of geometrical distortions given the small solvent effects in the $n_O\pi^*$ state, yielding a relative energy of 4.90 eV with respect to the FC region. The CI connecting the $n_O\pi^*$ and $\pi\pi^*$ L_b states, $(n_O/L_b)_{CI}$, has also been located, featuring a planar structure and differences in the bond lengths in the six-member ring, in particular in the differences in the N1-C2, N1-C6 bonds.

The differences observed in the geometries of the excited state minima and of the different CIs characterized both *in vacuo* and in solvent highlight the importance of the solvent that is considered explicit in our calculations, together with the explicit presence of the ribose and phosphate groups on GMP, providing more

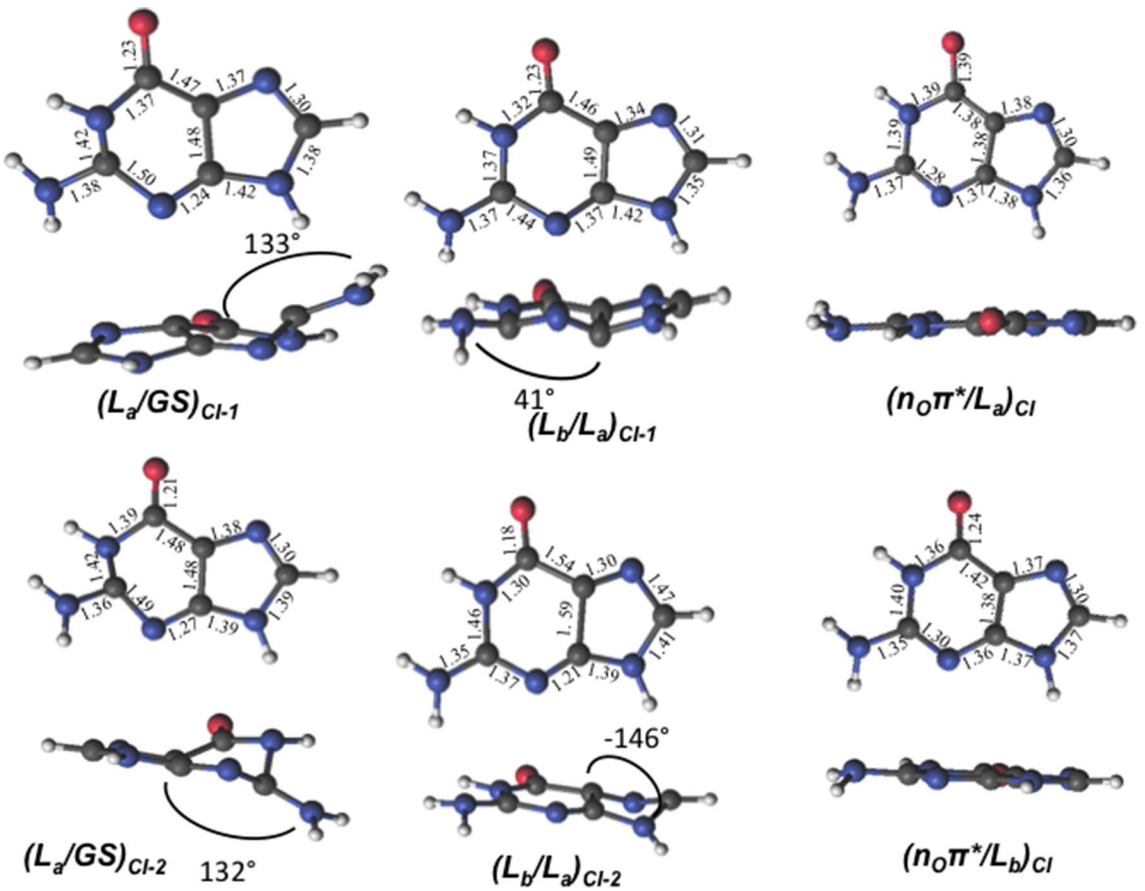

FIGURE 4 | GMP geometries and main geometrical parameters of the characterized conical intersections between the lowest-lying excited states computed at the CASSCF/6-31G* level of theory.

accurate estimates to relate to the photoinduced events in the cellular system.

Photophysics and Photochemistry of GMP: Elucidating Its Intrinsic Photostability

Figure 7 features a scheme with the tentative photo-processes occurring upon UV irradiation in GMP based on our present computations and the theoretical and experimental data available in the literature. Experimentally, time-resolved transient absorption in solution by Karunakaran et al. (2009) suggest either bi- or triexponential decay depending on the spectral region measured, providing $\tau_1 = 0.25$ ps, $\tau_2 = 1.0$ ps, and $\tau_3 = 2.5$ ps for the 270–400 nm region in the non-protonated GMP at neutral pH. (Karunakaran et al., 2009) justify these ultrafast signals in terms of TDDFT calculations due to ring-puckering CIs between the $\pi\pi^*$ L_a and GS states, in accordance to what was previously proposed *in vacuo* by Serrano-Andrés et al. (2008) on the basis of CASSCF/CASPT2 computations. Molecular dynamics simulations by Serrano-Andrés et al. (2008) proposed that the ultrafast decay from the $\pi\pi^*$ L_a state could occur already within the first 100 fs, an assumption that has been challenged by Barbatti et al. (2011), pushing the timescale toward the 500 fs mark. (Lan et al., 2009), on the other hand, support a biexponential decay based on their MD simulations where they obtain a faster ∼190 fs and a slower ∼400 fs decays through two different CIs between the $\pi\pi^*$ L_a and GS states, thus highlighting the complex process under study and the difficulty to simulate it coherently (Mai et al., 2014). The most recent experimental data to our knowledge is based on the photoelectron spectroscopy of GMP both *in vacuo* and in solution (Chatterley et al., 2014), yielding a biexponential decay of $\tau_1 = 50$ fs and $\tau_2 = 600$ fs *in vacuo* and $\tau_1 = 120$ fs and $\tau_2 = 680$ fs in solution, which reveals a striking similarity among the two different set of values as they are within experimental error and therefore provide evidence of the negligible role played by the solvent in the photoinduced decay paths present in this system. This biexponential decay is obtained through a 4.66 eV pump, which also suggests the possibility of only probing those kinetic processes undergone after direct $\pi\pi^*$ L_a population, whereas the time-resolved transient data by Karunakaran et al. (2009) yields a third exponent related to a slower timescale possibly arisen through an initial population of the $\pi\pi^*$ L_b state.

Our present results point toward an ultrafast deactivation along the L_a MEP characterized by a ring-puckering motion centered in the C2 atom, which brings the excited-state population to interact non-adiabatically with the ground state, funneling down the population that is further relaxed to the FC

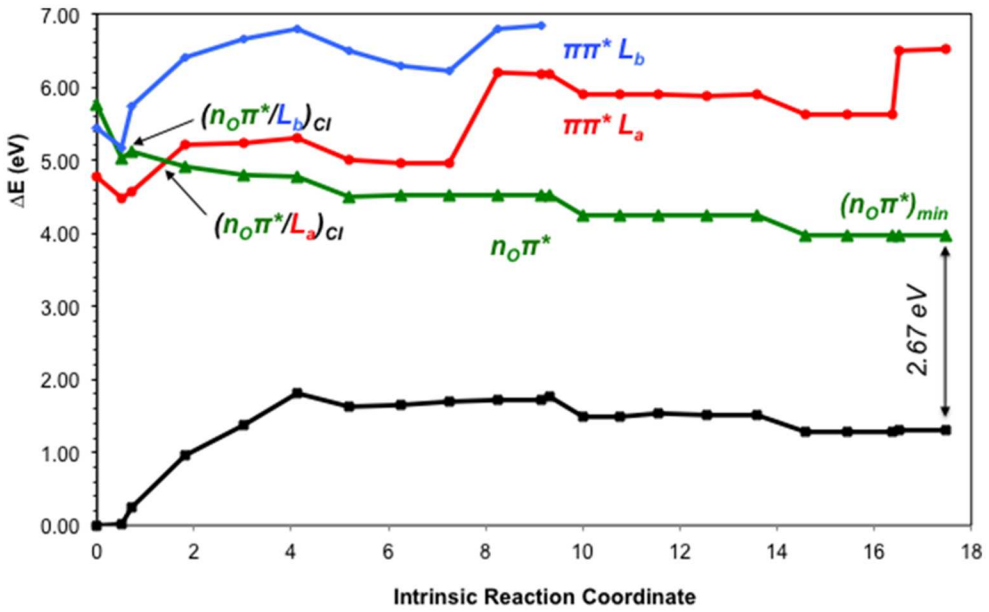

FIGURE 5 | CASPT2 energies of the ground (GS) and lowest-lying singlet excited states ($\pi\pi^*$ L_a, $\pi\pi^*$ L_b and $n_O\pi^*$) of the GMP from the FC geometry and along the $\pi\pi^*$ L_a CASSCF MEP.

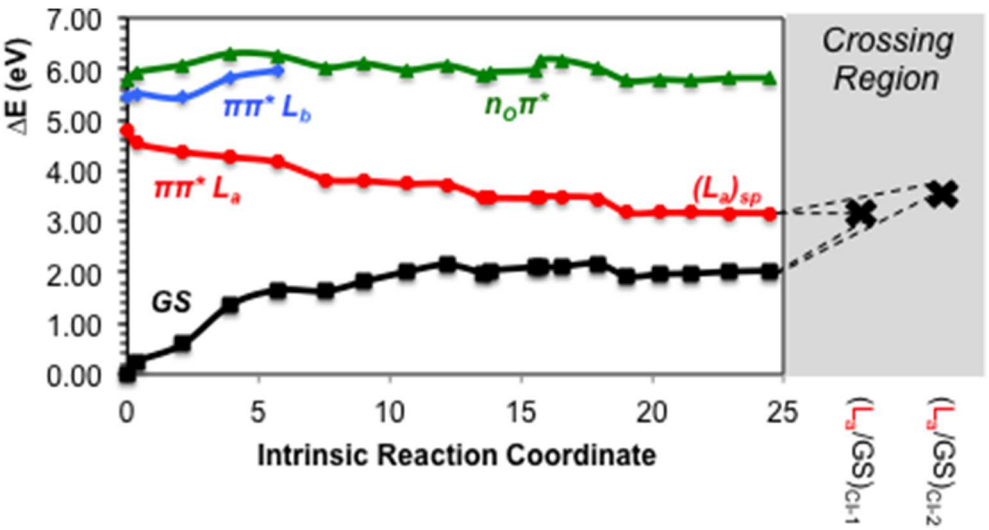

FIGURE 6 | CASPT2 energies of the ground (GS) and lowest-lying singlet excited states ($\pi\pi^*$ L_a, π π^* L_b and $n_O\pi^*$) of the GMP from the FC geometry and along the $n_O\pi^*$ CASSCF MEP.

region. This kind of process has been widely attributed to the DNA/RNA nucleobases and is permanently linked with their intrinsic photostability (Serrano-Andrés and Merchán, 2009) and therefore extends to the photostability of the genomic material. Our calculations in the presence of the solvent and the sugar and phosphate groups reveal a very shallow stationary point at the end of the MEP right before reaching the intersection seam (see **Figure 5**), which has also been previously documented in other nucleobases at a TDDFT level of theory to be related to a transition state with an imaginary reaction coordinate that drives the system toward the ring-puckering CI (Picconi et al., 2011). This stationary point is explained in terms of the planarity of the $\pi\pi^*$ potential energy hypersurfaces of all nucleobases (Giussani et al., 2013a; Improta and Barone, 2014), and is expected to be overcome in order to reach the CIs with the ground state in an ultrafast manner. In contrast, we have shown recently (Conti et al., 2010, 2015) that the corresponding internal conversion path in adenine is controlled by a larger barrier, which may explain its longer lifetimes. Two different CIs have been located between the $\pi\pi^*$ L_a and GS states, namely $(L_a/GS)_{CI\text{-}1}$

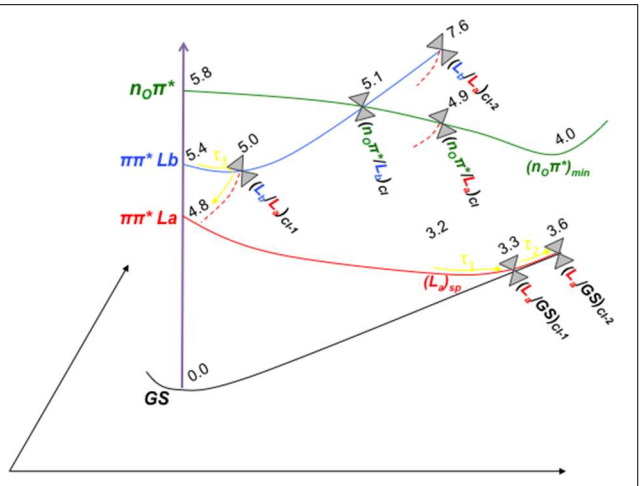

FIGURE 7 | Scheme of the photoinduced processes occurring in solvated GMP upon UV-light irradiation. The energetic values (in eV) and the different crossing points and minima depicted refer to the CASPT2 computations carried out in the present study. The associated time constants marked in yellow have been taken tentatively from the ultrafast pump-probe transient absorption experiments reported by Karunakaran et al. (2009). Three different decay channels have been assigned to the experimental evidence: τ_1 refers to the ultrafast decay path from an initially accessed $\pi\pi^*$ L_a excitation to the ring-puckering CI with the GS, τ_2 to the initial population of the $\pi\pi^*$ L_b state and subsequent non-adiabatic population transfer to the L_a state finalizing in the CI between L_a and GS, and τ_3 that is tentatively assigned mainly to deactivation processes along the L_b state (See text for details).

and $(L_a/GS)_{CI-2}$. These two CIs are analogous to those found *in vacuo* by Serrano-Andrés et al. (2008) but present an energetic inversion due to the embedding effect of the solvent. Both are expected to belong to the same intersection seam given their similar structures, and both are considered to be accessible from the L_a stationary point previously characterized. $(L_a/GS)_{CI-1}$, being the lowest-lying energy wise is expected to embody the fastest decay route, relating to the $\tau_1 = 0.25$ ps recorded through time-resolved transient and $\tau_1 = 120$ fs in time-resolved photoelectron spectroscopy experiments. This assignment is analogous to that previously reported for 9H-Guanine *in vacuo*, and supports recent experiments reporting analogous excited-state decays for GMP in gas-phase and in solution (Chatterley et al., 2014). The second conical intersection with the ground state, $(L_a/GS)_{CI-2}$, might be responsible for the second exponential measured at $\tau_2 = 1.0$ ps and $\tau_2 = 680$ fs in time-resolved transient and photoelectron spectroscopy, respectively, given its higher-lying energetic position and a relatively small barrier of ∼0.3 eV to be overcome in order to access it once reaching the intersection seam. Nevertheless, the existence of another CI between the L_a and GS states not characterized in the present contribution could better explain that second lifetime, which will be related to the L_a surface as it has been recently reported experimentally (Chatterley et al., 2014). These assignments are in line with the MD studies by Lan et al. (2009), reporting two different decay routes with their associated timescales to two distinct CIs between the $\pi\pi^*$ L_a and the ground state, and are in line with other theoretical CASPT2 and TDDFT studies that point toward the L_a state as the responsible for both ultrafast decay timescales.

The $\pi\pi^*$ L_b state is predicted to be involved in the photoinduced events being related possibly only to the longest-lived τ_3. This is explained in terms of an initial population of the L_b state, which presents a sizable oscillator strength, and subsequent funneling of the population toward the L_a state mediated by the $(L_b/L_a)_{CI-1}$, placed at ∼5 eV along the L_b relaxation pathway. The second CI characterized between L_b and L_a states, $(L_b/L_a)_{CI-2}$, is expected to be irrelevant to the photo-process due to its high-lying energetic position preventing its accessibility. The lone-pair excited state, $n_O\pi^*$, is blue-shifted in solution as has been already mentioned above. Its elevated vertical absorption energy prevents it to be one of the main spectroscopic states, yet its close-lying position to the absorbing $\pi\pi^*$ L_b state facilitates a possible population of this state and subsequent relaxation toward its minimum, $(n_O\pi^*)_{min}$. This minimum is placed at 3.97 eV adiabatically and 2.67 eV vertically from the GS, and could be partly responsible of the longest-lived signal reported experimentally at $\tau_3 = 2.5$ ps or at $\tau_3 = 167$ ps at low pH, given that such $n\pi^*$-mediated processes have been already characterized experimentally to be close to the ∼100 ps timescale on pyrimidines both *in vacuo* and in solution (Hare et al., 2007).

The present study elucidates the photoinduced events in GMP in terms of an ultrafast decay along the main spectroscopic and initially accessed $\pi\pi^*$ L_a state characterized by a ring-puckering motion, which would cover the experimental timescales τ_1 and τ_2 through different CIs with the ground state, whereas the longest-lived component would be attributed to the decay routes mediated through the $\pi\pi^*$ L_b and, to a minor extent, to the $n_O\pi^*$ state.

Conclusions

The present study encompasses a photophysical and photochemical appraisal of water-solvated GMP by means of theoretical multireference perturbation theory QM/MM techniques. An initial MD simulation has been carried out in order to characterize the geometrical parameters of the FC region. The vertical excitation energies have been computed and compared to recent data found in the literature and to the results obtained *in vacuo*, highlighting the importance of the environment yielding qualitative differences for the $\pi\pi^*$ L_a and $\pi\pi^*$ L_b states being red-shifted and for the $n_O\pi^*$ state being blue-shifted as compared to their gas-phase counterpart. The $\pi\pi^*$ L_a state is predicted to be the main spectroscopic state driving the ultrafast deactivation processes occurring in GMP upon UV-light irradiation based on a ring-puckering motion that enhances its non-adiabatic interaction with the ground state in a radiationless manner. A shallow stationary point toward the end of the $\pi\pi^*$ L_a MEP has been characterized, together with two different CIs with the ground state that help rationalize the two fastest decay times measured experimentally. Upon initial L_b absorption, two CIs between the $\pi\pi^*$ L_b and L_a states have also been located, one of them along the L_b decay path pointing toward a population funneling down to the L_a state and another being too high in energy to contribute prominently in the photo-process. The CIs connecting the $n_O\pi^*$ state and the $\pi\pi^*$ L_b and L_a states have also been characterized along its

relaxation route, yielding a minimum in the $n_O\pi^*$ state expected to emit vertically at ∼2.7 eV. Both $\pi\pi^*$ L_b and $n_O\pi^*$ are suggested to contribute to the longest-lived experimental timescale, the latter providing a lesser contribution given the relatively fast kinetic timescale and the long-lived timescales expected in $n\pi^*$ fluorescent states. Upcoming QM/MM dynamics simulations are expected to shed some more light on the photoinduced events occurring in water-solvated GMP and its specific decay timescales in order to provide a more specific molecular counterpart to the experiment and better explain the photochemical and photophysical processes resulting in the intrinsic stability of the genomic material.

Acknowledgments

MG acknowledges support by the European Research Council Advanced Grant STRATUS (ERC-2011-AdG No. 291198). We acknowledge the use of HPC resources of the "Pôle Scientifique de Modélisation Numérique" at the ENS-Lyon, France.

Supplementary Material

The Supplementary Material for this article can be found online at: http://www.frontiersin.org/journal/10.3389/fchem.2015.00029/abstract

References

Altoé, P., Stenta, M., Bottoni, A., and Garavelli, M. (2007a). A tunable QM/MM approach to chemical reactivity, structure and physico-chemical properties prediction. *Theor. Chem. Acc.* 118, 219–240. doi: 10.1007/s00214-007-0275-9

Altoé, P., Stenta, M., Bottoni, A., and Garavelli, M. (2007b). COBRAMM: a tunable QM/MM approach to complex molecular architectures. *Modelling the excited and ground state properties of sized molecular systems. AIP Conf. Proc.* 963, 491–505. doi: 10.1063/1.2827033

Andersson, K., Malmqvist, P.-Å., and Roos, B. O. (1992). 2nd-order perturbation-theory with a complete active space self-consistent field reference function. *J. Chem. Phys.* 96, 1218–1226. doi: 10.1063/1.462209

Aquilante, F., De Vico, L., Ferre, N., Ghigo, G., Malmqvist, P.-A., Neogrady, P., et al. (2010). Software news and update MOLCAS 7: the next generation. *J. Comput. Chem.* 31, 224–247. doi: 10.1002/jcc.21318

Aquilante, F., Pedersen, T. B., Veryazov, V., and Lindh, R. (2013). MOLCAS—a software for multiconfigurational quantum chemistry calculations. *Wiley Interdiscip. Rev. Comput. Mol. Sci.* 3, 143–149. doi: 10.1002/wcms.1117

Barbatti, M., Aquino, A. J. A., Szymczak, J. J., Nachtigallova, D., Hobza, P., and Lischka, H. (2010). Relaxation mechanisms of UV-photoexcited DNA and RNA nucleobases. *Proc. Natl. Acad. Sci. U.S.A.* 107, 21453–21458. doi: 10.1073/pnas.1014982107

Barbatti, M., Borin, A., and Ullrich, S. (2014). *Photoinduced Processes in Nucleic Acids*. Berlin Heidelberg: Springer.

Barbatti, M., Szymczak, J. J., Aquino, A. J., Nachtigallová, D., and Lischka, H. (2011). The decay mechanism of photoexcited guanine - a nonadiabatic dynamics study. *J. Chem. Phys.* 134:014304. doi: 10.1063/1.3521498

Barbatti, M. (2014). Photorelaxation induced by water–chromophore electron transfer. *J. Am. Chem. Soc.* 136, 10246–10249. doi: 10.1021/ja505387c

Bearpark, M. J., Robb, M. A., and Bernhard Schlegel, H. (1994). A direct method for the location of the lowest energy point on a potential surface crossing. *Chem. Phys. Lett.* 223, 269–274. doi: 10.1016/0009-2614(94)00433-1

Brash, D. E. (2015). UV signature mutations. *Photochem. Photobiol.* 91, 15–26. doi: 10.1111/php.12377

Cadet, J., Mouret, S., Ravanat, J.-L., and Douki, T. (2012). Photoinduced damage to cellular DNA: direct and photosensitized reactions†. *Photochem. Photobiol.* 88, 1048–1065. doi: 10.1111/j.1751-1097.2012.01200.x

Callis, P. R. (1983). Electronic states and luminiscence of nucleic-acid systems. *Annu. Rev. Phys. Chem.* 34, 329–357. doi: 10.1146/annurev.pc.34.100183.001553

Case, D., Darden, T. A., Cheatham, T. E., Simmerling, C., Wang, J., Duke, R., et al. (2011). *Amber 11*. San Francisco, CA: University of California.

Case, D. A., Cheatham, T. E., Darden, T., Gohlke, H., Luo, R., Merz, K. M., et al. (2005). The Amber biomolecular simulation programs. *J. Comput. Chem.* 26, 1668–1688. doi: 10.1002/jcc.20290

Chatterley, A. S., West, C. W., Stavros, V. G., and Verlet, J. R. R. (2014). Time-resolved photoelectron imaging of the isolated deprotonated nucleotides. *Chem. Sci.* 5, 3963–3975. doi: 10.1039/C4SC01493F

Chen, J., and Kohler, B. (2014). Base stacking in adenosine dimers revealed by femtosecond transient absorption spectroscopy. *J. Am. Chem. Soc.* 136, 6362–6372. doi: 10.1021/ja501342b

Chen, J., Thazhathveetil, A. K., Lewis, F. D., and Kohler, B. (2013). Ultrafast excited-state dynamics in hexaethyleneglycol-linked DNA homoduplexes made of A·T base pairs. *J. Am. Chem. Soc.* 135, 10290–10293. doi: 10.1021/ja4049459

Chen, J., Zhang, Y., and Kohler, B. (2014). *Excited States in DNA Strands Investigated by Ultrafast Laser Spectroscopy*. Berlin; Heidelberg: Springer.

Conti, I., Altoe, P., Stenta, M., Garavelli, M., and Orlandi, G. (2010). Adenine deactivation in DNA resolved at the CASPT2//CASSCF/AMBER level. *Phys. Chem. Chem. Phys.* 12, 5016–5023. doi: 10.1039/b926608a

Conti, I., Garavelli, M., and Orlandi, G. (2009). Deciphering low energy deactivation channels in adenine. *J. Am. Chem. Soc.* 131, 16108–16118. doi: 10.1021/ja902311y

Conti, I., Nenov, A., Höfinger, S., Flavio Altavilla, S., Rivalta, I., Dumont, E., et al. (2015). Excited state evolution of DNA stacked adenines resolved at the CASPT2//CASSCF/Amber Level: from the bright to the excimer state and back. *Phys. Chem. Chem. Phys.* 17, 7291–7302. doi: 10.1039/C4CP05546B

Crespo-Hernandez, C. E., Cohen, B., Hare, P. M., and Kohler, B. (2004). Ultrafast excited-state dynamics in nucleic acids. *Chem. Rev.* 104, 1977–2019. doi: 10.1021/cr0206770

Fingerhut, B. P., Dorfman, K. E., and Mukamel, S. (2013). Monitoring nonadiabatic dynamics of the RNA base uracil by UV pump–IR probe spectroscopy. *J. Phys. Chem. Lett.* 4, 1933–1942. doi: 10.1021/jz400776r

Fingerhut, B. P., Dorfman, K. E., and Mukamel, S. (2014). Probing the conical intersection dynamics of the RNA base uracil by UV-pump stimulated-Raman-probe signals; *ab initio* simulations. *J. Chem. Theory Comput.* 10, 1172–1188. doi: 10.1021/ct401012u

Frisch, M. J., Trucks, G. W., Schlegel, H. B., Scuseria, G. E., Robb, M. A., Cheeseman, J. R., et al. (2009). *Gaussian 09*. Wallingford, CT: Gaussian, Inc.

Garavelli, M. (2006). Computational organic photochemistry: strategy, achievements and perspectives. *Theor. Chem. Acc.* 116, 87–105. doi: 10.1007/s00214-005-0030-z

Giussani, A., Segarra-Martí, J., Roca-Sanjuán, D., and Merchán, M. (2013a). Excitation of nucleobases from a computational perspective I: reaction paths. *Top. Curr. Chem.* 355, 57–97. doi: 10.1007/128_2013_501

Giussani, A., Serrano-Andrés, L., Merchán, M., Roca-Sanjuán, D., and Garavelli, M. (2013b). Photoinduced formation mechanism of the thymine–thymine (6–4) adduct. *J. Phys. Chem. B* 117, 1999–2004. doi: 10.1021/jp307200g

González-Luque, R., Climent, T., González-Ramírez, I., Merchán, M., and Serrano-Andrés, L. (2010). Singlet-triplet states interaction regions in DNA/RNA nucleobase hypersurfaces. *J. Chem. Theory Comput.* 6, 2103–2114. doi: 10.1021/ct100164m

González-Ramírez, I., Segarra-Martí, J., Serrano-Andrés, L., Merchán, M., Rubio, M., and Roca-Sanjuán, D. (2012). On the N1–H and N3–H Bond dissociation in uracil by low energy electrons: a CASSCF/CASPT2 study. *J. Chem. Theory Comput.* 8, 2769–2776. doi: 10.1021/ct300153f

Gupta, A. P., Taylor, W. J., McGown, L. B., and Kempf, J. G. (2014). NMR studies of the chiral selectivity of self-assembled guanosinemonophosphate. *J. Phys. Chem. B.* 118, 14243–14256. doi: 10.1021/jp5075016

Gustavsson, T., Banyasz, A., Lazzarotto, E., Markovitsi, D., Scalmani, G., Frisch, M. J., et al. (2006). Singlet excited-state behavior of uracil and thymine in aqueous solution: a combined experimental and computational study

of 11 uracil derivatives. *J. Am. Chem. Soc.* 128, 607–619. doi: 10.1021/ja056181s

Hare, P. M., Crespo-Hernández, C. E., and Kohler, B. (2007). Internal conversion to the electronic ground state occurs via two distinct pathways for pyrimidine bases in aqueous solution. *Proc. Natl. Acad. Sci. U.S.A.* 104, 435–440. doi: 10.1073/pnas.0608055104

Hudock, H. R., Levine, B. G., Thompson, A. L., Satzger, H., Townsend, D., Gador, N., et al. (2007). *Ab initio* molecular dynamics and time-resolved photoelectron spectroscopy of electronically excited uracil and thymine. *J. Phys. Chem. A* 111, 8500–8508. doi: 10.1021/jp0723665

Improta, R. (2014). Quantum mechanical calculations unveil the structure and properties of the absorbing and emitting excited electronic states of guanine quadruplex. *Chem. Eur. J.* 20, 8106–8115. doi: 10.1002/chem.201400065

Improta, R., and Barone, V. (2014). *Excited States Behavior of Nucleobases in Solution: Insights from Computational Studies*. Berlin Heidelberg: Springer.

Jorgensen, W. L., Chandrasekhar, J., Madura, J. D., Impey, R. W., and Klein, M. L. (1983). Comparison of simple potential functions for simulating liquid water. *J. Chem. Phys.* 79, 926–935. doi: 10.1063/1.445869

Kamiya, Y., and Asanuma, H. (2014). Light-driven DNA nanomachine with a photoresponsive molecular engine. *Acc. Chem. Res.* 47, 1663–1672. doi: 10.1021/ar400308f

Karunakaran, V., Kleinermanns, K., Improta, R., and Kovalenko, S. A. (2009). Photoinduced dynamics of guanosine monophosphate in water from broad-band transient absorption spectroscopy and quantum-chemical calculations. *J. Am. Chem. Soc.* 131, 5839–5850. doi: 10.1021/ja810092k

Kleinermanns, K., Nachtigallova, D., and de Vries, M. S. (2013). Excited state dynamics of DNA bases. *Int. Rev. Phys. Chem.* 32, 308–342. doi: 10.1080/0144235X.2012.760884

Kohler, B. (2010). Nonradiative decay mechanisms in DNA model systems. *J. Phys. Chem. Lett.* 1, 2047–2053. doi: 10.1021/jz100491x

Krause, P., Matsika, S., Kotur, M., and Weinacht, T. (2012). The influence of excited state topology on wavepacket delocalization in the relaxation of photoexcited polyatomic molecules. *J. Chem. Phys.* 137:22A537. doi: 10.1063/1.4748580

Lam, E. Y., Beraldi, D., Tannahill, D., and Balasubramanian, S. (2013). G-quadruplex structures are stable and detectable in human genomic DNA. *Nat. Commun.* 4, 1796. doi: 10.1038/ncomms2792

Lan, Z., Fabiano, E., and Thiel, W. (2009). Photoinduced nonadiabatic dynamics of 9H-guanine. *Chemphyschem* 10, 1225–1229. doi: 10.1002/cphc.200900030

Mai, S., Richter, M., Marquetand, P., and González, L. (2014). *Excitation of Nucleobases from a Computational Perspective II: Dynamics.*Berlin Heidelberg: Springer.

Markovitsi, D., Gustavsson, T., and Vayá, I. (2010). Fluorescence of DNA duplexes: from model helices to natural DNA. *J. Phys. Chem. Lett.* 1, 3271–3276. doi: 10.1021/jz101122t

Martínez-Fernández, L., Corral, I., Granucci, G., and Persico, M. (2014). Competing ultrafast intersystem crossing and internal conversion: a time resolved picture for the deactivation of 6-thioguanine. *Chem. Sci.* 5, 1336–1347. doi: 10.1039/c3sc52856a

Martinez-Fernandez, L., Gonzalez, L., and Corral, I. (2012). An *ab initio* mechanism for efficient population of triplet states in cytotoxic sulfur substituted DNA bases: the case of 6-thioguanine. *Chem. Commun.* 48, 2134–2136. doi: 10.1039/c2cc15775f

McFarland, B. K., Farrell, J. P., Miyabe, S., Tarantelli, F., Aguilar, A., Berrah, N., et al. (2014). Ultrafast X-ray Auger probing of photoexcited molecular dynamics. *Nat. Commun.* 5:4235. doi: 10.1038/ncomms5235

Merchán, M., González-Luque, R., Climent, T., Serrano-Andrés, L., Rodriguez, E., Reguero, M., et al. (2006). Unified model for the ultrafast decay of pyrimidine nucleobases. *J. Phys. Chem. B* 110, 26471–26476. doi: 10.1021/jp066874a

Merchán, M., and Serrano-Andrés, L. (2003). Ultrafast internal conversion of excited cytosine via the lowest pi pi* electronic singlet state. *J. Am. Chem. Soc.* 125, 8108–8109. doi: 10.1021/ja0351600

Merchán, M., Serrano-Andrés, L., Robb, M. A., and Blancafort, L. (2005). Triplet-state formation along the ultrafast decay of excited singlet cytosine. *J. Am. Chem. Soc.* 127, 1820–1825. doi: 10.1021/ja044371h

Miannay, F.-A., Gustavsson, T., Banyasz, A., and Markovitsi, D. (2010). Excited-state dynamics of dGMP measured by steady-state and femtosecond fluorescence spectroscopy†. *J. Phys. Chem. A* 114, 3256–3263. doi: 10.1021/jp909410b

Murat, P., and Balasubramanian, S. (2014). Existence and consequences of G-quadruplex structures in DNA. *Curr. Opin. Genet. Dev.* 25, 22–29. doi: 10.1016/j.gde.2013.10.012

Nachtigallová, D., Zeleni, T., Ruckenbauer, M., Müller, T., Barbatti, M., Hobza, P., et al. (2010). Does stacking restrain the photodynamics of individual nucleobases? *J. Am. Chem. Soc.* 132, 8261–8263. doi: 10.1021/ja1029705

Nakayama, A., Arai, G., Yamazaki, S., and Taketsugu, T. (2013). Solvent effects on the ultrafast nonradiative deactivation mechanisms of thymine in aqueous solution: excited-state QM/MM molecular dynamics simulations. *J. Chem. Phys.* 139:214304. doi: 10.1063/1.4833563

Nenov, A., Rivalta, I., Cerullo, G., Mukamel, S., and Garavelli, M. (2014a). Disentangling peptide configurations via two-dimensional electronic spectroscopy: *ab initio* simulations beyond the Frenkel Exciton Hamiltonian. *J. Phys. Chem. Lett.* 5, 767–771. doi: 10.1021/jz5002314

Nenov, A., Segarra-Martí, J., Giussani, A., Conti, I., Rivalta, I., Dumont, E., et al. (2014b). FD 177: probing deactivation pathways of DNA nucleobases by two-dimensional electronic spectroscopy: first principles simulations. *Faraday Discuss.* doi: 10.1039/C4FD00175C. (in press).

Noonan, F. P., Zaidi, M. R., Wolnicka-Glubisz, A., Anver, M. R., Bahn, J., Wielgus, A., et al. (2012). Melanoma induction by ultraviolet A but not ultraviolet B radiation requires melanin pigment. *Nat. Commun.* 3, 884. doi: 10.1038/ncomms1893

Parac, M., Doerr, M., Marian, C. M., and Thiel, W. (2010). QM/MM calculation of solvent effects on absorption spectra of guanine. *J. Comput. Chem.* 31, 90–106. doi: 10.1002/jcc.21233

Picconi, D., Barone, V., Lami, A., Santoro, F., and Improta, R. (2011). The interplay between $\pi\pi^*/n\pi^*$ excited states in gas-phase thymine: a quantum dynamical study. *Chemphyschem* 12, 1957–1968. doi: 10.1002/cphc.201001080

Pierloot, K., Dumez, B., Widmark, P. O., and Roos, B. O. (1995). Density matrix averaged atomic natural orbital (ANO) basis sets for correlated molecular wave functions. IV. Medium size basis sets for the atoms H-Kr. *Theor. Chim. Acta* 90, 87–114. doi: 10.1007/BF01113842

Plasser, F., Aquino, A. J. A., Lischka, H., and Nachtigallová, D. (2015). Electronic excitation processes in single-strand and double-strand DNA: a computational approach. *Top. Curr. Chem.* 356, 1–37. doi: 10.1007/128_2013_517

Platt, J. R. (1949). Classification of spectra of cata—condensed hydrocarbons. *J. Chem. Phys.* 17, 484–495. doi: 10.1063/1.1747293

Pollum, M., Martínez-Fernández, L., and Crespo-Hernández, C. (2014). *Photochemistry of Nucleic Acid Bases and Their Thio- and Aza-Analogues in Solution*. Berlin Heidelberg: Springer.

Rivalta, I., Nenov, A., Cerullo, G., Mukamel, S., and Garavelli, M. (2014). *Ab initio* simulations of two-dimensional electronic spectra: the SOS//QM/MM approach. *Int. J. Quantum Chem.* 114, 85–93. doi: 10.1002/qua.24511

Roca-Sanjuán, D., Aquilante, F., and Lindh, R. (2012). Multiconfiguration second-order perturbation theory approach to strong electron correlation in chemistry and photochemistry. *Wiley Interdiscip. Rev. Comput. Mol. Sci.* 2, 585–603. doi: 10.1002/wcms.97

Roos, B. O., Andersson, K., Fulscher, M. P., Malmqvist, P. A., Serrano-Andrés, L., Pierloot, K., et al. (1996). Multiconfigurational perturbation theory: applications in electronic spectroscopy. *Adv. Chem. Phys. Vol. Xciii* 93, 219–331. doi: 10.1002/9780470141526.ch5

Santoro, F., Barone, V., Lami, A., and Improta, R. (2010). The excited electronic states of adenine-guanine stacked dimers in aqueous solution: a PCM/TD-DFT study. *Phys. Chem. Chem. Phys.* 12, 4934–4948. doi: 10.1039/b925108a

Saurí, V., Gobbo, J. P., Serrano-Pérez, J. J., Lundberg, M., Coto, P. B., Serrano-Andrés, L., et al. (2012). Proton/hydrogen transfer mechanisms in the guanine-cytosine base pair: photostability and tautomerism. *J. Chem. Theory Comput.* 9, 481–496. doi: 10.1021/ct3006166

Schwalb, N. K., and Temps, F. (2007). Ultrafast electronic relaxation in guanosine is promoted by hydrogen bonding with cytidine. *J. Am. Chem. Soc.* 129, 9272–9273. doi: 10.1021/ja073448

Schwalb, N. K., and Temps, F. (2008). Base sequence and higher-order structure induce the complex excited-state dynamics in DNA. *Science* 322, 243–245. doi: 10.1126/science.1161651

Segarra-Martí, J., and Coto, P. B. (2014). A theoretical study of the intramolecular charge transfer in 4-(dimethylamino)benzethyne. *Phys. Chem. Chem. Phys.* 16, 25642–25648. doi: 10.1039/C4CP03436H

Segarra-Martí, J., Roca-Sanjuán, D., Merchán, M., and Lindh, R. (2012). On the photophysics and photochemistry of the water dimer. *J. Chem. Phys.* 137, 244309. doi: 10.1063/1.4772187

Serrano-Andrés, L., and Merchán, M. (2009). Are the five natural DNA/RNA base monomers a good choice from natural selection? A photochemical perspective. *J. Photochem. Photobiol. C Photochem. Rev.* 10, 21–32. doi: 10.1016/j.jphotochemrev.2008.12.001

Serrano-Andrés, L., Merchán, M., and Borin, A. C. (2006). Adenine and 2-aminopurine: paradigms of modern theoretical photochemistry. *Proc. Natl. Acad. Sci. U.S.A.* 103, 8691–8696. doi: 10.1073/pnas.0602991103

Serrano-Andrés, L., Merchán, M., and Borin, A. C. (2008). A three-state model for the photophysics of guanine. *J. Am. Chem. Soc.* 130, 2473–2484. doi: 10.1021/ja0744450

Su, C., Middleton, C. T., and Kohler, B. (2012). Base-stacking disorder and excited-state dynamics in single-stranded adenine homo-oligonucleotides. *J. Phys. Chem. B* 116, 10266–10274. doi: 10.1021/jp305350t

Takaya, T., Su, C., Harpe, K. D. L., Crespo-Hernández, C. E., and Kohler, B. (2008). UV excitation of single DNA and RNA strands produces high yields of exciplex states between two stacked bases. *Proc. Natl. Acad. Sci. U.S.A.* 105, 10285–10290. doi: 10.1073/pnas.0802079105

Vayá, I., Gustavsson, T., Douki, T., Berlin, Y., and Markovitsi, D. (2012). Electronic excitation energy transfer between nucleobases of natural DNA. *J. Am. Chem. Soc.* 134, 11366–11368. doi: 10.1021/ja304328g

Werner, H.-J., Knowles, P. J., Knizia, G., Manby, F. R., and Schütz, M. (2012a). Molpro: a general-purpose quantum chemistry program package. *Wiley Interdiscip. Rev. Comput. Mol. Sci.* 2, 242–253. doi: 10.1002/wcms.82

Werner, H.-J., Knowles, P. J., Knizia, G., Manby, F. R., Schütz, M., Celani, P., et al. (2012b). *MOLPRO, Version 2012.1. A Package of ab Initio Programs*.

West, B. A., and Moran, A. M. (2012). Two-dimensional electronic spectroscopy in the ultraviolet wavelength range. *J. Phys. Chem. Lett.* 3, 2575–2581. doi: 10.1021/jz301048n

West, B. A., Womick, J. M., and Moran, A. M. (2011). Probing ultrafast dynamics in adenine with mid-UV four-wave mixing spectroscopies. *J. Phys. Chem. A* 115, 8630–8637. doi: 10.1021/jp204416m

West, B. A., Womick, J. M., and Moran, A. M. (2012). Interplay between vibrational energy transfer and excited state deactivation in DNA components. *J. Phys. Chem. A* 117, 5865–5874. doi: 10.1021/jp306799e

Conflict of Interest Statement: The authors declare that the research was conducted in the absence of any commercial or financial relationships that could be construed as a potential conflict of interest.

Copyright © 2015 Altavilla, Segarra-Martí, Nenov, Conti, Rivalta and Garavelli. This is an open-access article distributed under the terms of the Creative Commons Attribution License (CC BY). The use, distribution or reproduction in other forums is permitted, provided the original author(s) or licensor are credited and that the original publication in this journal is cited, in accordance with accepted academic practice. No use, distribution or reproduction is permitted which does not comply with these terms.

ADVANTAGES OF PUBLISHING IN FRONTIERS

FAST PUBLICATION
Average 90 days from submission to publication

COLLABORATIVE PEER-REVIEW
Designed to be rigorous – yet also collaborative, fair and constructive

RESEARCH NETWORK
Our network increases readership for your article

OPEN ACCESS
Articles are free to read, for greatest visibility

TRANSPARENT
Editors and reviewers acknowledged by name on published articles

GLOBAL SPREAD
Six million monthly page views worldwide

COPYRIGHT TO AUTHORS
No limit to article distribution and re-use

IMPACT METRICS
Advanced metrics track your article's impact

SUPPORT
By our Swiss-based editorial team

frontiers

EPFL Innovation Park · Building I · 1015 Lausanne · Switzerland
T +41 21 510 17 00 · info@frontiersin.org · frontiersin.org